12551

AD 200793

NTIS only
DDC-IR
10 May 66

UNCLASSIFIED

DATE 12/8/58 NEL NO. 1
RECLASSIFIED TO UNCLASSIFIED
AUTH. Jr. Underwater Acoustics
V. 8 no. 4 p. 593 Oct. 1958
E. Eyhmy 2420
SIGNATURE & CODE

Best Available Copy

TORPEDO STUDIES

NOTICE

This document is the property of the United States Government. It is furnished on a loan basis and shall be returned as specified, or upon recall by ASTIA to the following address: ASTIA Reference Center, Technical Information Division, Library of Congress, Washington 25, D.C.

CLASSIFICATION CHANGED TO
UNCLASSIFIED
AUTHORITY SEC Army by TAG per J205213
Dpt Army letter 11 Jul 58

Herbert M Jones
Maj Gen U.S.A.

FC

SUMMARY TECHNICAL REPORT
OF THE
NATIONAL DEFENSE RESEARCH COMMITTEE

Manuscript and illustrations for this volume were prepared for publication by the Summary Reports Group of the Columbia University Division of War Research under contract OEMsr-1131 with the Office of Scientific Research and Development. This volume was printed and bound by the Columbia University Press.

Distribution of the Summary Technical Report of NDRC has been made by the War and Navy Departments. Inquiries concerning the availability and distribution of the Summary Technical Report volumes and microfilmed and other reference material should be addressed to the War Department Library, Room 1A-522, The Pentagon, Washington 25, D. C., or to the Office of Naval Research, Navy Department, Attention: Reports and Documents Section, Washington 25, D. C.

Copy No.

129

This volume, like the seventy others of the Summary Technical Report of NDRC, has been written, edited, and printed under great pressure. Inevitably there are errors which have slipped past Division readers and proofreaders. There may be errors of fact not known at time of printing. The author has not been able to follow through his writing to the final page proof.

Please report errors to:

JOINT RESEARCH AND DEVELOPMENT BOARD
PROGRAMS DIVISION (STR ERRATA)
WASHINGTON 25, D. C.

A master errata sheet will be compiled from these reports and sent to recipients of the volume. Your help will make this book more useful to other readers and will be of great value in preparing any revisions.

SUMMARY TECHNICAL REPORT OF DIVISION 6, NDRC

VOLUME 21

TORPEDO STUDIES

OFFICE OF SCIENTIFIC RESEARCH AND DEVOLOPMENT

VANNEVAR BUSH, DIRECTOR

NATIONAL DEFENSE RESEARCH COMMITTEE

JAMES B. CONANT, CHAIRMAN

DIVISION 6

JOHN T. TATE, CHIEF

WASHINGTON, D. C., 1946

NATIONAL DEFENSE RESEARCH COMMITTEE

James B. Conant, *Chairman*
Richard C. Tolman, *Vice Chairman*

Roger Adams	Army Representative[1]
Frank B. Jewett	Navy Representative[2]
Karl T. Compton	Commissioner of Patents[3]

Irvin Stewart, *Executive Secretary*

[1]*Army representatives in order of service:*

Maj. Gen. G. V. Strong
Maj. Gen. R. C. Moore
Maj. Gen. C. C. Williams
Brig. Gen. W. A. Wood, Jr.
Col. L. A. Denson
Col. P. R. Faymonville
Brig. Gen. E. A. Regnier
Col. M. M. Irvine
Col. E. A. Routheau

[2]*Navy representatives in order of service:*

Rear Adm. H. G. Bowen
Capt. Lybrand P. Smith
Rear Adm. J. A. Furer
Rear Adm. A. H. Van Keuren
Commodore H. A. Schade

[3]*Commissioners of Patents in order of service:*

Conway P. Coe
Casper W. Ooms

NOTES ON THE ORGANIZATION OF NDRC

The duties of the National Defense Research Committee were (1) to recommend to the Director of OSRD suitable projects and research programs on the instrumentalities of warfare, together with contract facilities for carrying out these projects and programs, and (2) to administer the technical and scientific work of the contracts. More specifically, NDRC functioned by initiating research projects on requests from the Army or the Navy, or on requests from an allied government transmitted through the Liaison Office of OSRD, or on its own considered initiative as a result of the experience of its members. Proposals prepared by the Division, Panel, or Committee for research contracts for performance of the work involved in such projects were first reviewed by NDRC, and if approved, recommended to the Director of OSRD. Upon approval of a proposal by the Director, a contract permitting maximum flexibility of scientific effort was arranged. The business aspects of the contract, including such matters as materials, clearances, vouchers, patents, priorities, legal matters, and administration of patent matters were handled by the Executive Secretary of OSRD.

Originally NDRC administered its work through five divisions, each headed by one of the NDRC members. These were:

Division A—Armor and Ordnance
Division B—Bombs, Fuels, Gases & Chemical Problems
Division C—Communication and Transportation
Division D—Detection, Controls, and Instruments
Division E—Patents and Inventions

In a reorganization in the fall of 1942, twenty-three administrative divisions, panels, or committees were created, each with a chief selected on the basis of his outstanding work in the particular field. The NDRC members then became a reviewing and advisory group to the Director of OSRD. The final organization was as follows:

Division 1—Ballistic Research
Division 2—Effects of Impact and Explosion
Division 3—Rocket Ordnance
Division 4—Ordnance Accessories
Division 5—New Missiles
Division 6—Sub-Surface Warfare
Division 7—Fire Control
Division 8—Explosives
Division 9—Chemistry
Division 10—Absorbents and Aerosols
Division 11—Chemical Engineering
Division 12—Transportation
Division 13—Electrical Communication
Division 14—Radar
Division 15—Radio Coordination
Division 16—Optics and Camouflage
Division 17—Physics
Division 18—War Metallurgy
Division 19—Miscellaneous
Applied Mathematics Panel
Applied Psychology Panel
Committee on Propagation
Tropical Deterioration Administrative Committee

NDRC FOREWORD

As events of the years preceding 1940 revealed more and more clearly the seriousness of the world situation, many scientists in this country came to realize the need of organizing scientific research for service in a national emergency. Recommendations which they made to the White House were given careful and sympathetic attention, and as a result the National Defense Research Committee [NDRC] was formed by Executive Order of the President in the summer of 1940. The members of NDRC, appointed by the President, were instructed to supplement the work of the Army and the Navy in the development of the instrumentalities of war. A year later, upon the establishment of the Office of Scientific Research and Development [OSRD], NDRC became one of its units.

The Summary Technical Report of NDRC is a conscientious effort on the part of NDRC to summarize and evaluate its work and to present it in a useful and permanent form. It comprises some seventy volumes broken into groups corresponding to the NDRC Divisions, Panels, and Committees.

The Summary Technical Report of each Division, Panel, or Committee is an integral survey of the work of that group. The first volume of each group's report contains a summary of the report, stating the problems presented and the philosophy of attacking them and summarizing the results of the research, development, and training activities undertaken. Some volumes may be "state of the art" treatises covering subjects to which various research groups have contributed information. Others may contain descriptions of devices developed in the laboratories. A master index of all these divisional, panel, and committee reports which together constitute the Summary Technical Report of NDRC is contained in a separate volume, which also includes the index of a microfilm record of pertinent technical laboratory reports and reference material.

Some of the NDRC-sponsored researches which had been declassified by the end of 1945 were of sufficient popular interest that it was found desirable to report them in the form of monographs, such as the series on radar by Division 14 and the monograph on sampling inspection by the Applied Mathematics Panel. Since the material treated in them is not duplicated in the Summary Technical Report of NDRC, the monographs are an important part of the story of these aspects of NDRC research.

In contrast to the information on radar, which is of widespread interest and much of which is released to the public, the research on subsurface warfare is largely classified and is of general interest to a more restricted group. As a consequence, the report of Division 6 is found almost entirely in its Summary Technical Report, which runs to over twenty volumes. The extent of the work of a Division cannot therefore be judged solely by the number of volumes devoted to it in the Summary Technical Report of NDRC: account must be taken of the monographs and available reports published elsewhere.

Any great cooperative endeavor must stand or fall with the will and integrity of the men engaged in it. This fact held true for NDRC from its inception, and for Division 6 under the leadership of Dr. John T. Tate. To Dr. Tate and the men who worked with him—some as members of Division 6, some as representatives of the Division's contractors—belongs the sincere gratitude of the Nation for a difficult and often dangerous job well done. Their efforts contributed significantly to the outcome of our naval operations during the war and richly deserved the warm response they received from the Navy. In addition, their contributions to the knowledge of the ocean and to the art of oceanographic research will assuredly speed peacetime investigations in this field and bring rich benefits to all mankind.

The Summary Technical Report of Division 6, prepared under the direction of the Division Chief and authorized by him for publication, not only presents the methods and results of widely varied research and development programs but is essentially a record of the unstinted loyal cooperation of able men linked in a common effort to contribute to the defense of their Nation. To them all we extend our deep appreciation.

Vannevar Bush, Director
Office of Scientific Research and Development

J. B. Conant, Chairman
National Defense Research Committee

FOREWORD

One of the most serious obstacles to the use of torpedoes from aircraft is the likelihood of damage and consequent failure of the torpedo if the water-entry speed is high. Unless the speed is high, however, the attacking plane is a "sitting duck." This was brought home with tragic force in the Battle of Midway.

In July 1943, the Navy requested NDRC to undertake the design of an improved torpedo capable of withstanding the shock of water entry when launched at aircraft speeds as high as 400 knots. The project was assigned to Division 6 and thus initiated the studies reported in this volume.

It was soon discovered that the addition of a simple ring to the tail fins of the standard Mark 13 torpedo brought its performance up to the limiting speed of available torpedo planes. With this discovery, the pressure for immediate improvement with respect to water entry was further increased, and at the request of the Navy the project was broadened to include a study of every aspect of torpedo design. As a result of this comprehensive program, not only was a torpedo developed which fully met all requirements, but, of longer-term interest, an analysis was furnished of the basic physical factors affecting the overall design of any future torpedo.

The success of this project was made possible only by the cordial and effective cooperation of many individuals and agencies.

The technical program of the Division was carried out under contracts with Columbia University, California Institute of Technology, Massachusetts Institute of Technology, and the American Can Company.

The Navy, through the Bureau of Ordnance and the Naval Torpedo Station at Newport, not only provided test facilities, but made freely available the knowledge and skills gained through their long experience in design, production, and use of torpedoes. And at the suggestion of the Commanding Officer a project engineer was permanently stationed at Newport to assure complete and continuous exchange of information.

The Army, because of its interest in a related program, maintained close liaison throughout the duration of the project.

Division 3 of NDRC made possible crucial full-scale tests of high-speed water entry by providing through their contract with California Institute of Technology both personnel and facilities.

Division 7 of NDRC contributed consulting services on the control problem.

The General Electric Company gave to the groups working on power plant design the full advantage of their knowledge and experience in the design and construction of high-temperature gas turbines.

To all of these individuals and agencies, and in particular to Dr. W. V. Houston, Director of the Columbia University Special Studies Group who served as director of the entire program, the Division makes grateful acknowledgment.

John T. Tate

Chief, Division 6

PREFACE

This report was prepared by the Columbia University Special Studies Group as part of the studies made in connection with Project NO–176. It covers essentially the theoretical studies of torpedo performance and the corresponding indications as to proper torpedo design.

Although some of the theoretical work presented was done by the Special Studies Group, much of this report is a compilation of experimental results and theoretical developments carried on by various groups at a number of places. When possible, an attempt has been made to give credit to these groups for the work that they have done.

The work on the theory of torpedo control as discussed in this report is largely due to Dr. L. I. Schiff, while the studies associated with air flight and water entry have been compiled and developed by Marvin Gimprich.

W. V. Houston

CONTENTS

PART I

GENERAL DISCUSSION AND SUMMARY

PART II

HYDRODYNAMICS AND AERODYNAMICS

PART III

CONTROL SYSTEMS

PART I

GENERAL DISCUSSION AND SUMMARY

Chapter 1

GENERAL REQUIREMENTS FOR TORPEDOES

The term "torpedo" has been used at various periods in the history of modern warfare to mean a variety of weapons, but nearly always these have contained a charge of high explosive. In the naval warfare of the past 50 years the term has come to be applied almost exclusively to the automobile torpedo. This is a self-propelled and self-steered underwater vehicle that carries a charge of explosive to a point at which it will explode against the underwater part of an enemy ship. The principal problems of torpedo design can then be classified as those associated with its launching, its propulsion, its steering, and the means for exploding the charge.

The philosophy of torpedoes has always involved the idea that the explosive charge carried should be such as to cause decisive damage to the enemy. The rest of the torpedo, the power plant and the control mechanism, has been so elaborate and so expensive that economy of effort could be obtained only if one torpedo hit was sufficient to sink a ship. In fact, the fraction of the weight of a torpedo made up of the explosive charge is usually only somewhere between 0.2 and 0.3 so that the equipment necessary to convey the charge to its objective is much more elaborate than the charge and its firing mechanism.

In recent years, however, defenses against torpedoes have been built into all capital ships and many smaller ones so that the probability of sinking such a ship with a single torpedo is not very great. Furthermore, even cargo ships are so divided into compartments that usually a single torpedo will not be sufficient to sink one of them. It appears that a very large increase in explosive charge may be necessary materially to increase the probability of sinking from a single hit. For this reason, it may be more economical of effort to count on using two or more automobile torpedoes to sink even a merchant ship, but it is improbable that the complication of torpedo mechanism should ever be used to transport anything less than a very seriously damaging charge of explosive.

Another characteristic of torpedoes is that the explosion occurs against the part of the ship that is underwater. This is clearly more damaging than a hit on the superstructure, not only beeause a hole beneath the water line will cause the ship to lose buoyancy, but also because the presence of the water increases the effectiveness of the explosion. Modern battleships are so protected by armor plate in the neighborhood of the water line and for some distance below it that hits by shells in this region are considerably reduced in effectiveness. A hit by a torpedo on this armor belt will normally cause very little damage. Nevertheless, this kind of armor cannot be used to cover the entire hull for the buoyancy of the ship would be seriously reduced by it. A properly adjusted torpedo can hit the skin of the ship below this armor belt and do serious damage. For this reason a torpedo is a formidable weapon against any ship.

The automobile torpedo is normally fired at a considerable distance from its target. It normally travels in the water at a speed greater than that of the fastest ships. Nevertheless, even this speed is sufficiently low to make it necessary to predict the position of the target some time in advance. A torpedo traveling at 45 knots will require some 4 minutes to travel 6,000 yd. During this time, a ship making 30 knots will travel 4,000 yd. In case the firing of the torpedo could be detected, it would be quite possible for the target ship to avoid being hit by turning sharply. However, torpedoes can be launched in many cases without this launching being detected, and more often a number are launched almost simultaneously so that it is difficult for the target to avoid them all.

In the case of torpedoes used in naval engagements, long ranges are frequently used, and some torpedoes may need a range as great as 20,000 yd. It is clear, however, that no single aimed torpedo can be effective at such a range unless the target continues on a steady course throughout the full torpedo run. For such reasons, it is important to reduce the running time of a torpedo as much as possible. Apparently the most effective way to do this would be to increase the speed of the torpedo, but, since this is very difficult to accomplish, consideration must also be given to the possibility of reducing the length of the underwater run.

1.1 SPEED AND RANGE OF SUBMARINE AND DESTROYER LAUNCHED TORPEDOES

The torpedo is the ideal weapon for a submarine vessel. It can be fired in many cases before the enemy is aware of the presence of the submarine. If an electric torpedo, or some other torpedo without a visible wake, is used, the first warning of an attack may come from the explosion. Under these conditions a long range may be useful, and certainly a high torpedo speed is useful in increasing the aiming accuracy. Other things being equal, it is probable that more hits can be made with a high-speed than with a low-speed torpedo. On the other hand, speed can be obtained only by a sacrifice of other qualities and principally by a sacrifice of range or by a considerable increase in size and weight. Hence it is important to evaluate carefully the minimum useful range from which a torpedo can be fired and to emphasize its use. This would improve the accuracy of aiming, not only because of the shorter range and the reduced effect of aiming angle errors, but also because the maximum speed could then be obtained from the fuel carried.

1.2 SPEED AND RANGE OF AIRCRAFT TORPEDOES

In the case of aircraft torpedoes, the situation is somewhat different. The launching of the torpedo can usually be observed by the target, and the proper evasive action can be taken. It appears impractical to try to produce sufficient underwater speed in a torpedo to make this evasive action ineffective if much underwater travel is necessary. Since, however, the torpedo is dropped from an airplane, advantage can be taken of the speed of the plane and the altitude from which the torpedo is dropped to provide a long air travel. The speed of this travel in air is so much greater than any feasible underwater speed that most of the distance between the point of release and the target should be covered in the air travel. The principal requirement appears to be the development of a torpedo that can be launched from very high-speed planes and from high altitudes, with a sufficient power plant to travel a short distance under water at a moderate speed. Along with such a torpedo adequate torpedo directors must be provided.

If a torpedo can be released from 6,400 ft at 350 knots so as to strike the water 500 yd from its target, it will spend only about 20 sec in the air, traveling almost 4,000 yd. If its underwater speed is 40 knots, the 500 yd will require about 23 sec so that a total distance of nearly 4,500 yd can be covered in about 43 sec. This is not time enough for much manuevering on the part of the target.

1.3 REQUIREMENTS FOR STEERING AND DEPTH CONTROL

The specifications laid down for the steering and depth control of a torpedo will depend on the way in which it is to be used. It is necessary that the depth control be adequate to get the explosive to the desired depth on the target. When contact exploders are to be used and the target is a battleship, the depth mechanism must insure that the torpedo hits below the armor belt, and it must not fail to keep the torpedo from running completely under the ship. When influence exploders are used, the necessary accuracy of depth-keeping is not so great since the exploder will operate at any depth down to some distance below the keel.

The accuracy of steering required depends upon the length of the underwater run. The deviation from the set course must not be so great as to dominate other errors, but there is also no need to require of the steering equipment that it maintain its direction for a time longer than the torpedo will run or with an accuracy far greater than the accuracy of aiming that is possible. In general, it may be expected that a torpedo with a long underwater run will require greater accuracy than one with a short underwater run. Thus a submarine-launched torpedo with a run of some 5,000 yd would be expected to require roughly five times the steering accuracy of an aircraft torpedo with an underwater run of only about 1,000 yd. Nevertheless, the possible evasive action that may be taken by a target attacked by a long range torpedo and the use of salvos of long range torpedoes may again reduce the value of high accuracy steering in even these cases. Since the requirements of steering accuracy present some of the most troublesome problems in torpedo manufacture and maintenance, it is important to limit such requirements to those which really contribute to the effectiveness of the torpedoes.

In the case of an aircraft torpedo launched from a high altitude for a short underwater run it is necessary that: (1) the torpedo does not dive so deep as to strike the bottom and stick or be damaged; (2) the torpedo recover from its set depth and arm before reaching the target. These conditions, which are dependent only in part on the operation of the depth-control mechanisms, make necessary a complete understanding of the water-entry phenomena in designing such a torpedo. To a considerable extent, the water-entry behavior is determined by the external shape and the distribution of mass, as well as the torpedo orientation at entry.

The studies described in this report include many things common to all torpedoes, but particular emphasis has been placed on these problems of air travel, water entry, and control that are important in the design of aircraft torpedoes and, in particular, in the design of the Mark 25 aircraft torpedo.

Chapter 2

THE ELEMENTS OF A TORPEDO

A TORPEDO may be considered as being composed of several more or less independent elements properly balanced with one another to make a well-integrated weapon. For convenience of discussion, the general principles and basic underlying features of each of the elements can be developed separately.

2.1 EXTERNAL SHAPE

Torpedo bodies are usually cylindrical in shape and are provided with a rounded nose that may be either hemispherical or pointed, a tail which supports fins for stability, and rudders and elevators for steering and depth control.

This general shape has been found most suitable to furnish the volume required to contain the explosive charge, the power plant and control mechanism, and to provide for the dynamic stability and minimum drag necessary for proper behavior in water. These latter requirements are discussed in detail in Chapters 4 and 7.

These shape requirements hold for submarine-launched torpedoes and, in most cases, for torpedoes launched from surface vessels. For an aircraft-launched torpedo, however, the shape must be also suitable for proper travel through air and for proper entry into the water. In general, the shapes required for the three different phases of travel, air travel, water entry, and controlled underwater travel, are different. Stability in air travel is provided by equipping the torpedo with light wood appendages, which break off with entry of the torpedo into the water. These air stabilizers are of various types. Some are mounted on the tail, while others, such as the drag ring or "pickle barrel," are on the nose.

In most cases it has been possible to select a shape that is both adequate for water entry and satisfactory for the underwater run. However, various appendages have been tried, such as spoiler rings and Townend extensions to the nose, that are designed to stay on during water entry and to detach only when the steady run begins. It is probable that optimum control of the water-entry phase would require appendages on the tail as well as those that have been tried on the nose. Nevertheless, it has been found possible to get adequate performance, under certain conditions, by means of a shape that is also suitable for steady running.

2.2 THE EXPLOSIVE CHARGE AND THE EXPLODER

The size and nature of the explosive charge for a torpedo depend to a considerable extent on the kind of targets for which it is designed. Most torpedoes carry charges in the neighborhood of 600 to 800 lb of Torpex. This charge appears to be adequate to damage a battleship and to cause very serious damage to lighter vessels. It appears that an increase of a few hundred pounds would make relatively little difference and, unless it were decided to multiply the charge by a factor of at least 3 to 5, it would be hardly worth increasing at all.

An essential part of the torpedo warhead is the exploder mechanism. Exploder mechanisms are now available that will detonate the charge in the vicinity of the target rather than depending on an impact. This makes possible the use of greater depths and so minimizes the danger of hitting the armored belt of a capital ship.

The torpedo studies included in this report do not include studies of the explosive and the exploder mechanism.

2.3 PROPULSION MECHANISM

The propulsion mechanism occupies the major part of the torpedo both in volume and in weight. For this reason, the overall size is determined very largely by the requirements placed on speed and range. In order to get the maximum speed and range with a given weight, it is necessary that the power plant operate as efficiently as possible. The power necessary to drive the torpedo is approximately proportional to the third power of the speed at which it runs, provided the propulsive efficiency is independent of the speed. For the conventional propeller-driven type of torpedo, this is approximately true, but for some of the proposed types of drive, the efficiency increases rapidly with the speed so that the power required does not increase as rapidly as the third power of the speed.

The total energy required for a torpedo is proportional to the second power of the speed and to the range. Consequently, the amount of fuel necessary is similarly proportional to these quantities. A torpedo differs from a surface ship in that it must carry not only its fuel in the ordinary sense but also the oxidant. In most torpedoes, the oxidant has been in the form of compressed air. In fact, the original torpedoes were driven by compressed air alone. Later, a little fuel was added to warm up the air so as to make it more effective, and finally the process became one of complete combustion. For the purpose of combustion it is clear that compressed oxygen would be better than compressed air because the air is only about 30 per cent oxygen. Nevertheless, the hazards associated with the use of compressed oxygen have prevented its extensive adoption.

With either compressed air or compressed oxygen a heavy tank is necessary to contain the gas. In fact, approximately 4 lb of steel is necessary to contain 1 lb of air. For this reason, obviously it would be better if the oxidant could be carried in the form of a liquid since only about 1 lb of container is necessary for 1 lb of liquid. This 60 per cent reduction in the weight of the fuel and its container is a very important improvement in torpedo power plants, and such systems are now being developed. Probably the most advanced is that in which liquid hydrogen peroxide is used as the oxidant. On its way to the combustion chamber this is decomposed into oxygen and water. The oxygen combines with the fuel, and the water cools the flame to a point at which it can be used in the turbine.

Any such improvement in the weight of the fuel and its containers can be translated directly into torpedo range. If the use of hydrogen peroxide reduces the fuel and container weight by 60 per cent, it provides a means of increasing the range of a torpedo by a factor of 2.5 without increasing its weight. Whether the saving is put into increased range or into increased explosive depends on which of the two is regarded as the more important.

Propulsion mechanisms will not be discussed extensively in this report. An extensive study of them has been made by the Navy Department to be used as a basis for future torpedo development.

2.4 CONTROL MECHANISMS

The conventional automobile torpedo runs on a previously set course at a predetermined depth. The depth-control mechanism and the steering mechanism are to a large extent independent.

The operation of these mechanisms must be closely associated with the hydrodynamics of the torpedo body. This is particularly true of the pendulum, in which care must be taken that the natural period of the pendulum is not too close to the period at which the torpedo tends to oscillate in depth. Furthermore, the stability of the control depends not only on the control mechanism itself but also on the hydrodynamic constants of the body.

The development of torpedo-control mechanisms can then be divided into two parts. In the first part, it is important to measure the hydrodynamic constants of the torpedo and then to determine the properties of the control necessary to operate in the desired manner. In particular, it is important to determine the maximum time lag that can be permitted between the actuation of the mechanism and the final operation of the rudder and elevator. This is inversely

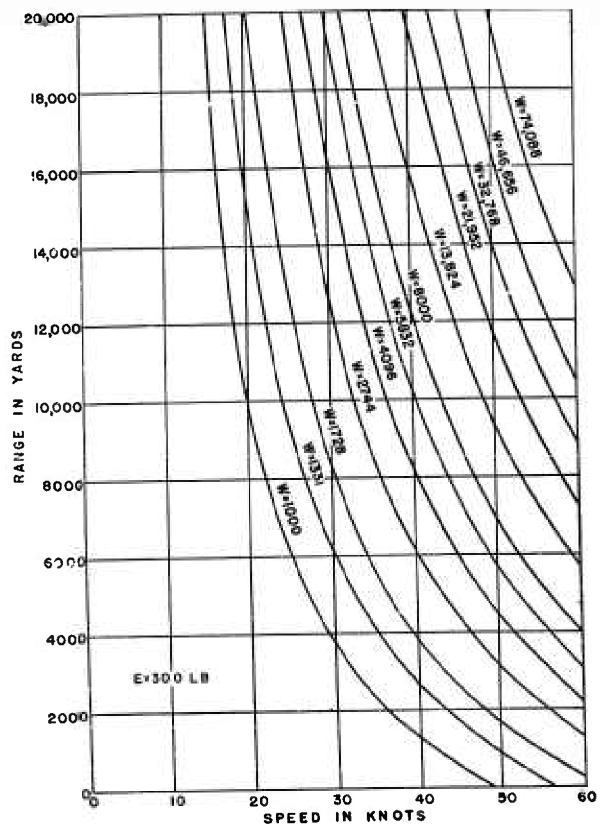

FIGURE 1. Estimated curves showing the speed and range attainable for various total weights and an explosive charge of 300 lb.

proportional to the velocity, and its value for any given torpedo depends on the hydrodynamic constants.

The second part concerns the design of mechanisms having suitable properties. The present report is concerned only with the theoretical analysis. The progress that has been made under Project NO-176 in the design of depth and steering mechanisms is reported in connection with the design of the Mark 25 torpedo.

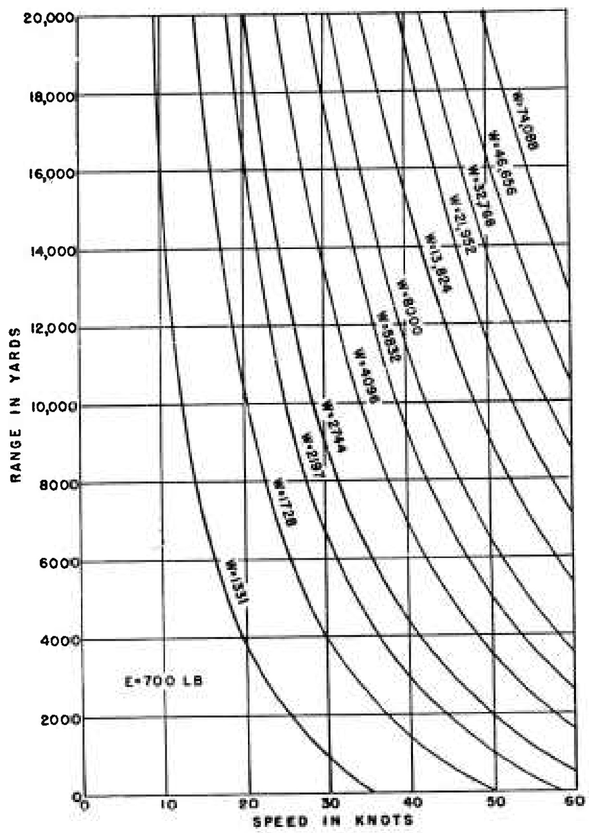

FIGURE 2. Estimated curves showing the speed and range attainable for various total weights and an explosive charge of 700 lb.

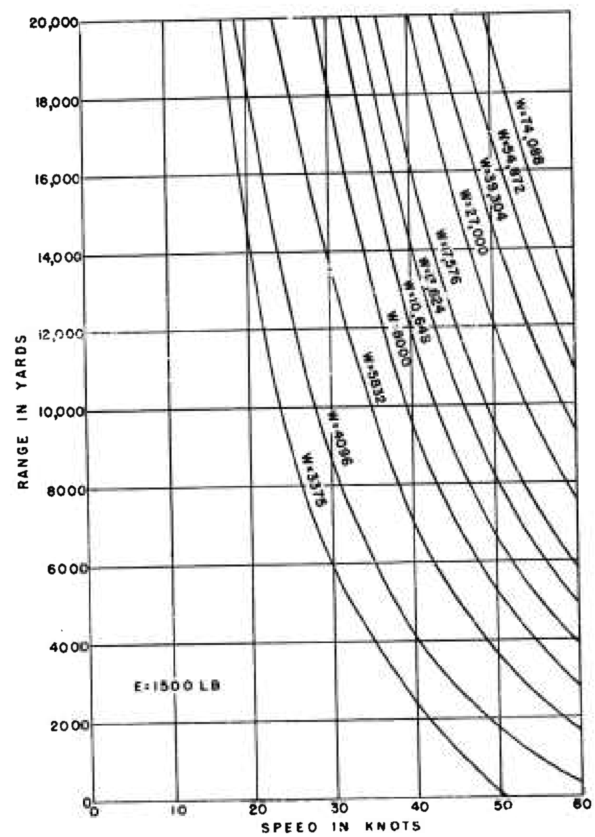

FIGURE 3. Estimated curves showing the speed and range attainable for various total weights and an explosive charge of 1,500 lb.

2.5 WEIGHT AND SIZE OF THE TORPEDO

The outstanding properties of a torpedo that must be correlated with each other are (1) range, (2) speed, (3) weight of explosive, and (4) overall weight. These four quantities are all related, and in the design of a torpedo suitable compromises must be made between the desire to have maximum weight of explosive, speed, and range and the desire to have a minimum overall weight.

In a very rough way the weight of a torpedo may be regarded as made up of four parts. These are E, the weight of the explosive; S, the weight of the external shell; F, the weight of the fuel and its containers; and P, the weight of the turbine, gear train, and propeller system. The weight of the shell is roughly proportional to the external surface of the torpedo and hence may be regarded as proportional to the two-thirds power of the total weight. Hence we may set $S = \gamma W^{2/3}$. γ is a constant that depends upon the material of which the shell is made, upon its thickness, and upon the shape of the torpedo.

The amount of fuel necessary is proportional to (1) the range of the torpedo, (2) the square of the velocity, and (3) the external surface. The amount of fuel necessary is proportional to the external surface because the drag is proportional to the external surface and hence to the two-thirds power of the weight. Hence we may accept $F = \alpha v^2 R W^{2/3}$. The constant α depends upon the fuel system used and will be very

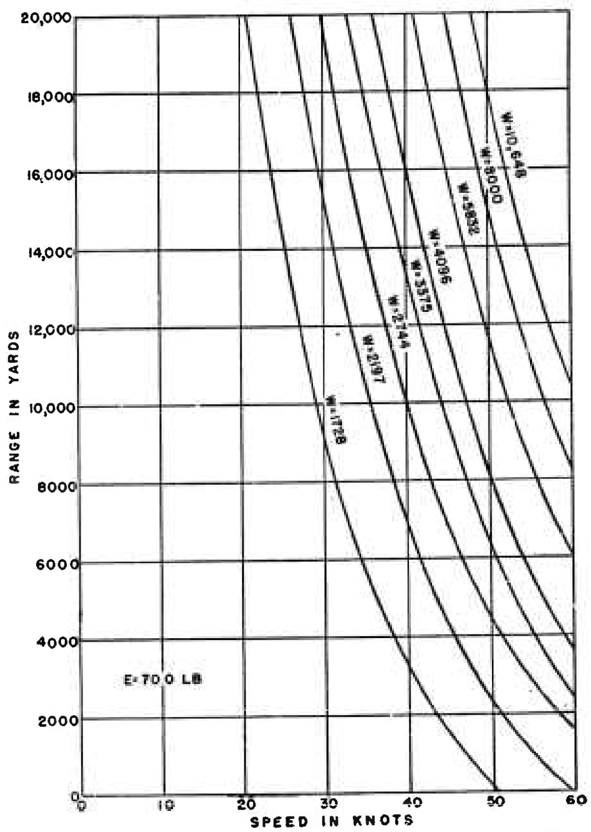

FIGURE 4. Curves showingt he estimated speed and range attainable for various total weights with the use of a liquid oxidant and an explosive charge of 700 lb.

much smaller in case hydrogen peroxide is used than when compressed air is used.

In a very rough way, the weight of the power plant may be set proportional to the cube of the speed and to the external torpedo surface. Hence we may regard $P = \beta v^3 W^{2/3}$.

Since the total weight of the torpedo is the sum of these four parts, it is possible to write an equation connecting the total weight of the explosive, the speed, and the range as follows:

$$W = E + (\gamma + \beta v^3 + \alpha v^2 R) W^{2/3}.$$

The constants, α, β, and γ must be determined from some known torpedo. If they are evaluated for the Mark 25 torpedo, the values are approximately

$$\alpha = 7.00 \times 10^{-7},$$
$$\beta = 2.45 \times 10^{-5},$$
$$\gamma = 4.00.$$

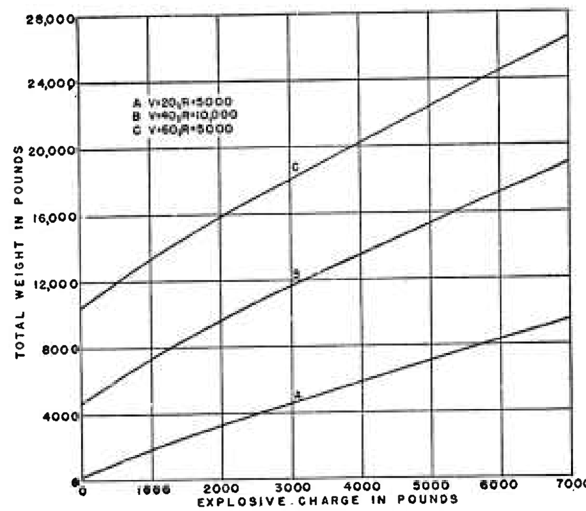

FIGURE 5. Total weight as a function of the weight of explosive for three cases. The power plant is assumed to be similar to that of the Mark 25.

By using these constants, it is possible to plot relationships between the various quantities in the equation. In particular, Figures 1, 2, and 3 show the speeds and ranges that can possibly be attained with given overall weight. Other curves present these data in slightly different ways.

These curves point out clearly the cost at which high speed and long range are attained. In most torpedoes, the explosive is a relatively small part of the total weight, while the fuel and power plant make up most of it. If the diameter is increased it is possible to increase the explosive charge with only a small increase in overall weight, but doubling the range or the speed makes a very serious change in the torpedo.

Chapter 3

OUTLINE AND SUMMARY

3.1 AIR TRAVEL

An aircraft torpedo is launched by dropping it from an airplane that is traveling at a high rate of speed, and the most important line of development of this weapon is concerned with increasing the speed and the altitude from which it can be launched. The initial travel of the torpedo through the air is equally important with its underwater travel, not only because the major part of the distance may be traversed in the air, but also because the torpedo must end its air travel in such a way as to make a proper entry into the water. The importance of this proper entry into the water is easily understood from the analogy between the torpedo and a diver. As is well known, a diver can safely dive from an elevation of 100 ft if he enters the water properly, while he can be seriously injured if he enters the water flat from a very much lower altitude.

The early experiments in launching torpedoes from aircraft were confined to dropping them from only a short distance above the water, such as 30 to 50 ft, and at speeds much less than 100 knots. These experiments emphasized the necessity for very rugged construction in order to withstand the shock of water entry. It appears, however, that in addition serious damage to the torpedo can only be minimized by providing for a clean entry. In fact, some evidence points to the fact that a 15-ft horizontal drop of a torpedo, such as has been frequently used for proof launchings, may be more damaging than a clean entry at speeds of over 200 knots.

For a clean entry it is necessary that the torpedo be traveling parallel to its axis at the time of impact with the water, and this requires proper stabilization of the torpedo in the air. Due to the action of the air forces, a simple cylindrical body tends to set itself perpendicular to its direction of travel, and a torpedo has somewhat the same tendency. If a bare torpedo is launched from a considerable elevation, it will enter the water flat and will suffer severe damage. To overcome this tendency, a large tail is required. Since this kind of tail is undesirable for the underwater run, it is constructed of light wood so as to break off on water entry.

A wide variety of stabilizers has been tried. Present practice in the United States Navy is to use a Mark 2-1 stabilizer combined with a drag ring or "pickle barrel" on the nose. The Mark 2-1 stabilizer is a simple wooden box that is slipped over the torpedo fins. The Mark 1 drag ring is a short wooden cylinder that slips over the nose. The combined effect of these two auxiliary devices is to cause the torpedo to be stable when traveling parallel to its air trajectory. The stabilizers also introduce sufficient damping so that during its air flight the torpedo will oscillate around its position of equilibrium with decreasing amplitude. If, then, the air flight is long enough, initial disturbances that are present due to conditions at release may be damped out, and the torpedo can enter the water smoothly and cleanly. This fact suggests that it is even more desirable to drop a torpedo from a high altitude than from a low altitude because a longer time is available in which this damping action can be effected.

A more important fact is that the damping effect of the stabilizers increases with the speed so that a high-speed launching may tend to be cleaner than one of lower speed. The damping is proportional to the speed, but the time of fall varies only as the square root of the altitude. Both high speed and high altitude therefore, are conducive to a good entry in the absence of a wind. These stabilizers also introduce a certain amount of drag so that there are some altitudes, depending on the release speed, from which the torpedo enters the water with a total velocity that is even less than the initial release velocity. For a low-speed launching this is only at a low altitude, but for a high-speed launching this may be true up to over 2,000 ft.

Other stabilizers have been used with more elaborate objectives. The British M.A.T. IV stabilizer is intended to cause the torpedo to strike the water slightly nose-up with respect to its trajectory. This can be easily accomplished by suitable shaping of the tail pieces, but it requires that roll in the air be prevented. To this end, the British M.A.T. IV stabilizer is a very elaborate device, incorporating a gyroscope and movable ailerons to correct any tendency to roll. Such elaboration is surely necessary if it is desired to make the torpedo enter in any other way than parallel to its trajectory. However, it would seem desirable to construct the torpedo so that entry parallel to its trajectory is adequate and so that very simple stabilizing devices can be used.

It is obvious that stabilizing appendages, such as have just been mentioned, can be effective only in causing the torpedo axis to remain parallel to its trajectory with respect to the air. If there is a wind, the trajectory with respect to the air will not be identical with the trajectory as seen from the ground, and it is the trajectory as seen from the ground that determines the water-entry conditions. As a consequence, a torpedo stabilized on its trajectory, and traveling with a tail wind, tends to enter the water effectively nose-down. A similar torpedo traveling in a head wind tends to enter effectively nose-up, and a torpedo traveling in a cross wind will enter with a certain amount of yaw. These effects of wind cannot be overcome by simple air stabilizers, and they cannot be neglected because they will affect the underwater behavior of the torpedo in a significant way. However, they can be recognized and understood, and proper allowance can be made for them in the tactical methods that are used.

In addition to making the torpedo stable on its trajectory, the stabilizers introduce a certain amount of drag. The Mark 2-1 stabilizer and the Mark 1 drag ring when used on the Mark 13 torpedo introduce enough air resistance so that the torpedo may enter the water at a speed somewhat less than the speed at which it is released. Most of this drag is due to the drag ring itself and not to the tail stabilizer. The analysis shows that the resultant speed of the torpedo first decreases because of the air resistance and then increases because of the acceleration of gravity so that it passes through a minimum. This increase does not continue indefinitely because the terminal velocity appears to be between 800 and 900 ft per sec. At this speed the air resistance is just equal to the weight so that there is no further acceleration. Because of this air resistance, the horizontal travel of the torpedo may be significantly less than that calculated when the air resistance is neglected, and the entry angle will also be different. This merely means that the more complete calculations must be used for predictions of the air flight.

It is clear that stabilizers could be designed to have increased drag and to reduce the velocity at impact to a low value. This, however, would result in a short horizontal range in air.

A detailed account of the air trajectory is given in Chapter 5, where the necessary properties of the stabilizers are analyzed.

3.2 WATER ENTRY

The water-entry phase of the aircraft torpedo trajectory is less subject to theoretical analysis than either the air travel or the underwater travel. At the beginning of the present study of the problem almost no information was available as to the essential features of the behavior of the torpedo during this stage. The air trajectory is subject to fairly complete theoretical analysis, and only certain constants need to be evaluated in order to apply the theory to any specific case. The same thing is true of the underwater run. The water entry, however, presents additional complications due to the presence of the water surface and the vastly different properties of the air and the water. For this reason, it has been possible only to establish a more or less phenomenological description of the torpedo behavior and to indicate certain convenient terms in which the initial underwater trajectory can be described. These are satisfactory for the water entry of the Mark 13 torpedo and the Mark 25 torpedo and presumably for other similar shapes.

When the torpedo nose first strikes the water, the torpedo experiences a very high force lasting over a very short time. It has not been possible to determine with any degree of reliability the exact magnitude or duration of this impact force. It is possible, however, to give some indication as to the total impulse associated with it. This produces both a sudden change of longitudinal velocity and a sudden access to angular velocity about a horizontal axis. The sudden change in linear velocity is a small fraction of the total velocity and seems to play no significant part in determining the subsequent torpedo behavior. The sudden access to angular velocity, however, is in such a direction as to cause the nose to rise and the tail to fall and determines whether the subsequent trajectory turns upward or downward. After the initial impact, the torpedo creates a cavity in the water, roughly conical in shape, so that only the nose is in contact with the water. This state continues until the torpedo is several lengths under the surface, and during this time the torpedo is subject to a decelerating force that can be described in terms of a drag coefficient and is proportional to the square of the velocity. The drag coefficient on a hemispherical nose is, at this stage, of the order of magnitude of 0.28.

The drag force on the torpedo when it is in the cavity, with its nose alone in contact with the water, is opposite in direction to the torpedo motion but does not usually act directly through the center of mass. If the torpedo is nose-down to its trajectory, this retarding force tends to turn it more nose-down and hence tends to overcome the initially produced nose-upward angular velocity. If the torpedo is nose-up to its trajectory, the retarding force adds to the initially produced angular velocity. As a consequence of this angular velocity about a horizontal axis, the tail of the torpedo will eventually strike either the top or bottom of the cavity. If it strikes the top of the cavity, the torpedo will travel in a roughly circular path concave-downward. If it strikes the bottom of the cavity, the path will be concave-upward. Which of these two things occurs depends upon the magnitude of the initially acquired angular velocity and the later angular acceleration that either adds to or subtracts from it. These depend on the entry pitch and trajectory angles. There can also occur an intermediate state in which the torpedo continues to travel for some distance without striking either side of the cavity.

If the torpedo enters directly along its trajectory, the initially acquired angular velocity will cause the nose to rise, and the subsequent retarding force will cause it to rise still farther. Under these conditions, the tail will strike the bottom of the cavity, and the trajectory will curve upward. If the torpedo enters slightly nose-down to its trajectory, the suddenly acquired angular velocity may be just enough to overcome the nose-down angular velocity produced by the retarding force. The nose-down pitch angle at which this occurs may be designated as the critical pitch angle and is found to be something over 2 degrees for the Mark 13 torpedo. If the torpedo enters much more nose-down than this critical angle, the nose-down turning produced by the retarding force will dominate the situation, and the tail of the torpedo will go to the top of the cavity. This produces a down-turning trajectory, and the torpedo will dive deep.

The forces producing the suddenly acquired angular velocity and the dependence of these forces on the entry conditions depend on the shape of the torpedo nose. Indeed, while for most nose shapes the torpedo receives an upward impulse, there are noses which are sufficiently blunt so that the torpedo nose receives a downward impulse at entry and hence the suddenly acquired angular velocity will be nose-downward in direction. For blunt noses, which are rarely used on projectiles entering water designed for an underwater run (except for antisubmarine weapons), the previous discussion must be somewhat modified in a manner indicated in Section 6.3. For the finer shaped noses which were implicitly assumed in the previous discussion, since the angular velocity acquired at impact depends on the nose shape, it is found that the critical pitch angle will vary with the nose shape.

After a moderately well-defined distance along the trajectory, the cavity will close in behind the torpedo, and the normal hydrodynamic forces will begin to act. Except for the continuing retardation, the behavior of the torpedo can then be described in the terms used for describing its steady underwater run.

It appears that the major features of the initial trajectory are determined before the cavity closes so that these major features are not influenced by the movement of the torpedo rudders or elevators and, consequently, are not dependent on the depth-control mechanism or the steering device. These mechanisms are important, however, in determining the trajectory after cavity closure. The hooks to the right or left, as well as the maximum depth of dive, are influenced by the behavior of the depth mechanism, the extent to which the elevators are reduced in effectiveness by a shroud ring and the extent to which the torpedo heels over. It appears also that a major part of the effect of a shroud ring on water-entry behavior is due to its shielding of the elevators and the corresponding reduction in curvature of the path. If the steady-state hydrodynamic constants of the torpedo are known, the trajectory after cavity collapse may be calculated (see Section 6.5).

On the basis of this kind of a picture of the initial underwater trajectory and the approximate determination of some of the constants involved, it is possible to predict with some degree of certainty the initial underwater behavior of the Mark 13 torpedo. Presumably the same can be done for the Mark 25, but this has not yet been thoroughly tested and verified. The situation is described in detail in Chapter 6, where equations are given that permit the computation of the expected depth of dive for various entry conditions. In this work the effect of wind is shown to be of great importance. Launching the torpedo in a tail wind can easily provide sufficient nose-down pitch so that the torpedo dives deep and may well strike the bottom in shallow water. Launching in a head wind may cause the torpedo to enter with a nose-up pitch such as to cause excessive broaching or to cause excessive torpedo damage on water entry.

By analogy with the above argument, it can be seen that, when the torpedo enters the water with a yaw either nose right or left, it will tend to move in a more or less circular trajectory to the right or to the left. This will introduce the initial hooks that are frequently observed. Although there are other more important reasons for hooks, it appears probable that a cross wind from the left will tend to make a torpedo hook to the left and a cross wind from the right will tend to make it hook to the right. In other words, there is a tendency to hook into the wind.

It would be highly desirable to find some shape of torpedo less sensitive than that of the Mark 13 to pitch angle and yaw angle at entry, and it seems quite possible that a proper combination of nose shape and large tail structure may do this. Nevertheless, there is at present no convincing evidence that any shape is significantly better than that of the Mark 13 torpedo with the shroud ring or that of the Mark 25 torpedo.

3.3 CONTROL OF UNDERWATER RUN

An aircraft torpedo, as well as any other kind of automobile torpedo, is equipped with steering and depth-control mechanism to make it travel on a prescribed course at a fixed depth. Since many torpedoes may travel for a considerable distance through the water, the steering performance is of importance in determining the probability of hitting the target. The depth-keeping performance is even more critical because it is desired to set the torpedo to strike the hull of a battleship between the lower edge of the armor belt and the bottom of the ship. For these reasons, the design of a torpedo requires particular attention to this steering and depth-control mechanism.

3.3.1 Hydrodynamic Stability

The studies that have been made in this connection have led to a fairly satisfactory theory of torpedo control. It has been shown that the behavior of the torpedo is the result not only of the control mechanism itself but also of the hydrodynamic characteristics of the torpedo body. These two things can be treated more or less separately, and the theory is now such that the necessary properties of the control can be fairly well specified when the hydrodynamic behavior of the body is known.

Some of the properties of a torpedo can be determined by the study of a model in a water tunnel or wind tunnel or by towing a full-scale body in a towing tank. Practically all torpedoes are statically unstable. This means that, if the torpedo is held at its center of mass while the water is pumped past it or if it is towed by an attachment at its center of mass, it will not continue to travel with its axis parallel to the direction of motion. A slight displacement will cause it to turn one way or another and set itself at a considerable angle. A bare torpedo body would probably set itself at nearly 90 degrees in the direction of motion, but, because of the presence of the tail fins and the shroud ring, an actual torpedo will not turn this far.

Although this type of static instability is very striking, it is of relatively little significance in connection with the running behavior of the torpedo. The reason for this is that, when the torpedo axis turns slightly one way or another, the direction of motion of a free torpedo driven by its own propellers also changes. It is possible to set up a criterion, as is done in Chapter 8, for what is called dynamic stability. A body is dynamically stable if, when it is displaced from its straight course, it takes up another relatively straight-line course in a direction slightly different from the original. On the other hand, if a body is unstable dynamically and is displaced slightly from its course, it will go into a circle and continue to turn with a definite radius of curvature. A body that is dynamically unstable can be steered, but it imposes a very considerable load on the steering mechanism. A body that is dynamically stable can be steered with much less anticipation in the rudder correction. A body that is statically stable will need very little steering since static stability usually corresponds to a high degree of dynamic stability, but it will be very difficult to turn. A body that is dynamically stable will always turn in the direction corresponding to its rudder position, while if it is dynamically unstable it may turn in the opposite direction for small rudder angles.

Owing to the simple shapes of conventional torpedo bodies, it is possible to set up a scale of stability in terms of the hydrodynamic constants of the body. At the one end is a region of dynamic instability, and at the other end is a region of static stability. Between these is a region of static instability but of dynamic stability, in which a steering device can turn the torpedo in a reasonable circle and also keep it on a straight course without too great limitations being imposed on the steering mechanism itself.

The criterion for dynamic stability cannot be expressed entirely in terms of coefficients that can be determined from straight-line motion in a towing tank or from ordinary measurements in a water tunnel. Additional measurements that can be made on a free-running body or that can be made by moving the body in a large circle in a towing basin can give these constants.

This indicates the importance of a careful hydrodynamic study of any torpedo body. Such a study must be made not only in straight-line motion but also in curved motion. In addition, it is important that the study be made with propellers attached and possibly even power-driven. The measured values of the hydrodynamic constants appear to depend strongly on whether the propellers are present or absent and possibly on whether they are driven or are free.

3.3.2 Steering Mechanisms

A steering mechanism may be either a two-position mechanism or a proportional mechanism. A proportional mechanism is such that the rudder displacement of the torpedo is proportional to the amount by which the torpedo axis departs from its prescribed direction. In a two-position mechanism the rudder is thrown hard over to one side or the other as soon as the torpedo departs more than a prescribed amount from its proper direction. There are also some other types that may be regarded as intermediate.

A proportional mechanism may be such that, combined with the hydrodynamic properties of the body, it results in unstable oscillations of increasing magnitude. This may be brought about if the control is too stiff, that is, if the rudder displacement divided by the deviation of the torpedo from the prescribed direction is too large a constant. Such an unstable system is, of course, unsatisfactory because the torpedo wanders widely from side to side. Instability of this kind can be corrected by reducing the amount of the rudder throw or by reducing the rudder area. Such a remedy reduces the curvature of the torpedo path and makes it more difficult to turn the torpedo in a prescribed direction. It also makes slower the correction of the course after a disturbance. In designing a steering mechanism, a proper balance must be struck between the necessity for stability and the necessity for a sensitive control or for a quick restoration after a disturbance.

Probably one of the most important sources of instability and unsatisfactory performance of the steering mechanism is the time delay that exists between the motion of the torpedo and the motion of the rudder. In an ideal control, the rudder is displaced just as soon as the torpedo departs from its course, but in most practical devices the rudder displacement lags a little bit behind the torpedo displacement. This lag may amount to one- or two-tenths of a second and is probably one of the principal reasons why some control mechanisms will work at low speeds and not at high speeds. The time delay that can be permitted is just inversely proportional to the speed at which the torpedo is running so that the time delay that is troublesome at 30 knots may cause instability if the torpedo runs at 40 knots or more.

The two-position control always results in oscillation of the torpedo about its course. If, however, this oscillation can be made of high enough frequency and of low enough amplitude, it is not serious. For example, if the torpedo oscillates at 1 c and turns through one-tenth of a degree in this time, the result will be quite insignificant.

The time lag in a two-position control will reduce the frequency of oscillation and will correspondingly increase the amplitude. Hence, in this type of control also, the time delay must be limited to an amount that does not produce too much oscillation. In fact, it is probable that the limitation on the time delay is more severe in the case of the two-position control than in the case of a proportional control. Nevertheless, if a two-position control is properly designed and built, it will steer just as well as a proportional control.

3.3.3 Depth-Control Mechanism

The depth-control mechanism may operate in the same two ways as the steering mechanism. It may produce an elevator deflection that is proportional to a given signal or combination of signals, or it may put the elevator either hard up or hard down.

The simplest form of depth mechanism might supposedly be a simple pressure bellows attached to the elevator in such a way that the deflection of the elevator is proportional to the amount by which the hydrodynamic pressure differs from its value at the desired depth. If, then, the torpedo were too deep, the pressure would be too great, and the elevator would turn up. It turns out, however, that such a mechanism is unstable and that the torpedo would oscillate widely about its set depth.

In order to get adequate depth-keeping, it is essential to have some kind of an anticipatory device. Thus, if the torpedo is running at its set depth and turns in order to start up, the depth mechanism must detect this initial change in pitch which takes place before the depth has changed at all. Similarly, when the torpedo is above its set depth but has turned so as to start down, the depth mechanism must recognize this fact and restore the elevator to its neutral or up position even before the torpedo has reached the proper depth.

Many kinds of anticipatory devices have been suggested. The one in most common use, and the one that appears the simplest, is a pendulum. This pendulum indicates the angle of inclination of the torpedo axis. In a proportional depth-control mechanism the position of the rudder is then made proportional to a combination of the departure from the set depth and the inclination.

This kind of depth control works very satisfactorily under suitable conditions. A suitably devised mechanism can control a torpedo, running at 45 knots, to within 6 in. of its prescribed depth. Nevertheless, the pendulum has numerous disadvantages. In the first place, the pendulum has a natural period of its own, and it is important that this natural period does not come too near to the natural period of depth oscillation of the torpedo. Furthermore, the torpedo can oscillate at a certain frequency at which the pendulum will not indicate any oscillation at all. This is called the frequency of antiresonance, and it depends on the location of the pendulum within the torpedo. These two points can be taken care of to a large extent in the design and location of the pendulum, but they do impose certain limitations upon the kind of pendulum that can be used.

Perhaps the most serious objection to the pendulum is its response to acceleration. Particularly in the case of an aircraft torpedo, the deceleration of the torpedo on entering the water moves the pendulum forward and turns the elevator up. If the torpedo remains right side up, this may lead to excessive broaching. If the torpedo rolls over 90 degrees to one side or the other, this action of the pendulum may cause large hooks, whereas, if it turns over completely, a deep dive may be the result. For the same reason a submarine torpedo tends to dive when ejected from the tube since it accelerates at that time, throwing the pendulum back and hence the elevator down. Furthermore, the pendulum is sensitive to changes in speed occasioned by the uneven supply of the fuel to the turbines. This may cause erratic depth-keeping. In spite of all these objections, however, no other mechanism has yet been extensively used, and it may well be that the pendulum, because of its simplicity, will always be the most satisfactory and that its disadvantages can be minimized by suitable design. Future changes may emphasize some disadvantages.

One of the means suggested for eliminating the pendulum is to use in its place a device sensitive to the time rate of change of depth. This is not too satisfactory because the torpedo does not begin to climb until after it has changed its inclination. Nevertheless, the analysis shows that such a mechanism can be constructed to give stable depth-keeping if the constants are carefully selected. In particular, if a pendulum is also included, stability can be guaranteed, and the disadvantages of using a pendulum alone can be minimized.

Another suggestion has been the use of a gyroscope for indicating the vertical. The principal difficulty with this method is that a free gyroscope will not maintain its direction with sufficient accuracy for the depth-keeping. It is possible, however, to introduce a procession to keep the axis of the gyroscope perpendicular to the main position of the axis of the torpedo. Although this device has been studied, it has not yet been given extensive service trials.

The principal result of the study of depth-keeping is the development of a theory by which it is possible to predict the performance of any projected mechanism. If a depth mechanism has been built, its characteristics can be examined in the laboratory on a tilt table or another similar device. If the device is only projected, its expected characteristics can be used to determine the behavior of the torpedo under its action. Tests have shown that the theory gives a close and fairly detailed description of torpedo behavior so that there is no longer any excuse for the laborious production of depth mechanisms that cannot be expected to operate at all.

PART II

HYDRODYNAMICS AND AERODYNAMICS

Chapter 4

HYDRODYNAMIC AND AERODYNAMIC FORCES AND MOMENTS

A torpedo is fundamentally an underwater weapon and so it is natural, although not necessarily correct, to consider its form primarily from a hydrodynamic point of view. The principal objectives have always been the minimization of drag and the achievement of a reasonable amount of stability within the limitations of overall dimensions imposed by the payload and the launcher. In an aircraft torpedo, however, the air travel and water entry must be given careful consideration as well. At the present time it appears that the water-entry phase of the motion is of dominant importance in determining the structure since less can be done to remedy the effects of poor form or inadequate strength in this connection than in others. For, in principle at least, the air travel can be stabilized by additional members that are removed on water impact, the underwater trajectory can be improved by the control system, and any extra drag can be offset by an increase in power plant. It is, however, still of the greatest importance to understand the hydrodynamic forces and moments experienced by the torpedo since some freedom in shape design is still available after water-entry requirements are satisfied and, in any event, the design of the control system and the power plant depends on these factors.

4.1 DRAG

The drag is the component of hydrodynamic force in the direction of the instantaneous velocity vector and always opposes the velocity. Since it is balanced mainly by the thrust of the propellers, it is of dominant importance in determining the power required. For very small speeds the drag is entirely due to viscous forces in the region of laminar flow surrounding the torpedo and hence is proportional to the speed. For speeds of practical interest the boundary layer is turbulent while the flow slightly farther out is smooth, and cavitation is usually not well enough developed to be significant. In this regime the drag tends to be more nearly proportional to the momentum transferred to the torpedo by turbulent masses of water in the boundary layer (dynamic pressure), that is, to the square of the speed. Experiments on models in the high-speed water tunnel, experiments on airships and airship models, and modern theories of the turbulent boundary layer indicate that the exponent is in the range 1.8 to 1.9. Thus the power required varies as the 2.8 to 2.9 power of the speed.

The influence of the drag on the underwater trajectory at entry is of secondary importance and shows up principally in the deceleration that continues after the collapse of the bubble. The effect of drag on the operation of the controls during the steady run is of still less importance. In both these cases it is a sufficiently good approximation to assume that the drag is proportional to the square of the speed, and this simplifies the analysis of Part III. Therefore, a drag coefficient can be defined as at the end of Section 4.3.

4.2 MOMENT

An elongated object such as a torpedo moving through a nonviscous fluid with a fixed acute angle of attack between its longitudinal axis and its velocity vector would be expected to experience an upsetting moment which would tend to increase the angle of attack. The moment observed experimentally in straight-line motion agrees with this prediction in sign, in the near proportionality to attack angle for moderate angles, and in the proportionality to the square of the speed. Since this moment, as well as the remainder of the hydrodynamic moments and forces, is made up of the totality of normal forces or pressures exerted on various parts of the hull and empennage, and since these pressures are proportional to the dynamic pressure $(\rho/2)V^2$ for fluid density ρ and speed V, it is convenient to define a dimensionless moment coefficient C_M by the relation

$$M \equiv \text{moment} = \left(\frac{\rho}{2}\right) V^2 A l C_M \,, \tag{1}$$

where A and l are the largest cross-sectional area and the overall length of the torpedo. This coefficient is found to be practically independent of speed. For a symmetrical body moving along its axis $C_M = 0$; its derivative with respect to attack angle is positive, meaning that the moment tends to increase the angle of attack.

The addition of tail fins or a shroud ring to the aft end of a bare torpedo hull always decreases the magnitude of the derivative of C_M with respect to attack angle and could, in principle, make it negative if carried far enough. Actual torpedoes appear always to have a positive derivative in the neighborhood of zero angle of attack. In a similar way the position of the control surfaces affects the value of C_M. When these are mounted on the ends of the fins, deflection of the control surface in one direction produces a force on them in the opposite direction and hence a moment that tends to swing the nose of the torpedo in the direction of the deflection.

4.3 CROSS FORCE

Although an object moving through a nonviscous fluid with constant velocity and orientation experiences no force perpendicular to its velocity vector, the actual torpedo does. This is due to the effect of viscosity in unbalancing the dynamic pressures on various parts of the body. The resultant lateral force L can be expressed in terms of a dimensionless force coefficient C_L:

$$L = \left(\frac{\rho}{2}\right) V^2 A C_L \,. \tag{2}$$

For a symmetrical body moving along its axis $C_L = 0$; its derivative with respect to attack angle is positive, meaning that an attack angle produced by deflection of the nose in one direction will result in a force in that direction. This agrees in sign with the well-known lift force observed in airships flying with nose up. From the discussion of Section 4.2 it follows that an increase in empennage area increases the magnitude of C_L and that a deflection of a control surface in one direction produces an increment of force in the opposite direction.

By analogy with the treatment of the lateral force, it is convenient to represent the drag force discussed in Section 4.1 in terms of a drag coefficient C_D:

$$D = \text{drag} = \left(\frac{\rho}{2}\right) V^2 A C_D \tag{3}$$

Although C_D is less independent of speed than C_M or C_L, it is often a useful approximation to regard it as constant with respect to changes of speed. Experimental evidence indicates that C_D is also independent of the attack angle and the deflection of the control surfaces for moderate values of these quantities.

4.4 DAMPING MOMENT AND FORCE

The discussion thus far in this chapter is limited to the forces and moments encountered in straight line motion. When the center of gravity [CG] of the torpedo moves in a curved path, it is convenient to divide the net forces and moments into two parts. The first is that experienced by the torpedo when moving along a straight line, with the attack angle that the CG has in the curvilinear motion. The second part is defined to be the remainder and is referred to here as the damping force or moment.

It is apparent that, in general, curvilinear motion of the CG results in rotation of the torpedo about a transverse axis that is perpendicular to the plane of the motion. This rotation combined with the forward motion results in an attack angle that varies along the length of the torpedo and hence a change in the pressure distribution referred to in Section 4.2. The damping force and moment would therefore be expected to be proportional to the angular velocity ω of the torpedo, at least for small ω, since the pressure at each point is proportional to $(\rho/2)V^2$ and the change in attack angle at each point is approximately $\omega x/V$, where x is the distance from the CG. The resultant force would be expected to be nearly perpendicular to the axis of the torpedo so this component is called $F\omega$ and the drag component is neglected. Similarly, the resultant moment will have the form $K\omega$. These can then be written in terms of dimensionless coefficients C_F and C_K that are expected to be independent of speed:

$$\begin{aligned} F\omega &= \left(\frac{\rho}{2}\right) V^2 A \left(\frac{\omega l}{V}\right) C_F \,, \\ K\omega &= \left(\frac{\rho}{2}\right) V^2 A l \left(\frac{\omega l}{V}\right) C_K \,. \end{aligned} \tag{4}$$

The damping moment always opposes the angular velocity, and, in general, a rotation that moves the nose in one direction gives rise to a lateral force in the same direction.

Although there is some evidence that C_F and C_K depend on attack angle for other bodies, the data on torpedoes is so meager that it is customary to regard them as constants. The discussion of Section 4.2 indicates that the magnitudes of both of these coefficients should increase with increase in empennage area.

Torpedo propellers generally add a cross force at the torpedo tail and hence influence all the hydrodynamic coefficients. This will be discussed further.

Chapter 5

AIR FLIGHT OF A TORPEDO

5.1 THEORY OF THE AIR FLIGHT

5.1.1 The Equations of Motion

In chapter 4 the forces acting on a torpedo during its motion through either air or water were described, and dimensionless quantities were defined in terms of which it is convenient to express them. In Chapter 7 the equations of motion of the torpedo in water will be more fully discussed in terms of these coefficients. Here the approximate equations will be written down and solved to the extent necessary for an understanding of the air flight.

Let the origin of coordinates be at the position of the torpedo CG at the time of release, and let the x axis be horizontal in the direction of forward motion. Let the y axis be vertically downward, and let the z axis be perpendicular to these two so as to make a right-hand system of coordinates.

If the effects of the air are to be neglected, the equations of motion are very simple and can be written directly as

$$\begin{aligned} \ddot{x} &= 0\,, \\ \ddot{y} &= g\,, \\ \ddot{z} &= 0\,. \end{aligned} \tag{1}$$

The solution of these equations gives the well-known parabolic trajectory.

If the resistance of the air is to be taken into account, the equations become a little more complicated for the drag is proportional to the square of the velocity and always acts opposite to the direction of motion. This leads to the equations

$$\begin{aligned} \ddot{x} &= -k\dot{x}V\,, \\ \ddot{y} &= g-k\dot{y}V\,, \\ \ddot{z} &= -k\dot{z}V\,, \end{aligned} \tag{2}$$

where $k = C_D\rho A/2M$. C_D is the drag coefficient defined in Chapter 4, ρ is the density of the air,[a] A is the cross-sectional area of the torpedo, and M is the effective mass of the torpedo. The drag coefficient C_D is that pertaining to the torpedo and its stabilizing appendages. These appendages may give rise to the major part of the air resistance.

[a] The change in density of the air with altitude is neglected, and the drag coefficient is constant over a sufficient range of yaw and pitch angles.

The solutions of equations (2) will be discussed in the Section 5.2 where it will be shown that, because of the air resistance, the horizontal velocity will tend to decrease during the drop. At the same time the vertical velocity will be less than it would be at the corresponding time if the drop were in vacuum. This can be described roughly by saying that the effective acceleration of gravity is somewhat reduced by the air resistance. It will also be shown that a torpedo dropped from a given height will have a reduced range and an increased time of drop compared with a corresponding drop in vacuum.

In addition, because of the air resistance, the vertical and horizontal motions will no longer be independent. For example, the time of drop for a torpedo launched horizontally from a given altitude will depend slightly on the release velocity.

It was shown in Chapter 4 that, in addition to the drag force due to the air, there are transverse forces. These are zero when the torpedo is traveling in a straight line parallel to its axis but come into play when the torpedo axis deviates from the direction of motion or when the direction of travel is changing. These forces will be neglected at first in the treatment given here because they are small and because the torpedo oscillates in its flight so that the forces act alternately in one direction and then in the other. For these reasons it appears that their neglect is usually justified in any practical treatment of the air trajectory.

In addition to the motion of the center of mass, it is necessary to study the motion of the torpedo about this center because the attitude of the torpedo as it enters the water is of the utmost importance. Let θ be the angle between the tangent to the trajectory and the x–z plane, and let θ be positive when the torpedo is falling. Then $\tan\theta = \dot{y}/\dot{x}$ when $\dot{z} = 0$. In addition, let α be the angle in a vertical plane between the torpedo axis and the trajectory, and let it be positive when the torpedo is nose-up. Similarly, let ψ be the angle in a horizontal plane between the torpedo axis and the trajectory. These two angles are small enough to be treated entirely independently. The equations of motion are then

$$\ddot{\alpha} + p\dot{\alpha} + q\alpha = p\dot{\theta} + \ddot{\theta}\,, \qquad (3)$$
$$\ddot{\psi} + p'\dot{\psi} + q'\psi = 0\,.$$

The first equation contains no term in θ because the restoring force is such as to urge the torpedo to lie parallel to the trajectory. The terms in $\dot{\theta}$ and $\ddot{\theta}$ appear because the direction of the trajectory is changing. The second equation has zero on the right side since, to the accuracy considered here, the projection of the trajectory on the horizontal plane is a straight line.

The coefficients q and q' are expressible in terms of the moment coefficient C_M defined in Chapter 4,

$$q = \frac{C_M}{\alpha}\frac{\rho}{2}Al\frac{V^2}{I}\,. \qquad (4)$$

In this expression C_M refers to the moment around a horizontal transverse axis through the center of mass, and I is the effective moment of inertia about this axis. q' can be expressed in a similar fashion in terms of the moment around the vertical axis. With some types of stabilizers these two moments are quite different, but the purpose of the stabilizers is to make them both positive. With air stabilizers making $q > 0$ and $q' > 0$ the torpedo, during the air flight, is statically stable, thus insuring a high degree of dynamic stability. Because of this high degree of dynamic stability and since the air disturbances are quite small, a torpedo in air does not have to be steered.

Similarly, referring to Chapter 4,

$$p = C_K\frac{\rho}{2}Al^2\frac{V}{I}\,. \qquad (5)$$

The solutions of equations (3) will be discussed and the nature of the motion illustrated in later sections.

5.1.2 Simplification for Solution

Although only parts of the complete equations are written down in the previous section, they are still too complicated to make a complete and rigorous solution profitable. Therefore, certain additional simplifying assumptions will be made to aid in understanding the nature of the motion.

In the first place, the axes were so chosen that $\dot{z}$ is zero at the time of release. It will then be assumed that $\dot{z}$ never becomes comparable with $\dot{x}$ so that in equations (2) V will be taken as $(\dot{x}^2 + \dot{y}^2)^{1/2}$. The equations to be treated will then be

$$\begin{aligned} \ddot{x} &= -k\dot{x}(\dot{x}^2 + \dot{y}^2)^{1/2}\,,\\ \ddot{y} &= g - k\dot{y}(\dot{x}^2 + \dot{y}^2)^{1/2}\,,\\ \ddot{z} &= 0\,. \end{aligned} \qquad (6)$$

The procedure will be to first get a suitable approximate solution to equations (6). This will then provide the value of θ as a function of the time to insert in equations (3).

The initial conditions to be used at the time $t = 0$ are as follows.

$x(0) = y(0) = z(0) = 0$ because of the location of the origin,
$\dot{x}_0$ = horizontal component of release velocity,
$\dot{y}_0$ = vertical component of release velocity,
$\dot{z}_0$ = 0,
α_0 = pitch angle of torpedo at release,
$\dot{\alpha}_0$ = pitching angular velocity of torpedo at release,
ψ_0 = yaw angle of torpedo at release,
$\dot{\psi}_0$ = yawing angular velocity at release.

5.1.3 Solution for the Trajectory

Even the simplified equations (6) cannot be solved exactly but must be given an approximate treatment. Hence define a quantity u as

$$u = \tan\theta = \frac{\dot{y}}{\dot{x}}\,. \qquad (7)$$

Then from equation (6) it follows that

$$\dot{u} = \frac{g}{\dot{x}}\,, \qquad (8)$$

and

$$\ddot{u} = gk(1 + u^2)^{1/2}\,. \qquad (9)$$

This last differential equation in u can be solved in a power series, so let

$$u = \sum_{n=0}^{\infty} c_n t^n\,. \qquad (10)$$

From the differential equation it follows that

$$c_0 = u_0 = \tan\theta_0\,,$$

$$c_1 = \dot{u}_0 = \frac{g}{\dot{x}_0}\,,$$

$$c_2 = \frac{\ddot{u}_0}{2} = \frac{gk}{2}\sec\theta_0\,,$$

$$c_3 = \frac{\dddot{u}_0}{6} = \frac{g^2k}{6\dot{x}_0}\sin\theta_0\,,$$

$$c_4 = \frac{\ddddot{u}_0}{24} = \frac{g^2k}{24\dot{x}_0^2}(g\cos^3\theta_0 + k\dot{x}_0^2\tan\theta_0)\,.$$

Each quantity desired can then be expanded in powers of t.

$$u = \tan\theta = u_0 + \frac{g}{\dot{x}_0}t + \frac{gk}{2}\sec\theta_0\,t^2 + \cdots \quad (11)$$

From (8) it follows that

$$\dot{x} = \frac{g}{\dot{u}} = \dot{x}_0\left[1 - k\dot{x}_0\sec\theta_0 t + \left(k^2\dot{x}_0^2\sec^2\theta_0 - \frac{gk}{2}\sin\theta_0\right)t^2\cdots\right] \quad (12)$$

so that

$$x = \int_0^t \dot{x}dt = \dot{x}_0 t - \frac{k\dot{x}_0^2}{2}\sec\theta_0 t^2 + \tfrac{1}{3}\left(k^2\dot{x}_0^3\sec^2\theta_0 - \frac{gk\dot{x}_0}{2}\sin\theta_0\right)t^3\cdots \quad (13)$$

Equations (11) and (12) show that the horizontal velocity is always less than the initial velocity and the horizontal distance traveled in a given time is less than would be traveled in vacuum.

Similarly, from equation (7),

$$\dot{y} = u\dot{x} = g\,\frac{c_0 + c_1 t + c_2 t^2}{c_1 + 2c_2 t} = \frac{\dot{y}_0 + gt + \dfrac{gk\dot{x}_0}{2}\sec\theta_0 t^2}{1 + k\dot{x}_0\sec\theta_0 t + \dfrac{gk}{2}\sin\theta_0 t^2}\,. \quad (14)$$

It is sometimes necessary to know the total velocity as a function of the time. The velocity at water entry is one of the initial conditions of the underwater trajectory, and the velocity in the air determines the forces acting on the torpedo. Since the velocity in the z direction is neglected,

$$V = (\dot{x}^2 + \dot{y}^2)^{\frac{1}{2}} = \dot{x}(1+u^2)^{\frac{1}{2}} = \frac{\ddot{u}}{k\dot{u}}\,. \quad (15)$$

If the terms containing t^2 are retained in both the numerator and the denominator, this becomes

$$V = \frac{2c_2 + 6c_3 t + 12c_4 t^2}{k(c_1 + 2c_2 t + 3c_3 t^2)}\,. \quad (16)$$

The velocity first falls off because of the air resistance and then later increases because of the acceleration of gravity. The initial decrease is not present when $k = 0$, and the later increase is less rapid than in the vacuum trajectory because of the air resistance. The value of t corresponding to a trajectory angle θ can be obtained from equation (11).

For some purposes, in particular for estimating the stabilizing moments on the torpedo during its air flight, it is convenient to use an average value of the velocity, $\bar{V}$. For torpedo launchings it is often desired to produce a specified entry angle, θ_e, and to know the time average of V up to the time this angle is attained. With sufficient accuracy the time over which the average is desired is given by

$$t_e = \frac{\dot{x}_0}{g}(\tan\theta_e - \tan\theta_0)\,. \quad (17)$$

Then

$$\bar{V} = \frac{1}{t_e k}\int_0^{t_e}\frac{\ddot{u}}{\dot{u}}dt = \frac{1}{kt_e}\log\frac{\dot{u}(t_e)}{\dot{u}(0)} = \frac{g}{k\dot{x}_0(\tan\theta_e - \tan\theta_0)}\log\left(\frac{c_1 + 2c_2 t_e + 3c_3 t_e^2 + 4c_4 t_e^3}{c_1}\right).$$

To the accuracy of this expression $\bar{V}$, the average velocity during the drop is a function only of the horizontal component of the release velocity, the trajectory angle at release, and the trajectory angle at entry. For many purposes, this may be treated as a constant velocity during the drop.

In the treatment thus far the air force has been considered as acting along the trajectory and through the center of mass. In other words, drag only has been considered. As a matter of fact, other forces are also acting. Among these the most important in its influence on the trajectory is the lift force. This acts perpendicular to the direction of motion and is proportional to the pitch angle of the torpedo. Since the torpedo oscillates during its flight so as to have alternately nose-up and nose-down pitch, this effect will be relatively small. There will be a small residual effect due to the fact that the torpedo oscillates about a position that is slightly nose-up because of the curvature of the trajectory. An additional mean pitch, either up or down, can be produced if the stabilizer is not symmetrical.

A significant effect on the trajectory may also be produced if the stabilizers are not quite symmetrical. A stabilizer, either intentionally or unintentionally, can be essentially an airplane wing and carry the torpedo much farther than it would travel without such an attachment. In case a stabilizer is designed to perform this function, provision must also be made to stabilize against roll. This has been done in the British air stabilizer, but it requires a considerable complication of the equipment.

5.1.4 Pitching and Yawing Motions

Pitch Oscillations

Thus far the trajectory of the torpedo has been treated by neglecting the effect of pitching and yawing motions. These motions have been neglected since their net effect is small because of their oscillatory nature. An expression for the resultant velocity V has been obtained and also a relation derived for the average velocity during the drop $\bar{V}$ so that for any drop V may be regarded as constant and equal to $\bar{V}$.

Since in the equations (3) for the pitching and yawing motions p and p' are proportional to V, and q and q' are proportional to V^2, we can regard these quantities as constant during the drop, and their magnitude will be given by the constant $\bar{V}$ which depends on the horizontal release velocity and trajectory angles at release and entry.

It is well known that if a torpedo is released in air without any appendages, such as stabilizers, it will tumble. It is necessary to install a stabilizer in order to create a moment that tends to line the torpedo up with its trajectory. With such a restoring moment, the torpedo, in general, will oscillate about its mean pitch angle, and it is also necessary to have these oscillations damp out as rapidly as possible. In the Mark 13 torpedo this damping is more than doubled by means of the drag ring, or pickle barrel.

If the axis of the torpedo makes an angle with the trajectory at release (the pitch angle at release) or if the axis of the torpedo is rotating with an angular velocity at release (the pitching angular velocity at release), the torpedo will proceed to oscillate while it is falling.

However, even if the pitch angle and pitching angular velocity at release are both zero, the torpedo will still oscillate during its fall. This is due to the fact that the center of gravity of the torpedo is moving along a curved trajectory and the axis of the torpedo at release may be along the trajectory, but it must turn to keep up with the changing direction of travel.

For the pitch, the first of equations (19) must be solved.

$$\ddot{\alpha} + p\dot{\alpha} + q\alpha = p\dot{\theta} + \ddot{\theta}. \tag{18}$$

The right-hand side of this will be treated as a known function of time since the approximate equations for the trajectory have already been solved. This is then an inhomogeneous differential equation, and its complete solution is obtained from the sum of the solution of the homogeneous equation

$$\ddot{\alpha} + p\dot{\alpha} + q\alpha = 0 \tag{19}$$

and a particular solution of the inhomogeneous equation. The solution of the homogeneous equation will be chosen so as to depend on the release conditions of the torpedo, the pitch angle, and pitching angular velocity at release. The particular solution will then be chosen to be independent of these initial conditions and will then represent the value the pitch angle α would have if both it and the pitching angular velocity at release were zero. The particular solution is then the part of α due to the fact that the torpedo traverses a curved trajectory.

The solution of the homogeneous equation is

$$\alpha_1(t) = e^{-pt/2}\left(\alpha_0 \cos \omega t + \frac{\dot{\alpha}_0 + p\alpha_0/2}{\omega} \sin \omega t\right), \tag{20}$$

where $\omega = \sqrt{q - (p/2)^2}$,
α_0 = pitch angle at release,
$\dot{\alpha}_0$ = pitching angular velocity at release.

It should be noted that: q is proportional to $\bar{V}^2$, and p is proportional to $\bar{V}$, so that ω is proportional to $\bar{V}$.

The particular solution of equation (18) leads to integrals which cannot be simply expressed. However, by partial integrations, a solution is obtained which is a very good approximation and is certainly sufficiently accurate for the problem being treated. Thus the particular solution of equation (18) may be taken as

$$\alpha_2(t) = \frac{p}{\omega r}\left[\dot{\theta}(t) \sin \eta + e^{-p/2t}\dot{\theta}(0) \sin (\omega t - \eta)\right] \qquad (21)$$

where $r = \sqrt{q} = \sqrt{\omega + (p/2)^2}$ and is proportional to $\bar{V}$,

$\eta = \tan^{-1}(-2\omega/p)$ and, since ω and p are both proportional to $\bar{V}$ for a given torpedo with given air appendages, η is a constant.

Equation (10) gives $\tan \theta$ as a function of the time and from it the value of $\dot{\theta}(t)$ and $\dot{\theta}(0)$ can be obtained. Combining the two integrals gives the complete solution for the pitching moment.

$$\alpha(t) = e^{-p/2t}\left\{\frac{1}{\omega}\left[\omega\alpha_0 - \frac{p}{r}\dot{\theta}(0)\sin\eta\right]\cos\omega t + \frac{1}{\omega}\left[\dot{\alpha}_0 + p\frac{\alpha_0}{2} + \frac{p}{r}\dot{\theta}(0)\cos\eta\right]\sin\omega t\right\} + \frac{p}{\omega r}\dot{\theta}(t)\sin\eta\,. \qquad (22)$$

Examination of the pitching motion given by this solution indicates that the motion may be described as damped oscillations about a mean position which is itself decreasing with time. The first term represents damped oscillations, while the second term is not oscillatory but decreases monotonically with time. It is clear that increasing p, which may be achieved by increasing the release velocity $\dot{x}_0$, decreases the magnitude of the pitch angle. This is even more effective than increasing the height of drop y_e since $p \propto \dot{x}_0(y_e)^{1/2}$.

Yaw Oscillations

We may now consider the yawing motion during the air flight. This is described by

$$\ddot{\psi} + p'\dot{\psi} + q'\psi = 0\,. \qquad (23)$$

The solution of this equation yields the yaw angle as a function of time, namely:

$$\psi(t) = e^{-p'/2t}\left(\psi_0 \cos\omega' t + \frac{\dot{\psi}_0 + p'\psi_0/2}{\omega'}\sin\omega' t\right) \qquad (24)$$

where $\omega' = \sqrt{q' - (p'/2)^2}$,

ψ_0 = yaw angle at release,

$\dot{\psi}_0$ = yawing angular velocity at release.

The solution is that of a damped harmonic motion. In this case, if the torpedo were released with zero yaw angle and yawing angular velocity ($\psi_0 = 0$ and $\dot{\psi}_0 = 0$), the yaw angle would always be zero during the drop.

5.1.5 Further Approximations

In this section the equations of motion were simplified and a solution obtained in which the forces acting on the torpedo were its weight and the drag forces. With these forces the trajectory was obtained and is given by equations (13) and (14). This trajectory lies in one plane since the forces perpendicular to the initial plane of motion are negligible. With these forces solutions to the pitching and yawing motion were obtained and are given by equations (22) and (24). The pitching motion may be described as damped oscillations of the axis of the torpedo about a mean position which is not zero but is slightly nose-up and decreases with time, while the yawing motion is that of damped oscillations about a mean position of zero yaw.

These results may be considered a first approximation. For, having obtained the solutions for $\alpha(t)$ and $\psi(t)$, one may apply a method of successive approximations. Thus, substituting the expressions for $\alpha(t)$ and $\psi(t)$ in more complete equations, the equations of motion of the trajectory may be solved again. The primary effect will be that the center of gravity of the torpedo will oscillate with very small amplitude about the trajectory. Then from this solution one may obtain an expression for $\theta(t)$ and $\mu(t)$. Using these expressions, a further approximation may be obtained for $\alpha(t)$ and $\psi(t)$.

These further approximations are not carried out here because the accuracy with which the various quantities are needed does not require them.

5.2 DISCUSSION AND ILLUSTRATION OF THE THEORY

Throughout Section 5.2, where illustrations and magnitudes are given, except when stated otherwise, they will always be given for the Mark 13 torpedo with shroud ring, fitted during the air flight with the Mark 2-1 stabilizer and Mark 1 drag ring (pickle barrel). The constants are given in Section 5.4.

5.2.1 Air Trajectory

Plot of Horizontal Distance as a Function of Time $x(t)$

Figure 1 is a plot of $x(t)$ for the special case of horizontal release, $\theta_0 = 0$, as given by equation (13)

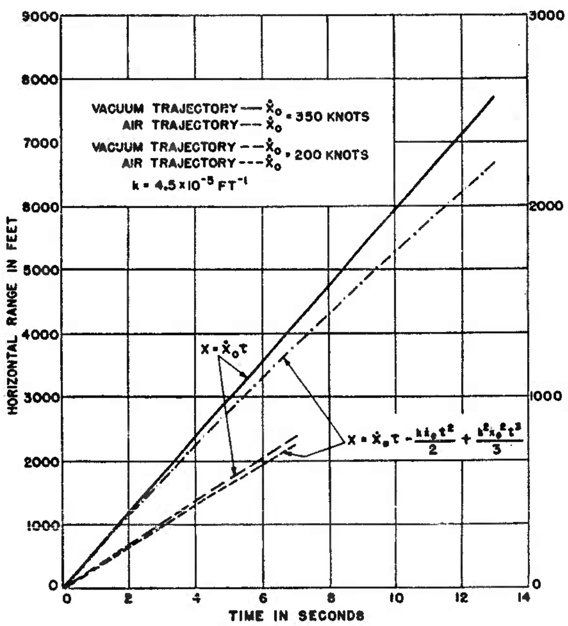

FIGURE 1. Horizontal range versus time from release.

in Section 5.1. From this figure one may readily see the effect of release velocity and drag coefficient (proportional to k) on the horizontal travel of the torpedo. Thus $x(t)$ is plotted for $\dot{x}_0 = 200$ knots and 350 knots, and at each of these release velocities the horizontal travel in a vacuum is plotted ($k = 0$), namely, $x = \dot{x}_0 t$.

From this figure it is readily seen that the horizontal range covered in any time is considerably less than the range covered in the corresponding time along a vacuum trajectory.

Also from this figure it is noticed that increasing the release velocity also increases the amount by which the actual range (with drag) is less than the vacuum range. This is exactly as expected since the drag forces are proportional to V^2.

Vertical Fall as a Function of Time $y(t)$

Figure 2 is a plot of $y(t)$ for the special case of horizontal release, $\theta_0 = 0$, as given by the integral of equation (14). Here again the graphs are drawn for release velocities of 200 knots and 350 knots, and, for comparison, the vacuum vertical falls, given by $y = gt^2/2$, are also drawn.

From this figure it is seen that in a given time the torpedo in a vacuum will fall through a greater vertical distance than a torpedo in air. Or, equivalently,

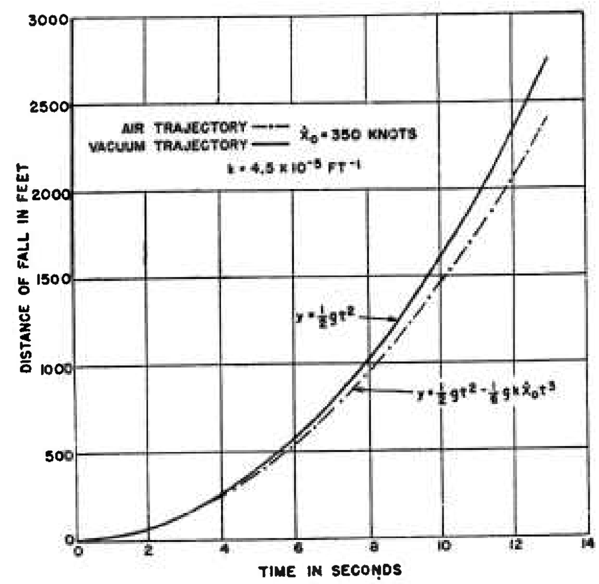

FIGURE 2. Distance of fall versus time from release.

when both torpedoes are launched from the same altitude, the one in air will take a longer time to strike the water than the one in a vacuum.

This effect is also seen to be larger the greater the release velocity. Here again this is true since the coefficient of the t^3 term which represents a retardation of the fall, increases roughly as $\dot{x}_0$.

Trajectory of the Torpedo y versus x

From the preceding graphs one may easily plot y versus x, which is the actual path of the center of gravity of the torpedo during the air flight as shown in Figure 3. This figure shows that, for two torpedoes launched from the same height, the one traveling in a vacuum (without air forces) would travel farther than the one launched in air, and the amount by which it would travel farther increases with the velocity of release because retarding forces increase as the square of the velocity.

HORIZONTAL VELOCITY AS A FUNCTION OF TIME $\dot{x}(t)$

In Figure 4 $\dot{x}(t)$ is plotted for horizontal release at velocities of 200 knots and 350 knots. For comparison, the vacuum horizontal velocity is drawn, this being a horizontal straight line on the graph with magnitude equal to the release velocity $\dot{x}_0$. It is seen that the horizontal velocity decreases with time instead of remaining constant, and the rate at which it decreases is approximately proportional to $\dot{x}_0^2$.

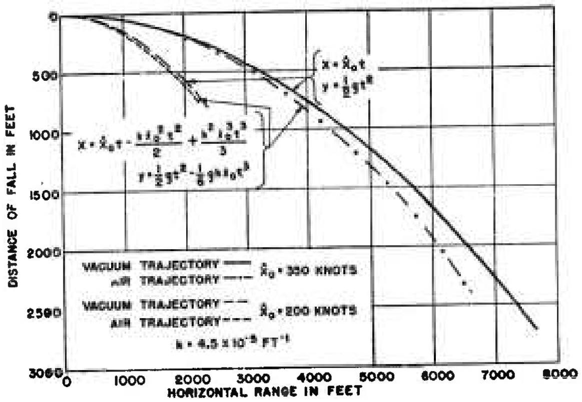

FIGURE 3. Distance of fall versus horizontal range.

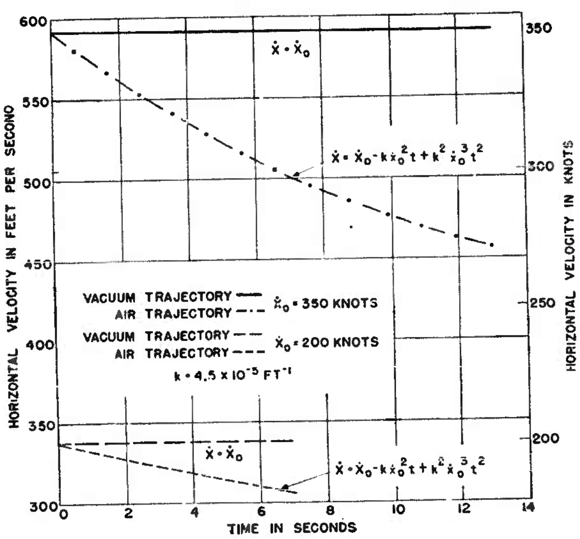

FIGURE 4. Horizontal velocity versus time from release.

VERTICAL VELOCITY VERSUS TIME $\dot{y}(t)$

From Figure 5 it is seen that the vertical velocity with air forces acting on the torpedo is less than the vertical velocity without the air forces. For a vacuum trajectory the graph, $\dot{y}(t)$ is a straight line with a slope equal to g. The drag force serves to decrease the slope with increasing time. Increasing the release velocity causes the vertical velocity to deviate more from the vacuum trajectory value.

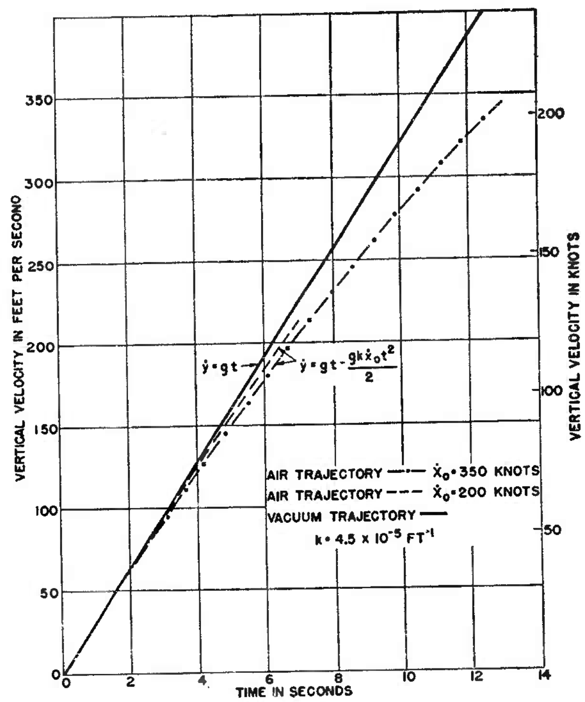

FIGURE 5. Vertical velocity versus time from release.

It is interesting to note the terminal velocity of the Mark 13 torpedo. This velocity is defined as the velocity the torpedo would have if it fell for an infinite time or, alternatively, the velocity the torpedo has when the drag forces are equal and opposite to the weight. This is readily seen to be terminal velocity $= \sqrt{g/k} = 848$ ft per sec, and without the Mark 1 drag ring $= 1{,}325$ ft per sec.

RESULTANT VELOCITY

In Figure 6 the resultant velocity $V = \sqrt{\dot{x}^2 + \dot{y}^2}$ as given by equation (16) is plotted for horizontal release, $\theta_0 = 0$. Curves are shown for a vacuum trajectory and for the trajectory with air forces acting on the torpedo, with release velocities of 200 knots and 350 knots. For horizontal release, one should expect V at first to decrease and be less than $\dot{x}_0$, whereas for larger values of t after the acceleration due to gravity has become important, V should be larger than $\dot{x}_0$. For a vacuum trajectory $V \geqq \dot{x}_0$ during the entire drop.

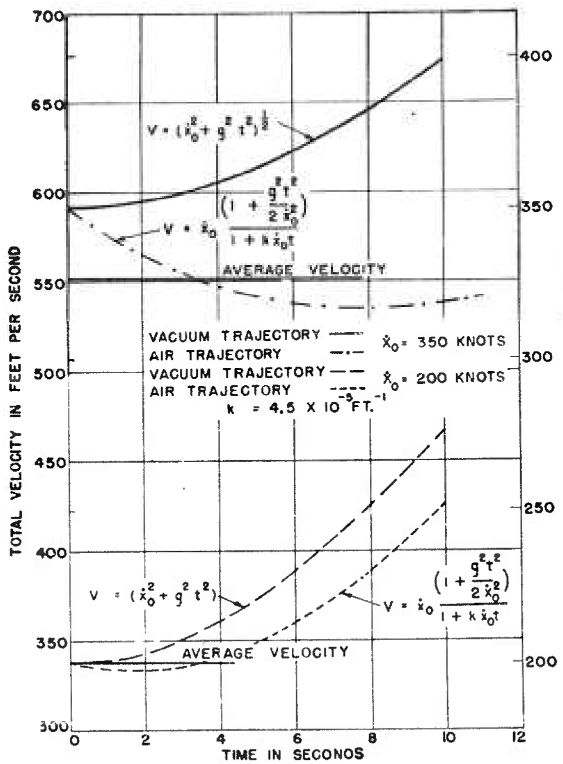

FIGURE 6. Resultant velocity versus time from release. Also average velocity in time corresponding to $\theta_e = 23°$.

From Figure 6 it is seen that the resultant velocity curve is of this form. At the higher release velocity of 350 knots the resultant velocity is less than the release velocity for times of drop of interest in most torpedo launchings. For the lower release velocity the resultant velocity is about equal to or larger than the release elocity for the times of interest. Thus, for example, if the torpedo enters the water with a trajectory angle θ_e of about 21 degrees, with a resultant velocity of about 317 knots, it would correspond to releasing the torpedo with a horizontal velocity of 350 knots from an altitude of about 630 ft. The entry velocity in this case is about 33 knots less than the release velocity, even though the torpedo was released from 630 ft.

In addition, in Figure 6 the value of $\bar{V}$ for $\theta_e = 23$ degrees as obtained from equation (17) is noted. From the form of $V(t)$ it is seen that, for the range of times of interest, one should be able to approximate $V(t)$ by some average value which is constant during the drop. For the two release velocities in question it is seen that $\bar{V}$ in the range of time of interest is always close to $V(t)$.

In Figure 7, for future use, $\bar{V}$ in knots is plotted against $\dot{x}_0$ in knots for horizontal release with $\theta_e = 23$

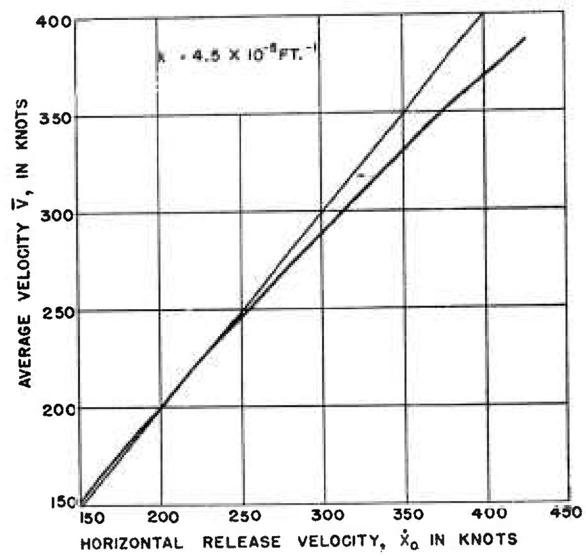

FIGURE 7. Average resultant velocity versus horizontal release velocity for $\theta_e = 23°$.

degrees. It is noticed that for low velocities $\bar{V} > \dot{x}_0$, while for the higher release velocities $\bar{V} < \dot{x}_0$.

TRAJECTORY ANGLE $\theta(t)$

For horizontal release at velocities of 200 knots and 350 knots, $\theta(t)$, as given by equation (11) and for a vacuum trajectory, is plotted in Figure 8. $\theta(t)$ would be the slope of the curves in Figure 3 as a function of time. From this plot it is seen that the trajectory angle with the air forces acting is greater than the vacuum value at any time during the drop. The difference is larger the greater the release velocity and is, in general, not negligible.

By means of graphs of $x(t)$, $\dot{x}(t)$, $y(t)$, $\dot{y}(t)$, $y(x)$, $V(t)$ and $\theta(t)$ for horizontal release, with velocities of 200 knots and 350 knots, with a k value corresponding to the Mark 13 torpedo fitted with the Mark 2-1 stabilizer and Mark 1 drag ring, and the corresponding graph for the vacuum trajectory, the theory de-

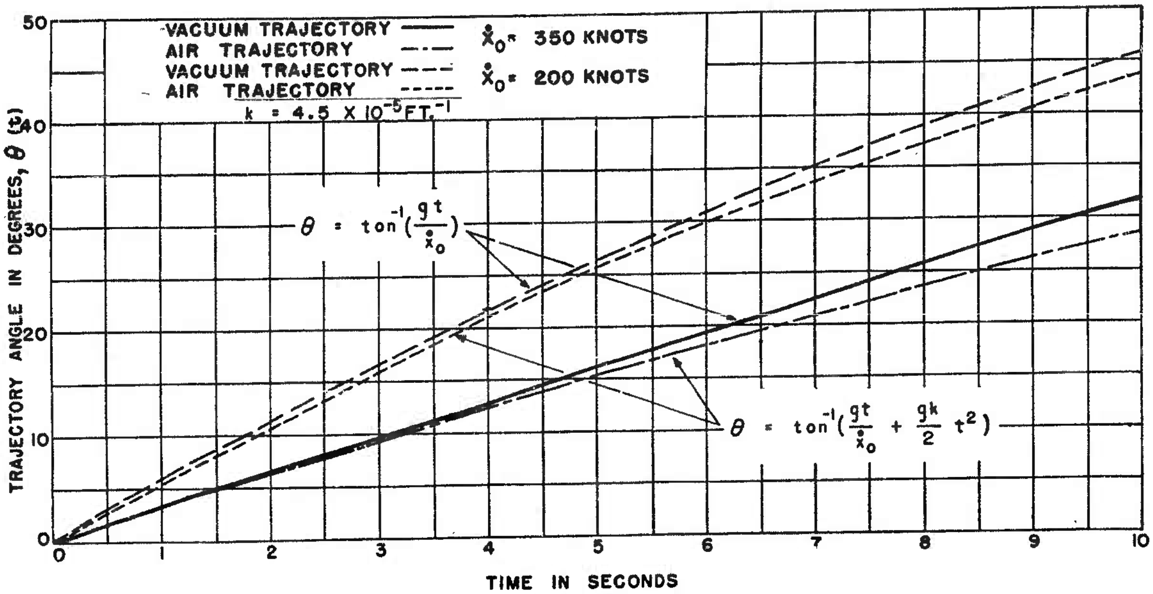

FIGURE 8. Trajectory angle versus time from release.

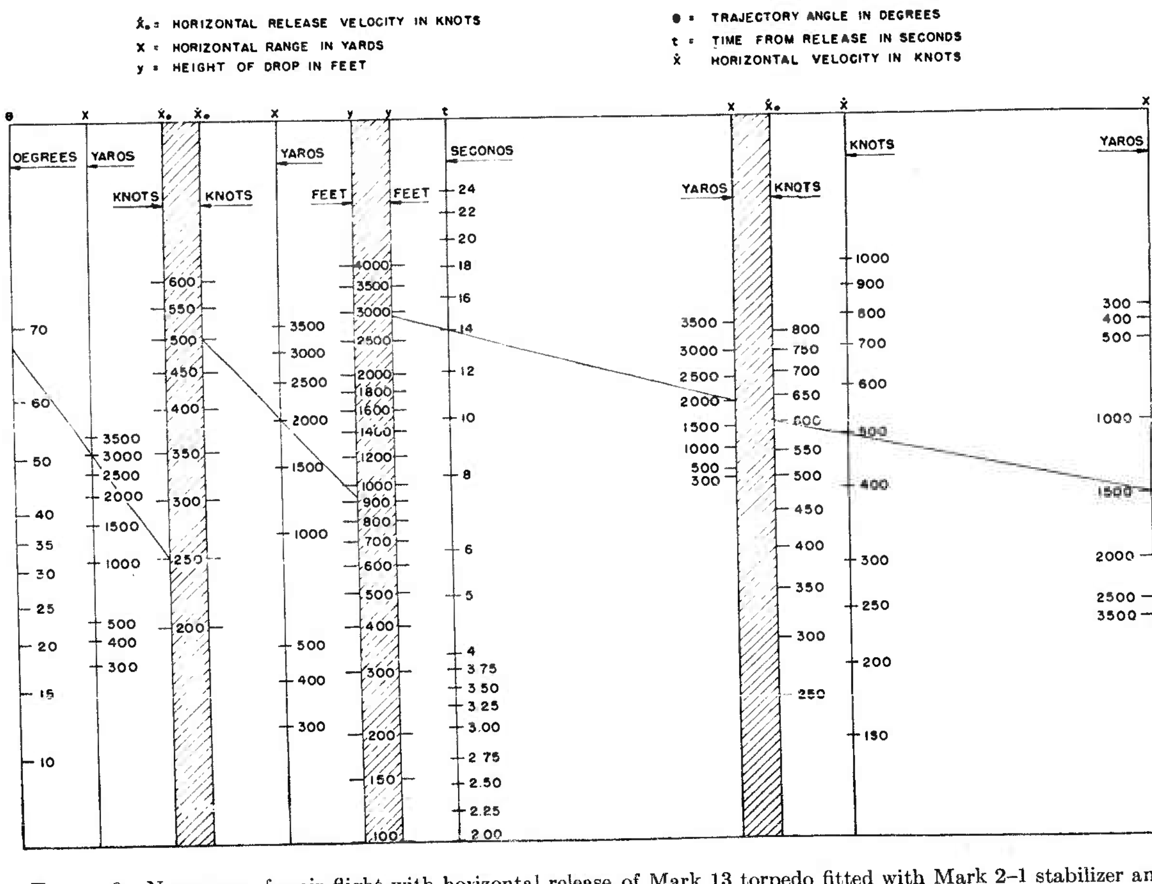

FIGURE 9. Nomogram for air flight with horizontal release of Mark 13 torpedo fitted with Mark 2-1 stabilizer and Mark 1 drag ring (pickle barrel).

veloped in Section 5.1 has been illustrated. In general, the nature of these curves may be explained by the fact that the external forces acting on the torpedo are proportional to V^2 and consequently will vary like $\dot{x}_0^2$, the square of the release velocity. Thus the amount by which the actual trajectory differs from the vacuum trajectory increases roughly as $\dot{x}_0^2$.

In general, the primary effect of the air forces is a deceleration so that from a given altitude it takes longer for a torpedo to reach the water when launched in air than when launched in a vacuum. The vertical velocity and the horizontal velocity and range are less than in a vacuum, and the vertical velocity V is usually less than the release velocity. Also, for the same launching condition, the torpedo will enter the water with a steeper trajectory angle when launched in air than when launched in a vacuum.

The results can also be combined into a nomogram as shown in Figure 9. From release velocity and altitude, the entry angle and horizontal range, for horizontal release, can be determined quickly.

5.2.2 Pitch Oscillations

When the torpedo axis is nose-up relative to the trajectory (flat pitch), α is the pitch angle and is positive. When the torpedo is nose-down (steep pitch) the pitch angle is negative.

Complete Solution of Pitch Oscillations

Figure 10 is a graph of the pitching motion with the initial conditions of $\alpha_0 = -4°$ and $\dot{\alpha}_0 = 15$ degrees per sec, as given by equation (42) for horizontal release with velocities of 200 knots and 350 knots. Using the constants corresponding to the value of $\bar{V}$ associated with this $\dot{x}_0$ we have

1. $\dot{x}_0 = 338$ ft per sec, $\bar{V}$ (knots) $= 200$ knots,
   $\omega = 2.76$, $p = 0.588$,

2. $\dot{x}_0 = 592$ ft per sec, $\bar{V} = 330$ knots,
   $\omega = 4.56$, $p = 0.97$.

From this figure it can be seen that increasing the release velocity increases the frequency of the motion and, for the same initial conditions, decreases the amplitude. ω which is the angular frequency of the motion is proportional to $\bar{V}$ which in turn varies like $\dot{x}_0$, and p which is a measure of the damping is also proportional to $\bar{V}$. Increasing $\bar{V}$ increases the frequency and the damping so that the amplitude of the oscillation is considerably smaller.

Particular Solution

From Figure 10 it can be seen that the oscillations are not symmetrical about zero pitch angle but that there is a bias to a nose-up angle. This bias is represented by the particular solution, $\alpha_2(t)$, of the equation of motion for the pitch oscillations. The particular solution is independent of α_0 and $\dot{\alpha}_0$, but it does depend on the release velocity. In Figure 11 the particular solutions are plotted for the two cases illustrated in Figure 10, $\dot{x}_0 = 200$ knots and 350 knots. It can be seen from this figure that for many applications, the magnitude of the particular solution is not negligible. For small values of time the particular solution is rarely more than 15 per cent of the complete solution, but for large values of time it is usually more than 25 per cent. In general, it may be said

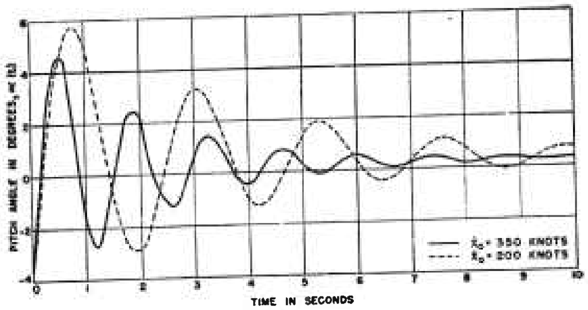

Figure 10. Pitch angle versus time from release $\alpha_0 = -4°$; $\dot{\alpha}_0 = 15$ degrees per sec.

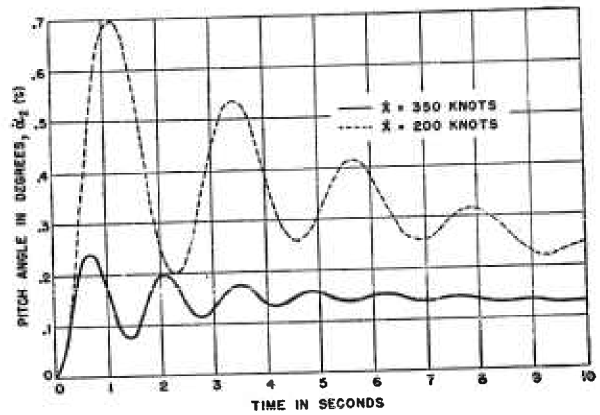

Figure 11. Pitch angle given by particular solution versus time from release $\alpha_0 = 0°$; $\dot{\alpha}_0 = 0$ degree per sec.

that, as release velocity increases, the particular solution becomes more negligible compared to the complete solution.

From Figure 11 it is evident that, as the release velocity increases, the magnitude of the particular solution decreases. The reason for this is that p, ω, and r are all proportional to $\bar{V}$, and $\dot{\theta}$ depends on the factor $C_1 = g/x_0$ so that as a result $\alpha_2(t)$ is roughly proportional to $1/\dot{x}_0^2$.

the expression (25) for $\bar{\alpha}(t)$. As $t \longrightarrow \infty$, $\bar{\alpha}(t) \longrightarrow 0$, or eventually the mean pitch angle approaches zero. This occurs within the limit in which the torpedo is falling straight down.

In Figure 12 $\bar{\alpha}(t)$ as given by (25) is plotted for horizontal release with the same velocities as Figures 10 and 11, 200 knots and 350 knots. To illustrate the behavior of $\bar{\alpha}(t)$, this figure has been plotted for time running up to 30 sec, although up to the present the

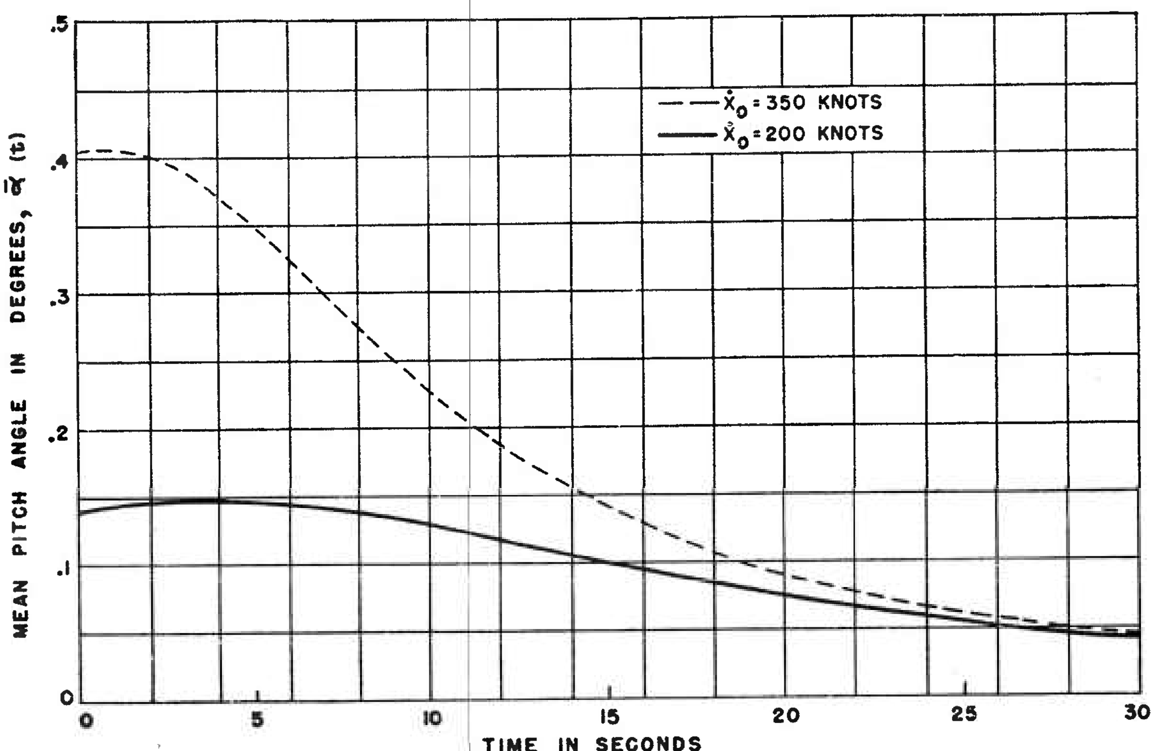

FIGURE 12. Mean pitch angle versus time from release.

Equation (22) represents damped oscillations about a mean pitch angle that is itself decreasing with time. The mean pitch angle is given by

$$\bar{\alpha}(t) = \frac{p}{r^2}\dot{\theta}(t) = \frac{p}{r^2\dot{x}_0}\,\frac{1 + k\dot{x}_0 \sec\theta_0 t}{1 + (c_0 + c_1 t + c_2 t^2)^2}. \quad (25)$$

This, of course, is also independent of α_0 and $\dot{\alpha}_0$. This mean pitch decreases relatively slowly with time because of the factor $1 + k\dot{x}_0 \sec\theta_0 t/[1 + (c_0 + c_1 t + c_2 t^2)^2]$, while the other factors in equation (22) decrease rapidly with time since they are multiplied by the exponential $e^{-(p/2)t}$. As t increases, the oscillations about this mean pitch angle damp out, and the pitch angle approaches the mean position given by

region of interest in torpedo launchings is up to about 10 sec for 350 knots and about 6 sec for the 200-knot release velocity. For small times the amplitude decreases with velocity; in fact, as has been shown, it decreases approximately like $\dot{x}_0^{-2}$. However, for large values of t this is no longer true since the terms involving t become much more important.

It is important in connection with the behavior at water entry to note that the mean pitch angle of the torpedo is slightly nose-up. This may be explained physically by the fact that the center of gravity of the torpedo is traveling along a curved path and consequently possesses an angular velocity and in addition an angular acceleration. The axis of the torpedo cannot "keep up" with the trajectory and so remains somewhat nose-up relative to it. As the time increases, the angular velocity of the trajectory decreases so that the torpedo axis gets closer to it. There is also a damping moment acting on the axis of the torpedo of amount $pI\dot{\theta}$. This moment is always acting in the same direction since $\dot{\theta}$ is always in the same direction, and it tends to keep the torpedo nose-up relative to the trajectory. Since the trajectory is curved, $\dot{\theta}$ is not zero. If we were dealing with a straight line trajectory, $\dot{\theta}$ would be zero, and the torpedo would damp out to zero pitch.

5.2.3 Release Conditions for Pitching Motions

The pitch angle at release, α_0, will vary from one airplane to another, and for a particular plane will depend on speed and also on the angle at which the torpedo is suspended in the plane. It probably will also depend on whether or not the airplane is moving horizontally at release and whether the airplane is accelerating, decelerating, or moving at constant speed. However, for roughly horizontal release and roughly constant speed we may say

$$\text{Weight of airplane} = \text{Lift force on plane} = K\dot{x}_0^2\alpha_{\text{plane}},$$

where K is a constant characteristic of the airplane.

The attitude of the thrust line of the airplane is inversely proportional to the square of the release velocity. For a particular airplane α_0 varies with $\dot{x}_0^2$ and with the loading.

Figure 13, showing a few standard airplanes, is a graph of the angle a reference line in an airplane makes with the horizontal and also the angle the torpedo axis makes with this line when suspended in the plane. These curves have been obtained experimentally, but the variation of α is as expected. Consequently, for each airplane, for roughly horizontal release and constant speed, the value of α_0 is known.

The situation with regard to $\dot{\alpha}_0$ is much more complicated. The pitching angular velocity at release will depend on the angular velocity of the axis of the torpedo and on the angular velocity of the trajectory $\dot{\theta}_0 = g\cos^2\theta_0/\dot{x}_0$. However, after being released, the torpedo falls through a region of disturbed air which imparts to it an additional angular velocity.

At the instant of release the angular velocity of the torpedo axis depends on many factors, such as the angular velocity of the airplane at release, the trajectory angle, the acceleration or deceleration, the pitch angle at release, and also probably on the release velocity and the weight of the airplane. The dependence on these factors is not known experimentally and can only be estimated theoretically. However, assuming the effect of most of these factors is known so that the pitching angular velocity at the instant of release is known, since the condition of the air beneath the plane is quite variable, the angular velocity of the torpedo when emerging from the small region of disturbed air is highly uncertain. From studying a number of photographs taken at the Newport Torpedo Station, showing launchings with various release velocities, the pitching angular velocity at release for a few standard airplanes was estimated. The average values of $\dot{\alpha}_0$ are listed in the table below.

	Number of drops	$\dot{\alpha}_0$ (Average pitching angular velocity at release)
TBM, TBF	6	+17 degrees per sec
PV1	6	−15 degrees per sec and +4 degrees per sec
F7F	7	−12 degrees per sec
SB2C	6	+10 degrees per sec and −7 degrees per sec
A-20	6	+10 degrees per sec and −8 degrees per sec
A-26	3	+ 2 degrees per sec
B-25	4	+ 8 degrees per sec and +14 degrees per sec
B-26	4	+ 3 degrees per sec

It should be remembered that there is a dispersion around the values listed in the table. Where two numbers appear for $\dot{\alpha}_0$ it means that a few of the observed launchings were found with each of the values for $\dot{\alpha}_0$.

Thus we may say that, while α_0 is known for the airplanes now in use and may be determined experimentally for future airplanes, $\dot{\alpha}_0$ is uncertain.

From water-entry considerations it is desirable to have the pitch angle at entry as small as possible. This requires keeping α_0 and $\dot{\alpha}_0$ small. Most airplanes are designed so that $\alpha_0 = 0$ near the middle of their velocity range. However, since from tactical and other considerations it is much better to release at as high a velocity as possible, it seems wise, if possible, to have $\alpha_0 = 0$ near the upper end of the velocity range for a given airplane.

5.2.4 Release at an Angle

In order to complete the illustration and discussion of theoretically predicted air trajectories, some examples of release at angles different from zero will be considered. We shall consider two cases in which the

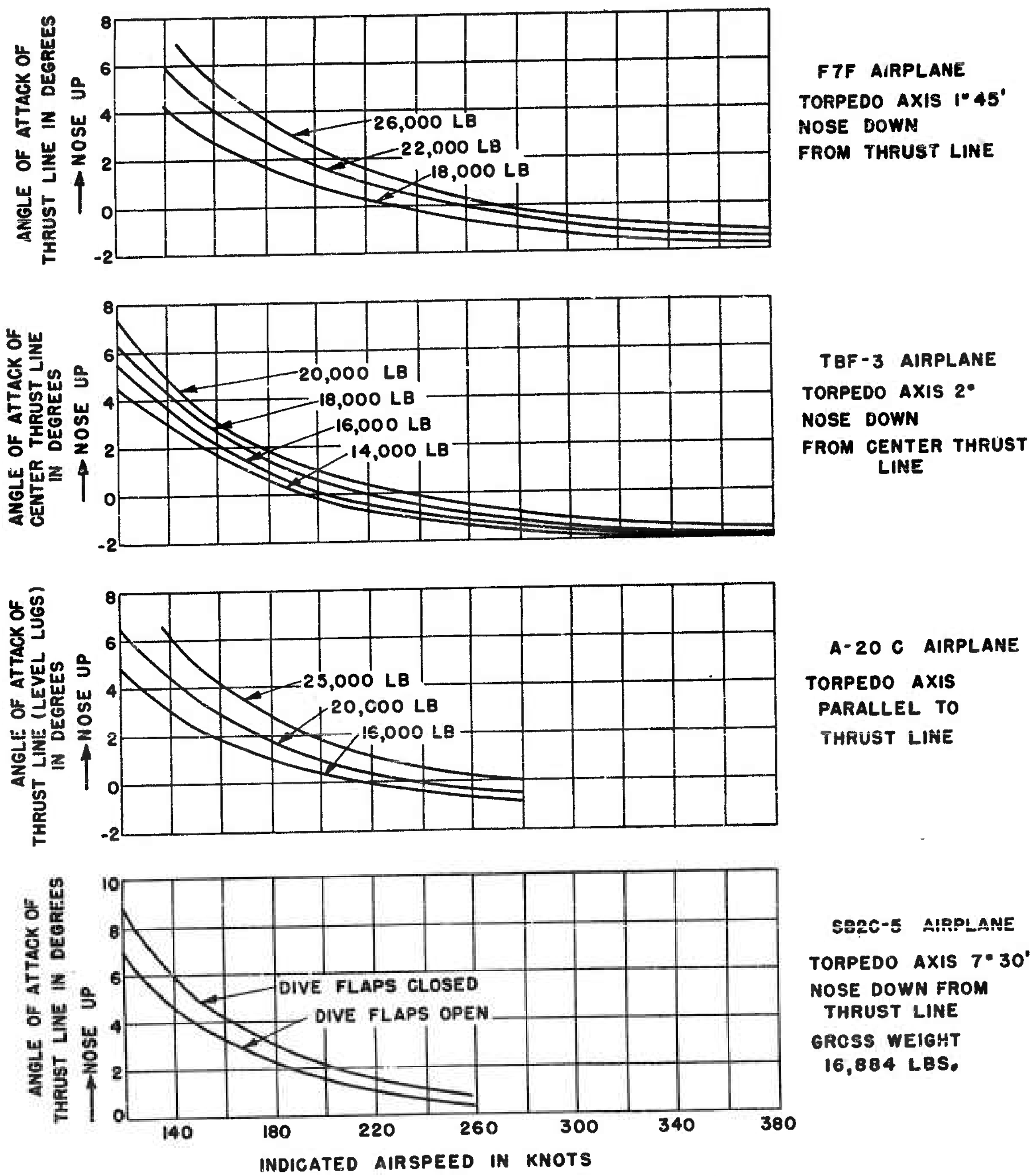

FIGURE 13. Airplane attack angle in level flight versus indicated speed.

torpedo is released with a velocity of 425 knots. It is to be remembered that, for release, while the airplane has an upward component of velocity, the trajectory angle at release is negative, $\theta_0 < 0$. In this case the torpedo is being "tossed," and this method of release is described as toss bombing. When the airplane is heading downward at release, θ_0 is positive, and the method of release is described as glide bombing. The release conditions for the two cases considered are:

Toss bombing:

1. $V_0 = 425$ knots, $\theta_0 = -10°$, height of release $= 800$ ft, $\alpha_0 = 5°$, $\dot{\alpha}_0 = 15$ degrees per sec.

Glide bombing:

2. $V_0 = 425$ knots, $\theta_0 = 10°$, height of release $= 800$ ft, $\alpha_0 = 5°$, $\dot{\alpha}_0 = 15$ degrees per sec.

The altitudes at release were chosen to conform to what is thought to be the minimum height at which the airplane can release the torpedo for the value of θ_0 chosen.

for a longer time than a torpedo having the same entry conditions but released horizontally.

Thus the range is less than that of the vacuum trajectory. In addition, due to the long time of flight, the pitching oscillations have markedly damped out so that the pitch angle at entry relative to air is very small.

From Figure 15 it is also seen that the range is less with the drag forces acting than with a vacuum trajectory. For this trajectory, even though the time of flight is small, the pitch oscillations have had time to damp out almost completely at entry. Due to the high release velocity the damping of the pitch oscillations is large in both trajectories and at entry there appears the small nose-up pitch.

A comparison of the two trajectories and the vacuum trajectories may be made from the table of release conditions, entry conditions, height at release, and time of flight. Also in the table are the conditions for a horizontal release which would have the same θ_e and V_e with the range and time of drop for such an "equivalent horizontal release."

From this table the advantages of a toss bombing

For all cases V_0 (release velocity) = 425 knots (= 708 ft per sec), $\alpha_0 = -5°$, $\dot{\alpha}_0 = 15$ degrees per sec.

Type of trajectory	θ_0	y_0 ft	t sec	θ_e	V_e ft per sec	R yds	V'_0	y'_0	t'	R'
Air	$-10°$	800	12.36	26.4	486	2,488	633	1,026	8.70	1,671
Vacuum	$-10°$	800	11.93	20.1	754	2,812	707	1,042	8.05	1,898
Air	$10°$	800	4.36	21.2	620	983	816	998	8.53	1,034
Vacuum	$10°$	800	4.17	20.1	754	1,025	707	1,026	8.05	1,939

θ_0 = trajectory angle at release.
y_0 = height at release.
t = time of drop.
θ_e = trajectory angle at entry.
V_e = entry velocity.
R = horizontal range in yards.

V'_0 = velocity when trajectory is horizontal (release velocity for equivalent horizontal release).
y'_0 = height when trajectory is horizontal (height for equivalent horizontal release).
t' = time of drop for equivalent horizontal release.
R' = horizontal range for equivalent horizontal release.

If the airplane is traveling in an upward circle at release, the pitch angle will be more nose-up than for horizontal release, and vice versa for a circle concave-downward.

In Figure 14 the trajectory for case 1, the vacuum trajectory for case 1, and the pitching oscillations are shown. (The trajectory without the Mark 1 drag ring would be intermediate between the vacuum trajectory and the trajectory with the drag ring.)

From Figure 14 it is readily seen that the effect of the drag forces is similar to horizontal release and is even more marked because essentially they are acting

method of release is clear. Thus with the Mark 13 torpedo the enormous range in air of 2,488 yd can be achieved with an entry angle of only 26.4°. The time of flight is not prohibitively large and the pitch angle at entry relative to air is very small. This is important from the point of view of water entry. It is clear that the vacuum trajectory will have a greater range (yards), a shorter time of flight, and a smaller entrance angle. The Mark 13 without a drag ring will have intermediate values. The very large range obtained by a toss bombing method of release (with very similar entry conditions to those for horizontal release) is of significance in tactical considerations.

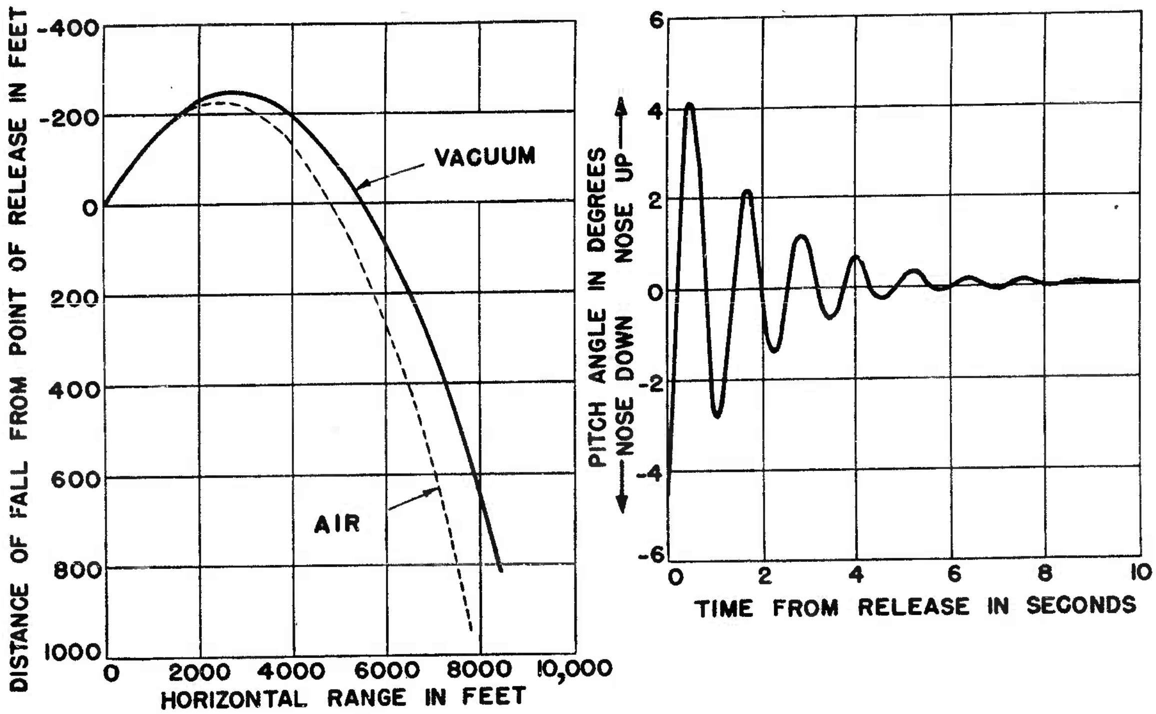

FIGURE 14. Trajectories and pitch oscillations for toss bombing release, torpedo tossed at $\theta_0 = -10°$, $V_0 = 425$ knots, released with $\alpha_0 = -4°$, $\dot{\alpha}_0 = 15$ degrees per sec.

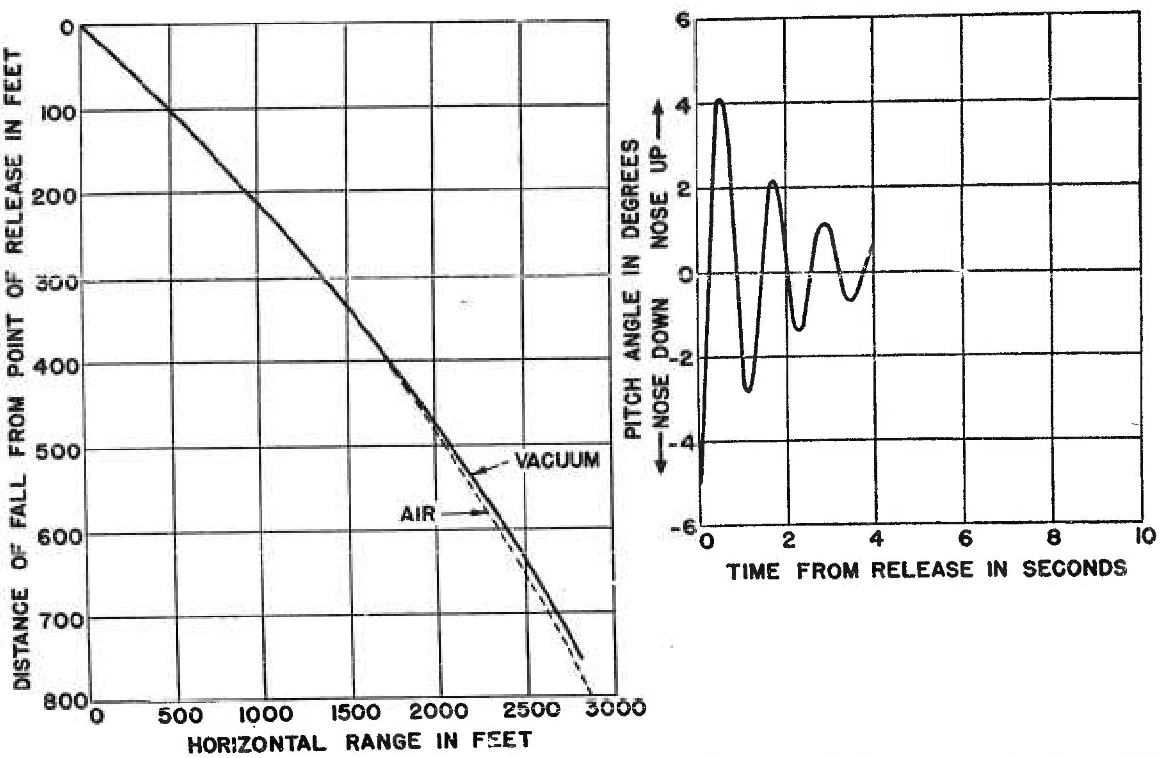

FIGURE 15. Trajectories and pitch oscillations for glide bombing release, torpedo gliding initially at $\theta_0 = -10°$, $V_0 = 425$ knots, released with $\alpha_0 = -4°$, $\dot{\alpha}_0 = 15$ degrees per sec.

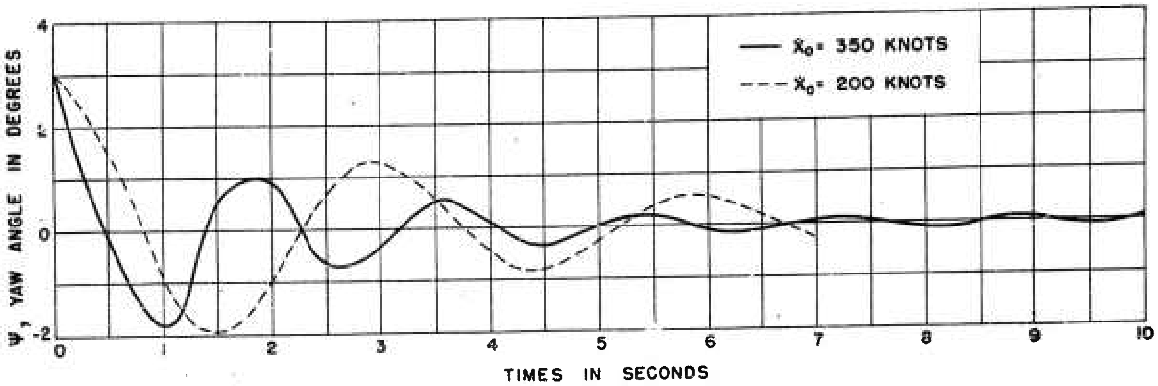

FIGURE 16. Yaw angle versus time from release $\psi_0 = 3°$, $\dot{\psi}_0 = 0$ degrees per sec.

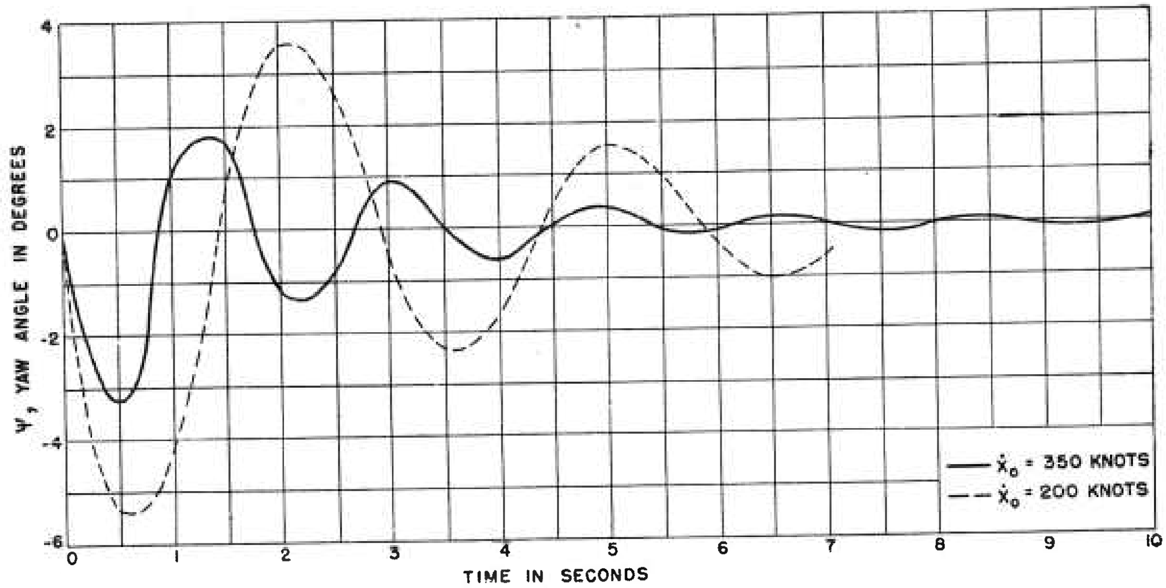

FIGURE 17. Yaw angle versus time from release $\psi_0 = 0°$, $\dot{\psi}_0 = 15$ degrees per sec.

For the glide bombing method of release, the horizontal range is comparatively small and pitch angle at entry may still be compara vely large. Obviously the only possible advantage for this method of release is the tactical one of a short time of flight.

5.2.5 Yawing Motion

In order to discuss the yaw oscillations, Figures 16 and 17 have been plotted. In Figure 16, using the constants for the Mark 13 torpedo, Mark 2-1 stabilizer and Mark 1 drag ring, two curves of the yawing motions are drawn. In Figure 16, $\psi_0 = 3°$ and $\dot{\psi}_0 = 0$ with one curve drawn for $\dot{x}_0 = 200$ knots and one for $\dot{x}_0 = 350$ knots, while in Figure 17 corresponding to these two release velocities curves are plotted for the release conditions $\psi_0 = 0$ and $\dot{\psi}_0 = 15$ degrees per sec.

These curves are seen to be ordinary damped harmonic oscillations about a mean yaw angle of zero degrees. From these curves we notice, as in the pitch oscillations, the amplitude of the yawing motion is more rapidly damped out as the release velocity is increased. Furthermore, it should be noted that the yawing motion is independent of the release angle θ_0, except insofar as θ_0 changes the time of drop.

From these curves the effect of an initial yaw angle and yawing angular velocity also can be seen. For present torpedo launchings the pilot must head the airplane in the direction he wants the torpedo to run and attempt to release the torpedo so that $\psi_0 = 0$ and $\dot{\psi}_0 = 0$. These conditions must be observed because the gyro is unlocked approximately 0.5 second after the torpedo is released. From Figure 16 it is seen that, if the plane is not heading in the right direction but is at yaw angle $\psi_0 = 3$ degrees, then the gyro can be off by 1.4 degrees when it is unlocked, while, if the airplane is spinning around to a lead angle and releases when $\dot{\psi}_0 = 15$ degrees per second, it is seen from Figure 17 that the gyro can be off by 5.3 degrees. Thus it is clear why the pilot must attempt to maintain $\psi_0 = \dot{\psi}_0 = 0$. Furthermore, it is clear that there would be advantages derived from releasing the gyro just before the torpedo is released.

5.2.6 The Effect of Roll

We have made no mention thus far of the rolling angular velocity of the torpedo during the air flight. The roll angle is the angle through which the torpedo rotates about its longitudinal axis. This angle is indicated by ϕ and the rolling angular velocity by $\dot{\phi}$. A torpedo may have a rolling velocity in air due to the release conditions. Thus the surface of the slings which release the torpedo is not smooth and, since the slings are released on one side first, due to friction the torpedo rolls off. Also, the slipstream beneath the airplane which acts on the stabilizer might induce a roll velocity. The effect of the slings may be minimized by greasing them or by the use of a single suspension bar. At the Newport Torpedo Station it has been observed that this bar releases the torpedo with very little roll velocity.

During the drop the roll angular velocity of the torpedo is practically constant since there is almost no damping of the motion. Due to the moments acting on the torpedo and the pitching and yawing motions, if the torpedo has a roll velocity, it must exhibit a gyroscopic effect. The magnitude of this effect has been calculated. The gyroscopic effect on roll or yaw should rarely be more than 0.17 degree at any time during the drop and for most launchings should not be more than one-quarter of this value.

The primary effect of the roll in air is due to the asymmetry of the stabilizer. Thus ω is different from ω' and the resulting motion is altered due to the change in the constants in any particular plane. This will be discussed further in a later section.

5.2.7 Roll Stabilization

Some torpedo air stabilizers, notably some employed by the British, Germans, Italians, and Japanese, possess gyro-controlled ailerons which serve to prevent large roll in air. It is necessary to prevent roll in air by such a device if it is desired to gain some particular advantage of an asymmetrical torpedo head at entry or if it is desired to have a torpedo enter the water with some mean pitch angle other than zero. For example, if the air stabilizer is preset so that the mean pitch angle is some amount nose-up, the torpedo must be prevented from rolling over in air since the nose-up pitch angle will become a yaw angle when rolled 90 degrees and will become a nose-down pitch angle if the torpedo rolls 180 degrees.

The gyro-controlled ailerons produce a torque about the longitudinal axis of the torpedo which is proportional to the square of the velocity (V^2) and for moderately small roll angles to the roll angle itself ϕ; thus the torque is $q_0\phi$, where q_0 is proportional to V^2. In addition, there is a damping moment which is probably small and is proportional to the velocity and to the rolling angular velocity $\dot{\phi}$; the damping moment is then $p_0\dot{\phi}$, where p_0 is proportional to V.

Thus the equation of motion is

$$C\ddot{\phi} + p_0\dot{\phi} + q_0\phi = 0\,, \tag{26}$$

where C is the moment of inertia of the torpedo about a longitudinal axis through the center of gravity. For the Mark 13 torpedo, $C = 30.4$ slug ft^2.

The roll angle as a function of time is then simply

$$\phi(t) = e^{-p/2t}\left(\phi_0 \cos \omega t + \frac{\dot{\phi}_0 + p\phi_0/2}{\omega} \sin \omega t\right) \tag{27}$$

where

$$p = \frac{p_0}{C}\,, \qquad \omega = \sqrt{\frac{q}{C} - \frac{p^2}{4C^2}}\,.$$

Generally, for most torpedo releases, $\phi_0 = 0$, and $\dot{\phi}_0 \neq 0$. The values of q_0/V^2 and p_0/V depend both on the size and position of the ailerons as well as the torpedo. p_0/V is probably small.

This motion is seen to be that of ordinary damped oscillations. If $\phi_0 = 0$, as appears to be the usual condition, the roll angle is always less than $\dot{\phi}_0/\omega$.

5.2.8 Other Approximations

For all the illustrations the complete expressions were used. For many applications, however, this is not necessary.

For quantities associated with the trajectory, the series expressions are usually sufficiently accurate and may be easier to use. For many purposes the t^3 term may be neglected. The succeeding terms become less significant the smaller the value of $k\dot{x}_0 t$. For all practical applications the expressions derived are sufficiently exact. The number of terms of the expressions to be retained in any problem depends on the particular application.

The complete expression (22) has been used for the illustrations of the pitching motion. However, for many applications the particular solution may be neglected,[b] and the solution of the homogeneous equation given in equation (20) should prove sufficiently accurate. From the illustrations given it appears that the particular solution is rarely more than 0.8 degree nose-up, the mean value rarely more than 0.4 degree nose-up, and they both decrease with time and also decrease rapidly with increasing release velocity. Consequently, using only the solution of the homogeneous equation is more accurate the greater the release velocity. However, again, the accuracy required of the solution depends on the particular application.

5.3 DISCUSSION OF EXPERIMENTAL RESULTS AND COMPARISON WITH THEORY

5.3.1 Comparison of Pitch Oscillation Theory and Experiment

Experimental curves of pitch angle against altitude or time can be obtained from the photographs of torpedo launchings at the Newport Torpedo Station. Some of these experimental curves have been matched by inserting appropriate values of p and ω into a slightly modified form of equation (22). From the experimental curves, α_0 and $\dot{\alpha}_0$ were obtained at a particular time, and, since p and ω were unknown, different values were tried until a good matching of the experimental curve by theory was obtained. Figures 18, 19, 20, and 21 are graphs of experimental curves obtained at the Newport Torpedo Station and of the curves fitted to them on the basis of the theory given in Section 5.1.

The experimental curves are based on photographs of airplane launchings. Since in most airplanes, especially those which have an internal installation of the torpedo, it is not possible to see the torpedo clearly until it has fallen for 0.5 sec (about 4 ft), the points on the experimental curves of pitch angle are really not known until about 0.5 second after release. Consequently, in equation (22) the initial conditions of the motion, which are specified by α_0 and $\dot{\alpha}_0$, were taken about 0.5 sec after release. Since the trajectory angle at release is zero and $t = 0$ was assumed to be about 0.5 sec after release, θ_0, the trajectory angle at the assumed $t = 0$ is given by

$$\theta_0 = \tan\theta_0 = 0.5C_1 = \frac{0.5g}{\dot{x}_0}.$$

For such a short time the single term gives sufficient accuracy.

In the graphs there is a close agreement between theory and experiment. There seems to be an indication of the fact that the torpedo tends to damp out to a slightly nose-up pitch angle for all usual times of drop. It is unfortunate that, due to the nature of the camera used, photographs of launchings from altitudes greater than about 450 ft could not be made.

To indicate why it was necessary to use a slightly modified form of equation (22), as well as to explain the lack of complete experimental verification of the theory of the air trajectory of the torpedo, the errors in the experimental data must be considered.

1. From an examination of a number of cases, it is estimated that there is a probable error of about 0.03 sec in the time of drop.
2. The probable error in determining the height of drop, which is determined from the time of drop, is about 4 ft.
3. The errors in determining the horizontal and vertical velocities relative to air during the drop are a result of the error in determining these velocities relative to ground (as obtained by the camera, in analyzing the photographs) together with the error in the wind velocity value which is used to convert the velocities relative to ground to those relative to air.
   a. There is a probable error of about 3 knots in determining the horizontal and vertical velocities relative to ground at any time during the drop. This error is due primarily to the

[b] This has been done in the approximate treatments given in reports issued by the U. S. Navy Torpedo Station at Newport and the British.[1]

probable error of about 2 per cent in determining the scale factor of the photographs. This estimate of the error was obtained by measurements of the small image of the torpedo.

b. The wind velocity for each launching at the Newport Torpedo Station is obtained by an anemometer on Gould Island at an altitude of 140 ft. A study of the distribution of wind

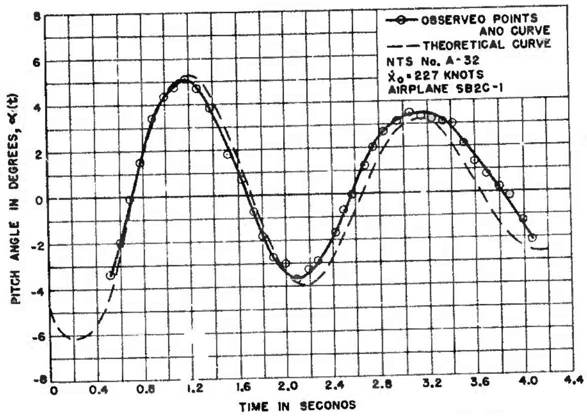

FIGURE 18. Theoretical and observed graph of pitch angle versus time.

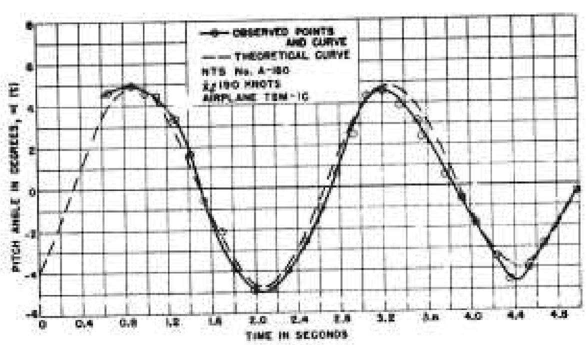

FIGURE 19. Theoretical and observed graph of pitch angle versus time.

velocity with height at Quonset Naval Air Station, which is five miles from Gould Island, during the months from September 1943 to September 1944, showed that the wind magnitude increases rapidly with altitude in the first 700 ft above the ground and that it veers in a clockwise direction. The effect is especially marked in the early morning hours, 0700, and diminishes towards noon as the wind stratification is destroyed by convective mixing.

It should be noted that the balloon data give the average wind through the first 700 ft above ground and that, therefore, the maximum wind in each layer may be considerably in excess of the average value.

Due to this variation in the speed and direction of the wind with altitude, the error in horizontal velocity due to the error in the wind data may be about 3 knots.

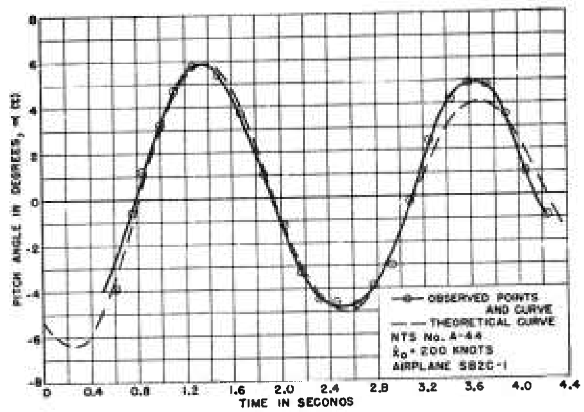

FIGURE 20. Theoretical and observed graph of pitch angle versus time.

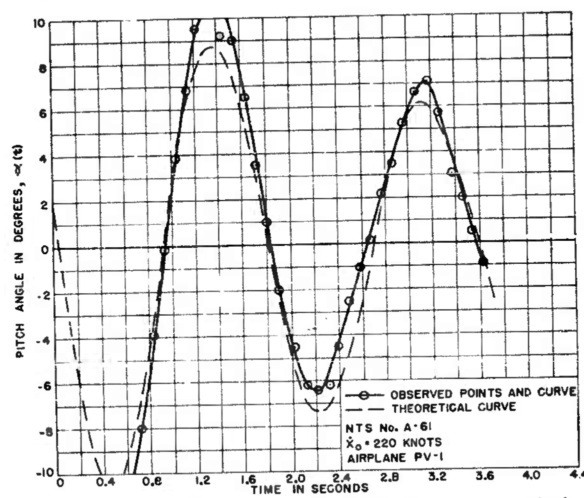

FIGURE 21. Theoretical and observed graph of pitch angle versus time.

4. The probable error in determining the trajectory angle θ, at any time during the drop, appears to be about 0.6 degree. This error is due to the error in the vertical and horizontal velocities relative to air.

5. The errors in obtaining the pitch angle relative to air at any time during the drop lie in the determination of the trajectory angle θ, and the measurement of the angle of inclination of the axis of the torpedo at that time.

Since the probable error in θ was found to be about 0.6 degree and the error in the measurement of the angle of the axis of the torpedo was found to be about 0.3 degree, the probable error in the pitch angle relative to air at any time during the drop is approximately 0.7 degree.

While the probable error in the pitch angle relative to air at any time during the drop is about 0.7 degree, the error in the smooth curve (in the statistical sense) through the points is probably very much less. Nevertheless, although the probable error in the pitch angle may be less than 0.7 degree, the actual error may be very much larger.

5.3.2 Discussion of Experimental Verification of Theory of Pitching Motion

In the analysis of the photographs a mean horizontal deceleration and vertical acceleration are obtained. From Section 5.1 it is seen that the trajectory cannot be described exactly by this method. Since constant accelerations are used, the values of $\tan \theta$ obtained do not correspond exactly to the expressions given in Section 5.1. In matching the experimental curves, the expressions for θ obtained from analysis of the photographs were used in each case. In this sense a slightly modified form of the theory was used. In general, there appears to be a good verification of the theory of the pitch oscillations given in Section 5.1.

However, examining many of the experimental curves of pitch oscillations reveals that some of them do not have the form predicted by the theory. Thus, if there were an error in the horizontal velocity, the trajectory angle θ would always be in error during the drop, and the calculated line of zero pitch on the curves would really not be zero pitch as assumed in the plotting. For example, if there were an error in the wind measurement and the actual tail wind were 10 knots greater than what was recorded, the pitch oscillation curve when plotted by the method outlined would appear asymmetrical. The torpedo would appear to favor a nose-down pitch since the amplitude of the oscillation in the nose-down direction would be larger in magnitude than the preceding amplitude in the nose-up direction, which is impossible according to the theory given in Section 5.1. There are quite a few experimental curves which appear to exhibit this type of error. It should be remembered that this is an error in the experimental pitch angle curves and the torpedo does not oscillate with respect to the air in the manner indicated by the curves. Since these curves do not represent the actual oscillations of the torpedo, they cannot be matched by theory.

Similarly, an error may often arise (which has somewhat the same appearance) due to the fact that the Mark 2-1 stabilizer or one flap of the stabilizer may have rocked during the air flight. This type of motion will represent the actual oscillations of the torpedo since the stabilizer behaves like one which is preset. By fixing the stabilizers this motion has been produced at the Newport Torpedo Station. These curves can be matched by the theory in Section 5.1 simply by adding to the equation (22) a constant mean pitch angle, which must be known, however.

Some irregularities in the curve may be due to the effect of the variation of the wind magnitude on ω and p. Thus, if the wind changes a certain amount, ω and p, which are proportional to the velocity, will vary accordingly, and the actual oscillations will not be periodic or described exactly by a theory which assumes a constant ω and p. However, the magnitude of this error is generally very small.

Again, as has been noted in Section 5.4.2, the ω in the pitching motion is affected by roll. This will alter the experimental curves. The quantitative effects will be discussed further in Section 5.4.

5.3.3 Discussion of Experimental Verification of the Theory of the Trajectory

As has been mentioned, the method used in the analysis leads to a mean horizontal deceleration and vertical acceleration. These cannot be the actual deceleration and acceleration. Nevertheless, for the short times of drop that are involved in the photographed launchings and for the relatively low release velocities, the terms involving higher powers of t than t^3 are negligible. The average time of drop was only some 4.6 seconds and the average speed some 175 knots. Neglecting the t^4 terms, the horizontal acceleration is $-k\dot{x}_0^2 + 2k^2\dot{x}_0^3 t$, and the vertical acceleration is $(g - k_1\bar{V}\bar{\alpha}\dot{x}_0) - gk\dot{x}_0 t$. In a time T, the average values of these would be $-k\dot{x}_0^2 + k^2\dot{x}_0^3 T$ and $(g - k_1\bar{V}\bar{\alpha}\dot{x}_0) - (gk\dot{x}_0/2)T$. The maximum errors in the accelerations produced by using these mean expressions are, at time T, $k^2\dot{x}_0^3 T$ and $-(gk\dot{x}_0/2)T$.

For the photographed drops the average value of $T = 4.5$ sec and $\dot{x}_0 = 296$ ft per sec. Consequently, the order of magnitude of the maximum error in the horizontal deceleration of 0.23 ft per sec per sec or about 5 per cent of the horizontal deceleration obtained by using only the t^2 term, and in the vertical acceleration the maximum error is 0.95 ft per sec per sec or about 3 per cent of the acceleration given by the t^2 term. These are small errors because the times of drop and release velocities are relatively low. However, for greater speeds and altitudes of release the error involved in using the average acceleration is not negligible.

In view of the previous discussion, since t and $\dot{x}_0$ are both relatively small for photographed launchings, the higher powers of t than t^2 in the expressions using for k the slope of the straight line in Figure 22 plus 5 per cent of the slope.

Again, in the y or vertically downward direction, because of the relatively small times of drop and release velocities, the effect of t^3 terms cannot be noticed. From the analysis of the photographs the mean vertical acceleration is obtained. We expect the slope of the graph of $y(t)$ obtained from the photograph to decrease somewhat with time, but, since t and $\dot{x}_0$ are small, the effect is only a change in slope of about 1.90 ft per sec per sec or about 6 per cent change in slope, which is hardly observable.

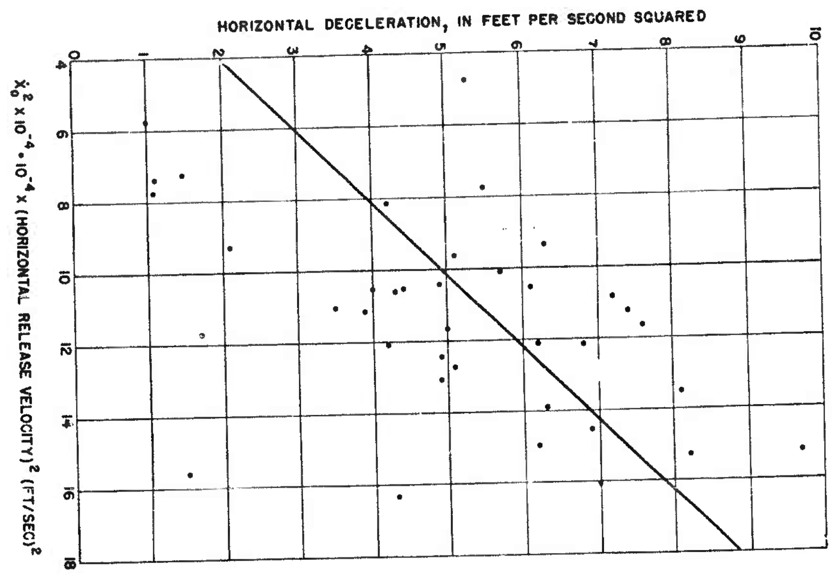

FIGURE 22. Horizontal deceleration versus (horizontal release velocity)^2 for the Mark 13-2 torpedo fitted with Mark 2-1 stabilizer and Mark 1 drag ring. Correlation coefficient = 0.94.

for the trajectory in Section 5.1 are small and consequently difficult to observe. Also they are usually masked by the experimental errors involved in analyzing the photographs. Consequently, it is extremely difficult to attempt to verify the higher power terms than t^2 in the expressions for the air trajectory. In spite of this, the method used to obtain k serves as some source of experimental verification. In order to determine k, a graph was plotted of the mean horizontal deceleration against $\dot{x}_0^2$. Since the effect of the t^3 term is small for this application, we should expect a good correlation between the deceleration and $\dot{x}_0^2$ from the plot, and the slope of this graph should give the value of k. Figure 22 shows this. There is a correlation coefficient of 0.94, which indicates the correctness of the theory. The effect of the t^3 term is approximately taken into account by

One might expect that, using the average value of the time of drop and release velocity, we might hope to obtain the average vertical acceleration and compare the result with the experimental averages of the launchings. This method breaks down due to the fact that, while the pitch oscillations about the mean value in any duration of time tend to cancel out to zero, actually in a relatively short time of drop there is not a complete cancellation. Thus the theory of Section 5.1 predicts an average vertical acceleration for the observed launchings of about 31.1 ft per sec per sec, while the average results yield the value of 31.5 ft per sec per sec. This slight difference may be explained by the fact that, for the airplanes used, the average pitch angle at release is about 3 degrees nose-down so that the net result in the relatively short time of drop will tend to be some small average pitch angle nose-down which will produce a lift force downwards and, consequently, could increase the average vertical acceleration from 31.1 ft per sec per sec to 31.5 ft per sec per sec.

5.4 AERODYNAMIC CONSTANTS OF THE MARK 13 TORPEDO

Thus far we have developed the theory of the air flight of the torpedo and discussed some of the experimental evidence that tends to support the point of view presented. We now proceed to the determination of the constants associated with the Mark 13 torpedo with its various air appendages.

5.4.1 Method of Obtaining Aerodynamic Constants and Tabulation of Results

The characteristics of the Mark 2-1 and Mark 2 stabilizers, with and without the Mark 1 drag ring, have been obtained by wind tunnel tests at various places including the Newport Torpedo Station, Wright Field, Langley Field, and the University of Michigan. In addition, strip camera photographs of airplane launchings at the Newport Torpedo Station can be interpreted in terms of the theory to give the same constants.

The model tests at the Newport Torpedo Station were carried out on a $\frac{1}{5}$-size model at a velocity of 100 ft per sec. At Wright Field a $\frac{1}{3}$-size model was used at a velocity of 100 miles per hour. A full-size model was used at Langley Field. The University of Michigan tests were carried out on a 0.2236-scale model, with a wind velocity of 88 ft per sec. All these models were tested without propellers.

From the wind tunnel tests it is possible to determine C_M/α, C_M/ψ, C_L/α, C_L/ψ, and C_D. However, with the facilities available, C_K and C_F could not be obtained in the tunnels. One result for C_K was obtained with an oscillating model, but otherwise these constants have not been determined from tunnel tests.

The method of obtaining C_M/α, C_K, and C_D from strip camera photographs may be described as matching. Using experimentally determined curves of $\alpha(t)$ and using the value of α and the slope $\dot{\alpha}$ at a particular time as the initial conditions of the motion, different values of p and ω were used in the modified form of equation (22) until a good matching of the experimental curve by the theoretical curve was obtained. Thus, from curves like those illustrated in Figures 18, 19, 20, and 21, where experiment is matched by theory, the values of p/V and q/V^2 were tabulated.

From p/V and q/V^2 and equations (4) and (5), C_K and C_M/α are obtained.

In order to obtain C_D, the horizontal decelerations as recorded at the Newport Torpedo Station (obtained from the strip camera photographs) were plotted against $\dot{x}_0^2$ and the best straight line fitted with the condition that it pass through the origin. This is plotted in Figure 22. If the t^3 term is negligible, the slope of this line is the value of k. The average contribution of the t^3 term to the deceleration in the cases considered is about 5 per cent of the t^2 term. Consequently, to the slope obtained from Figure 22, 5 per cent was added in order to find the value of k and hence C_D.

The following constants were used to describe the Mark 13 torpedo fitted with a shroud ring, Mark 2-1 stabilizer, and a drag ring.

I = moment of inertia about a transverse axis through the center of gravity = 972 slug ft^2.

ρ = density of air = 0.002378 slug per ft^3.

W = weight of the torpedo = 2,200 lb.

l = length of the torpedo = 13.4 ft.

We may then write C_M/α, C_K, C_D, etc., in terms of q/V^2, p/V, k, etc., and these constants.

The results obtained by the various methods are listed in Table 1.

5.4.2 Discussion of Aerodynamic Constants

Before proceeding to discuss the constants obtained by the various methods, the effect of propellers on the coefficients must be pointed out since this may account for a good part of the difference between tunnel tests and full-scale results obtained by matching. All the model tests were run without propellers. It has been found in wind tunnel tests that the restoring moments are markedly increased by the addition of propellers. In recent tests at the Newport Torpedo Station similar results were obtained over a large range of pitch angles. It is also found that the addition of propellers increases the damping coefficient considerably. Hence, due to the effect of propellers, it is to be expected that results from full-scale matchings should be somewhat different from results obtained in wind tunnels.

Restoring Moment Coefficient C_M/α

From the values of C_M/α presented in Table 1, it appears that the values obtained by matching experimental curves, which represent the full-scale torpedo in flight, are usually more negative than the values obtained in the wind tunnels. This is explained to some extent by the absence of propellers in the model tests. Furthermore, it is noticed that the Mark 1 drag ring seems to increase the negative value of C_M/α.

The value of C_M/α obtained by matching is subject to a probable error of about 10 per cent. The main cause of this dispersion seems to be the roll of the torpedo in air. During some part of the drop, the small face of the Mark 2-1 or Mark 2 stabilizer may have rolled into the pitching (vertical) plane, and the effective value of C_M/α would therefore be diminished. The Mark 2-1 stabilizer is not symmetrical, and the value of C_M/α varies with the angle of roll. From wind tunnel tests at the Newport Torpedo Station it was found that, for a stabilizer very similar to the Mark 2-1, when the torpedo rolled 45 degrees the value of C_M/α was 0.82 times the value at 0 degrees roll and, when the torpedo rolled 90 degrees it was 0.65 times the value at 0 degrees. It was not possible from the photographs to ascertain the magnitude of the roll of the torpedo during the air flight so that one might expect a dispersion in the values of C_M/α. The value of $C_M/\alpha = 1.50$ is, therefore, probably the value at some average roll angle other than 0 degrees.

For the Mark 2 stabilizer the area of the smaller face is much less than in the Mark 2-1 stabilizer so that the effect of roll in air on C_M/α will be greater than in the Mark 2-1. Consequently, the value of C_M/α will be too low, due to roll, by a larger factor than is expected from a comparison of the areas of the stabilizers in the pitching plane. That this does not appear as an increased dispersion may be due to the small number of observations.

Table 1. Results obtained for the constants of the Mark 13 torpedo with shroud ring fitted with Mark 2–1 and Mark 2 stabilizers with and without the Mark 1 drag ring (pickle barrel) by matching experimental curves with theoretical curves and by the wind tunnel tests at the Newport Torpedo Station (N), the University of Michigan (M), Wright Field (W), and Langley Field (L). All angles are in radians.

	Mark 2–1 with Mark 1 drag ring		Mark 2–1, no drag ring		Mark 2 with drag ring	
	Matching	Wind tunnel	Matching	Wind tunnel	Matching	Wind tunnel
C_M/α	−1.50±0.13	−1.19 (N) −1.39 (W) −1.36 (M)	−1.25±0.17	−1.16 (L)	−1.16±0.03	−1.13 (N)
C_K	−2.87±0.05	....	1.31±0.39 1.70±0.55	....	2.43±0.11	2.32 (P)
C_D	0.93	0.87 (N) 0.97 (W) 0.84 (M)	....	0.32 (N) 0.38 (W) 0.30 (M)	....	....
C_L/α	....	4.8 (N)	....	4.9 (L)	....	....
C_M/ψ	....	−0.717 (N) 0.774 (M)	....	−0.662 (N)	....	....

Damping Moment Coefficient C_K

As has been pointed out, elaborate arrangements are required in order to measure C_K in wind tunnels; consequently, very few results have been obtained. The drag ring probably produces damping of the oscillations of the torpedo by dissipating energy in shedding vortices. The damping effect of the stabilizer is due to the additional pitch angle at the tail of the torpedo caused by rotation. The moment due to the stabilizer caused by the rotation will therefore be affected by roll in the same way as C_M/α is altered by the roll in air. Therefore, roll will contribute to causing a dispersion in C_K, and this should be more marked without the drag ring since the drag ring contributes a constant amount to C_K. In addition, the mean value of C_K for the Mark 2 stabilizer may be expected to be lower than for the Mark 2-1 since the effect of roll is larger because of the greater difference of the areas in the pitching and yawing planes.

In Table 1, two values of C_K are given for the Mark 2-1 stabilizer without a drag ring. This is due to the fact that very large values of C_K obtained by matching raised the average value above what is probably the true value. It was found from an inspection of a number of curves of $\alpha(t)$ for launchings without drag rings that C_K is small so that the average value of C_K without a drag ring is in the neighborhood of 1.31. The dispersion in the value of C_K without a drag ring is considerably greater than with the drag ring, even for the value $C_K = 1.31$. This is to be expected from the discussion above and is explained by the roll in air. It is noticed that C_K with a drag ring is more than twice the value without it. This effect will be illustrated later.

Drag Coefficient C_D

The value in Table 1 was obtained from the graph in Figure 22 as has been pointed out earlier. This value is probably the most reliable one since it is based on full-scale actual flight tests of the torpedo. It is in fair agreement with wind tunnel results. The effect of propellers on C_D is not expected to be important, and this expectation appears to be confirmed.

Lift Coefficient C_L/α

This coefficient could not be obtained from analyzing strip camera records or photographs of airplane launchings. The photographs could not give a precise value for C_L because the times of drop were relatively low and the lift effect on the Mark 2-1 stabilizer is very small and masked by the pitch oscillations. Consequently, the only results for C_L/α are wind tunnel measurements.

Damping Force Coefficient C_F

Without the Mark 1 drag ring, $C_K = 1.31$. Without the drag ring, most of the damping arises at the tail of the torpedo. This also has been found true for airships. Consequently, the damping force is concentrated at the tail, and the damping force coefficient is $C_F = 13.4/6.7 = 2C_K$, where 6.7 ft is approximately the distance from the center of pressure of the air forces acting on the torpedo to the center of gravity. Now, when the torpedo is fitted with a drag ring, we find C_K is about doubled. Since most of the forces due to the drag ring, which produces this additional damping moment, are probably concentrated at the nose, when C_K is doubled, the damping forces at the nose must be roughly equal to those at the tail and in the opposite direction. Consequently, a couple is produced so that with the Mark 1 drag ring it seems probable that $C_F \cong 0$.

Moment Coefficients in the Horizontal Plane

The values of C_M/ψ and C_K in the horizontal plane cannot be obtained by matching experimental curves since, as yet, there are no accurate observations of yaw angle as a function of time in the horizontal plane for the Mark 13 torpedo with air appendages.

For C_M/ψ we can use the wind tunnel results to the extent of learning that C_M/ψ is about 0.6 times C_M/α so that taking 0.6, the value of C_M/α as obtained by matching experimental curves, we have $C_M/\psi = 0.9$. C_K in the horizontal plane is probably close to the value in the vertical plane. Although the area of the stabilizer effective in the horizontal plane is less than in the vertical plane, the effect of the edges in the horizontal plane should produce some damping which may result in about the same C_K as in the vertical plane. In addition, the part of C_K due to the drag ring is present in the same amount in the horizontal as in the vertical plane. Again, C_F should be about the same as in the vertical plane since C_K is about the same, that is, $C_F \cong 0$ in the horizontal plane, while without the drag ring $C_F = 2C_K$. For C_L/ψ there are no experimental results. However, since $C_M/\psi = 0.6C_M/\alpha$, one may estimate that $C_L/\psi = 0.6C_L/\alpha$.

5.4.3 Characteristic Aerodynamic Constants of the Mark 13 Torpedo with a Shroud Ring

Using the values obtained from actual air flight tests wherever possible, the following appears to be a reasonable set of constants.

1. Fitted with Mark 2-1 stabilizer and Mark 1 drag ring (pickle barrel)

$$
\begin{aligned}
C_M/\alpha &= -1.50,\\
C_K &= 2.87 \text{ (pitching and yawing)},\\
C_D &= 0.93,\\
C_F &= 0 \text{ (pitching and yawing)},\\
C_L/\alpha &= 4.8,\\
C_M/\psi &= 0.90,\\
C_L/\psi &= 2.88,
\end{aligned}
$$

$I = 972$ slug ft^2,
$A = 2.75$ ft^2,
$M = \dfrac{2200}{32.16}$ slugs,
$l = 13.4$ ft,
$\rho = 0.00238$ slug per foot^3.

The constants in the equations of motion become

$\omega = 13.8 \times 10^{-3}\,\bar{V}$ (knots) sec^{-1},
$p = 2.94 \times 10^{-3}\bar{V}$ (knots) sec^{-1},
$k = 4.47 \times 10^{-5}$ ft^{-1},
$r = 14.11 \times 10^{-3}\bar{V}$ (knots) sec^{-1},

where $\bar{V}$ (knots) may be obtained from Figure 7. These are the constants used in constructing the nomogram in Section 5.2.1, Figure 9.

2. Fitted with Mark 2-1 stabilizer, no drag ring,

$C_M/\alpha = 1.25$,
$C_K = 1.31$ (pitching and yawing),
$C_D = 0.33$,
$C_F = 2.62$ (pitching and yawing),
$C_L/\alpha = 4.9$,
$C_M/\psi = 0.75$,
$C_L/\psi = 2.94$,
$\omega = 12.6 \times 10^{-3}\bar{V}$ (knots) sec^{-1},
$p = 1.34 \times 10^{-3}\bar{V}$ (knots) sec^{-1},
$k = 1.60 \times 10^{-5}$ ft^{-1},
$r_1 = 12.7 \times 10^{-3}\bar{V}$ (knots) sec^{-1}.

It is both important and interesting to note the effect of the Mark 1 drag ring on the air flight of the torpedo. Besides the increased drag in air which may cause the velocity of the torpedo at entry to be as much as 40 knots less than the release velocity, the importance of the drag ring is due primarily to a large increase in the damping of the pitch oscillations. Consequently, for the same release conditions, torpedoes fitted with drag rings, in general, will have a much smaller pitch angle at entry than torpedoes without drag rings. The amplitude of the pitch angle at any time t without the drag ring divided by the amplitude with the drag ring is given roughly by a factor of the type

$$\frac{e^{-1.34 \times 10^{-3}\,\bar{V}t}}{e^{-2.94 \times 10^{-3}\,\bar{V}t}}$$

which may be seen to be of considerable importance in determining the subsequent underwater trajectory, as is shown in Chapter 6 (see end of Section 6.3). Incidentally, this ratio increases with time. This shows the great effect of the Mark 1 drag ring in changing the pitch oscillations and hence improving the water entry.

It should be noted that the *shroud* ring does not alter the constants of the torpedo in air since it is covered completely by the stabilizer.

The British aircraft torpedo is usually launched with the M.A.T. IV stabilizer which has an area in the pitching plane of about 1,200 sq in. (60 in. by 20 in.). With this relatively large stabilizer, the constants obtained by wind tunnel measurements are $C_M/\alpha = -4.53$ or about three times the value of the Mark 2-1 with drag rings. In addition, we may expect a correspondingly large C_L/α since most of the restoring moment comes from the lift at the tail. $C_M/\psi = -1.31$ or about 1.45 times the value of the Mark 2-1 with drag ring. These larger values may be considered as due primarily to the larger area of the M.A.T. IV stabilizer.

It is interesting to compare the constants of the Mark 13 torpedo in air with its underwater characteristics (where the stabilizer and drag ring have been removed). Thus it has been found in water and wind tunnel tests without propellers that for zero elevator or rudder angle the Mark 13 torpedo with shroud ring (using the density of water)

$C_M/\alpha = 0.69$ (destabilizing),
$C_K = 0.46$,
$C_F = 1.16$,
$C_L/\alpha = 2.24$,
$C_D = 0.13$.

It is noticed that the C_M/α and C_K produced by the Mark 2-1 stabilizer with a drag ring are quite large. In fact, in the air, due to the stabilizer, C_M/α is negative, or the center of pressure of the lift forces is aft of the center of gravity, producing a restoring moment, while underwater the center of pressure of the lift forces is forward of the center of gravity.

5.5 RELATIONSHIP OF QUANTITIES RELATIVE TO AIR AND TO GROUND

The primary reason for studying the air flight of the torpedo is to permit a prediction of the water-entry conditions from a knowledge of the release conditions. The condition of the torpedo at entry will determine its behavior in the entry stage and in the initial underwater trajectory. However, and this distinction is the essence of this part, *the underwater behavior of the torpedo will depend on the entry condition relative to the water.* Up to this point all the quantities which have been discussed, such as velocities, distances, pitch angles, etc., have been relative to the air.

5.5.1 Quantitative Considerations

The reason why the quantities used were relative to the air is that the lift and drag forces and the restoring moments acting on the torpedo in a fluid (air or water) are determined by the velocity relative to the fluid. Thus all quantities so far derived are as seen by an observer fixed in the air, and all quantities used are relative to air.

This fact does not alter any of the results obtained. However, since the underwater behavior depends on the entry conditions as an observer on the ground (or water) sees them and since the range relative to ground is an important tactical consideration, we must examine the results to see what additions must be made in order to convert quantities relative to air to quantities relative to ground.

First, it should be noted that, if no wind is blowing, that is, if the air has zero velocity relative to ground, there is no distinction between quantities relative to air and relative to ground. However, if there is, for example, a 20 knot head wind blowing, the velocity of the torpedo relative to the surrounding air is 20 knots greater than the velocity relative to ground. Similarly, if there is a 20 knot tail wind blowing, the velocity of the torpedo relative to air will be 20 knots less than its velocity relative to ground. The problem reduces itself to examining the effect of the wind on the results previously obtained.

In general, we may transform all quantities derived from quantities relative to air to quantities relative to ground by the vector relation

$$\mathbf{V}_{tg} = \mathbf{V}_{ta} + \mathbf{V}_{ag}\,. \tag{28}$$

$\mathbf{V}_{tg}$ = velocity of torpedo relative to ground,
$\mathbf{V}_{ta}$ = velocity of torpedo relative to air,
$\mathbf{V}_{ag}$ = velocity of air relative to ground, or the wind.

Since equation (28) is a vector equation, it is equally true for each of the components of the velocity, $\dot{x}$, $\dot{y}$, and $\dot{z}$. For example,

$$\dot{x}_{tg} = \dot{x}_{ta} + \dot{x}_{ag}\,,$$

where $\dot{x}_{ag}$ = component of the wind velocity in the x direction.

To consider the effect of the wind, we shall consider separately its effect on the trajectory and on the pitching and yawing motions. It will be assumed that the wind remains constant through the drop. Although this is rarely the case, the effect produced by varying winds is complicated and small and will be neglected. The wind velocity used will always be the velocity at release.

5.5.2 Effect of the Wind on the Trajectory

Let the wind velocity at release have the three components $\dot{x}_{ag}$, $\dot{y}_{ag}$, $\dot{z}_{ag}$.

1. *x Direction.* As has been pointed out from equation (28),

$$\dot{x}_{tg} = \dot{x}_{ta} + \dot{x}_{ag} \tag{29}$$

so that

$$x_{tg} = x_{ta} + \dot{x}_{ag}t\,,$$

where x_{tg} will be the horizontal range relative to ground that the torpedo will traverse in its air flight.

From these considerations it is seen that with a tail wind component the speed of the torpedo or plane at release relative to air is less than the speed relative to ground, while for a head wind the speed relative to air is greater than the speed relative to ground. In addition, the amount by which the range relative to ground is greater than the range relative to air is given by $\dot{x}_{ag}t$.

2. *y Direction.* If $\dot{y}$ or y relative to air are to be different from $\dot{y}$ or y relative to ground, then there must be a vertical component of the wind. There is not much information on this point, but the transformation is quite simple:

$$\dot{y}_{tg} = \dot{y}_{ta} + \dot{y}_{ag}\,,$$

where $\dot{y}_{ag}$ is positive for a wind blowing vertically downward toward the earth.

3. *z Direction.* In Section 5.1 the x, y, and z axes were chosen so that *relative to air* at release $\dot{z} = 0$. As a result, to the first approximation, the trajectory of the torpedo in air was in the vertical (x–y) plane. This would mean that at release the torpedo would not experience a cross velocity relative to the surrounding air. Consequently,

$$\dot{z}_{tg} = \dot{z}_{ag}\,,$$

or relative to ground the torpedo will be drifting perpendicular to its axis at a rate which is the magnitude of the cross wind at release. This is as expected for, if the torpedo is not to experience a cross wind, it must drift with this wind at release so that the relative velocity is zero. With a cross wind the torpedo will fall in a vertical plane relative to air (according to the way an observer on the torpedo would feel the relative air), while relative to ground the torpedo would be drifting in the horizontal plane. The distance the torpedo will drift relative to ground is $\dot{z}_{ag}t$.

Thus, for a given release velocity relative to air and with a tail wind, the trajectory angle relative to ground (θ_{tg}) is smaller than with a head wind.

Figure 23 illustrates these results. This figure shows the trajectories relative to ground that result from horizontal release for a constant velocity relative to air of 200 knots with no wind, a 35-knot head wind, and a 35-knot tail wind. The three trajectories are different, even though they are drawn for the same release velocity relative to air because, for the torpedo to be released at a constant velocity relative to air with a tail wind, its velocity relative to ground

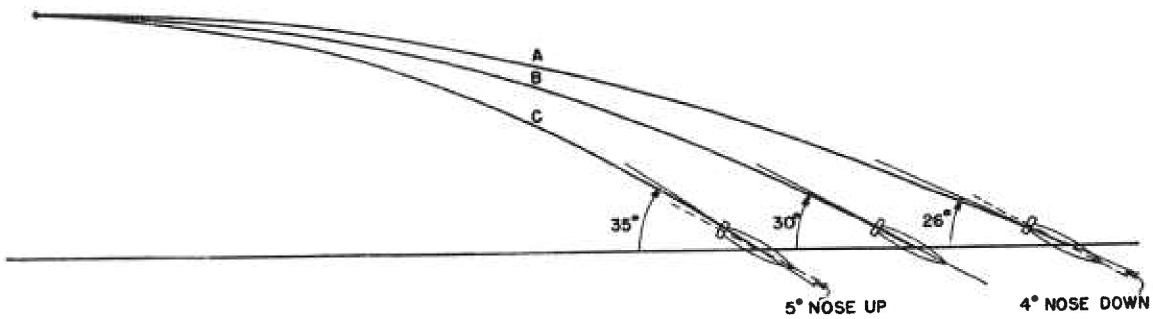

CURVE	WIND	GROUND RELEASE SPEED (KNOTS)
A	35 KNOTS - TAIL	235
B	0 KNOTS	200
C	35 KNOTS - HEAD	165

FIGURE 23. Trajectories, as seen from ground, for various winds. Constant release speed (relative to air) = 200 knots.

4. θ *Trajectory Angle*. The wind will cause the trajectory angle relative to ground to be different from that relative to air.

A good approximation for θ_{tg} at any time during the drop is obtained by retaining the first term in a Taylor series, thus

$$u_{tg} = \frac{\dot{y}_{ta}}{\dot{x}_{ta} + \dot{x}_{ag}} = \tan(\theta_a + \Delta\theta) .$$

Then

$$\Delta\theta \cong -\tfrac{1}{2} \sin 2\theta_a \frac{\dot{x}_{ag0}}{\dot{x}_0} ,$$

and

$$\theta_{tg} = \theta_a - \tfrac{1}{2} \sin 2\theta_a \frac{\dot{x}_{ag}}{\dot{x}_0} . \qquad (30)$$

θ_a is given according to Section 5.1.3 by

$$\tan\theta_a = c_0 + c_1 t + c_2 t^2 + \cdots .$$

must be larger than the release velocity relative to air; with a head wind the release velocity relative to ground will be less than the release velocity relative to air. Therefore, relative to ground, for constant release velocity relative to air, a tail wind tends to produce a smaller trajectory angle and a head wind a larger trajectory angle.

5.5.3 Effect of Wind on Angular Motion

PITCH ANGLE

The presence of a wind component in the direction of motion will also cause the pitch angle relative to ground, α_g, to differ from the pitch angle relative to air, α_a.

To find the relation between α_g and α_a it is to be remembered that

$$\alpha_g = \text{angle of axis of torpedo}, \theta_g ,$$
$$\alpha_a = \text{angle of axis of torpedo}, \theta_a .$$

Consequently,

$$\alpha_g = \alpha_a + (\theta_a - \theta_g) . \tag{31}$$

The meaning of this relation is readily understood. The torpedo axis is at a certain angle with the horizontal. The pitch angle is the angle between the axis and the tangent to the trajectory. Consequently, the difference between α_g and α_a is the difference between the two trajectory angles.

that computed from the release velocity relative to the air. However, only the correction to the vacuum trajectory will be changed, and a computation using the time average of the wind in which the torpedo is moving will give a close approximation to the exact result. In addition, the torpedo oscillation tends to damp out until its axis lies along the local air trajectory. Since this is changing differently from the way it changes with a constant wind, the mean position will be a little different. The primary effect of a var-

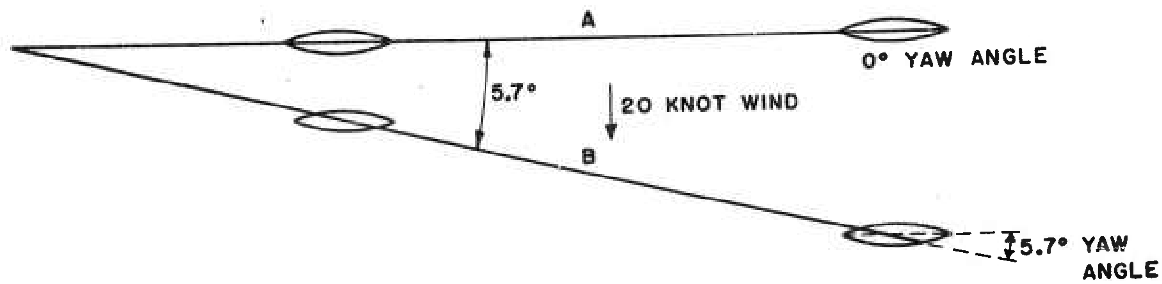

FIGURE 24. Trajectories relative to ground in horizontal plane at 200 knot release velocity.

From (30) it is therefore clear that

$$\alpha_g = \alpha_a - \tfrac{1}{2} \sin 2\theta_a \frac{\dot{x}_{ag}}{\dot{x}_0} . \tag{32}$$

Thus it may be concluded that, in general, a tail wind tends to produce a nose-down pitch relative to ground and a head wind tends to produce a nose-up pitch relative to ground.

This is illustrated in Figure 23 where we have the same air trajectory with a 35-knot tail wind, no wind, and a 35-knot head wind. In this figure, for simplicity, the pitch oscillations and mean pitch angle have been taken as zero.

Since the pitch of the torpedo α_g is an important quantity and the entry behavior is sensitive to small changes in this angle, it must be recognized that the neglect of the variation of the wind with altitude may not be completely satisfactory in this connection. The angle θ_a near the ground will not be exactly

iable wind is on α_a and hence α_g. The variation of the wind magnitude does not affect the solution of the homogeneous equation (20) but only alters the particular solution given in equation (21) by altering the value of $\dot{\theta}$. Taking this into account and using equation (30), one can easily compute α_a if the type of variation of the wind is known, and, knowing the wind at the water level, α_g at entry (which we shall call α_e) is then determined. However, for many purposes it appears that the use of a suitable mean wind might give a satisfactory approximation.

YAW ANGLE

For a constant cross wind ψ_g will differ from ψ_a. By analogous reasoning to that used to determine α_g,

$$\psi_g = \psi_a + (\mu_a - \mu_g) . \tag{33}$$

For constant cross wind $\mu_a = 0$ and equation (32) indicates that *a wind from the left will tend to produce a yaw angle to the left relative to ground and a wind from the right, a right yaw angle relative to ground.*

This may be understood by the fact that for a constant cross wind, neglecting the yaw oscillations, the torpedo will have zero yaw (at release the pilot tries to maintain zero yaw) so that the torpedo is drifting with the cross wind. Consequently, if a wind is blowing from starboard so that the torpedo is drifting to port and pointing straight ahead, the result is a starboard yaw angle. This is shown for $\dot{x} = 338$ ft per sec and $\dot{z}_{ag} = 55$ ft per sec in Figure 24.

5.5.4 Summary

In this part we have examined the effect of wind in altering the trajectory, trajectory angle, pitch and yaw angles relative to air and relative to ground. Given the release conditions of the torpedo and the wind, the condition of the torpedo relative to air and relative to ground at entry may be predicted. Because of the sensitivity of the entry behavior to the exact pitch and yaw angles, these effects of the wind are of great importance in prescribing the conditions for torpedo launching.

Chapter 6

WATER ENTRY

THE STUDY of the air flight was concerned with predicting the conditions of the torpedo at impact from a knowledge of the release conditions. In the study of the water entry, it is desired to prediet, from a knowledge of the entry conditions, the underwater behavior of the torpedo from the time of impact with the water to the time it settles down to its normal run.

The entry conditions of a torpedo may be described by the values of the following quantities at the instant of water impact.

1. Velocity, V_e,
2. Trajectory angle, θ_e,
3. Pitch angle, α_e,
4. Pitching angular velocity, $\dot{\alpha}_e$,
5. Yaw angle, ψ_e,
6. Yawing angular velocity, $\dot{\psi}_e$,
7. Roll angle, ϕ_e,
8. Rolling angular velocity, $\dot{\phi}_e$.

In the subsequent discussion, the effect of these quantities on the initial underwater trajectory will be traced through the various phases of the trajectory. In addition, the effect of physical parameters of the torpedo, such as head shape, moment of inertia, mass, length, diameter, position of the center of gravity, and center of buoyancy, and the tail structure, will be considered.

The phases into which the initial underwater trajectory will be divided for the subsequent discussion are

1. Impact (elastic wave in the water),
2. Flow forming (head is being submerged),
3. Motion in the cavity before tail slap,
4. Motion in the cavity after tail slap until cavity closure and during the subsequent cavity dissipation,
5. The subsequent noncavitating motion of the torpedo.

Although the discussion will be presented in general terms and will be specialized only for illustration and verification of the ideas presented, it must be remembered that most of the available information is based on studies of the Mark 13 torpedo. Most of the illustrations will be based on this torpedo and the points of view of the theory have largely developed around it. The Mark 13 torpedo head consists roughly of a hemisphere followed by a finely tapered

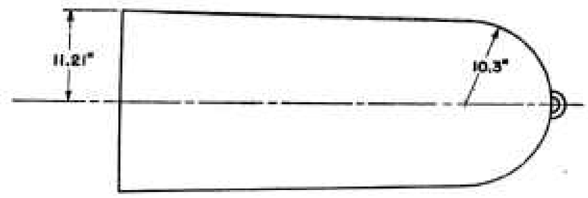

FIGURE 1. Mark 13 torpedo warhead—practically a hemisphere on a fincly tapered cone.

cone and is illustrated in Figure 1. Radical departures from this shape may alter the relative importance of various features of the analysis.

6.1 IMPACT STAGE (ELASTIC WAVE)

6.1.1 Pressure at Point of Impact

Except in the very extreme case in which the point of a pointed head makes the first contact with the water surface, the impact pressure exerted on the head, as calculated for a "perfect fluid" by potential hydrodynamic theory, is infinite since a mass of water is given finite kinetic energy in zero time. However, since water is compressible, it cannot sustain an infinite pressure, and the pressure on the head will be limited by the compressibility of the fluid.

When the torpedo strikes the water surface, the part of the nose that normally makes first contact is essentially flat so that a compression wave is generated, and the pressure behind this wave may be easily calculated.

The bulk modulus for water is given by

$$E = \rho c^2,$$

where ρ is the density of water, 2 slugs per cu ft, and c is the speed of sound in water, 4,800 ft per sec.

Consider a cylindrical element of water of length $c\Delta t$, of unit cross-sectional area and with its axis normal to the surface of the water at the point of contact. This cylinder, on impact of the torpedo, undergoes a compression of magnitude $V_{nr}\Delta t$, where V_{nr} is the normal velocity of the torpedo relative to the surface. The strain (compression) of the water is then

$$\frac{V_{nr}\Delta t}{c\Delta t} = \frac{V_{nr}}{c}$$

so that the pressure on the nose of the torpedo at the point of impact, which is the pressure behind the elastic wave, is

$$p = \frac{EV_{nr}}{c} = \rho c V_{nr} \, .$$

For a torpedo entering the water at a trajectory angle θ_e,

$$V_n = V_e \sin \theta_e$$

so that, if the water surface is initially at rest,

$$V_n = V_{nr}$$

and

$$p = \rho c V_e \sin \theta_e \text{ lb per sq ft.} \tag{1}$$

For the Mark 13 torpedo with $\theta_e = 20°$, and $V_e = 500$ ft per sec, $p = 11{,}400$ lb per sq in., which is many times the stagnation pressure.

6.1.2 Time Duration of Pressure at Point of Impact and Area over Which It Acts

We now inquire into the time during which this pressure at the point of impact may be regarded as constant and the area of the nose over which it acts. At impact, the point where the torpedo, water, and air meet usually recedes from the point of initial contact with a velocity greater than c, the velocity of sound in the water. This is because of the near flatness of the impact surfaces. As a result, the elastic wave that is generated at impact, and which produces the large pressure, cannot escape. At impact, the rate at which this point recedes is infinite. However, unless the head is really flat, this rate diminishes until its value is less than c, and the wave can then escape. The peak pressure persists during the time in which the pressure wave cannot escape, and it begins to damp out thereafter. The pressure wave begins to decay after a time which is roughly equal to twice the time required for the velocity at which the point

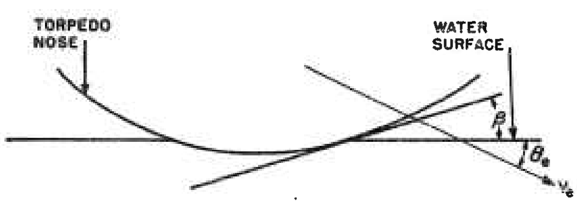

FIGURE 2. Diagram of torpedo nose entering the water.

of contact of the torpedo, air, and water, recedes to diminish to the speed of sound c. The factor of two arises since the wave is reflected from the point where the velocity of the contact point is just equal to c. From Figure 2 it is readily seen that the velocity of the point where air, water, and the torpedo meet is

$$V_e \sin (\theta + \beta) \csc \beta \, .$$

Consequently, this point of contact is moving faster than c until the surface of the torpedo makes an angle β such that

$$\frac{V_e}{c} = \frac{\sin \beta}{\sin (\theta_e + \beta)} \, .$$

The value of β corresponding to this condition depends on V_e and θ_e only and is independent of the shape of the head. Generally β is quite small so that

$$\sin \beta = \tan \beta = \beta \, .$$

Then

$$\frac{V_e}{c} = \frac{\beta}{\sin \theta_e + \beta \cos \theta_e}$$

or

$$\beta = \frac{\dfrac{V_e}{c} \sin \theta_e}{1 - \dfrac{V_e}{c} \cos \theta_e} \, .$$

For the Mark 13 torpedo, which has a hemispherical nose of radius r, since β is small

$$\sin \beta = \tan \beta = \beta = \frac{x^*}{r} \, .$$

x^* is the horizontal distance from the point of impact to the place where the contact point (air, water, and the torpedo) travels at the velocity c.

Then, since for most torpedo launchings

$$\frac{V_e}{c} \cos \theta_e << 1 \, ,$$

$$x^* = \frac{V_e \sin \theta_e r}{c} \, . \tag{2}$$

Similarly, for the spherical head it can be seen from the figure that the time necessary for the point at a distance x^* ahead of the point of initial contact to reach the undisturbed surface of the water is approximately

$$t^* = \frac{r(1 - \cos\beta)}{V_e \sin\theta_e} \cong \frac{x^*}{2c}\,.$$

During a time of about twice this length the pressure continues at near its peak value. Hence for the Mark 13 torpedo the pressure begins to decrease after the time

$$2t^* = \frac{V_e}{c^2}\sin\theta_e r\,. \qquad (3)$$

With $V_e = 500$ ft per sec and $\theta_e = 20°$ this time amounts to about 6.4 microseconds.

The area over which the pressure acts is given roughly by

$$A = \pi x^2$$

as long as $x < x^*$. The maximum value of this quantity, $A^* = \pi x^{*2}$ for the Mark 13 torpedo at 500 ft per sec and $\theta_e = 20°$, is about 0.58 sq in.

A similar approximate calculation can be carried through for any shape of nose, and an estimate can be obtained of the time and area over which the maximum pressure acts. The more pointed the nose, the faster the increase in β and hence the smaller t^* and x^*. The extreme roughness of the estimate, however, must always be kept in mind. The above calculation of x^* really only applies to the forward direction, and the values of the rear and to the sides will certainly be different.

6.1.3 Effect of Elastic Pressure Wave

With the physical description of the phenomena at impact, we may estimate the effect the elastic wave pressure on the nose has on the damage sustained by the torpedo and the influence of this pressure on the trajectory and underwater behavior of the torpedo.

From equation (1) we know the magnitude of pressure the head of the torpedo must withstand at the point of impact. This is not particularly significant for, as will be shown later, the nose must sustain even greater pressures at later stages in the entry.

Since the time for which this constant pressure wave persists is very small and the area of the nose over which it acts is also small, we can expect both the force and the impulse due to this pressure to be small.

The force in the longitudinal direction is given by

$$F_l = pA^* \sin\theta_e = \pi\rho c V_e \sin^2\theta_e (x^*)^2$$

and in the transverse direction

$$F_t = pA^* \cos\theta_e = \pi\rho c V_e \sin\theta_e \cos\theta_e (x^*)^2\,.$$

For the Mark 13 torpedo with $V_e = 500$ ft per sec, $\theta_e = 20°$, the numerical values are

$$F_1 = 2.26 \times 10^3\,\text{lb}\,,$$
$$F_2 = 6.22 \times 10^3\,\text{lb}\,,$$

and the impulse is given by

$$\int_0^t F dt < Ft$$

so that the longitudinal impulse for the Mark 13 is

$$I_1 < 1.45 \times 10^{-3}\,\text{lb sec}\,,$$
$$I_2 < 3.98 \times 10^{-2}\,\text{lb sec}\,.$$

Consequently, we can say that the resulting change in the linear or transverse velocities due to the elastic pressure wave is entirely negligible.

However, as will be shown shortly, in later stages of submergence of the nose, large compression wave pressures and smaller hydrodynamic pressures acting for a longer time are produced which have marked effects on both damage and the trajectory.

6.1.4 Effect of Drag Ring and Nose Cap

When the Mark 13 torpedo is fitted with the Mark 1 drag ring (pickle barrel), we cannot expect the pressures at the point of impact to be predicted by (1), but we expect them to be less than these values. The reason for this is that, when the drag ring is on the nose of the torpedo, it strikes the water first and has two effects:

1. The drag ring starts the water moving before the nose of the torpedo comes in contact with the water, with the result that the relative velocity of the torpedo to the water is diminished, $V_r < V_e$.

2. The drag ring serves as a "cushion" so that the pressure on the nose of the torpedo would be governed by the compressibility of wood which is greater than that of water.

In some launchings the Mark 13 torpedo is fitted with a nose cap over the drag ring (in order to reduce the drag while the torpedo is being carried by the airplane). If the torpedo entered the water with the nose cap, we should expect a similar reduction in the pressure at impact due to its presence for the same

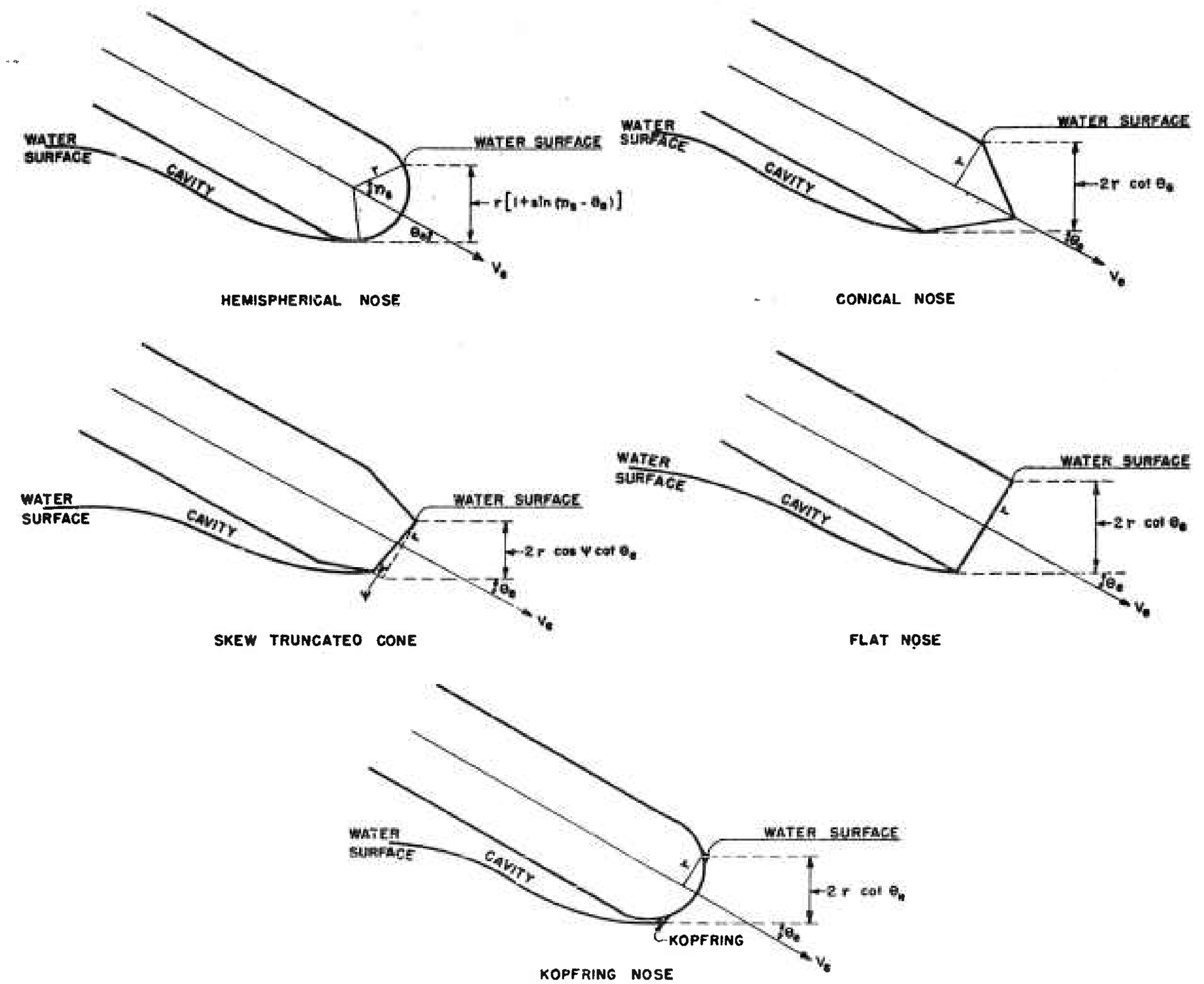

FIGURE 3. Illustration of flow separation on various noses.

reasons as the reduction due to the drag ring. These effects and the experimental verification of the previous analysis have been observed at the California Institute of Technology Torpedo Launching Range [CIT–TLR].

6.1.5 Summary of Elastic Impact Stage

At impact the water is compressed, forming a pressure wave. The magnitude of this pressure is given by (1) and is proportional to V_e and $\sin \theta_e$. For the Mark 13 torpedo with $V_e = 500$ ft per sec, $\theta_e = 20°$, we have a pressure $p = 11{,}400$ lb per sq in. acting for a time $t = 12.9 \times 10^{-6}$ seconds; the area over which this acts at this time is 0.38 sq in. The effect of the pressure wave on the damage is not important since the nose must sustain even greater pressure as will be seen later, and its effect on the trajectory is negligible. Furthermore, the pressure at the point of impact is considerably diminished by the drag ring or a nose cap. In fact, this entire stage is of such short duration that it is usually negligible.

6.2 FLOW-FORMING STAGE

This stage of the motion lasts until the head of the torpedo is submerged so that the flow breaks away from the top side of the nose. During this stage the torpedo undergoes a change in its longitudinal velocity and a change in its angular velocity. The details of these changes have not been observed, except in models, and, since they take place in a very short time, they will be treated as impulsive changes. The impulsive change in angular velocity in the vertical plane is called the whip. It is the magnitude and direction of the whip that is the important consequence of this stage of the motion. The phenomena occurring are understood qualitatively, and some quantitative results have been obtained experimentally; however, it is in this stage that a quantitative theoretical approach is most lacking.

This stage is also of importance from the point of view of shell damage since there is a high peak deceleration during the nose submergence.

The most important physical characteristic of the torpedo during this stage of the motion is its nose shape. It is the shape of the nose that primarily influences the whip at entry, and this in turn has a controlling effect on the subsequent underwater trajectory.

6.2.1 Duration of the Flow-Forming Stage

When the torpedo nose enters, the water will flow around it until separation occurs both from the top and from the bottom. One can say briefly that the flow will separate from the nose at any point where the total pressure on the nose is roughly zero or at any discontinuity on the surface of the nose for at a discontinuity the theoretical pressure becomes negatively infinite and the flow must separate. The point on the nose where the total pressure becomes zero depends on the pressure in the air or vapor near the torpedo head. Since at the time we are concerned with flow separation the torpedo head is still in the air, the pressure around the head is roughly atmospheric pressure or perhaps somewhat less than atmospheric pressure.[a]

Consequently, it is clear that the time duration of the flow-forming stage is intimately connected with the nose shape. In order to calculate the point at which the flow breaks away for "smooth" heads like spheres and ogives, the pressure distribution must be known. This point is, however, still somewhat obscure. Nevertheless, for noses with discontinuities, such as cones, flat heads, truncated cones, noses with kopfrings and spigots, examples of which are illustrated in Figure 3, the flow will separate at the discontinuity of the nose. Thus it is possible to calculate roughly the duration of the flow-forming phase of the motion for various shaped noses.

Let η_s be the angle at which the flow separates from the upper side of the nose. This angle is constant for all hemispherical heads, and different estimates of its magnitude vary from 42° to 65°. If r is the radius of the hemispherical nose, then the time to separation of the flow from the upper side of the nose is given roughly by

$$t = \frac{r[1 + \sin(\eta_s - \theta_e)]}{V_e \sin\theta_e}.$$

This is illustrated in Figure 3.

A rough picture of flow separation on a one-inch model of the CIT Steel Dummy is illustrated in Figure 4. In this figure the one-inch model is seen

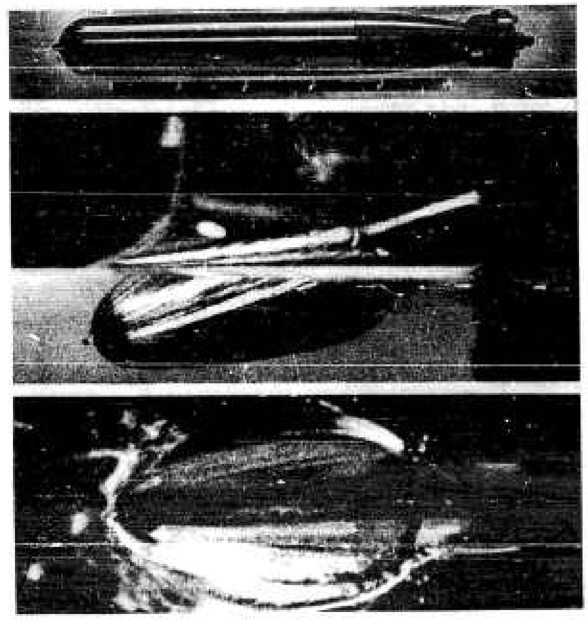

FIGURE 4. Flow separation on 1-in. model of Steel Dummy at end of flow-forming stage ($\theta_e = 19°$).

just after the end of the flow-forming stage. This is not necessarily an exact model of the full-scale torpedo behavior but it illustrates the concept of flow separation and flow-forming stage.

If $\eta_s = 55°$, for $\theta_e = 20°$, $V_e = 500$ ft per sec, $t = 8.6 \times 10^{-3}$ sec $= 8.6$ msec.

For heads of other shapes an approximate time to flow separation can be estimated along lines indicated in Figure 3.

It should be remembered that, while the flow separates from the nose at the various points discussed

[a] There may be some circulation of the air in the region near the place where the head, water, and air meet, which could reduce the pressure. It is estimated by the Morris Dam Group, which works on models, that this reduction of pressure is about ½ to 1 atmosphere.

above, if the cavity angle of the flow at separation is not great enough, it may easily reform on a part of the body further aft. This has been found with spigots in some experiments on nose shapes with rockets and on other projectiles like the Shark when yawed. Thus a second kopfring was put on the Shark head since the flow which broke away from the first kopfring when the projectile was pitched or yawed reformed on the body. The flow broke away from the second kopfring when the Shark projectile was yawed and then cleared the entire body.

6.2.2 Pressures Acting on the Torpedo Nose

During the time of submergence of the nose of the torpedo large pressures are acting on it. At the point of impact the pressure on the nose is approximately given by equation (1). As the torpedo enters the water and before the water has started to move, there will be points on the torpedo ahead of the point

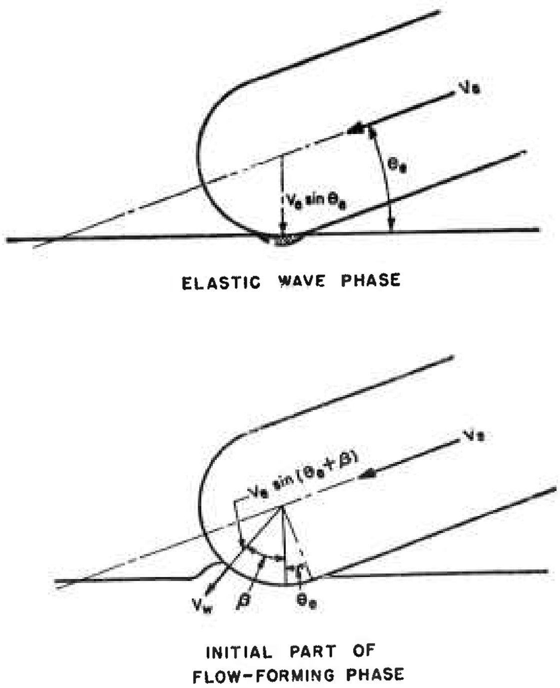

FIGURE 5. Schematic illustration of elastic wave and initial part of flow-forming stages.

of impact at which the relative velocity of the torpedo to the water will be greater than at impact (see Figure 5). Thus, at a point on the nose where the surface of the nose makes an angle β with the water surface, the velocity relative to the water is

$$V_e \sin (\theta_e + \beta) - V_w , \tag{4}$$

where V_w = velocity of the water. Consequently, if $V_w = 0$, the pressure at this point on the nose is given by

$$P = \rho c V_e \sin (\theta_e + \beta) . \tag{5}$$

Since $\sin (\theta_e + \beta) > \sin \theta_e$ for points forward of the point of impact, the pressure at points forward of the point of impact is expected to be greater than at the point of impact. Similarly, it is expected that the pressure aft of the point of impact should be less since the relative velocity is smaller. Presumably these peak pressures begin to attenuate immediately, somewhat as illustrated in Figure 6.

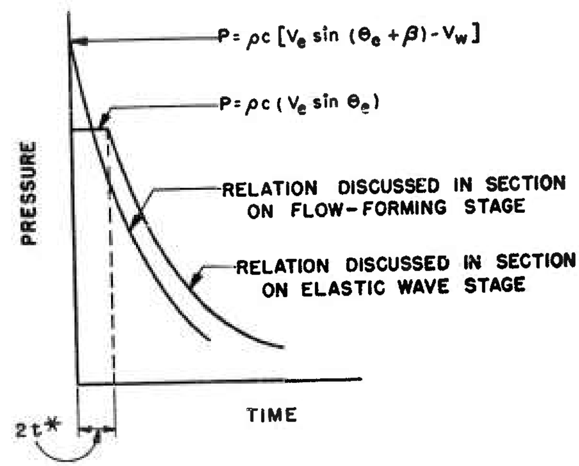

FIGURE 6. Pressure-time relations.

The CIT–TLR uses hydropressure plugs in order to record peak pressures at various points on the nose of the Mark 13 torpedo, as illustrated in Figure 7. About twelve plugs are inserted so that the distribution of the peak pressures over the nose is recorded. Examples of the results obtained are given in Figure 8. From this figure the effect of the drag ring and nose cap in reducing the elastic wave pressure is apparent. From equation (5) we might expect to predict the pressure distribution over the head except that the relative velocity of the torpedo to the surrounding water is not known. It is to be expected that, as the nose is submerged and momentum is imparted to the water, the water will flow and diminish the velocity of the torpedo relative to the surrounding water. However, in the neighborhood of the point of impact, the water has not had a chance to flow so that the recorded pressures should be roughly those pre-

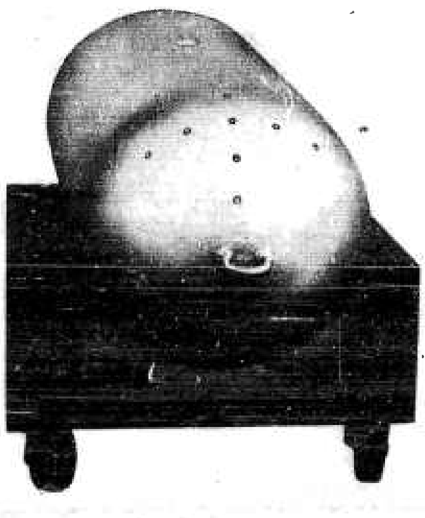

FIGURE 7. Mark 13 nose fitted with pressure plugs.

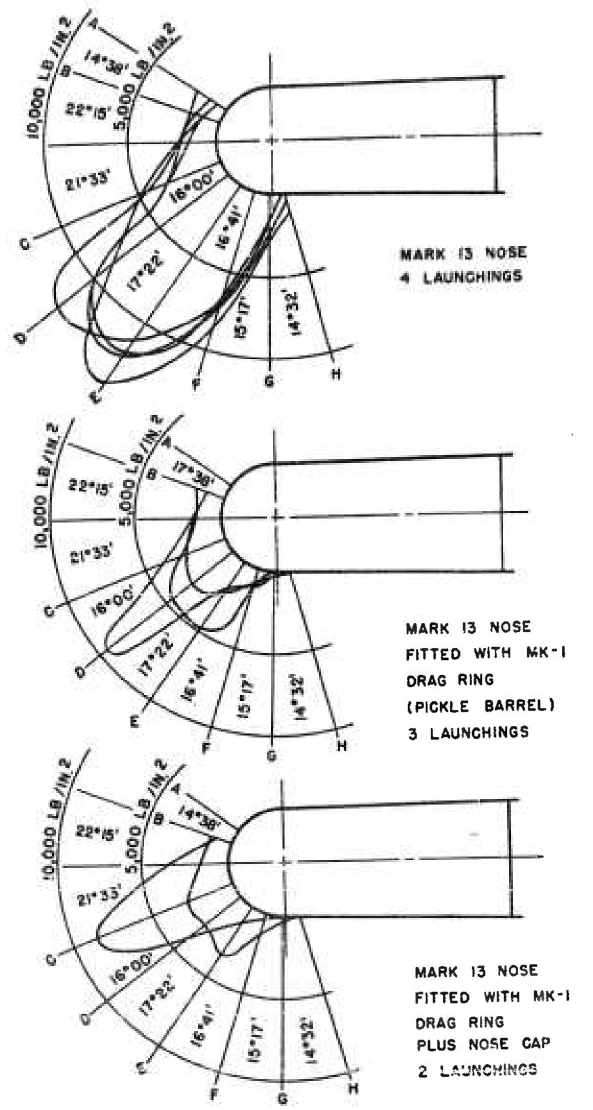

FIGURE 8. Maximum pressure distributions obtained by pressure plugs (A, B, etc.) at CIT–TLR.

dicted by equation (1), which is equation (5) with $\beta = 0$. In Figures 9, 10, and 11 the observed pressures at the point of impact ($\beta = 0$), at the point 16° forward of the point of impact ($\beta = 16°$) and 16° aft of the impact point ($\beta = -16°$), are compared with the pressures predicted by equation (5). On the whole, considering the experimental errors and the very crude nature of the theory, the agreement is good.

Forward of the position which is 16° forward of the point of impact, we notice from Figure 8 that the peak pressures are significantly less than indicated by the estimate. Here the water has had time to acquire a velocity so that $V_w > 0$, and the relative velocity of the torpedo to the water is less than V_e. We do not know the magnitude of V_w, but we do know that the calculated pressures must be too high.

As has been mentioned, these compression wave pressures attenuate very rapidly so that they only exist for a very short time. However, when they have damped out, the hydrodynamic pressures remain about a body which is decelerating in a fluid, but around which the flow is still forming so that the water has not yet separated from the top of the nose of the torpedo. These pressures probably vary as V^2. They are smaller in magnitude than the compression wave pressures, but on the other hand they act over a larger area and exist for a longer time.

Various theoretical attempts have been made to determine the distribution of these hydrodynamic, V^2, pressures over the nose of the torpedo for simple head shapes. So far, only some results for the vertical entry of a sphere have been obtained by two different theoretical approaches. These results are not directly applicable to the problem of oblique entry, which is the practical problem we are concerned with in the water entry of torpedoes. These results indicate that the V^2 pressures on the nose during this stage of entry are many times the stagnation pressure. The theoretical results obtained for this simplified case are in fair agreement with experimental results, but more work should be done along these lines.

Consequently, we have no theoretically reliable

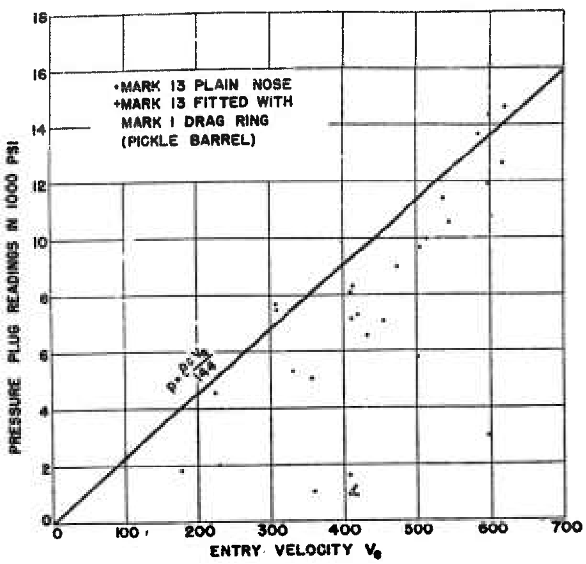

FIGURE 9. Pressure at point of impact ($\beta = 0°$) versus entry velocity for Mark 13 torpedo; Station F.

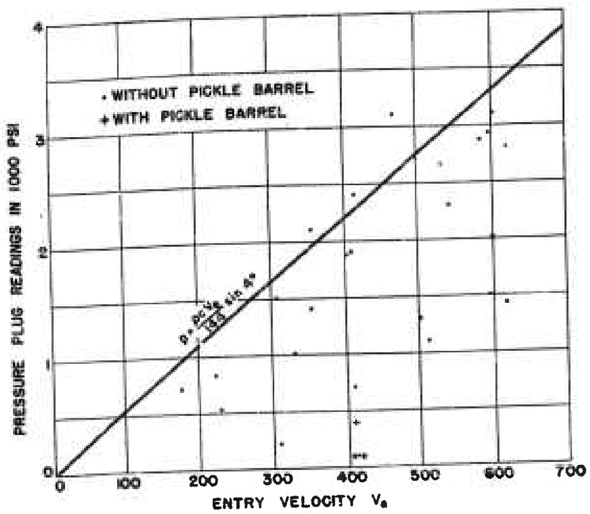

FIGURE 11. Pressure at point aft of impact ($\beta = -16°$); Station G.

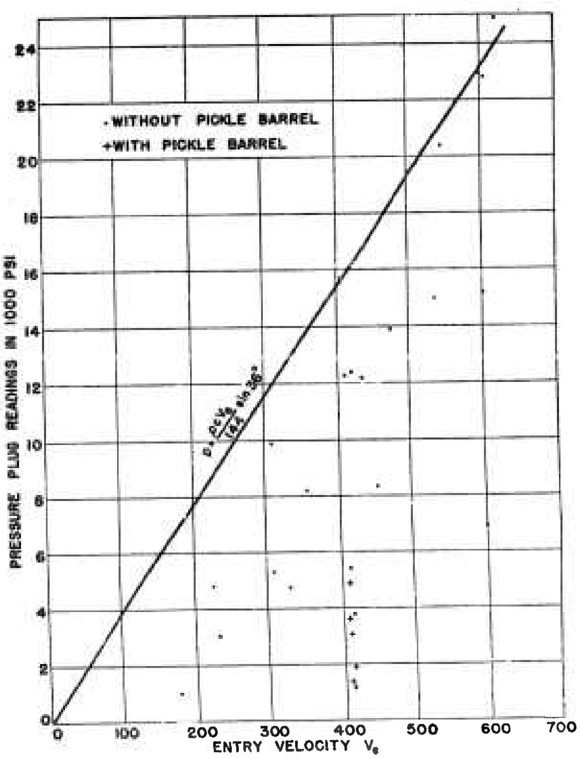

FIGURE 10. Pressure at point forward of impact ($\beta = 16°$); Station E.

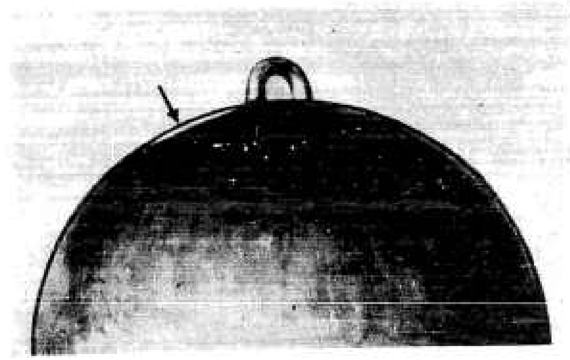

FIGURE 12. Mark 13 nose without drag ring "dimpled" by high-speed entry.

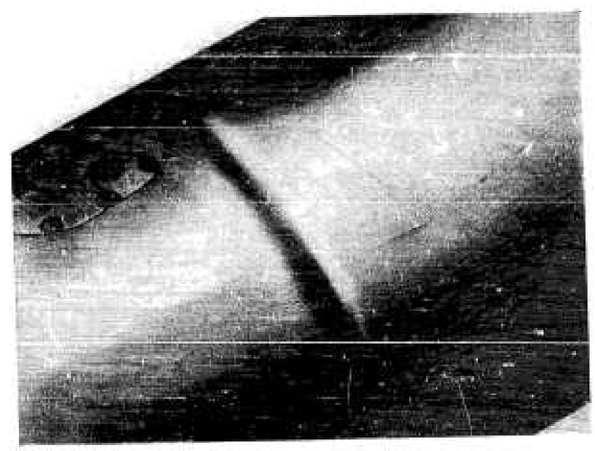

FIGURE 13. Mark 13 afterbody buckled ("accordion pleated") by high-speed entry.

quantitative results for the V^2 pressures on the nose of the torpedo for oblique entry, but we do have many qualitative results as well as experimentally obtained quantitative results. Many of these will be discussed when the trajectory in the flow-forming stage of the motion is described.

6.2.3 Damage During Flow-Forming Stage

The damage to the torpedo at entry may be divided roughly into damage to the shell and damage to the internal mechanisms of the torpedo.

DAMAGE TO THE SHELL

Damage to the shell of the torpedo is due to the high peak pressures which last for a relatively short time. In the case of the Mark 13 torpedo, the very large pressures predicted by equation (5) have been found to "dimple" the nose of the torpedo. This has been observed both at the Newport Torpedo Station and the CIT–TLR. In Figure 12 the photograph of the nose of a Mark 13 torpedo launching at the CIT–TLR in which the nose was "dimpled" is illustrated. The point of "dimpling" is about 30° off the axis of the nose and occurs close to the point of maximum pressure.

As has been discussed in Chapter 5, the drag ring diminishes the peak pressures, as may be seen from the pressure plug readings in Figure 8. Consequently, this type of nose damage should be considerably diminished by the presence of the drag ring. Further, it has been found that the peak deceleration of the Mark 13 torpedo during this stage of the motion is very large and varies roughly as V_e^2 or faster. These peak decelerations are only local in nature and have little relation to the motion of the torpedo. They are measured by accelerometers in the nose and represent local deformations. The recorded magnitudes are over 1,200g in a direction transverse to the torpedo axis. It is to be expected that the forces causing this high deceleration would damage the shell. With the drag ring on the nose, this peak deceleration is diminished to about 75 per cent its value without the drag ring. Thus it was found that, for $V_e = 400$ ft per sec for the CIT Steel Dummy ($M = 47.2$ slugs), for $\theta_e = 20°$, the accelerations as recorded by indenters in the nose are

Plain nose 505g,
Drag ring 405g,
Drag ring and nose cap 340g.

Further verification of these predictions and results have been obtained in launchings at the Newport Torpedo Station. There it was found that, for launchings for which roughly $V_e = 450$ ft per sec, without a drag ring the torpedo nose was "dimpled" at entry, and the afterbody was "accordion pleated," that is, it was buckled as is expected from a very high peak axial deceleration. This last type of damage has also been observed at the CIT–TLR and is illustrated in Figure 13. However, when fitted with a drag ring, none of these effects was noticed in the entire velocity range at which torpedoes were launched at the Newport Torpedo Station (up to about $V_e = 600$ ft per sec).

Another type of shell damage occurring during this stage of motion is the failure of the joints of the torpedo. Due to the nose-up angular velocity received during this stage of the motion, large stresses are experienced at the joints of the torpedo shell. This failure has been observed at the CIT–TLR and is more marked the more the pitch is nose-up at entry since this increases the nose-up whip.

COMPONENT DAMAGE

Component damage to the torpedo is rarely produced by this sudden peak deceleration except perhaps on some types of exploder mechanism in the nose. The behavior of the components when subject to a sudden short peak deceleration is as though they had suddenly received the impulsive velocity change sustained by the torpedo. Thus it may be proved that the acceleration sustained by the components of the torpedo is proportional to the impulsive change in velocity. The main source of component damage is the steady drag deceleration which will be discussed further under *Torpedo Damage* in Section 6.3.

6.2.4 Impulsive Axial Velocity Change

GENERAL CONSIDERATIONS

Since, during this relatively brief stage of the motion, momentum is conserved, we may say that

$$MV_e = (M + m)(V_e - \Delta V),$$

where m represents some suitable mass of water which is being accelerated. This may be called the induced mass. Consequently

$$\Delta V = \frac{m}{M + m} V_e, \qquad (6)$$

or the axial loss in velocity is proportional to the entry velocity. The value of the quantity m, the mass of water being accelerated, is obscure.

Several suggestions have been made for the value of m to be associated with the entry of a sphere in water.

1. It has been proposed that the value of m be taken as half the induced mass corresponding to the potential flow about a sphere whose radius is given by the radius of the circle of intersection of the water surface and the entering sphere, that is, $1/3\pi\rho r^3$, where r is the radius of the circle. (Of course, r is a function of the depth of penetration of the sphere.)

2. It has also been suggested that the value of m be taken as the induced mass corresponding to the potential flow about a disk whose radius is the radius of the circle of intersection of the sphere and the water, $4/3\rho r^3$.

In addition, in one theoretical attempt at the calculation of the vertical entry of a sphere in water the value of m has been obtained by replacing part of the sphere below surface by a lens with some refinements and using for the virtual mass the results obtained by hydrodynamic theory for the induced mass of a lens. The results were not too different from the results obtained using m associated with a sphere as above. However, no theoretically reliable estimates of the quantity m are at hand for oblique entry, so we can only say that it is expected that V will be proportional to V_e.

In order to discuss the magnitude of ΔV, we must decide on what distance of submergence of the head we are considering in the measurement of ΔV. The distance will be taken to equal the distance corresponding to flow separation from the upper side of the nose, which is defined as the duration of the flow-forming stage. It would probably be desirable to be able to attribute a certain amount of this change in axial velocity during the entire flow-forming stage to the compression-wave pressures which we found to vary as V_e and the balance to the hydrodynamic pressures which vary as V_e^2. However, there is not sufficient evidence, even for the Mark 13 torpedo, to be able to make this kind of division. Both types of forces usually exist at the same point on the nose at different times. Furthermore, for both types of forces the net impulse varies directly as the velocity. Thus:

1. Forces varying as V_e, since they are compression-wave forces and attenuate very rapidly, may be considered as acting for a very short time which is constant independent of V_e. The impulse is therefore proportional to V_e.

2. The hydrodynamic forces vary as V_e^2, and the time for which they act is roughly the time duration of the flow-forming phase of the motion. This varies as $1/V_e$. Consequently, for this type of force the impulse also varies as V_e.

As a result, from records on hand which give the axial velocity as a function of time for time intervals of a millisecond we cannot distinguish the effects of these two types of forces.

Magnitude of ΔV

Because of the inadequacy of the available theoretical estimates of m, the magnitude of ΔV can be obtained only from direct observation. Unfortunately, there are experimental results for only one shape nose, namely, the Mark 13 hemisphere.

For the Mark 13 it is found that, during the flow-forming stage, approximately $\Delta V = 0.034 V_e$. ΔV is proportional to V_e, and the time duration of this stage of the motion is proportional to $1/V_e$. Since $\Delta V = (a/2)\,\Delta t$, where a is the mean acceleration during this phase of the motion, we can say that $a \propto V_e^2$. At the CIT–TLR, accelerometer records obtained indicate this fact very clearly.

In general, as the dimensions of the nose increase, the time duration of the flow-forming phase increases so that ΔV during the flow-forming stage will increase with the dimensions of the nose. In addition, it is expected that, as the cross-sectional area of the nose increases, the area over which the hydrodynamic forces act will increase with the result that ΔV will increase roughly as the cube of the linear dimensions.

Not much experimental information has been obtained for other shaped noses. However, it is probably true that ΔV increases for blunter noses and decreases for finer noses. For cones up to moderately large cone angles, for ogives, and for spigots, ΔV is probably less than a hemisphere; while for truncated cones perpendicular to the axis of the torpedo with a large flat area, for flat noses, for cone noses with large cone angles, and for kopfring noses, ΔV is probably larger than a hemisphere.

Since, for a given set of entry conditions a certain amount of axial momentum is imparted to the torpedo, for $\Delta V << V_e$, and $m << M$, $M\Delta V =$ constant. As a result, $\Delta V \propto 1/M$, or the axial change in velocity is inversely proportional to the mass of the torpedo.

It should be noted that the drag ring on the Mark 13 torpedo does not alter ΔV, even though it diminishes the peak pressures as obtained by the pressure plugs and the peak local decelerations in the nose. This is perhaps further evidence for indicating the predominant effect of the V^2 forces in producing ΔV since the drag ring affects the peak values of the pressure and deceleration, but probably not the steady V^2 pressures.

6.2.5 Change in Angular Velocity of the Torpedo in the Flow-Forming Stage

The whip at entry, which is the change in angular velocity in the vertical plane, is probably the most important single quantity in determining the initial underwater trajectory of a torpedo. The forces producing the whip are determined primarily by the shape of the nose of the torpedo.

Two effects contribute to the whip. During the flow-forming stage, first the lower part of the nose is being wetted and then the upper part of the nose. As a result, while the lower part is in contact with the water and the upper part is still in air, large forces will be acting on the lower part of the nose with no compensating forces on the upper part. In general, this will apply a torque about the center of gravity of the torpedo and produce an angular velocity. The second cause of a whip is that, if the torpedo enters with a pitch angle α_e or a yaw angle ψ_e, the drag forces which produce the change in the axial velocity will have a moment about the center of gravity of the torpedo which is proportional to sin α_e and sin ψ_e and consequently result in a whip $\Delta\omega$ and a yawing angular velocity $\Delta\psi$.

Since the pressure distributions around the nose of the torpedo during this stage of the motion are not known, the whip cannot be calculated. The most important single unsolved theoretical problem connected with the water entry of torpedoes is a determination of the whip at entry and its dependence upon the entry conditions.

Although a completely theoretical approach has not been derived, some tendencies and simple relations may be obtained. The whip is very closely connected with the change in the transverse velocity in the flow-forming stage. The whip multiplied by the

FIGURE 14. Typical tail flare records showing refraction due to whip.

distance from the instantaneous center of rotation to the nose of the torpedo is equal in magnitude to the change in the transverse velocity of the nose.

The change in velocity at entry is proportional to V_e. Consequently, the whip at entry is proportional to V_e. To review briefly the reasoning: for forces proportional to V^2, the time while the forces are unbalanced (acting on the lower side of the head and not the upper side) varies as $1/V_e$ so that the impulse will vary as V_e. Similarly, the part of the whip which is proportional to $\sin \psi_e \cong \psi_e$ and $\sin \alpha_e \cong \alpha_e$, is also proportional to the axial change in velocity ΔV and hence is expected to be proportional to V_e. Finally, any part of the whip attributable to the elastic wave will vary as V_e.

Detailed discussion of the whip must be based on an assumed nose shape.

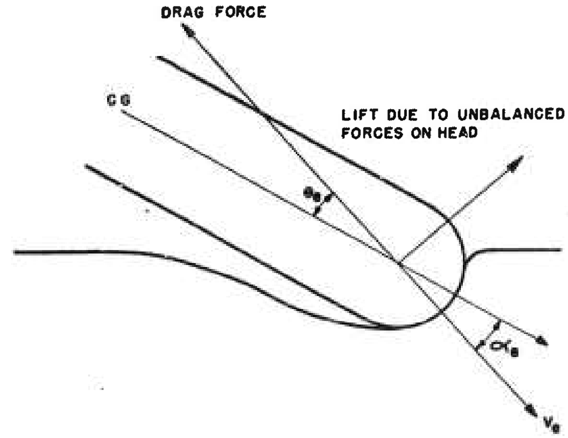

FIGURE 15. Forces independent of torpedo axis orientation; hence rotational moment of drag force is proportional to α_e.

HEMISPHERE

Whip Change in Angular Velocity. At the CIT–TLR, experimental results have been obtained for a hemispherical nose. By means of flares on the tail of the torpedo records like Figure 14 are obtained, and the change in angular velocity is recorded.

Since the whip is proportional to V_e and is expected to be proportional to α_e and ψ_e as may be seen from Figure 15, relations of the form

$$\frac{\Delta(I\omega)}{V_e} = a_1(\theta_e) + a_2(\theta_e)\alpha_e\,, \tag{7}$$

(Nose-up pitch and nose-up whip are positive.)

$$\frac{\Delta(I\psi)}{V_e} = a_3(\theta_e)\psi_e\,, \tag{8}$$

where I is the moment of inertia of the torpedo about a transverse axis through the center of gravity, are expected.

The coefficient a_1 is a function of θ_e. There will be a whip simply because one side of the nose is experiencing hydrodynamic pressures and the other side is in contact with air.

By means of flare records on the tail of the torpedo, the coefficients a_1 and a_2 were found at the Full-Scale Launching Range with $\theta_e = 20°$ for the Steel Dummy torpedo. The external shape of the Steel Dummy is the same as the Mark 13, but its moment of inertia $I = 800$ slug-ft² and $M = 47.2$ slugs, as compared to $I = 960$ slug-ft² and $M = 67.2$ slugs for the Mark 13 torpedo.

Thus, for the CIT Steel Dummy,

$$a_1(20°) = 187 \text{ slug-ft degrees}\,,$$
$$a_2(20°) = 21.2 \text{ slug-ft.}$$

In obtaining these quantities from the observations a correlation coefficient of 0.8 was found, which is an indication of the correctness of the expectations. In addition, although there is no experimental evidence to give a_3, since we are dealing with a hemispherical nose, it is clear from symmetry that $a_3 = a_2$.

We now inquire into the values of a_1 and a_2 for the Mark 13 torpedo. It is clear that the angular momentum transferred to the Steel Dummy will be the same as to the Mark 13 so that these coefficients will be the same. However, if the angular momentum imparted to both types of torpedoes is the same, then the quantities $\Delta\omega/V_e$ and $\Delta\psi/V_e$ will evidently differ, being in the ratio of the respective moments of inertia 800/960. Thus we may say:

Steel Dummy at $\theta_e = 20°$

$$\Delta\omega/V_e = 0.234 + 0.0265\,\alpha_e \text{ degree per ft}\,,$$

and

$$\Delta\psi/V_e = 0.0265\,\psi_e \text{ degree per ft.}$$

Mark 13 torpedo at $\theta_e = 20°$

$$\Delta\omega/V_e = 0.195 + 0.0221\,\alpha_e \text{ degree per ft}\,,$$

and

$$\Delta\psi/V_e = 0.0221\,\psi_e \text{ degree per ft.}$$

To be able to predict the whip at any value of θ_e, we have to know the dependence of a_1 on θ_e. On this point there is no experimental evidence on full-scale torpedo launchings since the whip has only been obtained for full-scale launchings with $\theta_e = 20°$. To find this dependence, detailed assumption on the type of

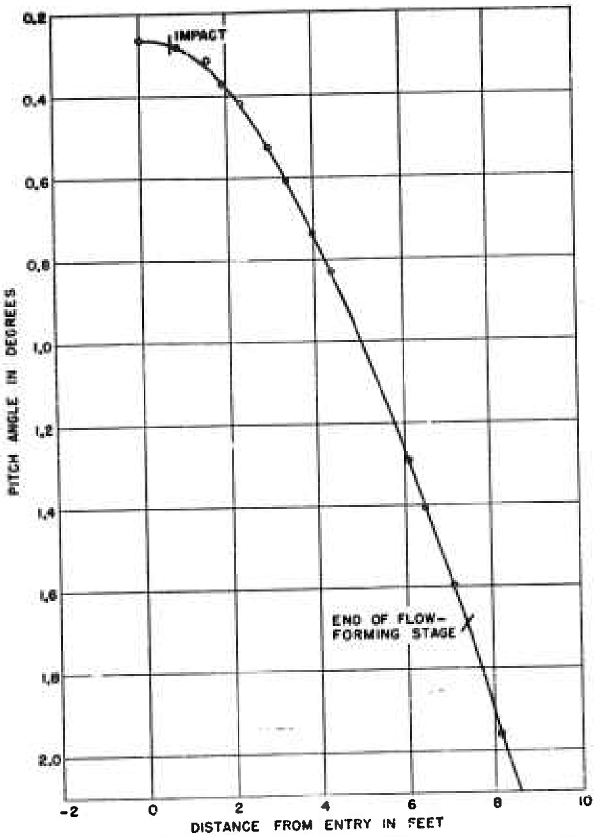

FIGURE 16. Pitch angle versus distance from entry for 1-in. model of Steel Dummy; $\theta_e = 12°$.

pressure distribution is unnecessary for one needs primarily only the dependence of the pressure distribution on θ_e. If the pressure distribution is independent of θ_e, as appears likely, for a hemispherical nose and if the mechanism of the whip is understood correctly as being due to an unbalanced pressure acting on the underside of the nose, the whip for zero pitch should be proportional to the time duration of the flow-forming stage, which was found to be proportional to cot θ_e. A theory which will give the complete pressure distribution, and hence the whip, will also yield the dependence of a_1 on θ_e. We can only say unequivocally that a_1 is a decreasing function of θ_e, and there is some indication that it decreases like cot θ_e.

By means of an optical whip recorder the Morris Dam Group working on 1-in. models of the CIT Steel Dummy recently obtained the whip as a function of distance along the trajectory during the flow-forming stage for $\theta_e = 12°$, 19°, and 34°. These are illustrated in Figures 16, 17, and 18. These whips are only about

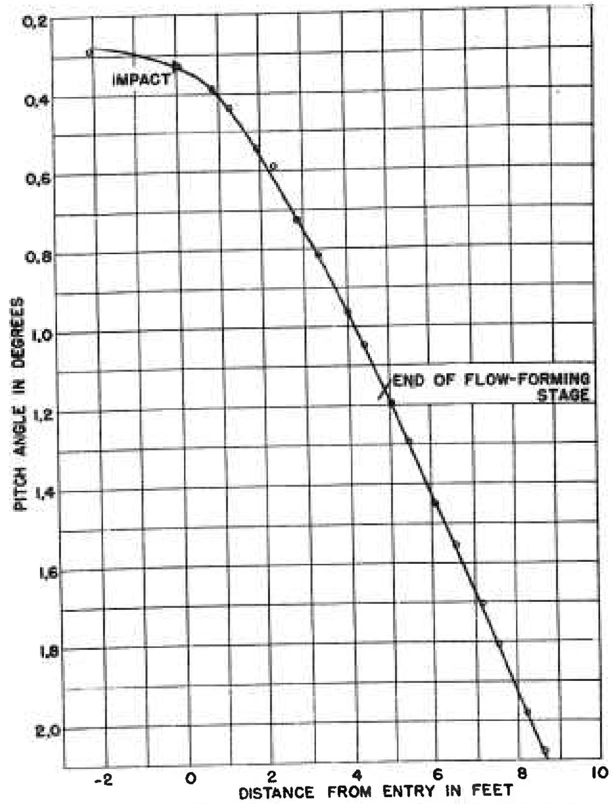

FIGURE 17. Pitch angle versus distance from entry for 1-in. model of Steel Dummy; $\theta_e = 19°$.

70 per cent of the values obtained for the full-scale dummy at the Torpedo Launching Range; nevertheless, the dependence of these whips on θ_e is interesting to note. Reading the whip, which is proportional to the slope of these curves at a distance corresponding to the end of the flow-forming stage, one finds that the whip varies like cot θ_e. This is illustrated in Figure 19. There are a number of discrepancies between the whip of the 1-in. model and the whip of the full-scale torpedo so that this is not conclusive evidence that $a_1 \propto \cot \theta_e$. However, it is a noteworthy experimental indication of the dependence of a_1 on θ_e.

There is even less experimental evidence on the behavior of a_2 and a_3 as functions of θ_e, but they probably both have finite values when $\theta_e = 90°$ and increase as θ_e decreases to small angles.

From relation (7) it is clear (with the sample values of a_1 and a_2) that for a hemispherical nose the nose-up whip at entry increases for nose-up (flat) pitch and decreases for nose-down pitch and also decreases with increasing trajectory angle at entry, θ_e. In other

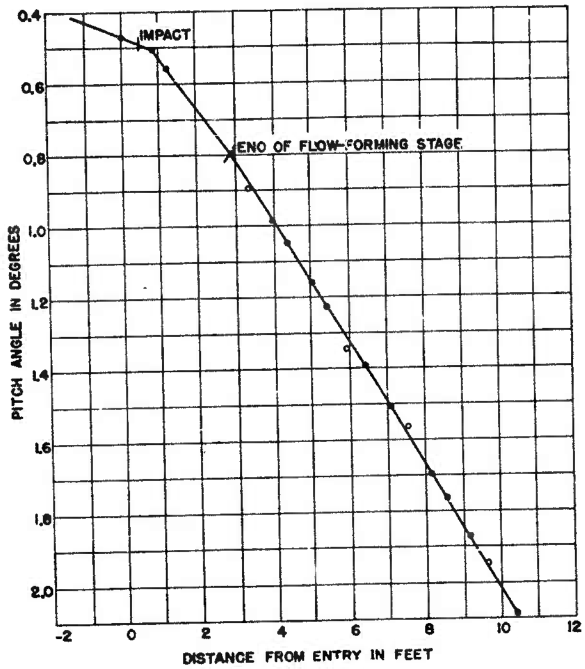

FIGURE 18. Pitch angle versus distance from entry for 1-in. model of Steel Dummy; $\theta_e = 34°$.

words, the torpedo tends to "stub its toe" as it enters with increasing nose-down pitch. It is also clear that a nose-right yaw angle will produce a nose-right angular velocity.

Of course, the quantities $\Delta\omega$ and $\Delta\dot{\psi}$ are not the angular velocities, but only the change in the angular velocities. In other words, they represent the angular velocities at the end of the flow-forming stage less the angular velocities at entry, which are usually relatively small.

Change in Orientation of the Torpedo Axis during the Flow-Forming Stage — Instantaneous Center of Rotation and Effect on Trajectory. For a hemispherical nose all forces act normal to the surface of the nose and the resultant force passes through the center of the nose. Furthermore,

r_1 = distance from the point of application of the impulsive forces to the center of gravity;

r_2 = distance from the center of gravity to the instantaneous center of rotation;

k = radius of gyration of the torpedo about the center of gravity;

then

$$r_1 r_2 = k^2 .$$

For the

CIT Steel Dummy, $r_1 = 4.9$ ft, $k^2 = 17$ ft^2,
Mark 13 Torpedo, $r_1 = 4.9$ ft, $k^2 = 14.3$ ft^2.

Consequently,

CIT Steel Dummy, $r_2 = 3.47$ ft,
Mark 13 Torpedo, $r_2 = 2.92$ ft.

Since the center of gravity is 5.8 ft from the nose, the instantaneous centers of rotation are

CIT Steel Dummy, 9.27 ft aft of the nose,
Mark 13 Torpedo, 8.72 ft aft of the nose.

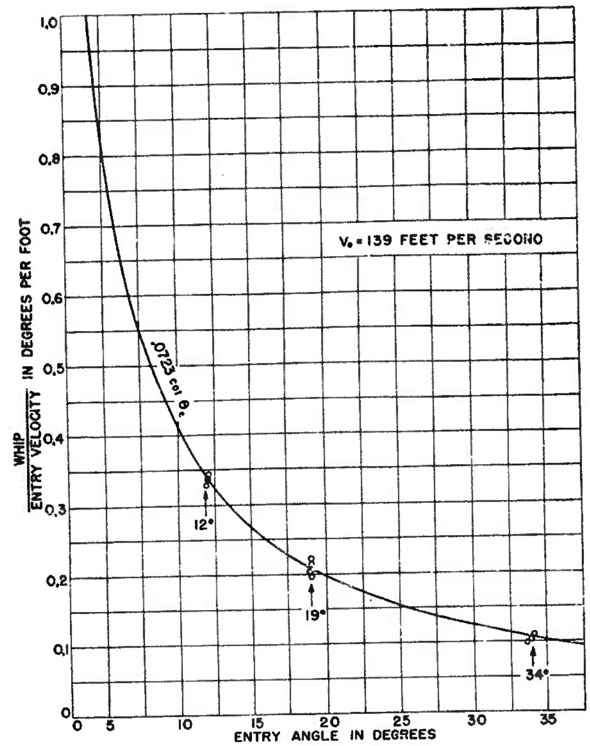

FIGURE 19. Whip at end of flow-forming stage versus entry angle for 1-in. model of Steel Dummy.

At the Full-Scale Launching Range the whip at entry is obtained from flares on the tail of the CIT Steel Dummy. If the torpedo receives a whip at entry, it is clear that the tail flare images will fall below the air flight line. If the whip is $\Delta\omega$ radians per sec and if the rate at which the flare images fall below the air trajectory is $\Delta\dot{w}$, then it follows that the distance between the tail flare and the center of gravity is given by

$$d = \frac{\Delta \dot{w}}{\Delta \omega} .$$

For the CIT Steel Dummy, $d = 4.3$ ft. Consequently, the distance from the instantaneous center of rotation to the nose of the Steel Dummy is $(13 - 4.3)$ ft $= 8.7$ ft, which is in fair agreement with the calculated position.

Since the instantaneous center of rotation is aft of the center of gravity, it is evident that during the flow-forming stage the center of gravity will experience a transverse velocity of magnitude:

$$v = r_2 \Delta \omega .$$

Consequently, the trajectory (the path of the center of gravity) will be refracted upward by an amount given by

$$\tan (\Delta \theta) = \frac{v}{V_e} ,$$

and, since $\Delta\theta$ is very small, then $\tan (\Delta\theta) = \Delta\theta$ so that

$$\Delta \theta = \frac{r_2 \Delta \omega}{V_e} = \frac{r_2 (a_1 + a_2 \alpha_e)}{I} . \qquad (9)$$

For $\alpha_e = 0$, using the calculated values of r_2,
$\Delta\theta$ (Steel Dummy) $= -0.81$ degree,
$\Delta\theta$ (Mark 13 Torpedo) $= -0.57$ degree.
For $\alpha_e = -2°$ (2° nose-down),
$\Delta\theta$ (Steel Dummy) $= -0.63$ degree,
$\Delta\theta$ (Mark 13 torpedo) $= -0.44$ degree,
where $\Delta\theta$ is negative since θ is being diminished.

Change in Pitch Angle during Flow-Forming Stage. Since the trajectory is refracted upward by an amount $\Delta\theta$, the pitch angle relative to the trajectory will be made more nose-down by the same amount. Consequently, due to the refraction of the trajectory the pitch angle during the flow-forming stage is made more nose-down by an amount given by equation (9). However, during the flow-forming stage, the torpedo is receiving a whip. The nature of the rate of increase of this whip during the flow-forming stage is not known. However, it is fairly safe to assume some sort of linear increase in the whip. As a result the pitch angle is made more nose-up by an amount

$$\Delta \alpha = \tfrac{1}{2} \Delta \omega \Delta t = \frac{(a_1 + a_2 \alpha_e) V_e \Delta t}{2I} . \qquad (10)$$

And from Section 6.2.1

$$\Delta \alpha \cong \frac{(a_1 + a_2 \alpha_e)}{2I \sin \theta_e} r \left[1 + \sin (\eta_s - \theta_e) \right] . \qquad (11)$$

Consequently, the sum of the changes in the pitch angle for a hemispherical head during the flow-forming stage from equations (9) and (11) is

$$\Delta \alpha = \frac{(a_1 + a_2 \alpha_e)}{I} \left[r_2 - \frac{r[1 + \sin (\eta_s - \theta_e)]}{2 \sin \theta_e} \right] .$$

The net result is that for the Mark 13 torpedo with $\theta_e = 20°$, $\eta_s = 50°$, the pitch angle is made more nose-down in the flow-forming stage by an amount depending on α_e and given by

$$\Delta \alpha_e (\alpha_e = 0°) = -0.18 \text{ degree (nose-down)} ,$$
$$\Delta \alpha_e (\alpha_e = -2°) = -0.14 \text{ degree} ,$$

which is a very small amount. However, it is seen to be a function of the trajectory angle and can even change sign for a small enough trajectory angle at entry.

For the yawing motion the change in yaw angle is given by

$$\Delta \psi = \frac{a_3 \psi_e}{I} \left[r_2 - \frac{r[1 + \sin (\eta_s - \theta_e)]}{2 \sin \theta_e} \right] ,$$

and is zero for $\psi_e = 0$, while for the Mark 13 torpedo with $\psi_e = 2°$, $\theta_e = 20°$, $\eta_s = 50°$, $\Delta\psi = 0.04$ degree.

Other Shaped Noses

For a hemispherical nose we have a great deal of quantitative evidence concerning the whip; for other shaped noses most evidence is qualitative.

It is not necessarily true that when a torpedo enters the water it should receive a nose-up whip for the direction of the whip will depend both on the entry conditions and on the nose shape. Even a hemispherical head can have a nose-down whip at entry if the pitch angle at entry is large enough nose-down.

By considering the general qualitative way in which the flow forms around a nose, some idea can be obtained as to the nature of the whip. A flat nose, for example, will be expected to whip nose-down as illustrated in Figure 20, while a sharp ogive will be expected to whip nose-up. Presumably the whip for almost any nose shape can be approximated by an

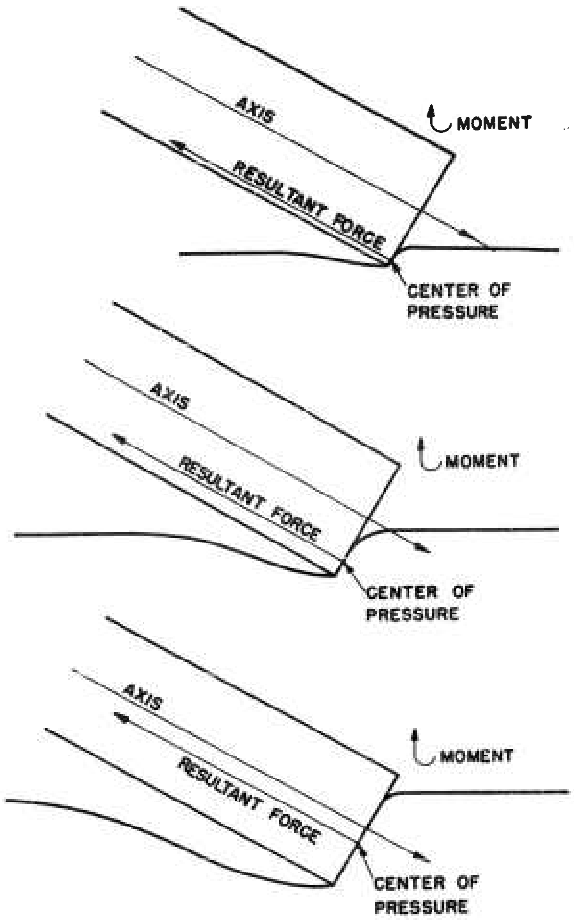

FIGURE 20. Flow-forming stage of flat nose torpedo showing nose-down moments.

expression of the form (7) but the functions $a_1(\theta_e)$ and $a_2(\theta_e)$ can only be determined by experiment or a further development of the theory.

In one case for a 90° cone tangent to the Mark 13 (hemispherical) nose, with a radius of about 7.29 in. at the end of the cone, values of the coefficients a_1 and a_2 were obtained at the CIT–TLR for $\theta_e = 20°$ with this nose fitted on the CIT Steel Dummy body. These were

$$a_1\,(20°) = 253 \text{ slug-ft degrees}\,,$$
$$a_2 = 35.5 \text{ slug-ft}\,.$$

It is clear that for this 90° cone angle on a hemisphere, with the flow separating at roughly the same position as on the Mark 13 nose, the whip at zero pitch is greater than for a hemisphere, and, as expected, the whip changes more rapidly with pitch angle with this cone nose than with a hemisphere. For a nose with a spherical cap of large radius, one may expect a small whip as may be seen in Figure 21.

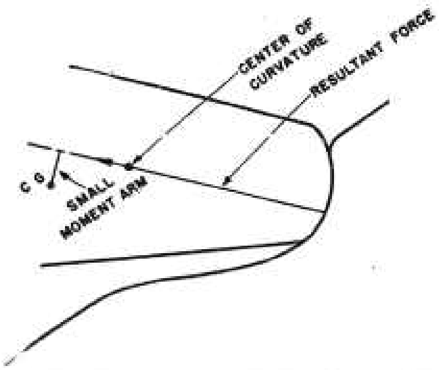

FIGURE 21. Small moment arm and hence small whip of torpedo with spherical cap of large radius.

EVIDENCE ON THE NATURE OF FORCES PRODUCING THE WHIP

It has been mentioned that the whip at entry is obtained at the Full-Scale Launching Range by means of flare records on the tail of the torpedo. From these records the entire change in angular velocity appears to occur in about one or two msec, as illustrated in Figure 22. (This figure is obtained from records like

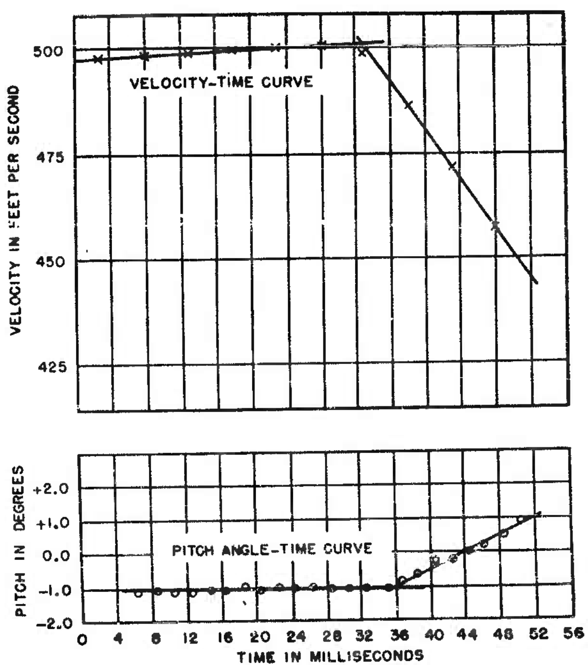

FIGURE 22. Typical velocity and pitch angle versus time data from flare records (CIT Steel Dummy).

that illustrated in Figure 14.) On the basis of the ideas developed, this time is much too short. For $V_e = 500$ ft per sec, it has been indicated that the angular velocity should continue to increase for about 8.6 msec. However, there is also observed a time delay of about 5 msec between impact and the first motion of the flare, which indicates that at entry the torpedo behaves like an elastic body. This fact may account for the apparently too short duration of the whip. There is another indication of the time duration of the whip from preliminary observations with shock-mounted accelerometers in the nose obtained at the CIT Torpedo Launching Range. From these it is found that when $V_e = 300$ ft per sec the transverse velocity for the CIT Steel Dummy is about 3 ft per sec in the first millisecond. For zero pitch at about 300 ft per sec, $\Delta\omega = 70$ degrees per sec. Since the instantaneous center of rotation is about 9 ft from the accelerometer, the transverse velocity at the accelerometer at the end of the flow-forming stage is about 11 ft per sec, which is much larger than is obtained in 1 millisecond. In fact, the accelerometer records indicate that in the time corresponding to the duration of the flow-forming stage, the transverse velocity will be in agreement with the value predicted by the whip.

By means of an optical whip recorder and the one-inch model of the CIT Steel Dummy, the Morris Dam Group has obtained very fine time resolution of the whip during the flow-forming stage. Typical curves of pitch angle versus distance from entry were presented in Figures 16, 17, and 18. On these figures the distance of travel from entry, corresponding to the flow separating from the top of the nose, has been indicated. Clearly, this distance depends on θ_c so that it differs in Figures 16, 17, and 18. In fact, it varies like cot θ_c. From these figures it is seen that the slope of the curve, which is a measure of the whip, continues to increase, although not uniformly, up to the end of the flow-forming stage. This is especially clear in Figure 16 where $\theta_c = 12°$ so that the torpedo has to travel a fair distance for the flow to separate from the top of the nose. Since these results have been on one-inch models where discrepancies appear between the whip observed and the full-scale results, they are certainly not conclusive. However, they do lend strong support to the statement that the whip will increase (due to the lift on the nose) during the entire flow-forming stage.

This indicates that the forces producing the whip are as described earlier, namely, hydrodynamic (V^2) forces acting on the lower part of the nose while the upper part is still in air. Further evidence along these lines arises from the fact that, although the drag ring will markedly decrease the elastic wave pressure, it is seen from flare records at the CIT–TLR that the drag ring does not alter the whip at entry. Consequently, it is believed that the V^2 forces, which are probably unaltered by the drag ring, produce the whip at entry.

These observations also indicate the care that must be taken in interpreting observations. The torpedo is an elastic rather than a rigid body, and due account must be taken of this fact.

Since in the vicinity of the point of impact the shape of the cone nose tested at the CIT–TLR is close to a hemisphere and since the whip is still markedly different from that of a hemisphere, we have further evidence that the V^2 type of forces produce the whip rather than elastic wave forces. Thus the elastic wave forces exist in the neighborhood of the impact point and should roughly be the same for both noses. Consequently, if the elastic wave pressures produced the whip, its magnitude and dependence on pitch would be approximately the same for the cone and the hemisphere, while, if the V^2 forces produced the whip, it will differ markedly for the two heads, as is seen to be the case.

Design Features Influencing Whip

It should be remembered that for all heads the whip is proportional to V_e. In addition, for all torpedoes with a given nose the whip varies inversely as the moment of inertia of the torpedo. Consequently, torpedoes with greater moments of inertia will possess smaller whips at entry, and torpedoes with smaller moments of inertia will have larger whips at entry.

As has been seen, the nose forces producing the whip at entry will vary considerably with the nose shape. However, for a given nose shape some indication can be given of the variation of these forces with the dimensions of the nose. For example, in general the whip will differ for a hemispherical nose of large radius and of small radius. The indication from previous discussions is that usually the nose forces producing the whip at entry for a given nose shape will increase in magnitude with larger nose dimensions. The reason for this is that the forces producing the whip, and hence the whip, appear proportional to the area of the nose. In addition, the whip appears to be caused by unbalanced forces acting on the nose of the torpedo. The time these hydrodynamic forces remain unbalanced is the time for separation of the flow from the nose, which is the time duration of the flow-forming stage. This has been calculated in Section 6.2.1 and from that section it is seen that the time increases with the dimensions of the head. Consequently, we can say that for a given nose shape the impulse and forces producing the whip at entry will increase with increasing head dimensions, roughly as the third power of the linear dimensions of the head. In all cases the time of the flow-forming stage, and hence the time of the whip, decreases with increasing trajectory angle at entry.

The nose shape and size determines the forces producing the whip at entry; however, the characteristics of the torpedo also determine the magnitude of the whip at entry.

As was pointed out, for a given set of entry conditions increasing the moment of inertia I will decrease the whip at entry. Thus, everything else remaining the same, the whip at entry is inversely proportional to the moment of inertia.

In addition, it is clear that the moment arm about the center of gravity of the nose-lift and nose-drag forces will be proportional to the distance from the center of gravity to the nose of the torpedo l_1. Hence, for a torpedo with given head shape and size and fixed I, the quantities a_1, a_2, a_3, and hence the whip, will be proportional to l_1.

We may say that, for a torpedo with a given density and *fixed shape* (primarily a fixed length/diameter) since the moment of inertia is proportional to the fifth power of the length, and since the density remains fairly constant, the whip will vary inversely as the first power of the linear dimensions.

6.2.6 Ricochet

In the discussion of the flow-forming stage of the motion it has been tacitly assumed that the head of the torpedo will be submerged sufficiently for the flow to separate and the torpedo head will continue to submerge. Actually, this is not necessarily true. Thus, when part of the nose becomes submerged, it is possible for the hydrodynamic lift forces to be sufficiently large so that the torpedo "bounces" off the water or ricochets. Ricochet means a motion such that the torpedo is never completely covered by water. Of course, it is expected that a ricochet will occur only for very shallow trajectory angles at entry.

Observations of the ricochet of spheres indicate that the trajectory angle at entry, which must not be exceeded if ricochet is to occur, is given roughly by $18°/\sqrt{\rho_s}$, where ρ_s = density of the sphere. As a matter of fact, this is the underlying principle of a German weapon "Kurt" (a sphere which enters with θ_e very small and at high speed so that it "bounces" along the water surface). The sphere would land on the water with $\theta_e = 6°$ and continue to ricochet until it lost sufficient speed.

Concerning the ricochet of a hemispherical-nose torpedo, the British could not make their 18-inch torpedo ricochet for θ_e down to 10° and $V_e = 250$ knots. In order for the Mark 13 torpedo to ricochet, it is seen from the rough relation $18°/\sqrt{\rho_s}$ that very approximately θ_e must be less than 4.4 degrees. Thus, for very shallow entry angles, it is possible that a torpedo with a hemispherical head will not enter the water but will ricochet.

For torpedoes with ogival heads there will probably be a greater tendency to ricochet; also, a nose-up pitch at entry will produce a greater lift force and hence increase the tendency to ricochet. A hemisphere would not be influenced by the nose-up pitch as would an ogival head. In general, for ricochet very shallow entry angles and high entry velocities are required and also nose shapes that have large nose-up whips at entry. Noses that whip down at entry probably will not ricochet at any entry angle.

6.2.7 Essential Data and Further Research on This Stage of the Motion

Because of its great influence on the future motion of the torpedo, the most important quantity which should be studied during this stage of the motion is the whip at entry.

Compared to the whip all other characteristics of this stage appear to be relatively unimportant. As we have seen, the whip depends both on the nose shape and on the torpedo body. Since the dependence on the body parameters are known, it is necessary to obtain the dependence of the whip on the nose shape. Hence, it appears profitable to tabulate the whip for various noses in the form of a nose-lift coefficient and determine the dependence of this coefficient on the entry conditions.

At present it appears that perhaps the most fruitful approach to a determination of the nose-lift coefficient is by direct experiment with various nose shapes. In this connection the success of some method of modeling the entry whip appears very important as smaller models rather than full-scale tests might be used. The most important unsolved theoretical problem in water entry is a theoretically sound determination of this lift coefficient. At the present stage of the development of the theory, the great analytical difficulties that arise in a determination of the nose-lift coefficient make it appear that a semi-theoretical experimental approach will be more profitable.

Thus future research in water entry should attempt to obtain nose-lift coefficients for various shaped noses and the dependence of the nose lift on the entry conditions.

6.3 MOTION IN THE CAVITY WITH THE NOSE IN CONTACT WITH WATER

The time duration of the stage of the motion which begins when the flow separates from the top of the nose and ends when the tail strikes the side of the cavity will depend on the shape and size of the cavity, on the orientation of the torpedo at the end of the flow-forming stage, on the head shape of the torpedo, and on various other physical characteristics.

In this part we shall discuss first what happens to the water during this stage of entry and then consider the forces acting on the nose of the torpedo. The determination of the behavior of the water and of the forces on the nose requires some knowledge of the pressure distribution about the nose. Finally, the trajectory and behavior of the torpedo in this stage will be discussed, with some mention of the damage sustained.

6.3.1 Flow Separation and Pressure Distribution about the Nose of the Torpedo

Remarks on Flow Separation

As has been mentioned, the flow separates from all sides of the nose of the torpedo, and in this stage of the motion the torpedo travels in a cavity. The water will remain in contact with the nose from the tip around to where the total pressure of the water on the nose falls to zero because of the velocity. Obviously, if the pressure falls below zero there will be no force to keep the water in contact with the nose.

In order to formulate this condition more quantitatively, we must consider the pressure acting on the nose. For the quasi-stationary flow conditions which exist in this stage, the integral of Bernoulli's equation for an incompressible nonviscous fluid is

$$P = \rho g h + P_0 + \tfrac{1}{2}\rho V^2 - \tfrac{1}{2}\rho v^2\,, \tag{12}$$

where P is the pressure at any point on the nose, v is the velocity of the fluid relative to the torpedo at this point, and $\rho g h$ is the gravitational static head. P_0 is the external pressure on the fluid; it is atmospheric pressure for all full-scale launchings, while for some model experiments in pressure tanks it may be controlled and differ from atmospheric pressure. V is the velocity of the torpedo relative to fluid at rest.

The flow will separate from the nose if $P = P_c$, where P_c is the pressure in the cavity. In this stage of the motion, P_c is probably very close to the external pressure P_0 since the cavity is open to the outside. However, it may be somewhat less than the external pressure in the neighborhood of the torpedo nose since the air may be circulating in the cavity.

When $P = P_c$, equation (12) may be written in the form

$$\frac{v^2}{V^2} = 1 + \frac{\rho g h + P_0 - P_c}{\tfrac{1}{2}\rho V^2}\,. \tag{13}$$

The quantity

$$K = \frac{\rho g h + P_0 - P_c}{\tfrac{1}{2}\rho V^2}$$

is defined as the cavitation parameter (also called cavitation number and cavitation index).

In the expression for K, the numerator consists of pressures which tend to prevent a cavity and to keep the flow in contact with the nose, while the denominator may be regarded as the pressure which tends to open a cavity.

Except for a possible circulation of air which may be due to air rushing in after the torpedo at entry, $P_c = P_0$, and, when the torpedo is still at the surface, $h = 0$ so that $K = 0$. As the depth increases, assuming $P_c = P_0$, K increases. In general, even when the cavity is open to the atmosphere $K > 0$, but not very much greater, as may be verified by inserting appropriate numerical values. For example, in Figure 23 for the Mark 13 torpedo with $\theta_e = 20°$ and $V_e = 500$ ft per sec, K is plotted against distance along the trajectory for the cases of $P_c = P_0$ and $P_c = 0$.

Pressure Distribution about the Nose

The flow will separate when $P = P_c$ or when the excess of the hydrodynamic pressure over the external pressure around the nose of the torpedo is zero. In order to determine at what point on the nose this will occur, it is generally necessary to know the pressure distribution around it. A knowledge of the pressure distribution about the nose of the torpedo is

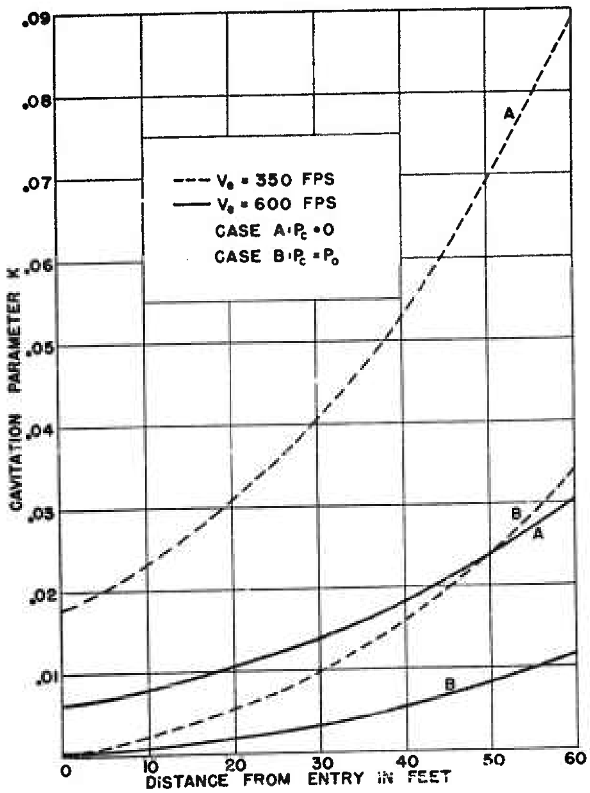

FIGURE 23. Mark 13 torpedo cavitation parameter versus distance from entry (before tail slap).

generally necessary, not only to determine where the flow will break away from the nose, but also to know the forces and moments acting on the torpedo during this stage of the motion.

The problem is quite complicated for, by classical hydrodynamic theory, even the steady-state equations of motion predicting a cavity lead to nonlinear, integro-differential equations that are exceedingly difficult to handle. Most attempts at obtaining the pressure distribution about the nose of the torpedo, the shape of the cavity, the drag force, etc., deal with a closed cavity, which is usually the flow about a larger body than the one under consideration, and knowingly neglect the fact that the cavity is closed at the rear. They then regard the pressures and the flow as of importance only up to the point where the flow breaks away. In addition, these attempts consider only steady state phenomena. Some of these attempts will be briefly discussed:

Potential Flow Method. One general attempt originated by Shaw[3] has been based on the assumption that the pressure distribution about the nose of the torpedo in a cavity is the same as the pressure distribution with potential hydrodynamic flow about the entire torpedo when moving in a steady state through the water without a cavity. The flow and pressure distribution around the nose of the torpedo are assumed to be unaltered by the cavity as long as the pressure is positive. Then the point where the flow breaks away is easily calculated for we know P in equation (12) and the point on the nose where $P = P_c$. By integrating the pressure over the nose of the torpedo up to the point where the flow breaks away, we obtain the drag and lift forces and moments.

Originally this was an ad hoc assumption. However, now there appears some experimental justification of it. The pressure distribution over various shaped noses fitted on a cylinder has been obtained in a water tunnel for various values of the cavitation parameter K, although it was practically impossible to lower K below the value of 0.20. However, since a series of pressure distributions are given for values $K > 0.20$, it appears possible to determine the dependence of the pressure distribution on K. Figure 24 is an example of such a pressure distribution. It is clear from the results of this work that, except for the finer conical noses, *the pressure distribution in the region where $P > 0$ is practically unaltered by changing the value of K.* In addition, from all the results it is clear that, assuming a linear extrapolation to $K = 0$, the point of zero pressure on the torpedo head can be located and the flow will break away at that point. These two observations both seem to justify the method of using the potential flow ($K \to \infty$) about the nose of the torpedo without a cavity to obtain the pressure distribution with a cavity ($K \to 0$).

Of course, a cavity may exist for values of K considerably greater than zero. At the surface $K \to 0$, but as the torpedo goes deeper K increases, and the pressure changes correspondingly.

As an example of an analytical use of this method we shall apply it to a sphere. We find from hydrodynamic theory that the pressure distribution about a sphere in steady flow is

$$P = \rho g h + P_0 + \tfrac{1}{2}\rho V^2 - \tfrac{9}{8}\rho V^2 \sin^2 \eta\,, \tag{14}$$

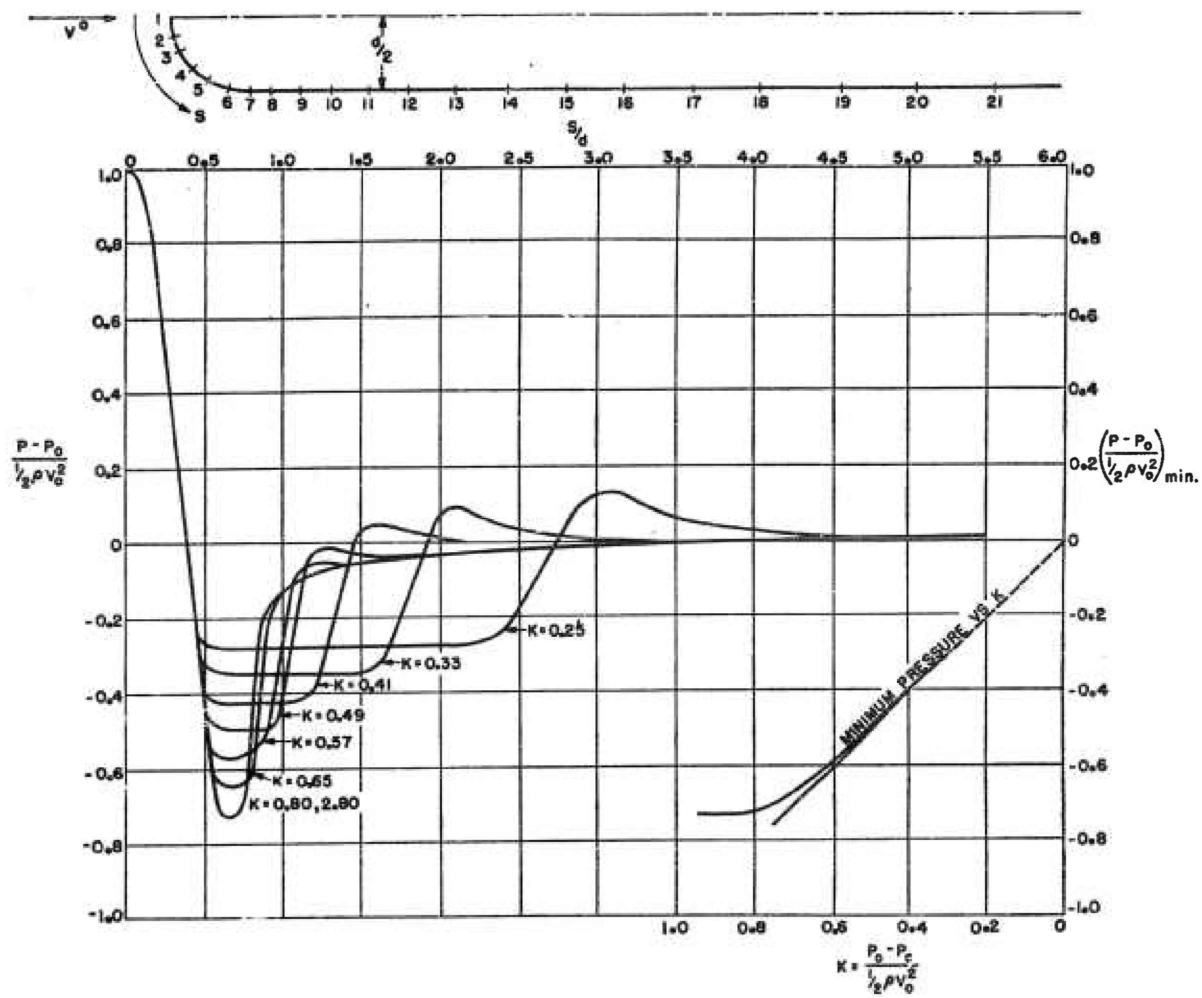

FIGURE 24. Effect of cavitation upon the pressure distribution around a cylindrical body with hemispherical head.

where η is the angle between the outward normal to the surface at the point under consideration and the direction of motion. The flow will separate when $P = P_c$, or at the angle where

$$\sin^2 \eta = \tfrac{4}{9}\left(1 + \frac{P_0 + \rho g h - P_c}{\frac{1}{2}\rho V^2}\right) = \tfrac{4}{9}(1 + K), \quad (15)$$

or at the angle

$$\eta_s = \sin^{-1}\left(\tfrac{2}{3}\right)(1 + K)^{\frac{1}{2}} .$$

Provided the flow does not reform on some part of the torpedo aft of the nose, the drag is given by

$$D = \int_{\substack{\text{over} \\ \text{wetted area}}} \vec{P} \cdot d\vec{A}$$

$$= \tfrac{1}{2}\rho V^2 \int_0^{\eta_s} 2\pi r^2 \sin\eta \cos\eta \left(1 + K - \tfrac{9}{4}\sin^2\eta\right) d\eta .$$

The drag coefficient is defined by

$$C_D = \frac{2D}{\rho} A V^2$$

so that

$$C_D = \left[(1 + K)\sin^2\eta_s - \tfrac{9}{8}\sin^4\eta\right] .$$

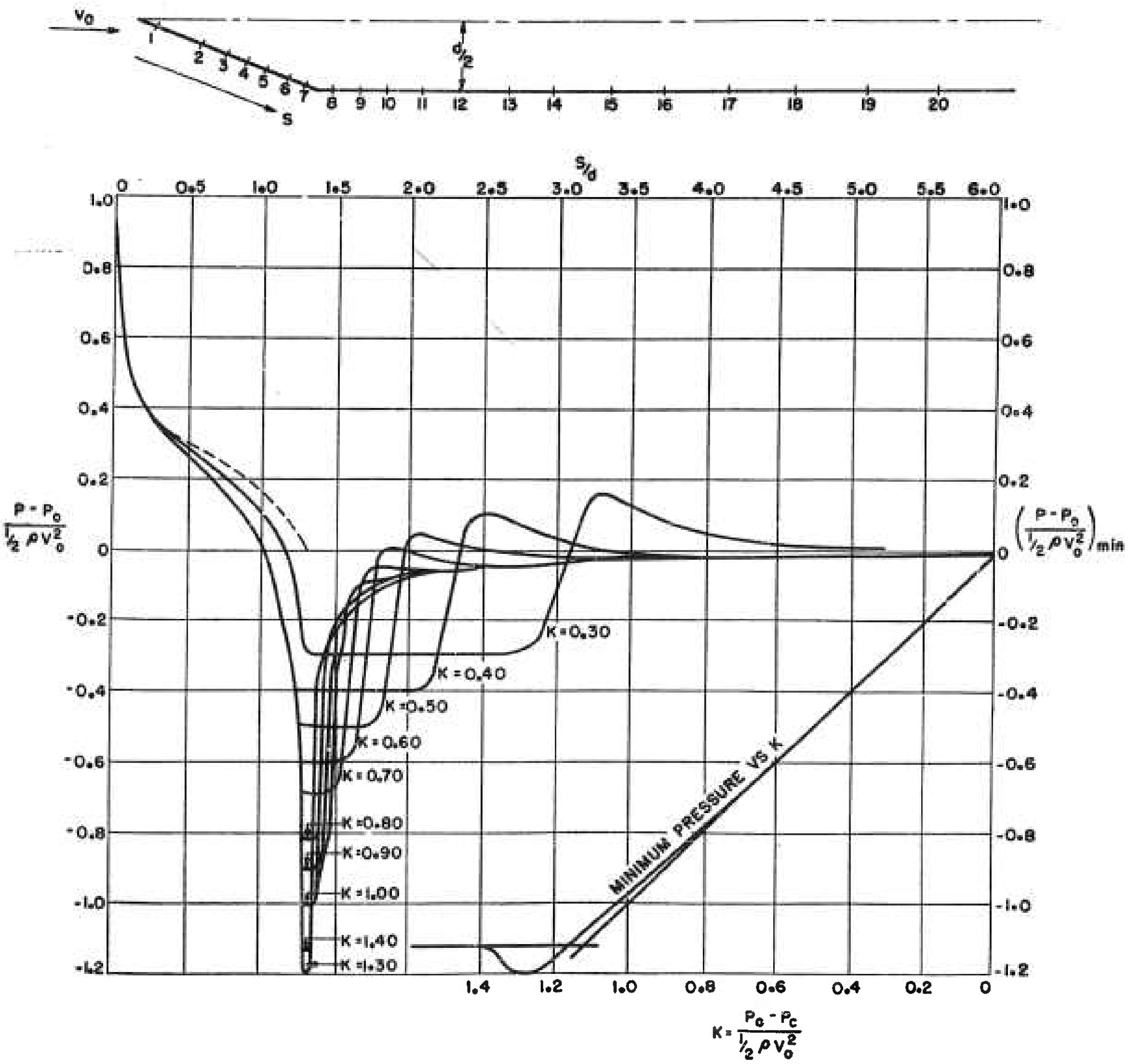

FIGURE 25. Effect of cavitation upon the pressure distribution around a cylindrical body with 45° conical head.

Therefore, from (15)

$$C_D = \tfrac{2}{9}(1 + K)^2 . \tag{16}$$

This Potential Flow Method permits the calculation of pressure distribution, point of flow separation, drag, lift, and moment on any head if the pressure distribution from potential hydrodynamic flow is known. The latter may be obtained by calculation for simple shapes, as has been illustrated for a sphere. However, the essence of usefulness and simplicity of the method is that the pressure distribution may always be obtained by wind or water tunnel measurements of the pressure distribution about a noncavitating projectile.

In general, this method is applicable to all shaped noses at arbitrary pitch or yaw angles as long as the flow does not reform at some point further aft. Clearly, if a torpedo head is at pitch or yaw angle, there will be a drag and lift force acting on the head and a moment about the tip of the head. If one obtains the pressure distribution from a wind or water tunnel, a numerical integration will give the desired coefficients. In some cases, such as fine cone heads, the distribution of positive pressure appears to change with K as shown in Figure 25. In such cases either the distribution must be extrapolated toward $K = 0$ before integration or the hydrodynamic coefficients extrapolated toward $K = 0$. The latter appears the easier method.

Approximate Method for a Sphere. There is perhaps only one result, obtained by G. I. Taylor, in which a cavity is predicted by potential hydrodynamic theory (for a nondecelerating body). In this result the flow about a paraboloid, which would have an infinite drag, is combined with a flow about the body with zero drag to produce the flow about a body which approximates a sphere with finite drag and a cavity. The method is essentially that of combining a series of infinite line sources with a steady stream. By this method the approximate cavity flow about a sphere is obtained, but has not been obtained for other shaped noses.

Source in Infinite Stream. The cavity flow about a sphere has been approximated (in reference 9) by a point source in an infinite stream. Here again, the drag is obtained by integrating the pressures up to the point where the pressure falls to zero. By this method the pressure is given by

$$P = P_0 + \rho g h + \tfrac{1}{2}\rho V^2 \frac{2b^2 r^2 \cos\eta - b^4}{r^4}, \qquad (17)$$

where $b = \frac{3}{4} \times$ radius of a sphere, r is the distance from the point source to the point at which the pressure is being measured, and η is the azimuthal angle measured from the direction of motion with the origin at the point source. By a very similar method to that employed for potential flow one may easily calculate the point of separation and the drag coefficient.

Semiempirical Method. Recently a semiempirical attempt at calculating the pressure distribution was made. In this method a form of the pressure distribution is assumed with constants which are adjusted to produce agreement with experiment. In this attempt it is assumed that for $K = 0$:

$$\frac{P}{\frac{1}{2}\rho V^2} = B \sin\beta_1 \left[1 - b \sin^2(\beta_1 - \beta)\right], \qquad (18)$$

where B = a constant independent of head shape,

β = angle between direction of motion of the torpedo and the tangent to the torpedo nose at the point under consideration,

β_1 = semiangle at the nose of the torpedo ($\beta_1 = 90°$ for a sphere),

b = constant for a particular head shape, depending on the angle at which the flow separates from the head.

Probably numerous other expressions could be written which, with the substitution of suitable determined constants, would give adequate approximations to the pressure distribution. In each case, however, such expressions must be verified by comparison with some other method so that it is ultimately useful only if it is especially convenient for integration.

A Variational Method. One result has been obtained for the flow about a sphere in a closed cavity. By means of a doublet and a series of sources, a flow is set up, and then, by means of a variational method, the cavity is shaped so that the boundary condition (namely, that the pressure on the free streamline is the same as at the point of separation) is satisfied. By this method the separation point is chosen initially, and a corresponding value of K results. Thus far, not many results have been obtained as the method is quite lengthy. In addition, it has been applied only to the case of a sphere.

Noses with Discontinuities. Some separate consideration must be given to noses with discontinuities. By a discontinuity is meant a sudden change in slope (such as a cone on a cylinder) at some point of pressure on the head so that, if the water is to remain in contact with the torpedo, it must flow around a corner. The determination of the point of flow separation for these heads does not require a knowledge of the pressure distribution.

From hydrodynamic theory it may be proved that at such a discontinuity the velocity of the water relative to the nose of the torpedo becomes infinite (limited only by viscosity), and hence the pressure becomes negatively infinite; that is, infinite suction of the water is required to cause it to flow around a discontinuity without leaving the surface about which it is flowing.

Of all these suggested methods of estimating the pressure distribution, the only one that appears really useful is the potential flow method. This is really a method for interpreting pressure-distribution measurements that can be made under noncavitating conditions in terms of the pressures that exist in a cavity. In the last analysis its justification is empirical, and it is not really a theoretical method.

Point of Flow Separation

As has been indicated above, the point of flow separation is just one aspect of the pressure distribution and can be seen when the pressure distribution is known. For a hemisphere the potential flow method gives separation at $\eta = 42°$, and water tunnel measurements give 45°. The other methods that seem to have less satisfactory foundations suggest values between 55° and 75°. The exact point of zero pressure may be varied considerably without affecting the integrated forces and moments appreciably.

The point of separation for ogives and spherogives can be determined by water or wind tunnel measurements. If the spherical nose of a spherogive has an angle greater than 45°, the separation will probably occur on it and be entirely independent of the ogive that follows.

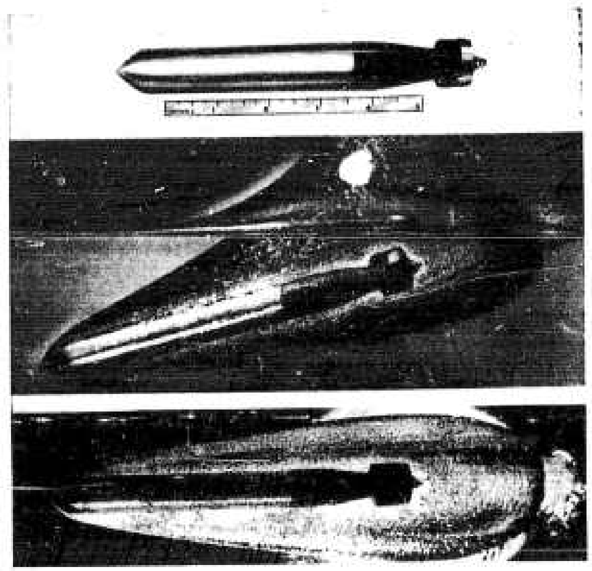

FIGURE 26. Flow separation on 1-in. model of the Steel Dummy with a conical nose smoothly joined to the torpedo. Notice that the nose appears to be the only part of the model in contact with the water.

In the case of cone heads the flow will break away at the shoulder of the cone. This is illustrated in Figure 26. Similarly for flat heads, kopfrings, and truncated cones the flow will break away at the discontinuity.

Kinematic Theory of Cavity Shape

As long as only the nose of the torpedo is in contact with the water, the behavior of the rest of the cavity is of little importance. However, the torpedo soon falls over so as to be in contact with the cavity wall, and it is important to know something about the cavity size and shape to tell how far the torpedo will fall. In undertaking a theory based on the laws of hydrodynamics, very great difficulties are encountered and no significant progress has been made. The best that can be done is an empirical description based on an observation by Blackwell[6] that the diameter of the cavity at any point can be described as a parabolic function of the time.

The observations upon which the description is based were made on the cavities due to spheres dropped vertically into water. It was observed that the water started to move radially with a velocity proportional to the velocity with which the sphere passed the point in question. Hence there may be defined a coefficient λ such that

$$\lambda = \frac{\text{Initial radial velocity of the cavity}}{\text{Velocity with which the torpedo nose passed this point}}$$

The second observation was that the radial velocity of the cavity wall decreased with a deceleration proportional to the depth.

To apply this kind of description to a torpedo entry cavity it is necessary to neglect many things, some of which may be important. Gravity is neglected, and the torpedo is considered to follow a straight path at an angle θ_e with the horizontal. Furthermore, the effect of the water surface is neglected, and the cavity is regarded as a surface of revolution about the axis. Any effect due to air pressure inside the cavity is also ignored.

The axis of x is taken along the axis of the cavity with the origin at the surface of the water. The radius of the cavity y is then regarded as a function of x and of the time. If $t(x)$ is the time measured from the time at which the separation radius of the head, r_s, passes the point x, the above assumptions give

$$y(x, t) = r_s + \lambda V(x)t(x) - \frac{\mu x \sin \theta_e}{2r_s} t^2(x) \,. \quad (19)$$

With the r_s in the denominator, the constant quantity μ can be expected to be independent of the scale of the cavity if the Froude law holds.

Since the torpedo moves with a deceleration proportional to the square of the velocity,

$$V(x) = V_e e^{-kx} \,,$$

$$t(x) = t - \frac{1}{kV_e}(e^{kx} - 1) \,,$$

with $k = C_D \rho A/2M$. Here t is measured from the time of impact, but the expressions are valid only for such t and x that $t(x) > 0$.

As a result, the radius of the cavity at the time t after impact and at a distance x along the path is

$$y(x,\, t) = r_s + \lambda V_e e^{-kx}\left[t - \frac{1}{kV_e}\,(e^{kx} - 1)\right]$$
$$- \frac{\mu x \sin \theta_e}{2r_s}\left[t - \frac{1}{kV_e}\,(e^{kx} - 1)\right]^2. \quad (20)$$

The two constants λ and μ must be experimentally determined. λ appears to be about 0.15 for a hemispherical nose. This means that the initial cone angle is considerably less than would be indicated by the angle of flow separation on the sphere. This is associated with the fact that the empirical description of the cavity covers only its major features and not all details. For blunter or sharper noses it is expected that λ will be correspondingly greater or less than 0.15.

There is some indication that μ is about 8 ft per sec per sec although this is only very crudely known.

Later on we shall want to know the cavity width at a given value of x at a time such that the tail of the torpedo reaches the point x. Let us say we want $y(x)$ at a time t when a point b feet aft of the nose reaches the point x under consideration. From equation (20) it is clear that we are interested in $y(x, t)$ for $t = (1/kV_e)\,(e^{k(x+b)} - 1)$.

Hence

$$y(x) = r_s = \frac{\lambda}{k}\,(e^{kb} - 1) - \frac{\mu x \sin \theta_e e^{2kx}\,(e^{kb} - 1)^2}{2k^2 V_e^2 r_s}. \quad (21)$$

It is clear from this expression that the cavity width at a point on the torpedo b feet aft of the nose (near the tail of the torpedo) will decrease with (1) increasing distance along the trajectory, (2) decreasing entry velocity, (3) increasing trajectory angle at entry.

6.3.2 Forces and Moments Acting on the Torpedo Nose

In the previous section, various methods of estimating the pressure distribution about the nose of the torpedo were mentioned. Since, during this stage of the motion, only the nose is in contact with the water, a knowledge of this pressure distribution will determine the torpedo motion. The resultant force can be resolved into a drag force that acts along the trajectory and a lift force that acts perpendicular to it. The effective point of application can be specified by giving the moment of the force about the tip of the nose. These forces and this moment can be described in terms of coefficients C_D, C_L, and C_M since it is assumed that all forces are proportional to the velocity squared.

Hemispherical Nose

Most of the studies of forces have been carried out on spheres or hemispherical noses because of the simplicity introduced by the symmetry. Since the forces are pressure forces they act perpendicular to the surface and hence through the center of the sphere. As a consequence only the drag force and its coefficient C_D are of importance.

Experimental Determinations. Numerous experimental determinations of C_D have been made for spheres dropped vertically into water. In such cases the observed deceleration will depend on the density of the sphere since much of the momentum that is destroyed will reside in the water itself. One way in which to formulate the results is to assume an effective mass of water that partakes of the motion of the sphere. The equation of motion is then written

$$(M + M')\,\frac{dv}{dt} = -C^\circ_D\,\frac{\rho}{2}\,AV^2. \quad (22)$$

If now the forces on the sphere alone are considered, one has

$$M\,\frac{dv}{dt} = -C_D\,\frac{\rho}{2}\,AV^2, \quad (23)$$

where

$$C_D = \frac{M}{M + M'}\,C^\circ_D. \quad (24)$$

Since M is proportional to the density of the sphere and M' to the density of the water, this relationship may be written

$$C^\circ_D = \left(1 + \frac{c}{\sigma}\right) C_D, \quad (25)$$

where σ is the density of the sphere and c is a proportionality constant.

The assumptions involved in equation (25) are largely gratuitous and can be justified only in case the observations lead to a value of $C°_D$ that is independent of density. The evidence on this point is not entirely conclusive. Values between $C°_D = 0.26$ and 0.37 appear to have been obtained.

For a torpedo with a hemispherical nose the proportionality constant c will be very small, and the observed value of C_D should be close to $C°_D$. The extensive set of measurements at the CIT–TLR give $C_D = 0.28$ when the area used in the expression is the projected area of the sphere and is not the maximum cross section of the torpedo.

Theoretical Estimations. The value of the drag coefficient based on the Potential Flow Method has been shown to be $\frac{2}{9}(1 + K)^2$. This coefficient has also been obtained by integrating the observed pressure distribution. The results obtained by these two methods are similar but differ by a constant factor.

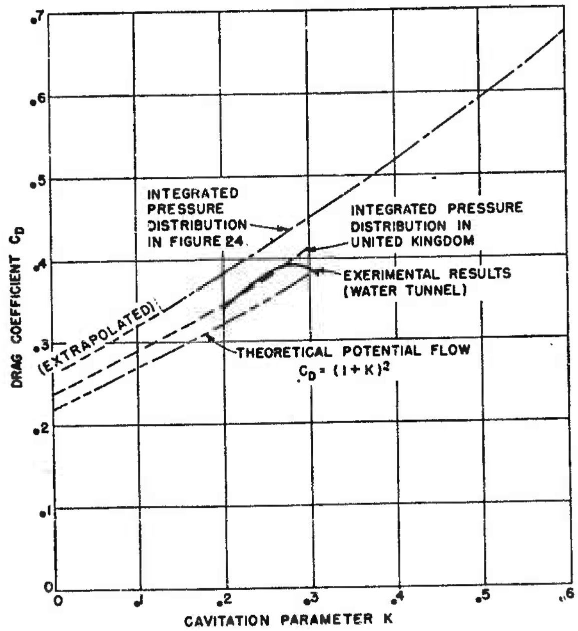

FIGURE 27. Drag coefficient versus cavitation parameter for spherical nose.

K	$\frac{2}{9}(1 + K)^2$	Integrated pressure
0.0	0.22	0.24
0.1	0.27	0.29
0.2	0.32	0.35
0.3	0.38	0.41

Figure 27 illustrates some values of the drag coefficient as a function of cavitation parameter. One curve represents the results of numerieally integrating the pressure distributions in Figure 24 for the accessible values of K and then extrapolating to $K = 0$. Another represents similar integrations carried out in the report by Shaw.[3] The third represents the theoretical coefficient based on potential flow, and the fourth represents some observed values.

The drop-off in the observed values as K increases is due to the reforming of the flow on the afterpart of the body. Taking this into account, the agreement with the theory is reasonably good. The difficulty in associating these values with those observed for torpedoes is partly due to a lack of knowledge of the proper value of K to use for the torpedo launchings.

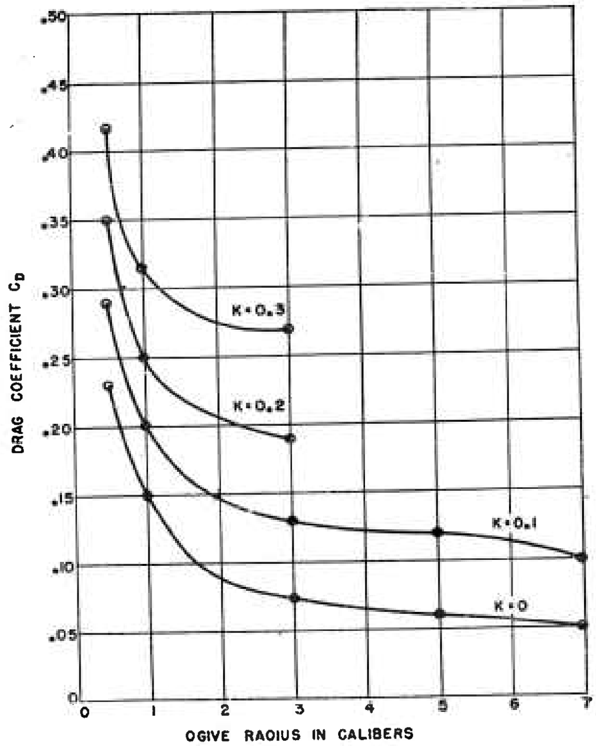

FIGURE 28. Nose-drag coefficients versus ogive radius in calibers obtained by numerically integrated potential flow pressure distributions in region where $P/\frac{1}{2}\rho V^2 + K > 0$.

Other Shaped Noses

Figure 28 gives some values of the drag coefficient C_D based on observed pressure distribution over ogive heads. There are no suitable experimental observations with which to compare these results. Similarly, by integration of the pressure distributions the other coefficients can be obtained.

It is frequently desirable to treat the forces parallel and perpendicular to the torpedo axis rather than parallel and perpendicular to the trajectory. These will be designated as C_D' and C_L'. Some values of these coefficients are given in the following table for a 1.4 caliber ogive.

1.4 Caliber Ogive

K	0	0.05	0.10	0.20
		$\alpha = 0°$		
C_D'	0.120	0.145	0.169	0.226
		$\alpha = 6°$		
C_D'	0.120	0.141	0.164	0.218
C_L'	0.046	0.053	0.061	0.079
$-C_M'$	0.038	0.046	0.056	0.080
		$\alpha = 15°$		
C_D'	0.117	0.135	0.156	0.203
C_L'	0.113	0.131	0.150	0.195
$-C_M'$	0.102	0.124	0.146	0.210

Thus it appears that for $K = 0$

$$\begin{aligned} C_D' &= 0.119\,, \\ C_L'/\alpha &= 0.0076\,, \\ -C_M'/\alpha &= 0.0065 \text{ (destabilizing)}\,. \end{aligned}$$

Other values may easily be obtained from the table.

For a flat nose, experiments on 1-in. models seem to indicate $C_D = 0.77$. Various other values have been obtained by experiment, all of them being within about 20 per cent of this value and scattering about it.

By integration of observed pressures $C_D = 0.72$, which is in very close agreement with experimental results. C_L has not been calculated.

It appears that the force coefficients can be estimated with fair accuracy from the measurement of pressure distributions in the cavitating state in water tunnels or with slightly less certainty from similar measurements in the noncavitating state or in wind tunnels. It is then possible to predict the motion of a body from measurements that can be made on such models.

6.3.3 Motion of the Torpedo during This Stage

The object of the study of the forces on the nose of the torpedo when in the cavity and of the changes in size and shape of the cavity itself is to describe the motion of the torpedo during this stage.

After the flow-forming stage the axis of the torpedo possesses a whip (angular velocity in the vertical plane) given by

$$\frac{\Delta(I\dot{\alpha})}{V_e} = a_1(\theta_e) + a_2(\theta_e)\alpha_e\,, \tag{26}$$

where α_e is the pitch angle at entry. a_1 and a_2 are experimentally determined functions that depend on the nose shape and area. a_1 and a_2 probably have similar dependence on the trajectory angle at entry θ_e in some manner which is not completely known. There are indications that they may vary as $\cot \theta_e$. In the horizontal plane the angular velocity of the axis of the torpedo is

$$\frac{\Delta(I\dot{\psi})}{V_e} = a_3\psi_e\,, \tag{27}$$

where ψ is the yaw angle at entry. Probably $a_3 = a_2$. It was pointed out that at the end of the flow-forming stage α differs from α_e and ψ differs from ψ_e, but the difference is usually not large. It is less than about 0.2° for the Mark 13 torpedo.

From these relations it is clear that, as long as the center of pressure of the nose forces lies forward of the center of gravity of the torpedo, the more nose-down the pitch angle is at entry, the smaller the whip; that is, the torpedo tends to "stub its toe." With a nose-down pitch at entry the drag force on the nose usually produces a moment about the center of gravity of the torpedo which tends to make the torpedo rotate tail-up or nose-down, while with a nose-up pitch the moment of the drag forces is in the opposite direction, thus tending to make the torpedo rotate tail-down and nose-up. It is therefore clear that for a nose-up pitch, due to the large nose-up whip and the drag moment, the torpedo rotates tail-down and the tail soon strikes the bottom wall of the cavity; while for a large enough nose-down pitch, the nose-up whip is small and the drag forces will produce a moment which will cause the torpedo tail to strike the top of the cavity wall. For some intermediate value of α this reversal occurs. One of the results of the subsequent calculations is the magnitude of the pitch angle α_c separating these two types of motion.

In the horizontal plane it is clear that, for a fine nose, a nose-right yaw will produce a nose-right angular velocity and a drag moment pushing the tail left or nose right, thus insuring that the torpedo tends to rotate to the left wall of the cavity.

The behaviors in the vertical plane and in the horizontal plane are generally quite different for noses in which the center of curvature of the nose is aft of the center of gravity. In this case the quantities a_1, a_2, and a_3 are negative with a resulting angular velocity in the opposite direction to the usual case, that is, we get a stabilizing moment for this type of a nose as opposed to a destabilizing moment for the finer noses.

From Figure 29 we see the forces acting on the torpedo and may readily write down the equations of motion. Gravity is neglected since this force is quite

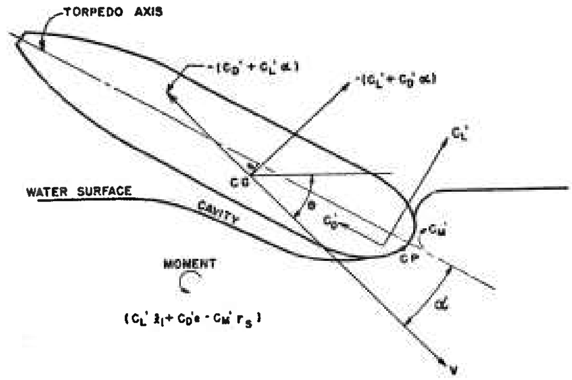

FIGURE 29. Forces and moments acting on torpedo (nose) before tail slap. To obtain forces and moments multiply coefficients by $(\rho/2)AV^2$.

negligible compared to the other forces involved. In addition, in so far as the moment of the lift force about the nose is large compared to the moment of the drag force at the nose, the ratio $-C_M'/2C_L'$ gives the fraction of a diameter of the nose by which the lift force lies aft of the tip of the nose. Hence we know l_1, the distance from the point of application of the lift force to the center of gravity. In the following analysis we shall consider the drag moment about the axis described by the moment coefficient C_M'. The equations of motion for $\sin\alpha = \alpha$, $\cos\alpha = 1$ are, along the trajectory,

$$M\frac{dV}{dt} = -\frac{\rho}{2}(C_D' + C_L'\alpha)AV^2\,; \tag{28}$$

perpendicular to the trajectory in the vertical plane,

$$MV\frac{d\theta}{dt} = -\frac{\rho}{2}(C_L' - C_D'\alpha)AV^2\,; \tag{29}$$

rotation about CG in the vertical plane,

$$I(\ddot\alpha - \ddot\theta) = \frac{\rho}{2}C_L'l_1AV^2 - C_M'\frac{\rho}{2}r_sAV^2 + \frac{\rho}{2}C_D'e\cos\phi AV^2\,; \tag{30}$$

where l_1 is the distance from the center of pressure of the lift forces to the center of gravity.

Similar equations hold in the horizontal plane:

C_L' and C_M' are linear functions of α for small angles, and it is to be remembered that the effective pitch angle is

$$\alpha - \left(\frac{l_1}{V}\right)(\dot\alpha - \dot\theta)\,.$$

Then

$$C_L' = C'l\left[\alpha - \frac{l_1}{V}(\dot\alpha - \dot\theta)\right],$$

$$C_M' = C_m'\left[\alpha - \frac{l_1}{V}(\dot\alpha - \dot\theta)\right].$$

It was found in earlier sections that for almost all noses C_D' is constant, practically independent of α and ψ. Hence $C_L'\alpha$ in equation (28) is of second order in α and is certainly negligible compared with C_D'.

The equations of motion then become

$$\frac{dV}{dt} = -\frac{\rho A}{2M}C_D'V^2\,, \tag{31}$$

$$V\frac{d\theta}{dt} = -\frac{\rho A}{2M}\left\{C'l\left[\alpha - \frac{l_1}{V}(\dot\alpha - \dot\theta)\right] - C_D'\alpha\right\}V^2, \tag{32}$$

$$\ddot\alpha - \ddot\theta = \frac{\rho A}{2I}\left\{(l_1C'l - C_m'r_s)\left[\alpha - \frac{l_1}{V}(\dot\alpha - \dot\theta)\right] + C_D'e\cos\phi\right\}V^2\,. \tag{33}$$

Since $d/dt = V(d/ds)$ where s is the distance along the trajectory, these equations can be combined to give

$$\alpha'' + 2G\alpha' - B\alpha = Q\,, \tag{34}$$

where the primes indicate differentiation with respect to s and

$$2G = \frac{\rho A}{2M}\left[C_l'\left(1 + \frac{Ml_1^2}{I}\right) - C_m'r_s\frac{M}{I}l_1 - 2C_D'\right],$$

$$B = \frac{\rho A}{2I}\left(l_1C_l' - r_sC_m'\right)\left(1 + \frac{\rho A}{2M}C_D'l_1\right) + \left(\frac{\rho A}{2M}\right)^2 C_D'\left(C_l' - C_D'\right),$$

and

$$Q = \frac{\rho A}{2I}C_D'e\cos\phi\left(1 + \frac{\rho A}{2M}C_l'l_1\right).$$

For many purposes the roll angle ϕ may be treated as a constant in the study of pitching and yawing and the solution of (34) with Q a constant can be easily written down. If α_0 and α_0' are the values of α and α' respectively when $s = 0$,

$$\alpha = \frac{1}{2F}\left[(F+G)\left(\alpha_0 - \frac{Q}{B}\right) + \alpha_0'\right]e^{(F-G)s}$$

$$+ \frac{1}{2F}\left[(F-G)\left(\alpha_0 - \frac{Q}{B}\right) - \alpha_0'\right]e^{-(F+G)s} + \frac{Q}{B}, \quad (35)$$

where $F = (G^2 + B)^{1/2} > G$. The initial pitch angle, α_0, is the pitch angle with which the torpedo strikes the water plus a small correction for the refraction of the trajectory at impact. The initial rate of change, α_0', is connected with the pitching angular velocity by $\alpha_0' = \dot{\alpha}_0/V_e$. $\dot{\alpha}_0$ is essentially the angular velocity of the whip.

Since $F > G$, and in fact for the Mark 13 torpedo $F >> G$, the first exponential in equation (35) is increasing and the second is decreasing. Hence after a sufficient distance the sign of α is governed by the sign of $[(F + G)(\alpha_0 - Q/B) + \alpha_0']$. If this quantity is positive the torpedo will swing to the bottom of the cavity. If it is negative the swing will be to the top of the cavity.

In the limiting case, in which $[(F + G)(\alpha_0 - Q/B) + \alpha_0'] = 0$, the final value of α is Q/B. The pitch angle for which this occurs is called the critical pitch angle and satisfies the relationship

$$\alpha_c = -\frac{\alpha_0'}{F+G} + \frac{Q}{B}. \quad (36)$$

Since

$$\alpha_0' = \frac{a_1(\theta) + a_2(\theta)\alpha_c}{I},$$

this reduces to

$$\alpha_c = \frac{-a_1(\theta) + \left(\dfrac{Q}{B}\right) I(F+G)}{a_2(\theta) + I(F+G)}. \quad (37)$$

This critical pitch is of great importance because it represents the dividing line between those launchings in which the torpedo swings to the bottom of the cavity and makes only a shallow dive and those in which the torpedo swings to the top and may dive very deep.

A similar analysis can be made of the yawing motion, but because of the symmetry of the situation the critical yaw angle is zero.

Motion in the Vertical Plane

At this point we may understand the reason for the great emphasis placed on the value of the whip at entry in the last part. From equation (36) it is clear that the greater the whip at entry the more nose-down the critical pitch, and hence the greater the nose-up whip at entry the smaller the chance that the torpedo will rise to the top of the cavity and, as we shall see later, dive deeply. Thus it is the whip at entry, which is obtained from θ_e and α_c, that determines how large a nose-down pitch angle can be permitted for finer heads before the torpedo goes to the top of the cavity. It should be carefully noted that both in the vertical plane and in the horizontal plane α_c as well as α_0 and α_0' in equation (36) are all independent of the entry velocity V_e. *Thus the behavior of the torpedo and the trajectory of the torpedo during this phase of the motion is practically independent of the entry velocity V_e.*

For noses whose center of curvature lies aft of the center of gravity (such as flat noses), $a_1 < 0$ and $a_2 < 0$ so that a critical pitch angle exists. This is generally nose-up since $[a_2(\theta) + I(F + G)]$ is usually positive. Hence it appears that for a flat nose α_c will be positive, that is, even for a small nose-up pitch, the torpedo will go to the top of the cavity. This is just the reverse of what will happen with, let us say, a hemispherical nose.

The critical pitch angle α_c depends on θ_e through the dependence of a_1 in equation (26) on θ_e. As has already been indicated this dependence is not known. There are indications that a_1 varies as cot θ_e. At any rate, for finer noses it is clear that the absolute magnitude of α_c decreases with increasing θ_e.

α_c depends on the roll angle through the term Q/B. However, this term is generally small since the metacentric height e is small. The magnitude of α_c for different values of ϕ for the Mark 13 torpedo will be given a little later.

For torpedoes to be used in shallow water it is desirable to have α_c sufficiently nose-down so that the torpedo will almost always swing to the bottom of the cavity. This is true even though the upturning trajectory leads to a broach for the torpedo can frequently withstand a broach but not an impact with the bottom.

Equation (37) shows the way in which the various design features of the torpedo affect the critical pitch angle. The head shape affects the coefficients $a_1(\theta_e)$ and $a_2(\theta_e)$ as well as the various coefficients appearing in F, G, Q, and B. The effect of the moment of inertia is also clear.

As illustrations of the use of these equations, let us consider the behavior of a Mark 13 torpedo and of the CIT Steel Dummy. These two bodies have the same external shape but different values of I and M. For the Steel Dummy $e = 0$.

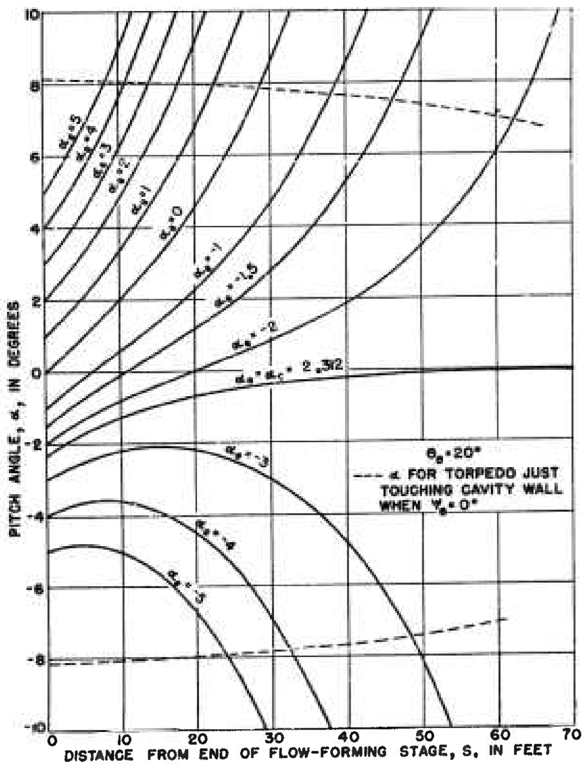

FIGURE 30. Mark 13 torpedo (neglecting metacentric height). Pitch angle versus distance from end of flow-forming stage for various pitch angles at entry (equation 26).

Both of these bodies have hemispherical noses so that $C_l' = C_D = C_D' = 0.28$ and $C_m' = 0$. The constants in equation (37) are then

Mark 13	Steel Dummy
$G = 0.0033$	$G = 0.0029$
$F = 0.059$	$F = 0.065$
$B = 0.0035$	$Q = 0$

Figures 30 and 31 show the pitch angle α as determined from equation (35) plotted against distance for various values of the pitch at entry α_e. In plotting these curves the pitching angular velocity has been obtained from the whip as given by equation (26).

Figures 32 and 33 show the yaw angle calculated in a similar fashion with the assumption that there is no initial yawing angular velocity.

Similarly Figures 34 and 35 give the rate of change of pitch with distance along the trajectory and Figures 36 and 37 give the corresponding rate of change of yaw angle. To obtain the time rate of change, these

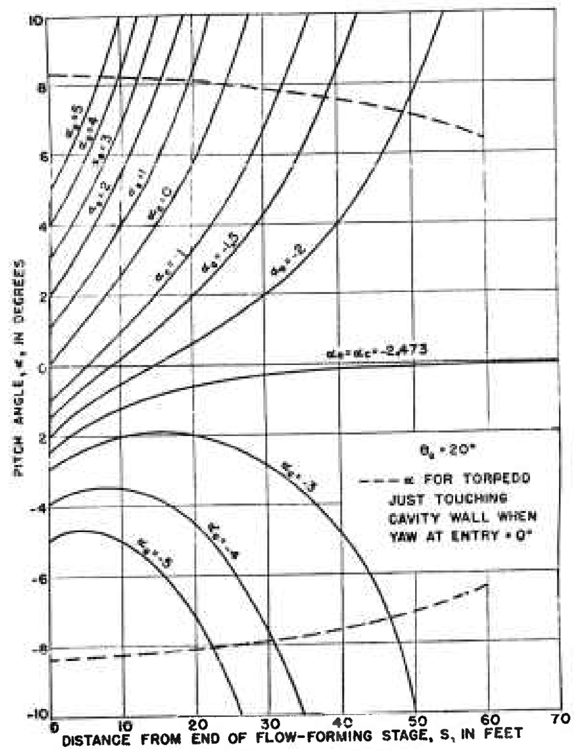

FIGURE 31. Steel Dummy. Pitch angle versus distance from end of flow-forming stage for various pitch angles at entry (equation 26).

values must be multiplied by the corresponding velocity, $V = V_e e^{-ks}$.

POSITION OF TORPEDO AT TAIL SLAP

As the torpedo swings to one side or the other of the cavity it soon comes in contact with the cavity wall. This is an important point in the history of the water entry since new forces are brought into play that must be taken into account. The analysis thus far given is valid only up until the tail slap.

Equation (21) gave the radius of the cavity at a point b feet aft of the nose as

$$y_b(x) = r_s + \frac{\lambda}{k}(e^{kb} - 1) - \frac{\mu x \sin\theta_e e^{2k}(e^{kb} - 1)^2}{2k^2 V_e^2 r_s},$$

with μ approximately 8 ft per sec per sec and $\lambda = 0.15$ for a hemispherical nose. The condition that the torpedo strikes the cavity wall at a point b feet aft of the nose is that

$$b(\alpha^2 + \psi^2)^{1/2} + r_b = y_b$$

or

$$(\alpha^2 + \psi^2)^{1/2} = \frac{y_b - r_b}{b},$$

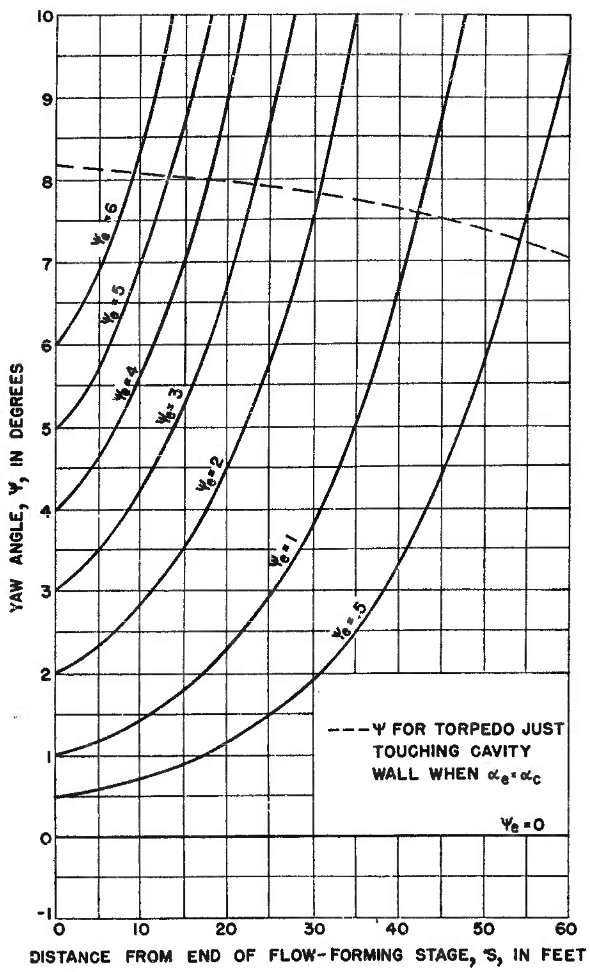

FIGURE 32. Mark 13 torpedo. Yaw angle versus distance from end of flow-forming stage for various yaw angles at entry. The curves are symmetrical about $\psi_e = 0$.

where r_b is the radius of the torpedo at the point of contact.

Figures 30 and 31 show also the value of α that satisfies this condition when b is taken as 9 ft and $\psi = 0$. There is clearly a positive as well as a negative value of α that satisfied this condition. These correspond to the torpedo striking the bottom or the top of the cavity. The significance of the critical pitch angle is brought out very clearly in these curves. For $\alpha_e = -2°$ the Mark 13 torpedo strikes the bottom of the cavity at about 64 ft from impact and with a pitch about 7° nose-up. However, for $\alpha_e = -3°$ the torpedo never strikes the bottom at all but strikes the top about 48 ft from the impact and with a nose-

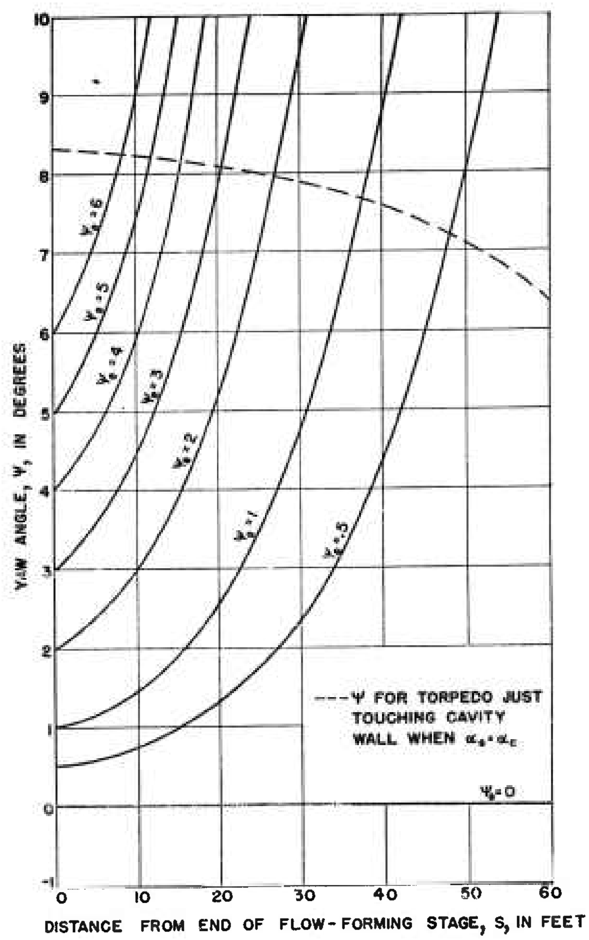

FIGURE 33. Steel Dummy. Yaw angle versus distance from end of flow-forming stage for various yaw angles at entry. The curves are symmetrical about $\psi_e = 0$.

down pitch of about 7.5°. To these distances should be added some 4.5 ft as the distance the torpedo travels during the flow-forming stage.

In Figures 38 and 39 the distance to tail slap is plotted against α_e for the Mark 13 torpedo for $\phi_e = 90°$ so that the metacentric height is zero, and for the Steel Dummy. The solid curve is for $\psi_e = 0$ while the dotted curve is for $\psi_e = 3°$. As is expected, S is diminished with increasing ψ_e. On the curve of S versus α_e for the Steel Dummy are included points of observed distance to tail slap versus α_e obtained at the CIT–TLR. These points are obtained from an indication on sound records when the torpedo tail strikes the cavity wall. Generally, at the CIT–TLR $\psi_e = 1°$ so that these points are expected to lie near the curve for $\psi_e = 0$ and possibly slightly below it.

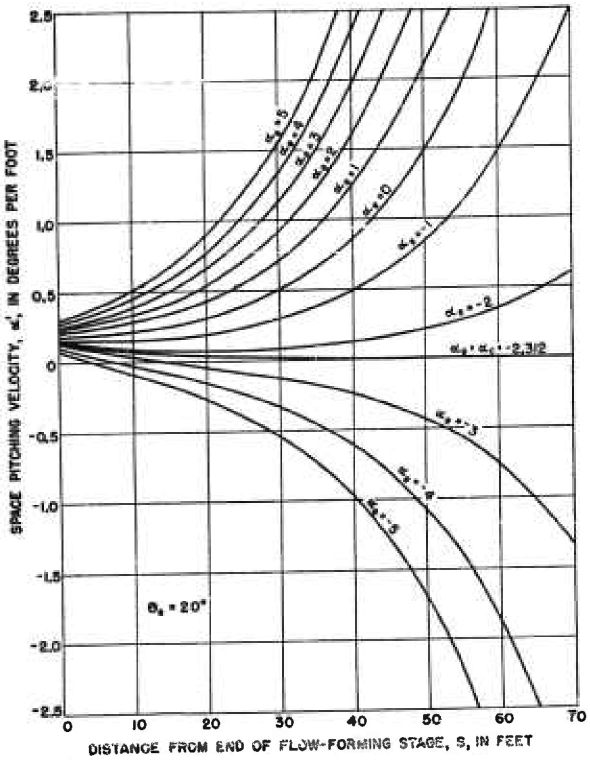

FIGURE 34. Mark 13 torpedo (neglecting metacentric height). Space pitching angular velocity versus distance from end of flow-forming stage for various pitch angles at entry.

The agreement between theory and experiment is quite clear and is gratifying. Besides serving as a verification of the theory of the torpedo motion during this stage, it also offers some corroboration of the kinematic theory of cavity shape and the constants λ and μ which were used.

The angle the plane which includes the trajectory and the point of tail slap makes with the vertical plane is given by

$$\delta_1 = \tan^{-1}\left(\frac{\psi(S)}{\alpha(S)}\right),$$

and the angle the direction of motion of the torpedo at tail slap makes with the vertical plane is given by

$$\delta_2 = \tan^{-1}\left(\frac{\psi'(S)}{\alpha'(S)}\right),$$

where (S) denotes the value of the quantity at tail slap. It is clear that δ_1 and δ_2 are small when $\psi_e \sim 0$ and are large when $\alpha_e \sim \alpha_c$.

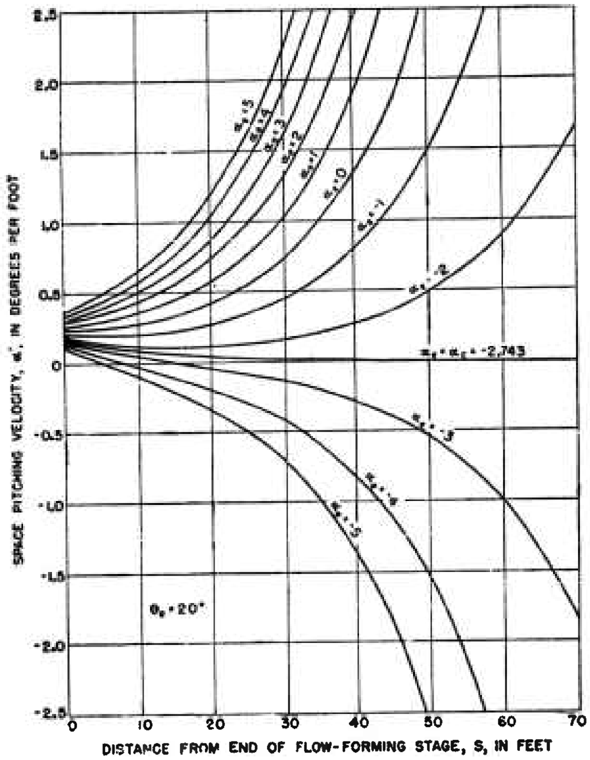

FIGURE 35. Steel Dummy. Space pitching angular velocity versus distance from end of flow-forming stage for various pitch angles at entry.

For the critical pitch angle at entry we find, by inserting the numerical values in the expression (37), the following magnitudes for $\theta_e = 20°$:

Mark 13 torpedo

$\alpha_c = -2.67°$ for zero roll,
$\alpha_c = -2.31°$ for 90° roll,
$\alpha_c = -1.94°$ for 180° roll.

CIT Steel Dummy torpedo

$\alpha_c = -2.47°$.

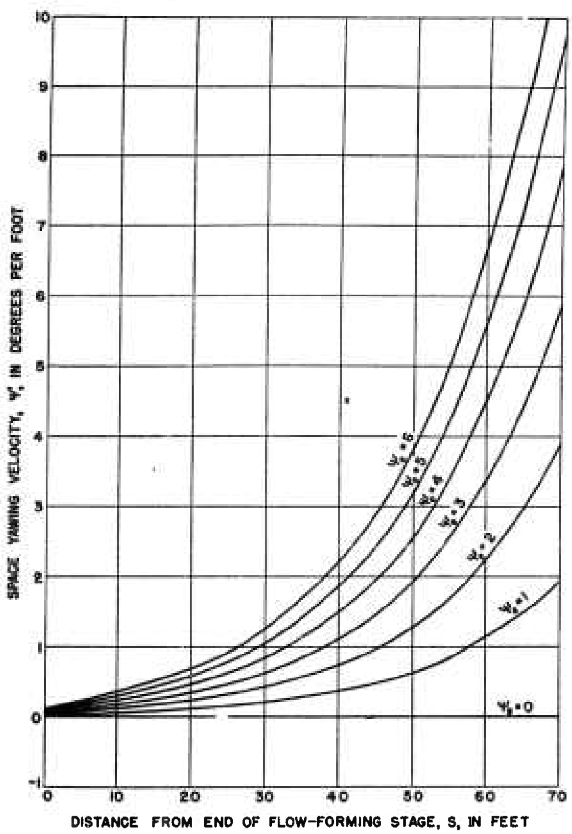

FIGURE 36. Mark 13 torpedo. Space yawing angular velocity versus distance from end of flow-forming stage for various yaw angles at entry. Figure is symmetrical about $\psi_e = 0$.

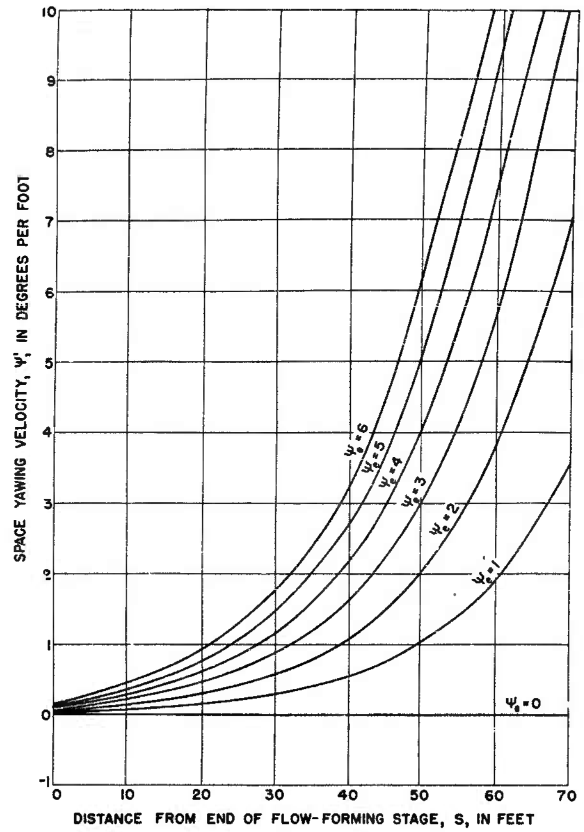

FIGURE 37. Steel Dummy. Space yawing angular velocity versus distance from end of flow-forming stage for various yaw angles at entry. Figure is symmetrical about $\psi_e = 0$.

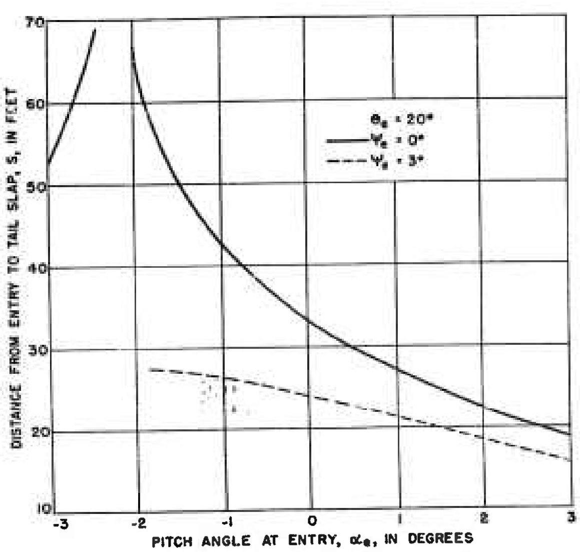

FIGURE 38. Mark 13 torpedo (neglecting metacentric height). Distance from entry to tail slap versus pitch angle at entry.

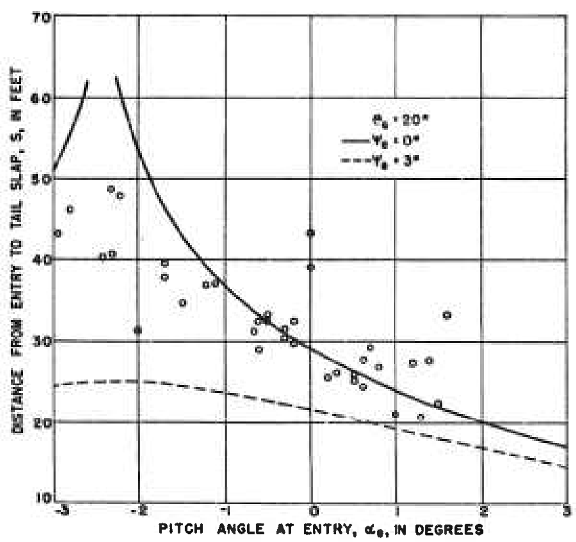

FIGURE 39. Steel Dummy. Distance from entry to tail slap versus pitch angle at entry. Points are observations of this distance from sound records at CIT-TLR.

These results appear to be in agreement with observations at the CIT–TLR. The question of the dependence of α_c on θ_e is quite important and awaits the knowledge of the dependence of entry whip (or

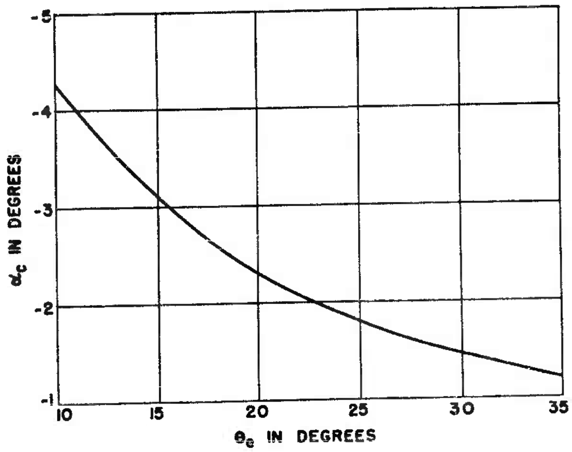

FIGURE 40. Mark 13 torpedo (neglecting metacentric height). Possible relation between critical pitch angle α_c and trajectory angle at entry θ_e. It is essentially assumed that $\alpha_c = (-a_1 \cot \theta_e)/[I(F + G) + a_2(20°)]$.

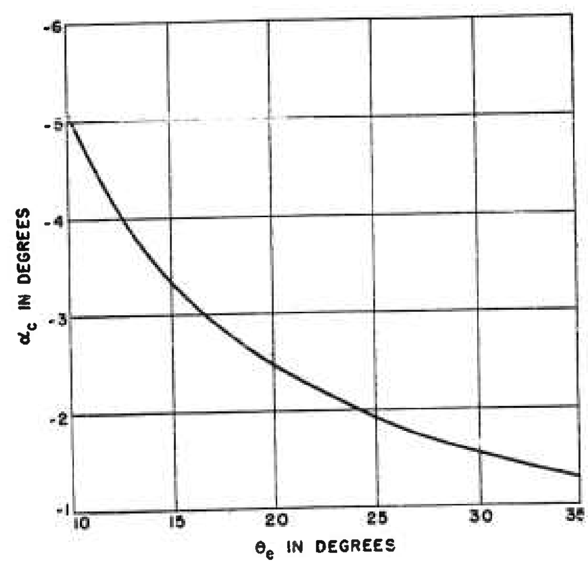

FIGURE 41. Steel Dummy. Possible relation between critical pitch angle α_c and trajectory angle at entry θ_e. It is essentially assumed that $\alpha_c = (-a_1 \cot \theta_e)/[I(F + G) + a_2(20°)]$.

α_0') on θ_e. It was pointed out in Section 6.2 that there are indications that $a_1 \propto \cot \theta_e$ and $a_2 \propto$ constant + cot θ_e. In the quantity a_2, the coefficient of cot θ_e is probably small, and we might expect that the constant term is very much larger than the cot θ_e term. This is based on the fact that a marked sensitivity of whip to pitch should be observed for $\theta_e = 90°$. Hence, as a crude approximation, if the indications are correct that $a_1 \propto \cot \theta_e$, α_c will vary with θ_e in a manner illustrated in Figure 40 for the Mark 13 torpedo neglecting the metacentric height ($\phi = 90°$) and as in Figure 41 for the Steel Dummy.

At the CIT–TLR a recorder is sometimes inserted in the torpedo which records the angle the axis of the

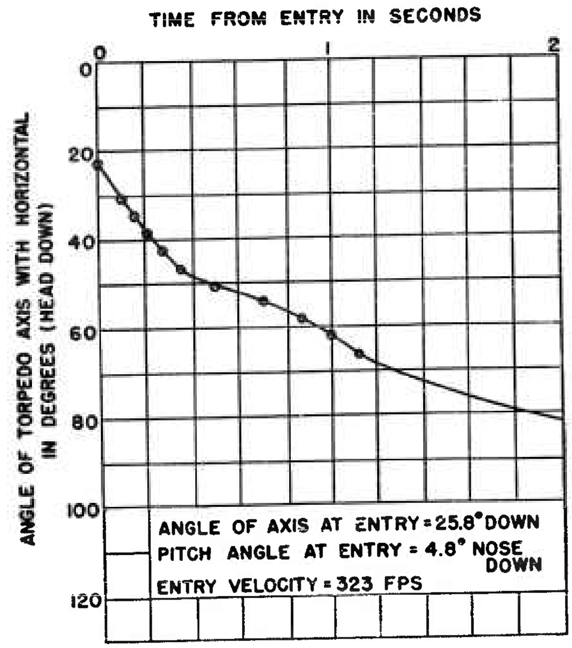

FIGURE 42. Illustration of torpedo, entering with large nose-down pitch angle, going to top of cavity. Angle of torpedo axis with horizontal versus time from entry for dummy.

torpedo makes with the horizontal. This instrument, known as the *gyroscopic orientation recorder* [GOR], will be mentioned further a little later. One record was obtained showing clearly a Steel Dummy going to the top of the cavity for the very steep pitch angle of $\alpha_c = -4.8°$. This record is illustrated in Figure 42. The axis orientation angle increases steadily from its entry value of 25.8 in distinction to the case of a torpedo going to the bottom of the cavity for which this angle decreases.

DEPENDENCE ON ENTRY VELOCITY

It should be emphasized that the motion of the torpedo expressed in terms of the distance along the trajectory is independent of the entry velocity. The critical pitch angle, the point of tail slap, and the attitude of the torpedo at various points does not depend on whether it enters at 200 ft per sec or 600 ft per sec. This assumes, of course, that it is moving fast enough that an open cavity exists and is due to the assumption of forces proportional to the (velocity)^2.

The available evidence seems to bear out this conclusion.

Torpedo Damage

Although it is not difficult to build a torpedo shell strong enough to withstand the drag force on the torpedo, the forces brought in to play at tail slap may crush the afterbody and fins. These forces increase with increasing angular velocity, and, as is shown in Figures 34 and 35, the angular velocity increases with increasing departures from the critical pitch angle and with the velocity. Hence the importance of a clean entry for preventing damage.

Even though the shell may not be damaged by the drag forces, the sustained acceleration due to them may amount to a hundred times the acceleration of gravity and presents a vital problem in the design of the internal torpedo mechanism.

6.3.4 Further Research

Further research and experiment on this stage of the motion should probably deal with (1) Cavity Shape and (2) Nose Forces.

In the direction of cavity shape a theoretical hydrodynamic theory is most lacking. However, since very great difficulties appear, perhaps more work on the kinematic theory is warranted. This implies a tabulation of the quantity λ as obtained by experiment for various nose shapes and further measurements to determine the quantity μ.

In order to obtain a better knowledge of the nose forces, the drag, lift, and moment coefficients for various shaped noses must be determined. In this direction further experiment is highly desirable. Also, some general semi-analytical method should be developed and checked. The Potential Flow Method seems, at present, most likely to be useful, but its results must be checked.

6.4 MOTION OF THE TORPEDO IN A CAVITY AND WHILE CAVITATING

When the tail of the torpedo strikes the wall of the cavity, additional forces come into play in determining the motion. Under the influence of these forces the torpedo continues to slow down in a curved path until it is moving in a noncavitating state.

We shall first consider the behavior of the cavity and its closure by the method outlined in Section 6.3.1. We shall then investigate the equations of motion of the torpedo during that stage and examine what is known about the forces necessary to describe the behavior of the cavity and the motion of the torpedo. Subsequently, the dissolution of the cavity will be treated.

6.4.1 Cavity Shape and Closure

Deep Closure

In Section 6.3.1 a semiempirical approach to the cavity shape was developed. From equation (20)

$$y(x \leqq S, t) = r_s + \lambda V_e e^{-kx}\left[t - \frac{1}{kV_e}(e^{-kx} - 1)\right] - \frac{\mu x \sin\theta_e}{2V_s}\left[t - \frac{1}{kV_e}(e^{kx} - 1)\right]^2 \quad (38)$$

for

$$t \geqq \frac{1}{kV_e}(e^{kx} - 1),$$

where $k = C_D\,(\rho A/2M)$. The value of C_D depends on the nose shape of the torpedo. During the present stage of the motion, since both the tail and the nose are in contact with the water, obviously C_D will be larger than the value for the nose alone, and k will be correspondingly larger.

One might expect that the proper way to treat the torpedo motion in the cavity would be to handle separately the situations before and after tail slap. In the present state of knowledge, this results in a fairly complicated procedure that is of doubtful value in view of the uncertainties in the constants that must be used. It seems more practical to use an estimated mean value of k that may be called $\bar{k}$ and to treat the motion before and after tail slap as a unit.

The type of mean k must be adjusted to the observed facts of the situation. For high speed rockets most of the underwater trajectory may be after tail slap. For torpedoes of the Mark 13 type, possibly the length of the trajectory after tail slap will be twice that before. The average used must take into account these facts. It is clear that, as the torpedo travels along its trajectory, the cavity width ($2y$) for a given x eventually decreases until the cavity walls come together. We wish to determine at what time this occurs and where the torpedo is at this instant. This phenomenon, which we will call deep closure, can be seen clearly in photographs of model projectiles launched into water. At a given point, the diameter of the cavity first increases after the projectile has passed and then decreases until the cavity closes. This closure will not occur at the same time at various points. For this reason one desires to find the time and place at which the cavity walls first come together, thus sealing off the torpedo from the atmosphere. Call this time of first closure t_c and its position x_c.

From equation (38) setting $y = 0$, we find

$$t = \frac{1}{\bar{k}V}(e^{\bar{k}x} - 1) + r_s\frac{\lambda V_e e^{-\bar{k}x} + \sqrt{\lambda^2 V_e^2 e^{-2\bar{k}x} + 2\mu x \sin\theta_e}}{\mu x \sin\theta_e}. \quad (39)$$

This equation gives the time of closure at a given position x. To find the time at which the cavity seals off, it is necessary to use the position at which the time of closure is a minimum. Writing

$$T = \bar{k}V_e t, \qquad T_S = (e^{\bar{k}S} - 1),$$
$$X = \bar{k}x,$$
$$G = \frac{2\bar{k}^2 V_e^2 \lambda r_s}{\mu \sin\theta_e}, \qquad H = \frac{2\mu \sin\theta_e}{k\lambda^2 V_e^2} = \frac{1}{G}\frac{4\bar{k}r_s}{\lambda}.$$

Then equation (39) becomes

$$T = e^X - 1 + \frac{Ge^{-X}(1 + \sqrt{1 + HXe^{2X}})}{2X}. \quad (40)$$

To minimize T set $dT/dX = 0$, which yields

$$\frac{2X^2e^{2X}}{G} = 1 + X + \frac{1 + X}{\sqrt{1 + HXe^{2X}}} + \frac{HXe^{2X}}{2\sqrt{1 + HXe^{2X}}}. \quad (41)$$

The solution of these equations gives $X_c(G, H)$. Then, substituting in equation (40), we may obtain T_c, and the position of the torpedo may be calculated from the relation

$$s = \frac{1}{\bar{k}}\ln(1 + \bar{k}V_e t_c) = \frac{1}{\bar{k}}\ln(1 + T_c). \quad (42)$$

Thus, if we know the value of λ and μ for a given torpedo and can select a suitable mean value of $\bar{k}$ it is possible to estimate the distance and time to cavity closure.

To facilitate the use of these results, the quantities T_c and X_c are plotted against G in Figures 43 and 44 for some values of H. In Figure 45 $\ln(1 + T_c)$ is plotted as a function of G for some values of H since

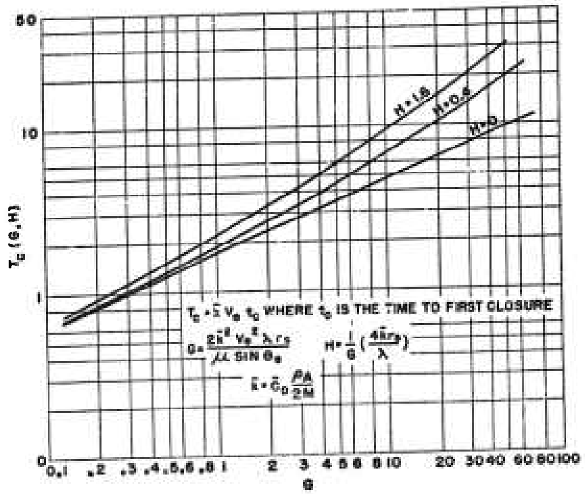

Figure 43. Graph determining time to first closure as a function of the torpedo characteristics and entry conditions.

the distance traversed by the torpedo from entry to cavity closure is given approximately by

$$s_c = \frac{1}{\bar{k}}\ln(1 + T_c).$$

As an example of the use of these figures, consider the Mark 13 torpedo with $V_e = 600$ ft per sec and $\theta_e = 20°$. Before tail slap $C_D = 0.28$, and after tail

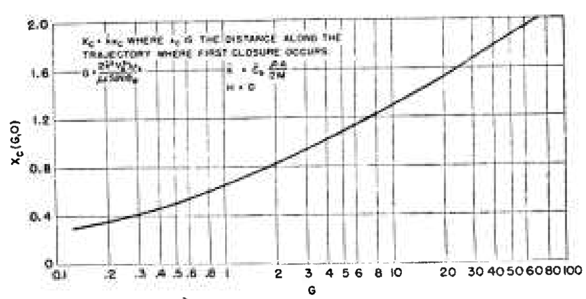

Figure 44. Graph determining point along the trajectory where the cavity first closes as a function of the torpedo characteristics and entry conditions.

slap $C_D' = 0.45$. As a result, $\bar{k}$ may be taken as 0.0143. We found in Section 6.3.1 that $\lambda = 0.15$ and $\mu = 8$ ft per sec per sec. Hence we find $G = 4.16$ and $H = 0.06$. According to Figure 43 we find

$T_c = 3.1$ and the cavity seals off from the atmosphere 0.36 sec after entry. From Figure 44 we see that the cavity closes first at a distance of 72 ft from entry. At the time of closure the approximate position of the torpedo is given by Figure 45 and is seen to be about 101 ft from entry. An entry velocity of 350 ft per sec for the Mark 13 torpedo makes $t_c = 0.40$ sec, $x_c = 51$ ft, $s_c = 77$ ft. For the same entry conditions

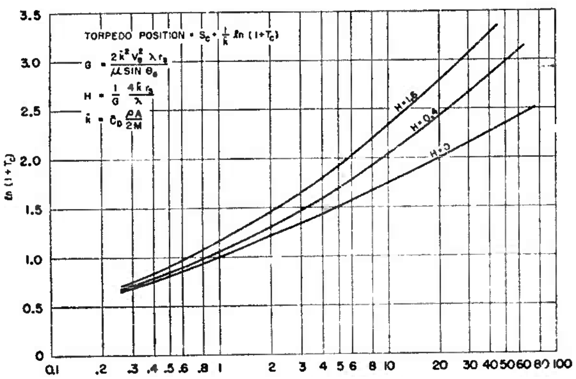

FIGURE 45. Graph determining position of torpedo at first closure.

with the Steel Dummy, but with $V_e = 600$ ft per sec, the corresponding values are $t_c = 0.35$ sec, $x_c = 61$ ft, $s_c = 83$ ft, and, with $V_e = 350$ ft per sec, $t_c = 0.39$ sec, $x_c = 46$ ft, $s_c = 65$ ft. The velocity of the torpedo at this point is given by

$$V_c = V_e e^{-\bar{k}s_c}\,.$$

From Figures 43 and 44 for t_c and x_c it is found that t_c decreases slowly with increasing V_e. It is also found that s_c (the position of the torpedo at cavity closure) will increase with increasing V_e.

The values for t_c agree with the sound records of cavity collapse as observed in rocket trials in the United Kingdom and with the time that the depth and roll recorder begins to record in the British 18-inch torpedo. The values predicted also agree with values obtained in many model experiments of the vertical entry of spheres into water.

Using the value of $\bar{k}$ presented above, another interesting and useful graph is the angle between the trajectory and the torpedo when the torpedo is just touching the cavity wall during the open cavity stage. This is given by $(y - r_b)/b$ and is drawn in Figure 46. This figure is only approximate since among other assumptions is that of a straight line trajectory.

Surface Closure

Numerous times in model water-entry studies, a phenomenon of what may be called surface closure has been observed rather than deep closure that has been discussed up to now. By surface closure is meant the phenomenon whereby the cavity closes

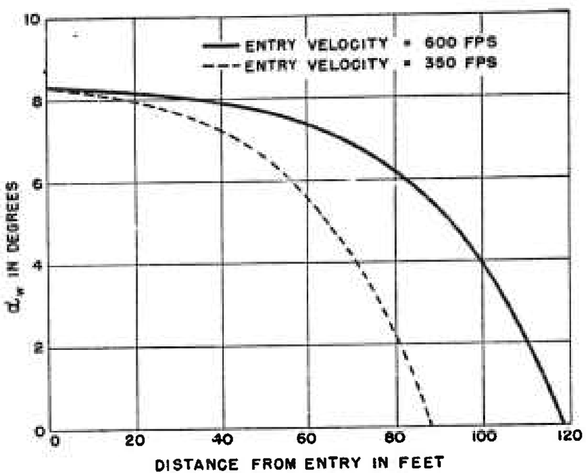

FIGURE 46. Approximate curve of mean angle between the trajectory and the Mark 13 torpedo when it is just touching cavity wall.

near the surface due to the splash folding over the cavity opening forming a roof. This often occurs quite soon after entry compared to the time for deep closure. The primary cause is possibly the aerodynamic force acting on the splash near the surface of the water.

The time at which surface closure occurs decreases with increasing V_e, and it appears that, as V_e increases, surface closure will occur before deep closure, at least for small models. It is, therefore, desirable to know how surface closure will affect deep closure. On this point there is not much experimental evidence. It is expected that after surface seal the pressure in the cavity, at least at first, will tend to fall below P_0 (external pressure) since the volume occupied by the entrapped air increases. In the empirical theory of the cavity shape which was used to determine the time to deep closure, one of the assumptions was that the pressure in the cavity is P_0. However, if surface closure occurs and $P_c < P_0$, there is another force accelerating the cavity walls inward, and the time to closure will be somewhat diminished. From the water entry of torpedo models there are indications that $P_c \sim P_0$. In addition, deep closure has been observed to occur after a surface closure has occurred in the vertical entry of spheres in water and appears to be relatively unaffected by the surface closure.

Just how surface closure scales up has as yet not been determined. However, it appears that, while it may occur in model tests, it probably does not occur in the full-scale tests; furthermore, even if it does occur, it appears that it probably does not affect the deep closure and the subsequent torpedo motion.

6.4.2 Motion with Tail in Contact with Cavity Wall

When the torpedo strikes either the top or bottom of the cavity or possibly one side, forces at the tail are produced in addition to the forces on the nose which were discussed in Section 6.3. The tail forces are primarily a lift perpendicular to the axis of the torpedo near the tail, at some distance l_2 aft of the center of gravity, and also a small tail drag. Although the equations of motion are essentially of the same form as given in Section 6.3, they are quite difficult to handle. During this stage of the motion gravity may or may not be neglected, depending on the V_e and the distance from entry to tail slap (essentially the velocity). To obtain equations amenable to simple treatment, we shall make the simplification that the torpedo is resting at some equilibrium pitch and yaw angle against the cavity wall. These equilibrium angles are such that the sum of the moments about the center of gravity is zero. When the torpedo first strikes the cavity wall it will tend to go past this equilibrium position and then execute damped oscillations about it. In addition, at the tail of the torpedo the cavity is contracting, and also the torpedo is generally rolling in the cavity during this stage of the motion.

Motion along the Trajectory

For the motion along the trajectory, there is the usual equation

$$M \frac{dV}{dt} = -C_D \frac{\rho A}{2} V^2 , \qquad (43)$$

but the drag coefficient C_D may be divided into two independent parts

$$C_D = C_{Dn} + C_{Dt} ,$$

where C_{Dn} represents the drag due to the torpedo nose, and C_{Dt} represents the drag due to the tail.

Equation (43) gives directly the velocity V and the time t in terms of the distance s that the torpedo has traveled along its trajectory from the position at tail slap

$$V = V_0 e^{-C_D \frac{\rho A}{2M}(s-S)} , \qquad s \geqq S . \qquad (44)$$

V_0 is the velocity at the beginning of this stage of the motion. This is given in terms of the entry velocity and the distance to tail slap S by

$$V_0 = V_e e^{-C_{Dn} \frac{\rho A}{2M} S} .$$

Also

$$t = \frac{2M}{C_D \rho A V_0} \left[e^{C_D \frac{\rho A}{2M}(s-S)} - 1 \right] + t_S , \quad s \geqq S ,$$

where t_S is the time to the tail slap.

Motion in the Vertical Plane

In case the torpedo strikes the cavity top or the bottom, it will become subject to additional forces in the vertical plane and perpendicular to the trajectory. Subject to these forces in the vertical plane, the trajectory will curve up or down depending on whether the torpedo is in contact with the cavity top or bottom.

The equation of motion is

$$\begin{aligned} MV^2 \frac{d\theta}{ds} &= -C_L \frac{\rho A}{2} V^2 + Mg \\ &= -(C_L' - C_D'\alpha) \frac{\rho A}{2} V^2 + Mg . \end{aligned} \qquad (45)$$

The angle θ is assumed close enough to zero to permit setting $\cos\theta = 1$ and writing Mg for $Mg \cos\theta$. Since the effect of this term is small, such an approximation appears acceptable. The coefficient C_L is composed of two parts. One represents the lift at the nose and is called C_{Ln}. The other is the lift at the tail and is called C_{Lt}.

$$C_L = C_{Ln} + C_{Lt} . \qquad (46)$$

The primed coefficients describe the resultant forces along and perpendicular to the torpedo axis, while the unprimed coefficients describe the components parallel and perpendicular to the trajectory. The relation between these quantities (in the usual case where α is sufficiently small so that $\cos\alpha = 1$, $\sin\alpha = \alpha$) is

$$C_L' = C_L + C_D\alpha\,,$$
$$C_D' = C_D - C_L\alpha\,,$$

this being true for the coefficients of the nose, the tail, or the entire torpedo.

To obtain a relationship between C_{Ln} and C_{Lt}, it is only necessary to make use of the assumption that the torpedo is resting on the side of the cavity at an equilibrium pitch angle $\bar{\alpha}$. The sum of the moments about the center of mass is then zero so that

$$l_1 C_{Ln}' = l_2 C_{Lt}'\,, \tag{47}$$

where l_1 is the distance the center of pressure of the nose lift lies forward of the center of mass, and l_2 is the distance the center of pressure of the tail lift lies behind the center of mass.

Concerning the lift forces, two assumptions are made that will be shown later to have some experimental basis. It is assumed that the nose lift is proportional to the pitch angle α and that the tail lift and drag are proportional to the departure of the pitch angle from the value for which the tail of the torpedo just touches the wall of the cavity, α_w.[b] This last assumption is clearly valid only when $\alpha > \alpha_w$, but this is the case of importance. Hence let

$$C_{Ln}' = C_{ln}'\alpha C_{Lt}' = C_{lt}'(\alpha - \alpha_w) \text{ and } C_{Dt}' = C_{dt}(\alpha - \alpha_w)\,. \tag{48}$$

The condition of equilibrium, equation (47) then gives the equilibrium pitch angle to be

$$\bar{\alpha} = \frac{C_{lt}' l_2 \alpha_w}{C_{lt}' l_2 - C_{ln}' l_1}\,. \tag{49}$$

Equation (45) then becomes

$$\frac{d\theta}{ds} = \frac{1}{R} = -\left[C_{ln}'\left(1 + \frac{l_1}{l_2}\right) - C_D'\right]\bar{\alpha}\,\frac{\rho A}{2M} + \frac{g}{V^2}\,. \tag{50}$$

This result shows that under the assumptions made the torpedo moves in a vertical circle as long as $\bar{\alpha}$, or α_w, is constant and g/V^2 does not change too much. The negative sign implies a circle concave-upward, while if $\bar{\alpha}$ is negative the circle is concave-downward. As the velocity decreases the last term in (50) becomes more important and may eventually change an upturning trajectory to a downturning one.

Equation (50) was based on the assumption of a constant $\bar{\alpha}$ and this depends on a constant α_w. Since the shape of the cavity changes with the time, α_w will not be constant but will decrease as the torpedo moves along. Equation (21) gives the radius of the cavity at a distance b back of the torpedo nose so that α_w can be evaluated.

$$\alpha_w \approx \tan\alpha_w = \frac{y_b - r_b}{b}$$

$$= \frac{r_s - r_b}{b} + \frac{\lambda(e^{\bar{k}b} - 1)}{\bar{k}b} - \frac{s\sin\theta_e e^{2\bar{k}s}(e^{\bar{k}b} - 1)^2}{2(\bar{k}V_e)^2 b r_s} \tag{51}$$

with y_b = radius of cavity at distance b back of the nose,
r_s = radius of torpedo at the point of flow separation from the nose,
r_b = radius of torpedo at a distance b back of the nose,
$\bar{k}$ = mean deceleration coefficient,
s = distance along trajectory.

This expression for α_w can be used in equation (49) to get $\bar{\alpha}$ for use in equation (50). The value of $1/R$ as a function of s can then be obtained and integrated with respect to s to obtain the angle through which the torpedo turns in a given length of trajectory.

Motion in the Horizontal Plane

If the torpedo enters the water near the critical pitch angle α_c, it may swing to one side or the other of the cavity so that the force due to contact with the cavity will be horizontal. To the extent to which gravity can be neglected, the motion will then be confined to the plane defined by the direction of this force and the initial direction of the trajectory. Since the torpedo is probably symmetrical about its longitudinal axis, the force coefficients for the horizontal forces will not differ significantly from those for the vertical forces, and the radius of curvature will be given by equation (50). The force of gravity will not affect the radius of curvature but will tend to distort the motion out of the plane.

[b] Strictly, the nose lift is proportional to the effective pitch angle at the nose, $\alpha - l_1/V(\dot{\alpha} - \dot{\theta})$ and the tail lift to $\alpha + l_2/V(\dot{\alpha} - \dot{\theta})$. However, due to the uncertainty in the coefficients and for simplicity the effect of the angular velocity terms are omitted in this analysis. No analytical difficulties are present if one wishes to include them.

General Case

In case the torpedo strikes the wall of the cavity at an arbitrary angle, the forces called into play will lie in the plane defined by the axis of the torpedo and the direction of motion at the time of impact. In so far as gravity can be neglected, the motion will continue in this plane with a radius of curvature indicated by equation (50). In this approximation, the horizontal displacement and the change in depth can be estimated for any given condition at tail slap. It is assumed, of course, that the torpedo does not roll around the cavity. For no rolling of the torpedo, the radius of curvature of the path in the vertical plane increases slowing with increasing s. In other words, if the torpedo is on the bottom side of the cavity, the torpedo trajectory is curved (and essentially circular) concave-upward, with the radius of the curve increasing as the torpedo travels along its trajectory. Thus it becomes less concave-upward until finally, if the torpedo is traveling sufficiently slowly, it may reverse sign and become concave-downward. However, if the torpedo is on the top side of the cavity, the trajectory is concave-downward with the torpedo tending to dive and the radius of curvature tending to increase slowly. Due to the gravitational term the radius of curvature tends to decrease slowly, and the net result depends on the hydrodynamic constants and entry conditions. This general type of behavior is due to the fact that the cavity is contracting near the torpedo tail and its shape is changing slowly so that the equilibrium pitch angle is decreasing and thus, also, the lift force increasing the radius of curvature.

For launchings, like those of rockets and high speed aircraft torpedoes, V_e is very large, and the gravitational term may be neglected. In this case, the trajectory does not differ much from a circular arc since the cavity contracts very slowly, and thus the radius of curvature of the path increases very slowly. On the other hand, for sufficiently low V_e, even though the torpedo strikes the bottom wall of the cavity at some distance along the trajectory, the path may become concave-downward, and the torpedo will dive. This has been clearly observed in model experiments.

In the horizontal plane the behavior is very similar. For no roll, if the torpedo tail strikes the right side of the cavity the path is concave to the left with slowly increasing radius of curvature, and if the torpedo tail strikes the left side of the cavity the torpedo path will curve to the right with slowly decreasing curvature.

The change in the trajectory angle in the vertical and the horizontal planes during this stage of the motion follows immediately from the discussion of the radius of curvature. Thus for the torpedo on the bottom side of the cavity the trajectory angle decreases at a slowly diminishing rate, while if the torpedo is on the top of the cavity it increases at a rate which may diminish or increase depending on the hydrodynamic constants of the torpedo during this stage of the motion and the entry conditions. Thus for torpedoes on the bottom side of the cavity, the pitch angle at entry being more nose-up than the critical pitch angle ($\alpha < \alpha_c$) (unless V_e is very low), θ will decrease with a resulting upturning trajectory, while if at entry $\alpha_e < \alpha_c$ the torpedo will strike the top of the cavity the trajectory angle will increase with a resulting down-turning trajectory.

It is evident from the preceding discussion of the equation of motion solution that the motion in the horizontal plane depends also on the entry conditions in the vertical plane, and a similar statement may be made for the motion in the vertical plane.

Illustration of Motion

The general behavior of a torpedo going to the bottom of the cavity may be seen qualitatively from a series of photographs obtained from 1-in. models at the Morris Dam Group, California Institute of Technology. This is illustrated in Figures 47A to 47D. This series of photographs is taken from the trajectory of the 1-in. vented model of the CIT Steel Dummy. From these pictures, which probably do not duplicate all the aspects of the trajectory and cavity shape of the full-scale CIT Steel Dummy, one may nevertheless see the qualitative behavior of the torpedo as described earlier. Clearly the torpedo strikes the cavity wall, and the tail digs in until the torpedo settles around some equilibrium pitch angle, as illustrated in Figures 47A and B. The torpedo then pursues a curved path (concave-upwards since it is on the bottom side of the cavity) at roughly constant pitch angles as seen in Figures 47B, C, D. The cavity then can be seen sealing off (deep closure) from the atmosphere. The trajectory after closure differs more markedly from the full-scale and will be discussed later. However, it should be noted that even after the closure, while a cavity (although closed) may exist, the torpedo path is curved. In addition, one

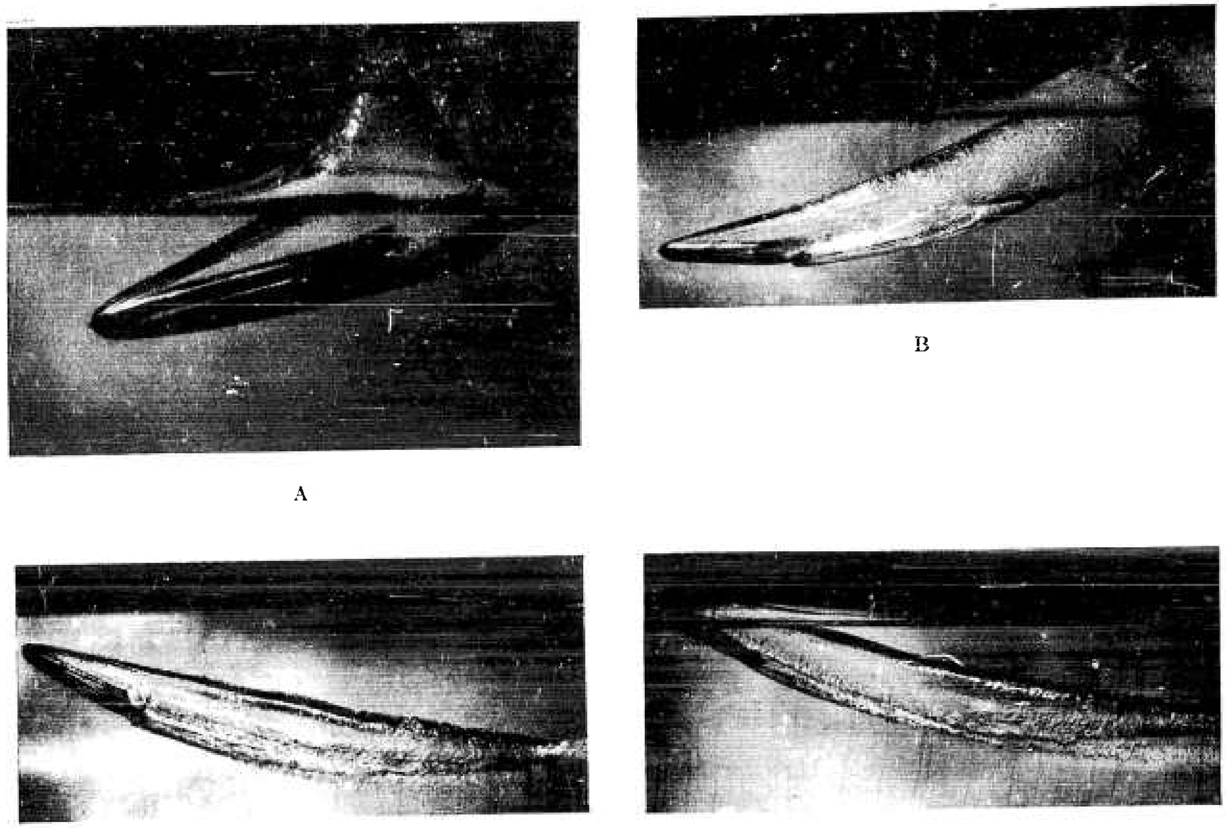

A B C D

FIGURE 47. Illustrations of the underwater trajectory of the 1-in. vented model of the Steel Dummy with a finer nose. $\theta_e = 19°$. $V_e = 105$ ft per sec.

A. 10 diameters from entry. Torpedo going to bottom wall of cavity.

B. 22 diameters from entry. Tail slap has just occurred and torpedo tail is digging in.

C. 67 diameters from entry. Torpedo riding on bottom wall of the cavity at roughly constant pitch angle and pursuing an upturning trajectory (roughly circular arc).

D. Torpedo broaching after approximately circular path. Cavity behavior appears different from prototype.

sees the diminishing trajectory angle and the nose-up pitch angle during, and at the end of, the open cavity stage of motion.

Other Types of Motion during Open Cavity Stage

The foregoing discussion has more or less implicitly assumed a type of head on the torpedo in which the center of curvature of the nose is forward of the center of gravity. However, if the center of curvature of the nose is aft of the center of gravity (as on a flat nose) then it was seen (Section 6.2.5) that a restoring moment acts on the nose tending to return the torpedo axis to zero pitch. In this case the torpedo may strike the cavity wall, but the corresponding pitch angle will not be the stable equilibrium pitch angle. After striking the cavity wall, due to the restoring moment at the nose, the torpedo may rebound from the wall, oscillate past its equilibrium position to the opposite cavity wall, and then rebound from that wall. Thus a periodic oscillation in pitch may be expected with an attendant periodic oscillation in the trajectory. This entire phenomenon has been observed in model experiments with flat noses. This is the type of behavior which has sometimes been called an oscillatory type of trajectory.

Generally, the entire preceding discussion is for torpedoes in which the length to diameter ratio is not too small. If this ratio becomes small a comparatively wide cavity is produced, and it is possible that a very large value of $\bar{\alpha}$ must be attained for equilibrium (which may not necessarily be a position of stable equilibrium) and the motion will tend to be that of broadsiding.

It has also been assumed that l_2 (the distance between the center of pressure of the tail lift and center of gravity) remains constant during this stage of the motion. Generally, this is satisfactory. However, it clearly depends on the shape of the tail section of the torpedo and may easily involve $\bar{\alpha}$ and the cavity angle. For the broadsiding motion mentioned above, l_2 will probably vary during this stage.

Roll in the Cavity

Up to now, it has been assumed that the torpedo does not roll about the cavity during this stage of the motion. Actually, this assumption may not be completely correct. In order to examine this point, the roll velocity of the torpedo must be investigated.

During the stage before tail slap, it was observed that a rolling velocity of the torpedo about its longitudinal axis was produced and that this velocity is proportional to the yaw angle at entry ψ_e. This roll velocity was caused by the moment of the hydrodynamic forces perpendicular to the torpedo axis, multiplied by the metacentric height. Thus for the Mark 13 torpedo entering right side up, since the center of gravity is below the torpedo axis, a nose-right yaw produces a clockwise rolling angular velocity, while for the torpedo upside down with the same entry conditions a counterclockwise roll velocity would be produced. For intermediate roll angles the hydrodynamic forces perpendicular to the torpedo axis in the vertical plane also produce a rolling moment.

Thus, at tail slap, the rolling angular velocity of the torpedo is its roll velocity at entry, $\dot{\phi}_e$, plus the rolling velocity induced during the previous stage of motion.

At tail slap, an additional rolling angular velocity is produced due primarily to three causes, the metacentric height of the torpedo (arising in an entirely similar manner to the roll velocity induced during the previous stage of motion), the torpedo propellers, and the torpedo fins. We will discuss each of these effects separately.

Effect of Metacentric Height. The roll velocity produced by the moment of the hydrodynamic forces multiplied by the metacentric height has already been mentioned. Clearly, roughly the same type of forces will act on the nose of the torpedo as in the previous stage of the motion where the nose alone was in contact with the water. The magnitude of the transverse forces are proportional to ψ in the horizontal plane and $\bar{\alpha}$ in the vertical plane.

Effect of Propellers. The effect of the propellers in producing a roll velocity depends primarily on their sense of rotation. At tail slap, the propellers first come in contact with the water, and therefore a hydrodynamic force is produced. By far the largest component of this force is that normal to the propeller blades. The force normal to the blades produces a rolling impulse and hence a rolling velocity about the longitudinal axis of the torpedo. The direction of this rolling velocity will depend on the direction of the force normal to the propeller blades, which in turn depends on the direction the propellers are pitched. The torpedo experiences a rolling moment since at tail slap the propellers probably are not up to their normal running speed and, in any case, the torpedo velocity is much greater than the steady running value. For a given set of propellers, the force and hence the rolling velocity would be a maximum when the propellers are fixed to prevent rotation.

It is evident that the direction of the force on a single propeller which is left-handed is such that a counterclockwise roll velocity is expected, while if the propeller is right-handed a clockwise roll velocity is expected. With counter-rotating propellers, with which most propeller-powered torpedoes are fitted, the problem is somewhat more complex. However, it is probably correct to assume that the direction of pitch of the forward propeller will determine the direction of the roll velocity induced at tail slap.

From this discussion of the mechanism whereby propellers produce a rolling velocity, it may be inferred that the rolling impulse and hence the rolling velocity will increase with increasing propeller blade area, increasing propeller blade pitch, and certainly with increasing entry velocity V_e. In addition, the rolling velocity will probably also depend on how much the propellers sink into the cavity wall. As a result, one might expect an increasing roll velocity with a larger propeller diameter even though the blade area is constant.

Effect of Fins. The third possible cause of torpedo roll after tail slap is the action of the water on the torpedo fins. If there is any relative velocity, perpendicular to the torpedo axis, between the water bounding the cavity and the torpedo in contact with it, there will be a torque tending to roll the torpedo.

Very little is known as to the detailed motion of the water at the surface of the cavity, but it is in accord with the simple description of cavity shape already given to assume that all of the motion is in a plane containing the axis of the cavity. Hence any relative motion must be a motion of the torpedo in the cavity.

If the torpedo were initially in the center of the cavity and moved directly over to make contact with the surface, there would be no relative motion between the torpedo and the water, perpendicular to the axis. It appears, however, that the situation is not so simple. In the first place, the torpedo is away from the axis of the cavity by amounts corresponding to the yaw angle ψ_e and the pitch angle α_e at entry. In the second place, the pitch angle will change much more rapidly due to the entry whip than will the yaw angle. Hence, when the torpedo strikes the cavity surface, it will not be travelling along a radius but along a chord of a section of the cavity. Hence directions of roll due to the fins are to be expected as follows:

Pitch at Tail Slap	ψ_e	Roll Velocity
Nose-up	Nose-right	Clockwise
Nose-up	Nose-left	Counterclockwise
Nose-down	Nose-right	Counterclockwise
Nose-down	Nose-left	Clockwise

Experimental Verification. We may now undertake to investigate the available experimental data on the roll velocity produced at entry and examine the agreement with the qualitative and semiquantitative theory of the phenomena presented above.

Practically all of the data obtained on initial underwater roll in this country was observed at the CIT–TLR by means of a gyroscope orientation recorder. Roll records have been obtained in which the effect of the metacentric height, the propellers, and the fins have been studied. These tests were carried out on the CIT Steel Dummy which, incidentally, is generally not fitted with propellers. The effect of the fins was to a large extent isolated by experimenting with the so-called MBB Dummy, illustrated in Figure 48. This dummy has the same physical characteristics as the CIT Steel Dummy, except, as is seen, most of the fin area is removed. With the MBB Dummy as the basis, the effect of metacentric height, fixed propellers, and fins was examined one at a time.

Since on the normal MBB the metacentric height is zero, there are no propellers, and the fin area is a minimum, we expect the observed roll velocity (which is defined as the maximum roll velocity observed within the first second after entry) to be a minimum, but with some residual roll due to the fact that the fin area is not completely removed. The observed roll velocity in this case is expected to have the same de-

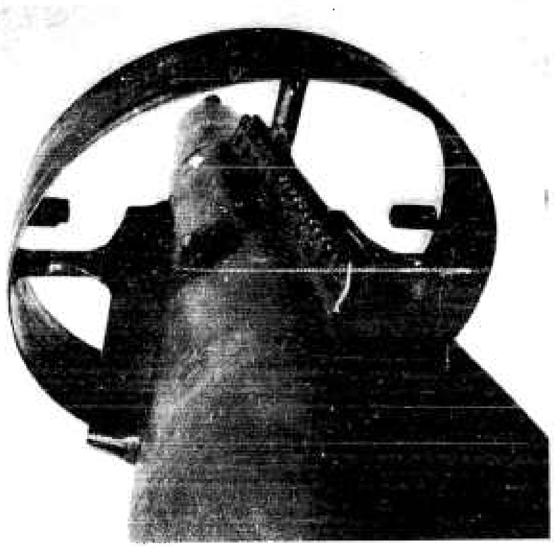

FIGURE 48. CIT MBB Dummy minimum fin installation.

pendence on yaw at entry as that due to the fins alone so that, in the light of our previous discussion, a nose-right yaw is expected to produce a clockwise roll velocity. These roll velocities are not however expected to be nearly so large as with normal fins. In Figure 49 the observed roll velocity for the MBB

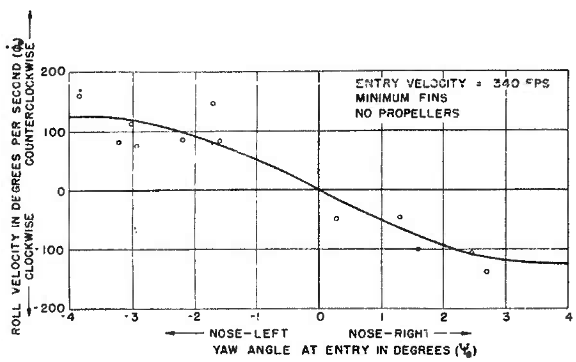

FIGURE 49. Induced roll velocity for CIT MBB Dummy (zero metacentric height).

Dummy is plotted against yaw at entry, and the relationship is seen to be as expected. At the origin, the slope of the curve is approximately 50 degrees per sec per degree yaw.

The next step in the measurements of roll velocity was to put the center of gravity 0.53 in. below the axis of the dummy and obtain the dependence of ϕ on ψ_e. It is expected from the previous discussion that for a given nose-right yaw angle the clockwise roll velocity will increase with increasing metacentric height. The dummies entered with $\alpha_e > \alpha_c$ and right side up. Examining Figure 50, which represents the

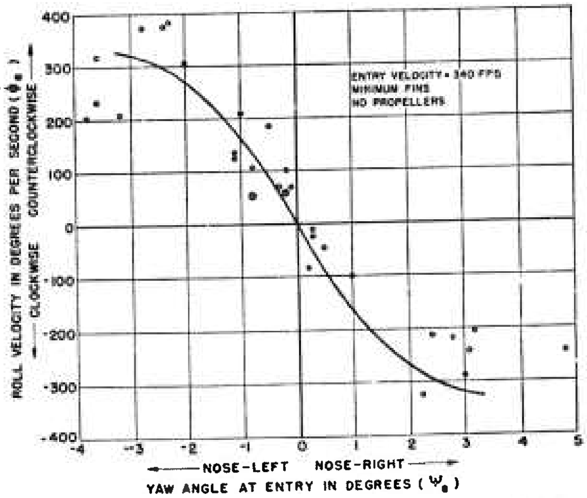

FIGURE 50. Induced roll velocity for CIT MBB Dummy (metacentric height = 0.53 in.).

results of these tests, indicates that the observed roll velocity is altered by the metacentric height in the manner predicted. From this figure it is seen that for the MBB Dummy the sensitivity of $\dot{\phi}$ to ψ_e is increased to 150 degrees per sec per degree yaw so that, due to the metacentric height of 0.53 in., the roll velocity is increased approximately 100 degrees per sec per degree of yaw.

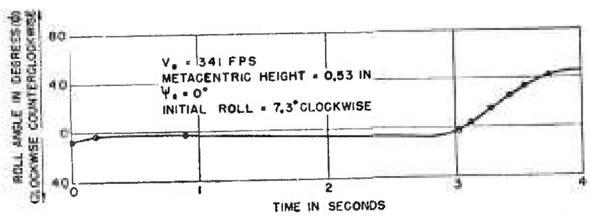

FIGURE 51. Roll angle versus time for CIT MBB Dummy.

On the basis of the discussion of the causes of roll given earlier, it is expected that the effect of the metacentric height in producing a roll velocity is zero for $\psi_e = 0$ since in this case there is no force acting on a hemispherical nose normal to the torpedo axis in the horizontal plane. In addition, the effect of minimum fins for $\psi_e = 0$ is expected to be zero since the fin effect varies with ψ_e as discussed earlier. Hence for $\psi_e = 0$, we expect $\dot{\phi} = 0$. One roll record was obtained with the MBB Dummy with the center of gravity 0.53 in. below the axis in which $\psi_e = 0$. The record is presented in Figure 51. It is seen that the roll velocity is practically zero as expected.

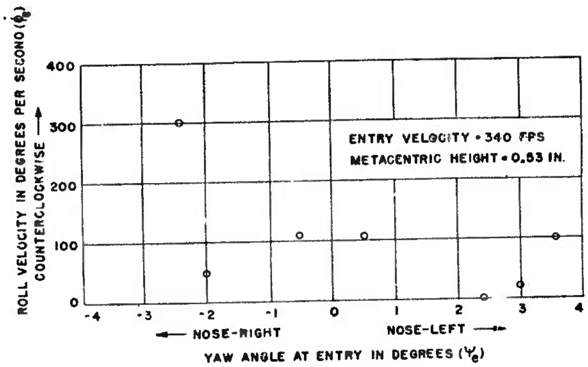

FIGURE 52. Induced roll velocity for CIT MBB Dummy (fixed Mark 13 propellers with minimum fins).

To test the effect of propellers, the MBB Dummy was fitted successively with Mark 13 and Mark 14 propellers fixed to prevent rotation. The Mark 14 propellers are somewhat larger than those of Mark 13. It should be noted that the Mark 13 and Mark 14

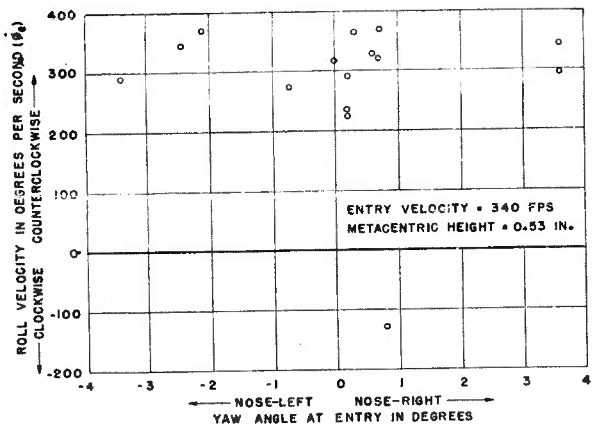

FIGURE 53. Induced roll velocity for CIT MBB Dummy (fixed Mark 14 propellers with minimum fins).

forward propellers are left-handed. The result obtained with the Mark 13 propellers is illustrated in Figure 52 and indicates that with left-handed propellers at zero yaw a counterclockwise roll velocity is produced averaging about 125 degrees per sec.

Thus a constant roll velocity is superposed on the roll velocity caused by the metacentric height and minimum fins. In Figure 53 a similar result is observed with fixed Mark 14 propellers. In this case the roll velocity due to propellers is some 300 degrees per sec or about 2½ times the roll velocity due to Mark 13 propellers. This is as expected since the area of the Mark 14 propellers is somewhat greater than that of the Mark 13 propellers.

To study the effect of the fins in producing a rolling velocity the MBB Dummy was launched with normal fins. The observed results are presented in Figure 54. From this figure it is clear that the fins produce a

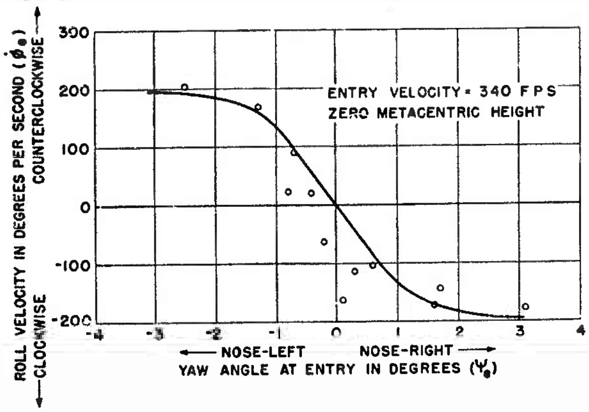

FIGURE 54. Induced roll velocity for CIT MBB Dummy (no propellers and normal fins).

rolling velocity in a manner predicted earlier. The decreased influence of the yaw angle on the roll velocity for larger yaw angles is quite apparent. Near $\psi_e = 0$ it is found that the slope of the roll velocity curve is approximately 150 degrees per sec per degree of yaw which represents an increase of about 100 degrees per sec per degree of yaw over the value observed with minimum fins.

We thus see that the discussion of the causes of roll at tail slap appears to be verified by the available experimental data at least for torpedo shapes similar to the Mark 13 torpedo.

On the basis of the observed values of the roll velocity, it is possible to estimate the extent to which a Mark 13 torpedo might roll around the cavity during this stage of the motion and hence the extent to which the plane of the trajectory might be distorted.

It appears that this stage of the motion will not last longer than 0.4 sec and, if the roll velocity of the torpedo is less than 200 degrees per sec, it will turn less than 80°. This will correspond to a change in angular position in the cavity that is less than 32° since the ratio of the torpedo radius to the cavity radius is about 0.4. This value of 32° based on no slipping at all is an upper limit, and its low value justifies the qualitative picture of the plane trajectory as a first approximation.

6.4.3 Observed Values of Hydrodynamic Constants after Tail Slap

In order to obtain the magnitudes of the radius of curvature of the path, the time and velocity distance relationships, as well as the cavity shape during this stage of the motion, the additional drag and lift forces due to the contact of the tail with the water must be known.

METHODS OF OBTAINING C_D DURING THIS STAGE OF THE MOTION

In general, we can say that $C_D = C_{Dn} + C_{Dt}$, where C_{Dn} is the drag coefficient due to the torpedo nose, which was discussed in detail in the last part, and C_{Dt} is the drag coefficient of the tail of the torpedo. The magnitude of C_{Dt} may be thought to be attributable to the extra drag of the tail section coming in contact with the cavity wall or the additional drag caused by the increased wetted area of the torpedo in this stage. Hence it is expected that for any torpedo C_D will be a function of the tail shape and structure. Possibly the only method for obtaining C_D is experimentally, and the simplest method for obtaining C_D or C_{Dt} is probably by obtaining a velocity distance, velocity time, or distance time record during this stage of the trajectory. A usable drag coefficient for a rocket, based on full-scale and model tests, has been determined. This drag coefficient is generally averaged over the entire trajectory. Hence it is expected that the value of C_D quoted would be slightly less than $(C_{Dn} + C_{Dt})$ since it generally includes a small region where $C_D = C_{Dn}$ (the previous stage of the trajectory) and possibly, for low V_e, some region after cavity closure.

Another possible method for investigating the value of C_D during this stage of the motion makes use of water tunnel tests with the torpedo at a pitch angle $\bar{\alpha}$ that is estimated to be roughly the value in the open cavity. With the cavitation number K appropriate to this stage of the trajectory (which is probably of the order of $K = 0$) the value of C_D, and also other coefficients like C_L, may be measured. The increase in the value of C_D during this stage of the trajectory is expected to occur almost discontinuously since the immersion of the tail in the cavity wall takes place very suddenly.

In addition, since the wetted area of the tail usually increases considerably with increasing $\bar{\alpha}$ we should expect C_{Dt} and hence C_D to increase with increasing $\bar{\alpha}$ during the open cavity stage. Indeed, as was mentioned before, we expect $C_{Dt} \propto (\bar{\alpha} - \alpha_w)$. The model tests of the forces on a long cylinder planing on water have shown that C_{Dt} is apparently a linear function of $(\bar{\alpha} - \alpha_w)$ as was expected.

Observed Values of C_D

During this stage of the motion, C_{Dn} is approximately the same as the value of C_D in the previous stage, and C_{Dt} is a function of the tail structure.

For the CIT Steel Dummy (which is fitted with a shroud ring) it was found by repeated distance-time measurements at the CIT–TLR that, based on body diameter, during this stage of the motion $C_D \approx 0.35$ approximately. Based on the actual nose-sphere diameter, $C_D \approx 0.42$ is in fair agreement with the values for hemispherical-nose rockets. The value of C_D for the full-scale Mark 13 torpedo with shroud ring is probably in the same neighborhood and may be somewhat larger due to an additional drag force introduced by the propellers. From distance-time curves obtained with the 1-in. vented model of the Steel Dummy, it is estimated that during this stage of the motion $C_D \approx 0.33$ based on body diameter and when based on nose-sphere diameters $C_D \approx 0.38$. Hence it appears that without propellers $C_{Dt} \approx 0.14$ at the particular $(\bar{\alpha} - \alpha_w)$ holds for that torpedo. Adding propellers tends to diminish $\bar{\alpha}$ and henee should diminish that part of C_{Dt} due to the torpedo tail. However, the propellers also contribute to C_{Dt}. As a very crude approximation, the value of C_D for a flat plate of the same area may be used for C_{Dp}. For the Mark 13 propellers this appears to be using the area of two blades (presumably two of the four blades may be completely immersed). Very roughly $C_{Dp} \sim 0.06$. Due to the propellers there is also an increase in C_{lt} and as a result $\bar{\alpha}$ will diminish somewhat, thus decreasing C_{Dt}, possibly by 0.03. Hence, by this very rough method, for the Mark 13 torpedo $C_{Dt} = 0.17$ and $C_D = 0.45$. As a notation, it is here, for the first time, that the shroud ring has been considered since this is the first stage of the motion in which the tail structure has made contact with the water. It is estimated that the shroud ring drag will be small. Therefore, the value of C_D for the Mark 13 torpedo without a shroud ring is expected to be approximately the same. The reason for this is that the ring surface makes an angle of 4° with the torpedo axis. If the cavity were conical, then the shroud ring would also make roughly a 4° angle with the water when just touching the cavity wall. However, at the rear of the torpedo the cavity wall begins to curve inwards with the result that the flow past the shroud ring will be roughly in the direction of the ring when just touching the cavity wall. As the torpedo tail digs into the cavity wall, there is probably an angle of attack of the flow on the shroud ring as to result in a lift. The total increase in drag appears however to be negligible.

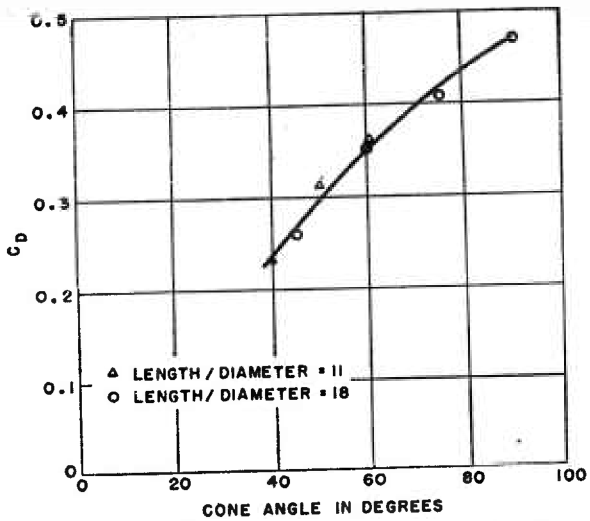

FIGURE 55. Drag coefficient versus cone angle for cone heads on a cylinder. (Obtained in the United Kingdom.)

The value of C_D measured for the Mark 13 torpedo is at the equilibrium angle $\sqrt{\bar{\alpha}^2 + \bar{\psi}^2}$. The magnitude of this angle is not known and is not constant during this stage of the motion. It is estimated that the magnitude of this angle is in the neighborhood of 10°, based on the kinematic theory of cavity shape and from gyroscopic orientation recorder records at the CIT–TLR of the angle of the torpedo axis in the vertical plane.

Results have been obtained in the United Kingdom for the C_D of models of cone head rockets. These results are probably averaged over the entire trajectory, and as a result the drag coefficients observed are probably low for this stage of the motion. The results indicate that C_D appears practically independent of the length over diameter ratio for the rockets. Figure 55 is a plot of the results obtained of C_D versus cone angle. They are all for $l_1/l = 0.4$. Comparing these results with the C_D observed for cone noses before tail slap, the value appears lower. This illustrates somewhat the inherent inaccuracies in measurements, but primarily it indicates that C_{Dt} for a cylinder is almost negligible. It appears, as is expected, that C_D increases with the cone angle. Results obtained for C_{Dn}' for cone noses by model experiments and integrated pressure distributions may be compared with the results in Figure 55, and from the comparison an estimate of the tail drag coefficient can be made. In addition, the tail drag is shown to be small by the fact that a smooth velocity-time relation is found in these model tests over the entire trajectory rather than the almost discontinuous curve observed for the Mark 13 torpedo.

It was also found that C_{Dt} increases somewhat as the center of gravity is moved back from the nose. This may be attributed to a greater lift required for equilibrium on the cavity wall and increased submersion of the tail.

A rocket with the Admonitor CIT head, which is a head looking like a large-caliber ogive, was found by the British to have $C_{Dn} = 0.11$ and $C_D = 0.16$. The tail of the rocket is roughly cylindrical in shape. The same rocket with the Armo head (a flattish nose) was found to have a mean C_D over the entire trajectory of $C_D = 0.16$ and to vary between 0.13 and 0.19. Various results for the C_D of rockets (based on nose area) are presented in the following table.

TABLE 1. C_D for rockets with various noses

	Radius in calibers	Connecting region of nose on to cylinder in calibers	C_D (based on nose area)	Radius of curvature
	Hemispherical noses			
HVAR	0.22	20	0.41	
	0.31	5	0.43	
	0.25	20	0.43	
	Ogive noses			
JMA 2				
11.75″ AR	0.6	20	0.32	
2.25″ AR	1.4		0.33	50
3.5″ AR	1.4		0.25	200
	1.14	20	0.25	620
5.0″ HVAR 6	1.4		0.25	170
	1.0	20	0.25	
1.75″ AR long motor	1.5		0.21	550
11.75″ AR short motor	1.5		0.20	500
3.25″ Mark 7	1.8		0.31	
	2.4		0.29	
	4.0		0.16	

The 600-lb A/S bomb was found to have $C_D = 0.43$. The nose of this bomb is roughly spherical. The 250-lb A/S bomb has a spherical capped nose of radius $\sim l/3$. It was found that for this bomb $C_D \approx 0.95$.

On the basis of the results presented it may be possible to estimate the magnitude of C_{Dt} for various shaped torpedoes. C_{Dt} appears small for rockets. Using the C_{Dn} for various noses given in Section 6.3, it appears possible to estimate C_D for this stage of the trajectory and to use this value in obtaining the cavity behavior and the motion of the torpedo

Lift Coefficient

By far the greater effect of the torpedo tail resting on the cavity wall is the lift that is produced near the tail. From the equations of motion it appears that it should be possible to determine the trajectory during this stage of the motion if the quantities C_{lt}' (vertical plane) and C_{ct}' (horizontal plane) are known, as C_{ln}' and C_{cn}' were derived in Section 6.3.

From equation (50) for the first order approximation of the trajectory during the open cavity stage, it is apparent that three quantities enter into the equation, the radius of curvature R, the mean pitch angle $\bar{\alpha}$, and the lift rate coefficient of the nose C_{ln}'. The quantity C_{ln}' for various shaped noses was discussed in Section 6.3. Thus, since the approximate value of C_{ln}' is known, it is necessary to know $\bar{\alpha}$ to determine $1/R$ or to know $1/R$ in order to determine $\bar{\alpha}$. In order to determine $\bar{\alpha}$ without knowing R, C_{lt}' must be known. Actually, the quantity that is usually measured is the radius of curvature of the path (which is closely circular), and sometimes from this there is inferred the quantity C_L.

In tests of a series of cone head rockets (cone heads on a cylinder) the following procedure was used. The value of R was found for various cone angle noses with different positions of the center of gravity (and thus different values of l_1 and l_2 in equation (47). The values found are given in Figure 56 (Shaw and Naylor[5]) for various values of the length divided by diameter, position of center of gravity, and cone angle of the nose. It is clear from this figure that the smaller the cone angle the larger the value of C_L and hence the smaller the value of R. This is expected since the smaller the cone angle the larger the nose lift. Also the quantity C_L varies much as might be expected. Thus clearly C_L increases with $\bar{\alpha}$ and from equation (49) it is clear that as the center of gravity is moved back, since l_2/l_1 decreases, $\bar{\alpha}$ will increase and hence C_L will increase. In addition, it is clear that, as l and hence length divided by diameter increases, the inclination of the torpedo in the cavity becomes smaller due to the increased length of the rocket and curvature of the cavity. As a result $\bar{\alpha}$ will decrease with increasing l.

Many underwater trajectories have been observed at the CIT–TLR for the full-scale Mark 13 torpedo and for the Steel Dummy. However, due to the relatively short path length during which this stage exists and due to the large radius of curvature it has been quite difficult to estimate R with much precision.

For a hemispherical nose $C_{ln}' = C_{Dn}' = 0.28$. Also, since $C_D' = C_D - C_L\bar{\alpha} = 0.45 - (1 + l_1/l_2)C_{Dn}'\bar{\alpha} = 0.45 - 0.63\bar{\alpha}$ ($l_1 = 5$ ft, $l_2 = 4$ ft), we may say

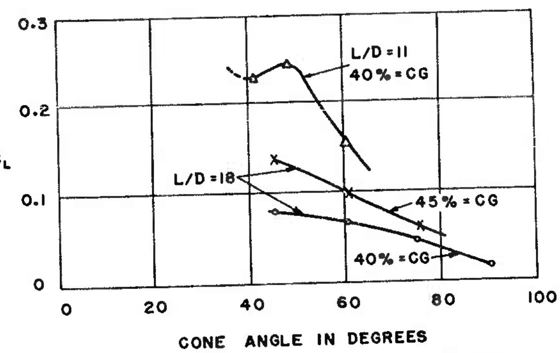

FIGURE 56. Lift coefficient versus cone angle for cone heads on a cylinder. (Obtained in the United Kingdom.)

from equation (50), neglecting the dependence on V, that

$$\frac{1}{R} = -\frac{\rho A}{2M}\left[\left(1 + \frac{l_1}{l_2}\right)C_{ln}' - C_D'\right]\bar{\alpha}$$

$$= -\frac{\rho A}{2M}\left(0.18 + 0.63\bar{\alpha}\right)\bar{\alpha}\,.$$

Hence we have an approximate relationship between $1/R$ and $\bar{\alpha}$. If either of the quantities is known, the other is determined. As has been mentioned, from the underwater trajectories one cannot easily measure R on the relatively short region from tail slap to cavity closure. However, one may obtain the radius of curvature of the trajectory from records of the gyroscopic orientation recorder. In the approximation indicated by the equation above, $\bar{\alpha}$ is assumed constant and hence the path is circular. The gyroscopic orientation recorder yields records of the angle that the axis of the torpedo makes with the horizontal as a function of distance or, as illustrated in Figure 57, time. Since the path is assumed circular, R is determined simply by $R = (s_c - S)/\Delta(\theta - \alpha)$. In this manner the results listed below were obtained for cold shots. These values are only very approximate and are subject to considerable error.

R (ft)	Weight (lb)
600	1,861
500	1,648
500	1,862
450	1,635
450	1,681

However, it is remembered that the cavity contracts at the torpedo tail during the open cavity

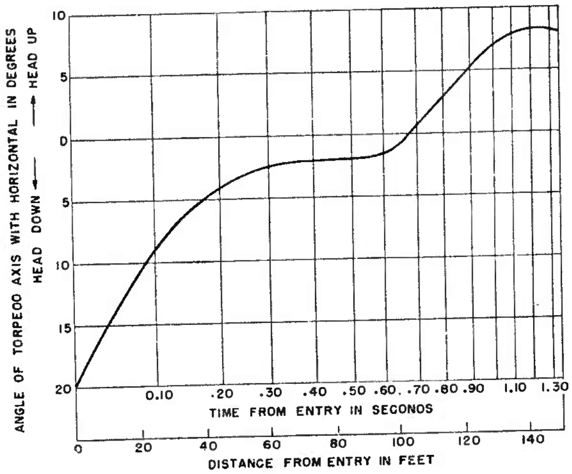

FIGURE 57. Typical record of angle of axis of torpedo versus time. This record is for a cold shot.

stage. From Figure 46 it appears that the contraction might be taken as decreasing $\Delta(\theta - \alpha)$ by approximately 3° and probably more. This is a very significant correction and must be applied. Making this correction in R and adjusting the results to a common weight of 2,160 lb, by the relation expected from the equations, $R \propto M$, we find that for the Mark 13 torpedo $R \approx 400$ ft. Then, from the equation above, it is found that for the Mark 13 torpedo roughly $\bar{\alpha} = 13°$. The value of $\bar{\alpha}$ computed for the cold shots seems in fair agreement with the observed gyroscopic orientation recorder records.

With the value of R, $\Delta\theta$ can be computed. Thus $\Delta\theta = (s_c - S)/R$, or θ_c, the trajectory angle at cavity closure, is given by

$$\alpha_e > \alpha_c\,, \qquad \theta_c = \theta_e - \Delta\theta\,,$$
$$\alpha_e < \alpha_c\,, \qquad \theta_c = \theta_e + \Delta\theta\,.$$

Taking a typical case where $V_e = 350$ ft per sec and 600 ft per sec, it is found that θ_c versus α_e for the Mark 13 torpedo is given in Figure 58, for $\theta_e = 20°$ and $\psi_e = 0°$. Altering θ_e with the same α_e will change θ_c through the quantity S.

From this figure we see that a small change in α_e from 2° nose-down to 3° nose-down changes θ_c from 15° to 27°.

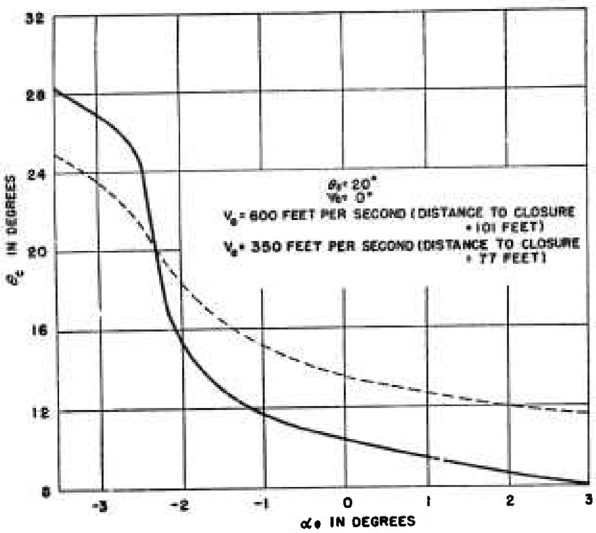

FIGURE 58. Mark 13 torpedo. Trajectory angle at cavity closure versus pitch angle at entry.

From the expression for $\bar{\alpha}$ given by equation (49) it is possible to solve for C_{lt}'. Hence knowing $\bar{\alpha}$ (or knowing R which determines $\bar{\alpha}$) should presumably determine C_{lt}' by the equation

$$C_{lt}' = \frac{C_{ln}' \dfrac{l_1}{l_2}}{1 - \dfrac{\alpha_w}{\bar{\alpha}}},$$

where α_w is determined by the nose shape. Thus C_{lt}' can be calculated for the various rockets in Table 1. The method by which this could be carried out is clear. These calculations will not all be exhibited, but C_{lt}' will be examined for the Mark 13 torpedo with and without a shroud ring based on the very rough values of R obtained at the CIT–TLR.

For the Mark 13 torpedo it was found that $\bar{\alpha} = 10°$. Then during this stage $\alpha_w/\bar{\alpha} \cong 0.5$, $C_{ln}'(l_1/l_2) = 0.35$, C_{lt} (Mark 13 torpedo with shroud ring) $= 0.70$.

From some three cold shot launchings without a shroud ring it is found (correcting to $W = 2{,}160$ lb) that $R \approx 200$ ft and as a result $\bar{\alpha} \approx 20°$. Consequently, C_{lt}' (Mark 13 torpedo without shroud ring) $= 0.50$ is then found.

Very similar calculations may easily be carried out for the horizontal plane.

On the basis of the various values of R and $C_D = C_D' + C_L'\bar{\alpha}$, one may calculate C_{lt}' and it appears possible to make a rough guess at the values for arbitrarily shaped projectiles. However, this is still very crude.

The possible oscillatory behavior of flat-nose torpedoes has already been mentioned. The trajectory resulting is essentially oscillatory with no general curvature.

EFFECT OF PROPELLERS DURING THIS STAGE OF THE MOTION

The effect of propellers during this stage of the motion is to produce a rolling velocity, to produce a small increase in tail drag C_{Dt}, and to produce a cross force at the torpedo tail. It is this cross force that is of major importance since it may produce large changes in the underwater trajectory. If a torpedo enters with $\alpha_e > \alpha_c$ so that it strikes the bottom of the cavity wall and if there is a sufficiently large cross force at the tail, it may rebound to the top wall, and the subsequent trajectory would be of the downturning type instead of the expected upturning trajectory.

In model tests by the British of their aircraft torpedo it has been observed that without propellers the torpedo rested on one side of the cavity, while with propellers the torpedo rebounded from the wall which it struck originally. Model tests of the Mark 13 torpedo in the United States made without propellers indicated no rebounding. In addition, tests have been made with a full-scale powered Mark 13 torpedo equipped with propellers. From these tests a clear sensitivity of depth of dive to pitch angle was observed. For $\alpha_e > \alpha_c$ the depth of dive was relatively shallow, while for $\alpha_e < \alpha_c$ the torpedo struck bottom or at least dived very deep. If rebounding occurred, one should have observed some deep dives and some shallow dives for $\alpha_e > \alpha_c$. Since this was not observed, it is inferred that the Mark 13 powered torpedo does not rebound. Records obtained with the gyroscopic orientation recorder on Mark 13 shots under power indicate that during the open cavity stage there is no marked change in the inclination of the axis of the torpedo in the vertical plane as would appear with rebounding.

From a single gyroscopic orientation recorder record it appears that R is practically unaltered by the removal of propellers. However, the crudeness of the measurements and the fact that there is only one record makes the evidence extremely inconclusive. Further experiments were made at the CIT–TLR with Steel Dummies fitted with fixed Mark 14 and Mark 15 propellers. For these launchings (where $\alpha_e > \alpha_c$) the gyroscopic recorder clearly indicated the torpedo rebounding from the bottom cavity wall.

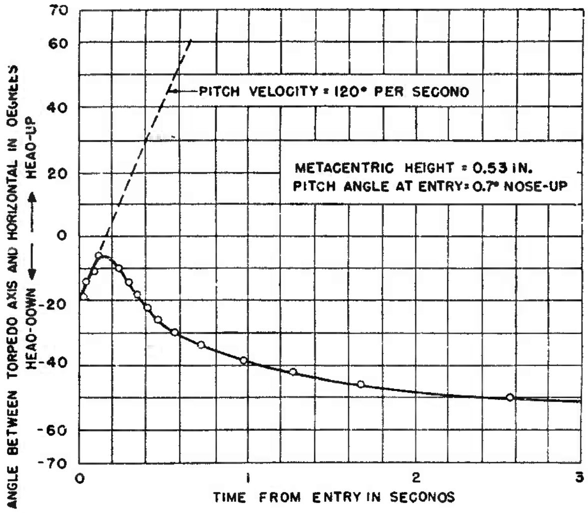

FIGURE 59. Inclination of torpedo axis versus time for MBB Dummy with fixed Mark 14 propellers. Notice nose-up pitching velocity at entry and rebounding from bottom cavity wall.

Typical records obtained are illustrated in Figures 59 and 60. For launchings of this type the trajectory data indicated a very deep dive. In addition, some records have been obtained with fixed propellers showing that the dummy rebounded from the bottom wall and down again from the top wall. From these results it is inferred that the cross force on fixed propellers is considerably greater than the cross force on moving propellers. This is perhaps what might be expected since the relative velocity and angle of attack on the propellers is reduced when they are revolving. In any case, it is probably true that C_H' with propellers is greater than without propellers.

As far as is known, the rebounding of the British torpedo has not been proved by observations on a full-scale torpedo. However, there are elements in that torpedo which make it more likely to rebound than the Mark 13 torpedo. The nose area of the British torpedo is 1.5 times the area of the Mark 13 nose, and hence the moment holding it in the cavity wall is greater. In addition, since the British torpedo is some three feet longer, $\bar{\alpha}$ is smaller; thus a smaller moment holds the torpedo against the cavity wall. There may also be a larger cross force on the British propellers than on the Mark 13 propellers.

6.4.4 Transition Region

The behavior of the torpedo in the transition region, that is, from its position at cavity closure to the

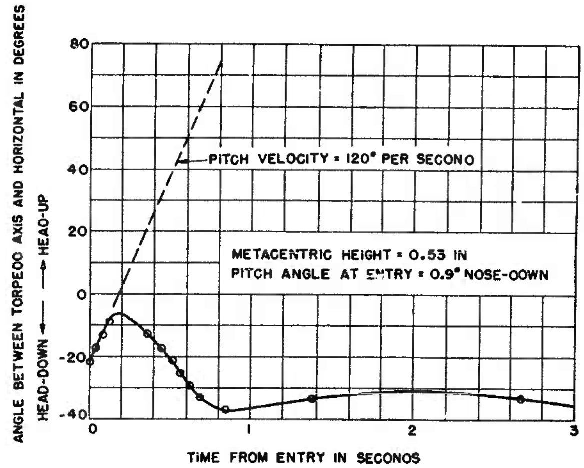

FIGURE 60. Inclination of torpedo axis versus time for MBB Dummy with fixed Mark 13 propellers. Notice nose-up pitching velocity at entry and rebounding from bottom cavity wall.

point where it is in practically noncavitating motion is about the most obscure part of the underwater trajectory.

EXTENT OF THE TRANSITION REGION

The point where this region begins is quite definite: it is the location of the torpedo at cavity closure and is given approximately by equation (42) and Figure 45. The point where this region terminates is somewhat arbitrary. The method that will be used to determine it is based on the fact that, after this transition region is traversed, it is desired to treat the torpedo as though it were in noncavitating motion. Hence the termination of this transition stage will be governed by the fact that the cavitation parameter K attains a value K^* such that effectively the torpedo is in noncavitating motion. The word "effectively" has been used since water tunnel tests indicate that an advanced stage of cavitation must be reached for the hydrodynamic parameters, especially C_D, to differ significantly from their values for noncavitating motion. Furthermore, since the fins of the torpedo and the control surfaces are very effective in controlling the motion when the torpedo is in a noncavitating state, the value of K corresponding to the end of the transition region is also determined by the requirement that there be no effective cavitation on the fins or control surfaces. Having found this value of K^* we may determine the approximate position of the termination of the transition stage. Thus

$$K^* = \frac{\rho g h^* + P_0 - P_c}{\frac{1}{2}\rho (V^*)^2}.$$

Now roughly

$$h^* = s^* \sin \theta_c ,$$

and

$$V^* \approx V_c \, e^{-Ks_c} e^{-\bar{k}(s^* - s_c)} ,$$

where s_c is the position of the torpedo at cavity closure and is given by equation (16). k'' is given by $k'' = C_D'' (\rho A/2M)$, where C_D'' is the average drag coefficient in this region. P_c, the pressure in the (closed) cavity, is not known and this point will be discussed later. However, the length of this transition stage $(s^* - s_c)$ is relatively insensitive to changes in P_c. It is therefore assumed that $P_c = P_0$. Hence we may say that the transition stage terminates approximately at the distance s which satisfies the equation

$$K^* \frac{\rho}{2} V_c^2 \, e^{2(k'' - \bar{k})s_c} e^{-2k''s^*} = \rho g s^* \sin \theta_c . \qquad (52)$$

For example, from water tunnel tests it appears that for the Mark 13 torpedo $K^* \approx 0.35$. For $\theta_c = 20°$, $V_c = 350$ and 600, it was found $s_c = 77$ ft and 101 ft. Using for k'' the value based on $C_D = 0.25$ it is found that s corresponding to the end of the transition region is 113 ft and 145 ft, or only 36 ft and 44 ft after cavity closure.

At cavity closure some air is entrapped with the torpedo. It appears that, due to the fact that the cavity closes in on the air surrounding the torpedo and since this air is at a depth corresponding to a considerable hydrostatic pressure, the pressure of the entrapped air tends to rise above atmospheric pressure P_0. At the same time some of the entrapped air is being entrained in the wake of the closed cavity and transported away. This phenomenon tends to diminish the pressure in the cavity during this stage of the motion. In addition, the cavitation parameter K is still sufficiently low so that the torpedo is cavitating, and as the torpedo moves along this tends to increase somewhat the volume of the cavity. By cavitation is meant the phenomenon whereby the pressure around some part of the torpedo falls to the value of the vapor pressure of the water (due to the velocity being sufficiently high) so that local vaporization of the water immediately commences, and ceases only when the pressure is greater than the vapor pressure of water. It is clear that the pressure cannot fall below the vapor pressure of water.

Thus it is clear that there are a number of effects tending to alter the pressure in the cavity, and it is difficult to say which one predominates. It is believed that the net result is that the pressure in the cavity may perhaps increase a small amount after cavity closure. This probably does not affect the motion significantly. Earlier in this section, in order to find the distance to where the torpedo is effectively in noncavitating motion it was assumed that during this stage $P_c = P_0$. This appears sufficiently accurate for such a calculation since the distance is relatively insensitive to changes in P_c.

The mechanism by which the air or cavitation cavity is carried away after deep closure is still obscure. It may be that small bubbles are entrained and carried away in the wake.

It appears from what has been said that the volume of the closed cavity diminishes since the pressure tends to increase and the mass of air in the cavity tends to decrease. Hence we may expect that the cavity width at the torpedo tail will probably diminish somewhat. The magnitude of this change in the cavity width at the torpedo tail is not known precisely, but as a very rough approximation the expression for the cavity width at the torpedo tail used previously might be used here and apply also to the short transition region. At the conclusion of the transition region α_c is assumed to be in the neighborhood of the value at the beginning of the region. It appears from water tunnel tests that for $K \sim 0.25$ there is a linear relation between the maximum closed cavity diameter and the radius of the hemispherical nose, as is expected from equation (51), where at a given cavitation parameter y is seen to be a practically linear function of r_s. This point lends further support to extrapolating the cavity width equation to the transition region.

A consideration of the forces on the torpedo during this stage of the motion indicates that any attempt at estimating their magnitude other than by experiment leads to almost unsurpassable difficulties. The expectation is that during the earlier part of this transition region C_D is approximately the same as in the stage with the open cavity, since $P_c = P_0$, and that the flow has not yet reformed on the afterbody. As the torpedo progresses during this stage, the cavitation parameter K increases until the cavity no longer envelopes the entire torpedo but begins to close in and the flow to reform on the afterbody. As soon as this occurs it is clear that a sudden reduction in the value of C_D will result since there will be pressures acting on the tapered afterbody of the torpedo in the opposite direction to the drag forces. Hence it is expected that the resultant drag force will continue to decrease as the flow proceeds to reform on more of the torpedo afterbody. As an illustration of how the flow around the torpedo changes with cavitation parameter K and yaw or pitch angle, Figure 61 is inserted. These are photographs of models in a water tunnel. It is clear that the size of the cavity increases for decreasing K. Calculating the value of C_D is therefore seen to be nearly impossible due to the lack of knowledge of the back pressures.

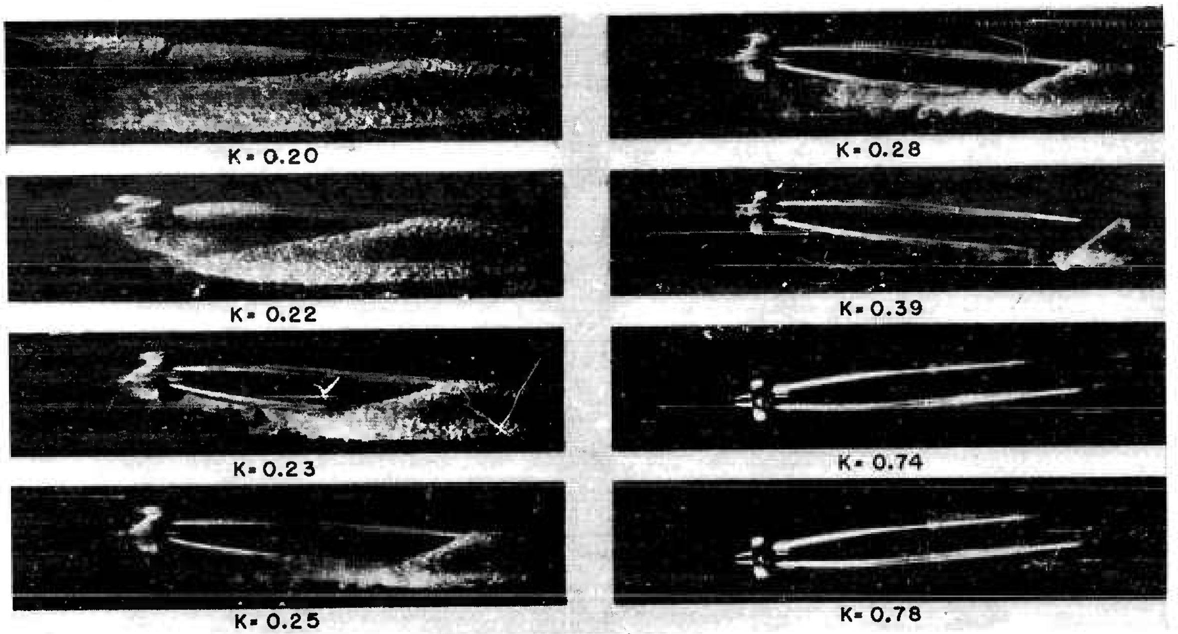

FIGURE 61. Illustration of change of flow in water tunnel about a 2-in. model of the Mark 13 torpedo with decreasing cavitation parameter, $K = (P_0 - P_c)/\frac{1}{2}\rho V^2$, for a pitch or yaw angle of 6°.

For the Mark 13 torpedo it appears from both full-scale and water tunnel results that C_D decreases during the transition region. Thus C_D, as defined by the relation $C_D = -(2M/\rho A)\ (dV/dt)$, diminishes from about 0.45 to approximately 0.1 in this small transition interval. In connection with the magnitude of C_D, it should be noted from Figure 62 that C_D does not increase significantly for the Mark 13 torpedo without propellers until K is well below the value for incipient cavitation.

The difficulty with the experimental approach to the problem is that with most apparatus one cannot reduce K sufficiently to reach the value existing during the transition region. Thus at the beginning of the transition region $K = 0$, and at the end of the stage K has a value K^* which will be different for each projectile. As will be seen $K^* \sim 0.35$ for the Mark 13 torpedo. Thus most of this stage of the motion is difficult to duplicate. There is some promise in apparatus now being constructed of ability to measure the forces and observe the cavitation for very low values of K, theoretically, almost down to $K = 0$. Some investigation of the forces acting on various torpedo bodies has been carried out in the variable pressure water tunnel at the CIT Hydrodynamics Laboratory. The essential results obtained are given in Figure 62. From these figures it is seen that precisely in the region of greatest interest (low K) the coefficients C_M, C_c, and C_D (for the Mark 13 torpedo body) vary so rapidly that extrapolation is unreliable. The precision of the results is not entirely known.

The value of K^* was chosen on the basis of photographs of the flow about the torpedo in the water tunnel for various values of K. From Figure 62 we might expect that roughly $K^* = 0.35$. Actually it would be necessary to measure effectiveness of fins and control surfaces as a function of K and to ascertain from these tests what value to use for K^*. However, with the present apparatus it is not feasible to run such tests. For calculations involving C_D during the transition stage, the mean value of C_D (and hence K) during this stage is used, namely, $C_D = 0.27$. This C_D is the mean between the open cavity value and the value at the termination of this stage.

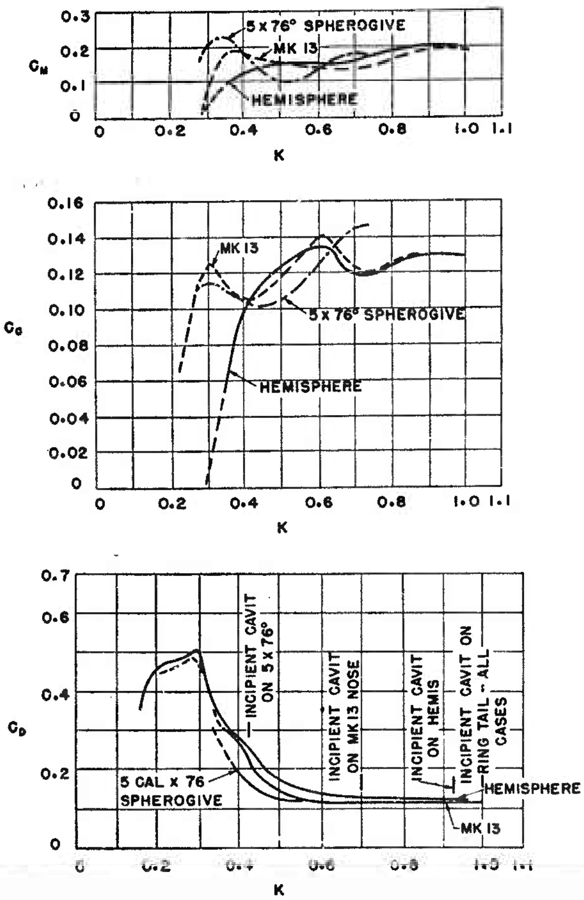

FIGURE 62. C_M, C_C, and C_D versus K for various nose shapes. Measurements on a projectile 7.18 calibers in length with center of gravity 42 per cent of the length from the nose.

During this transition stage, as the torpedo makes increasingly better contact with the water, the buoyant force on the torpedo increases from its value of close to zero in the open cavity stage to approximately its value in still water at the end of this stage. In addition, it appears that during this stage the torpedo continues to roll with a somewhat decreasing angular velocity due to some damping moments.

Since the magnitude of the forces acting on the torpedo during the transition stage is obscure, the trajectory of the torpedo during the transition stage may be taken, in a first approximation, to be a continuation of the trajectory in the open cavity stage and may be roughly described as a curve with increasing radius of curvature.

For the value of $\bar{\alpha}$ at the end of the transition region one may use as a first approximation the $\bar{\alpha}$ during the open cavity stage. However, there is some evidence pointing to a smaller value. First of all, from Figure 46 we see that α_w decreases considerably and quite rapidly during the transition region since it depends on a term of the form se^{ks}. Secondly, from Figure 62 which gives an indication of the approximate static moment coefficient of the forces on the torpedo, there are indications that there is close to zero moment on the torpedo at $K \sim 0.25$ and $\bar{\alpha} = 3°$. Based on these considerations it can be indicated that toward the end of the transition region $\bar{\alpha}$ for the Mark 13 torpedo is approximately 5°.

Condition of the Torpedo When Effectively in Noncavitating Motion

At the end of the transition region the torpedo is in the initial state for the subsequent run. The speed is given by

$$V = V_e\, e^{(k^* - \bar{k})s_e} e^{-k''s}.$$

The pitch angle will be determined by the nose shape (cavity width) and the values of θ_e, V_e, and ψ_e, and critically by α_e. If α_e is more nose-up than α_c the pitch angle at this point will be roughly the same number of degrees nose-down. For example, with the Mark 13 torpedo it was determined that at this point $\bar{\alpha} = 5°$ nose-up for $\alpha_e > \alpha_c$, while $\bar{\alpha} = -5°$ for $\alpha_e < \alpha_c$.

The yaw angle will also depend on these variables.

The roll orientation clearly depends on θ_e, and θ_e, as well as ψ_e, and the propellers. It is probably correct to say that any orientation is equally likely with the probability that the torpedo is a little closer to right side up than upside down.

The condition at cavity closure of the torpedo for which $\alpha_e \approx \alpha_c$ (so that the torpedo never really strikes the cavity wall) has to be considered a little more in detail. Thus for a torpedo entering in this manner we can estimate $\alpha(s)$ and $\psi(s)$, and the indications are that these remain fairly close to zero. The tail of the torpedo does not touch water until the cavity closes in about the torpedo. It must then be determined at what distance $\sqrt{\alpha^2 + \psi^2}$ = the angle of the cavity. Up to this point, C_D corresponds to C_{Dn} as given in Section 6.3. Hence, up to the distance S where the cavity closes in around the torpedo, the path is straight for a hemispherical nose, and, from that point to the end of the transition region, it is curved, depending further on whether the torpedo is toward the top or bottom cavity wall. For the limiting case of $\alpha_e = \alpha_c$, $\theta^* = \theta_e$, $\alpha^* = \alpha_e$, $D = s^* \sin \theta_e$. Clearly, if the cavity is closing in about the torpedo, the distance ($s^* = S$) is going to be relatively small. From the methods presented for handling the underwater trajectory, it is clear that these intermediate cases can be calculated.

6.4.5 Further Research and Experiment during the Open Cavity Stage and Transition Region

Despite the fact that a fairly clear qualitative description of the torpedo behavior during this stage of the motion has been presented, the quantitative results are very uncertain.

It appears that future research could determine some of the fundamental quantities considered. To be more precise, future study of the water entry of torpedoes should attempt to obtain with greater precision the C_{Dt} (tail drag coefficient) value during the open cavity and transition stage for various tail structures. Similarly, the value of C_{lt} (tail lift coefficient) is of importance and should be tabulated for various types of torpedo tails.

Presumably, on the basis of the theory presented, these coefficients might well determine the underwater trajectory of the torpedo during this stage of the motion. However, the cavity shape also enters into these considerations, and the theory of the cavity shape is only approximate. Hence during this stage of the motion the importance of a more precise theory of cavity shape is clear. It is especially important in the transition region since the pitch angle at the end of the transition region could then be determined.

If the value of the radius of curvature were known with some degree of precision or if $\bar{\alpha}$ were known, then C_{lt}' could be determined.

The most promising approach to practical results appears to be of the experimental type. Two general attacks appear hopeful. In the first method, observations are made either on full-scale torpedoes with recording apparatus or on reliable models with cameras. From these observations C_D, R, and $\bar{\alpha}$ may be determined and hence C_{Dt}' and C_{lt}'. The second approach is to obtain sufficiently low cavitation parameters in some water tunnel arrangement so that in this tunnel the forces and moments on the torpedo may be measured and the coefficients then determined directly.

As far as the cavity shape is concerned, the present kinematic theory may prove adequate. However, further experimental verification and research on the constants in the equation is necessary. Particular attention must be paid to the cavity shape during the transition region. Thus future research should obtain the basic constants entering into the equations of motion C_{Dt}' and C_{lt}', as well as the change in cavity shape during the transition region. This will determine the motion in this stage and the condition of the torpedo at the conclusion of this stage. The condition of the torpedo at the conclusion of this stage to a large extent determines the subsequent motion.

Modeling

The study of water entry by means of small-scale models is very attractive since underwater trajectories and many details of behavior may then be observed at a comparatively small expense.

The conventional method used for studying water entry is Froude modeling. By this method the scale factor for length of the model S_l is the square root of the scale factor for time S_t, or $S_l = \sqrt{S_t}$. As a consequence, accelerations on the prototype and the model are the same. This may be seen from the fact that accelerations have the dimensions l/t^2 on the prototype and $S_l l/(S_t t)^2 = l/t^2$ on the small model. As a result the effect of the acceleration of gravity (or the weight) is properly modeled.

This type of modeling has appeared to give realistic results in studying the water entry of blunt nose antisubmarine weapons and, in fact, for most projectiles studied in the past.

However, in the fall of 1944 the illusion of the universal success of a Froude model was shattered. As part of a program for studying head shapes, the CIT Morris Dam Group studied the water entry of a finer shaped nose than the hemisphere fitted to the Steel Dummy. With this fine nose the dummy actually dove to the bottom with a 4° nose-up pitch rather than having the expected shallower trajectory. Then the CIT–TLR fitted this head to a full-scale dummy, and the trajectory was of the rapidly upturning type until a pitch angle of 1.5° nose-down was reached. Hence an important violent discrepancy between full-scale and model trajectories was observed. This appears to be the first time that Froude modeling was noticed to be markedly unsuccessful in modeling water entry. The recognition of this fact appears to be a major step in the study of modeling, and the means of correcting this defect is the major problem which still appears to be wanting a complete solution. The discussion of the discrepancies, their causes and methods of partial solution are best considered under the various stages of entry.

Flow-Forming or Whip-Producing Stage

In the light of the theory presented in Section 6.3, one might expect that the reason why the model dove when it was expected to turn upward should probably be due to the fact that the whip at entry was not properly modeled. Hence, it was decided at the Morris Dam Group that the whip at entry of the models should be studied. To this end an optical whip recorder was designed whereby the whip at entry of the models could be measured. The results obtained by this recorder indicated that the whip of the models was radically different in many respects from the prototype whip.

It is remembered, from Section 6.2, that the prototype exhibits a large nose-up whip which varies as the first power of the entry velocity, or the whip divided by the entry velocity was a constant independent of the entry velocity. On the models the following startling results were observed:

1. At a Froude prototype velocity of 475 ft per sec the whip of the model of the Steel Dummy was only about one-third of the whip of the prototype, thus indicating why the trajectories were different from the prototype and the critical pitch results smaller.

2. At this same velocity, with the finer nose on the dummy, the whip at entry was *actually nose-down* instead of the very large nose-up whip observed on the prototype.

3. In addition, on the 1-in. model of the Steel Dummy the whip was observed to increase as the square of the entry velocity, while with the finer nose it increased very much more rapidly than the square of the entry velocity.

These results indicated the truly bad state of affairs in the modeling of the water entry of finer noses.

The next obvious question was what caused this very anomalous behavior of the 1-in. Froude model. Clearly, a different set of forces was controlling the model behavior than was controlling the prototype behavior. This is perhaps most clearly seen from the very large dependence of the whip on entry velocity.

It was evident that a large nose-down lift was acting on the torpedo nose during the flow-forming stage, and the various possible causes of this nose-down lift were systematically investigated. These investigations are reported in reference 14. The result of this study indicated that the cause of the nose-down lift appears to be associated with the narrow air space which exists when the flow separates from the finer shaped noses. There is a pressure drop in this narrow air space due to the viscous flow of air in it.

For the 1-in. model the Reynolds number in this space is estimated to be only around 5. Rough calculations indicate that due to this viscous flow of air the pressure reduction on the underside of the nose is of the order of ½ atmosphere, while on the top side of the nose is roughly atmospheric pressure. It appears that the downward lift force on the nose depends on the area and thickness of this laminar space between the solid and liquid and hence on the curvature of the nose, as is expected from the anomalous behavior of the finer noses.

Generally, it appears that the magnitude of the down lift varies with the Reynolds number. The ratio of the down lift to the normal nose-up lift caused by the hydrodynamic V^2 forces should decrease with increasing entry velocity and size as well as probably with decreasing density of air.

These contentions are supported somewhat by photographs of a launching of the finer head. One photograph is illustrated in Figure 63. On this photograph is clearly seen the fact that the water tends to "stick" to the underside of the nose. This is in marked contrast with Figure 4 in which the flow separates from all parts of the model nose.

In order to equalize the pressure in the air space on the underside and top side of the nose, a scheme which has proved moderately successful is known as "venting." By this method, holes are drilled in the torpedo model which permit free passage of air from the underside to the top side of the nose. As a result the pressure in the air on the underside of the nose tends to be the same as on the top side of the nose, which is the desired result. Many types of venting were tried using different shape and size holes and grooves. One fairly successful vented model in which the nose alone was vented is illustrated by the nose in Figure 65. (The other vents in this figure will be discussed subsequently.)

With this type of venting the model whip more nearly duplicated the prototype whip, although the problem is still far from being completely solved.

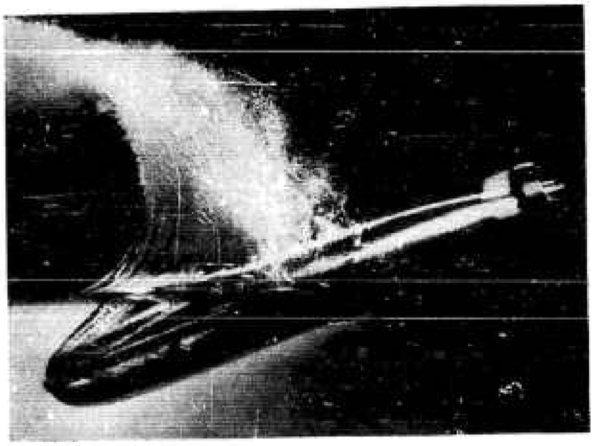

FIGURE 63. Water entry of unvented fine nose 2-in. model of Steel Dummy. Notice water "sticking" to bottom side of nose. Compare with Figure 4.

With venting, the model whip reached the value of only 70 per cent of the prototype whip. However, even with venting, the whip increases faster than the first power of the entry velocity, which is still in disagreement with the prototype results.

The results obtained with the Steel Dummy (with the Mark 13 nose) are illustrated in Figure 64. From this figure the discrepancy with the prototype is noticed.

Another troublesome point that was observed is that with the 2-in. model, which, since it is larger, should more closely duplicate the prototype whip, actually exhibited a smaller whip than the 1-in. model both when unvented and when vented.

Thus it is seen that, although much progress has been made in understanding the modeling of the entry whip, the state of the problem is still far from being satisfactory and discrepancies with the prototype results still remain. However, with blunter noses and with heads possessing discontinuities small models will probably not exhibit this very anomalous effect to any marked extent.

From the present understanding of the cause of the smaller whips in 1-in. models, one might expect that the modeling will improve with increasing entry velocity, thus indicating that stress modeling ($S_e = S_t$) is perhaps much better than Froude modeling during the flow-forming stage. Decreasing the density of the air also seems to be a step in the right direction.

UP TO TAIL SLAP

The lack of modeling of this stage is probably due to lack of modeling of the entry whip.

CAVITY BEHAVIOR AND TRAJECTORY AFTER TAIL SLAP

In the oblique entry of 1-in. models surface closure is practically always seen to occur. This may not be

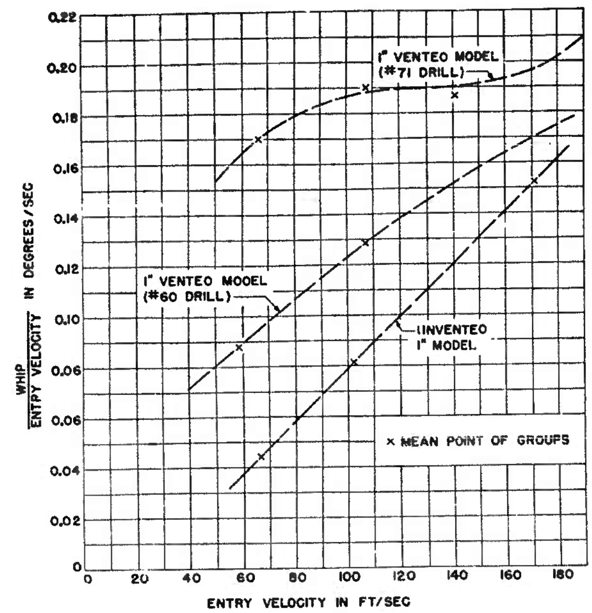

FIGURE 64. Whip/entry velocity of prototype and 1-in. model Steel Dummies versus entry velocity where $\theta_e = 19°$. Points represent averages of a number of observations.

the case on full-scale launchings, however, as yet no data on this point exist. It is observed that in the 1-in. model launchings the cavity appears to persist very much longer than what is believed, and sometimes seen, to occur on the full scale. In 1-in. vented model launchings, the cavity is sometimes seen to persist even to the broach of the model. The reason for this difference has not been investigated by the Morris Dam Group.

The trajectories after tail slap of the 1-in. Froude model were seen to dive after traversing about the first seven torpedo lengths despite the fact that the torpedo struck the bottom cavity wall and started to turn up. This is not a weight effect since the velocity is too large, and it differs very markedly from the prototype where the trajectories turn up.

This behavior appeared to improve (differ less from the prototype) the larger the entry velocity.

The cause of this behavior appears, as before, to be a down lift on the torpedo during the cavity stage. Hence the same remedy, namely, venting, was tried. Whereas, before, only the nose was vented to improve the whip, now the entire torpedo was vented, as illustrated in Figure 65. The result was a marked improvement in the subsequent underwater trajectory. Before the rest of the dummy was vented, the model

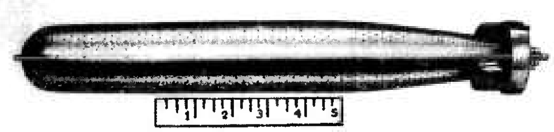

FIGURE 65. Illustration of the 2-in. vented model of CIT Steel Dummy.

appeared to dive, and, after the venting, it actually broached. However, as in the whip, the solution was not complete. The trajectories depend on velocity, and for a Froude prototype velocity of about 300 ft per sec even the vented models dive while the prototype continues to turn up.

Conclusions

The study and results of modeling indicate that effects which may truly be regarded as second order in prototype actually become first order for small, fine nose Froude models and hence cause very large discrepancies between the model and full-scale results.

For blunt noses or nose with discontinuities, much more faith can probably be put in the Froude model since the fine air space no longer exists.

The modeling of fine noses has definitely been improved by venting; however, experimental results clearly indicate that the problem is far from a satisfactory and complete solution. Hence small Froude model results must be used with a great deal of caution and experienced judgment.

6.5 RECOVERY STAGE

6.5.1 Introduction

During this stage the torpedo is in effectively noncavitating motion and is decelerating down to its running speed if it is powered or decelerating down to zero speed if unpropelled. If the torpedo is controlled, it will tend to return to the set depth and direction for its steady run. With the ordinary controls now in use, if the torpedo has rolled (as it generally does), a hook results, but it finally heads in the direction as directed by the gyro.

During this stage we know the equations of motion, and their solution is relatively simple. It appears that the motion of the torpedo can be predicted by the use of eight hydrodynamic constants together with a knowledge of the control mechanism. The subsequent discussion is equally applicable to torpedoes without controls, with fixed controls which are ideal, or with actual control systems. The specialization to ideal and actual controls will be given a little later.

6.5.2 Assumptions and Equations of Motion

Assumptions

In the general case, the torpedo is at a roll angle $\phi(s)$ and possesses a rolling angular velocity so that, at the beginning of this stage of the motion, the orientation about its longitudinal axis may be described by some roll angle and angular velocity. During this stage of the motion the controls, if they are operating normally, will call for hard up elevators since the torpedo is well below set depth. If the control includes a pendulum, it will be against the forward stop due to the deceleration of the torpedo, and this also will call for an up elevator. The vertical rudders, during the earlier part of this stage, will be hard over in a direction to prevent a change in heading due to the effect of the elevators in the horizontal plane that is associated with the roll displacement $\phi(s)$ and due to the initial heading error (at the beginning of this stage) arising from the fact that the torpedo may have gone to one side of the cavity in the previous stage and may therefore be pursuing a curved path. Clearly, if the torpedo is without controls (like rockets and the Steel Dummy), the effect of roll on the motion during this stage will be practically negligible. In view of the fact that the elevators are hard up, at least until the torpedo reaches a depth, inclination, and speed at which the controls call for a different elevator angle, it may be assumed that during the earlier stages of the motion the elevator angle ξ has a constant value ξ_0, corresponding to the limit of the up elevator throw or $\xi_0 = 0$ in the particular case that the torpedo has no controls. Similarly, the vertical rudder angle δ has the constant value δ_0 corresponding to the maximum rudder throw.

In Section 7.2 the equations of motion are derived for a torpedo in the steady state, which is right side up, ($\phi = 0$). Strictly speaking, the equations are derived either for a torpedo for which ϕ = constant = $0, \pi/2, \pi, 3\pi/2$. The general case is to be considered here of a torpedo at a roll angle $\phi(s)$ which is not constant. For a first approximation the roll will be introduced as an independent effect, assuming that the roll influences the motion of the torpedo only through the changing components of the elevator and rudder forces and moments. This assumption is probably accurate enough for a first order theory, provided the torpedo is somewhat symmetrical. Generally, torpedoes are composed of a body which is a solid of revolution with perhaps an appendage which is rotationally symmetrical like the shroud ring so that the body has an infinite number of axes of symmetry. To this body are generally added the fins and controls. It is the latter two appendages which, if they are present, cause the torpedo to deviate from a body of revolution. For a torpedo with four fins which are equal in area, the torpedo appears the same when rotated through 90°, 180°, 270°, and 360° angles; in other words, the torpedo then has a fourfold axis of symmetry. With controls there is generally only a twofold axis of symmetry. In the assumption mentioned above it is assumed that, for example, in the horizontal plane the hydrodynamic coefficients of the torpedo (excluding controls) are to the first approximation insensitive to changes in roll orientation ϕ. The error in this assumption is not very great and certainly decreases with increasing rotational symmetry. Thus, in this first order approach, the equations developed in Chapter 7 may be used if the effect of both elevators and rudders in the vertical and horizontal planes is considered. For example, for the elevator against the bottom stop and the vertical rudder against the side stop, the lift coefficient in the vertical plane when the torpedo is rolled through an angle ϕ would be given by

$$-C_{\lambda_e}\xi_0 \longrightarrow -C_{\lambda_e}\xi_0 \cos\phi - C_{\lambda_r}\delta_0 \sin\phi\,.$$

In Chapter 7 no account is taken of changes in speed of the torpedo since only the steady running state is considered where speed changes are negligible. As a matter of fact, even the very large deceleration during the recovery stage affects the motion only as it affects the control mechanism. This is true because of the assumption that all of the forces are proportional to the square of the instantaneous velocity and independent of the acceleration.

The only exception is the case of the gravitational forces and moments. These lead to the terms

$$\frac{2(W-B)}{\rho A V^2} \quad \text{and} \quad \frac{2aB}{\rho A V^2}$$

so that they become more important as the velocity diminishes.

If the thrust of the propellers were independent of the velocity it would be possible to write

$$M_1 V V' = -C_D \frac{\rho A}{2}(V^2 - V_r^2)\,, \tag{53}$$

where V_r is the running speed. Some observations have led to the value of $C_D = 0.45$ based on this equation. This is obviously too large a value to represent a true drag coefficient and it must be concluded that equation (53) does not really represent the true situation.

That equation (53) is incorrect is really quite understandable for the thrust of a propeller depends upon its motion through the water. If the torpedo is moving faster than the speed corresponding to the propeller rotation, the propeller might even produce a drag instead of a thrust. A good estimate is probably obtained by neglecting the propeller altogether and setting

$$M_1 V V' = -C_D \frac{\rho A}{2} V^2 \tag{54}$$

as long as $V > V_r$ and treating V as constant after it gets near the value V_r. Then

$$\frac{2(W-B)}{\rho A V^2} = \frac{2(W-B)}{\rho A V_0^2}\, e^{C_D \frac{\rho A}{M_1} s} \tag{55}$$

until

$$e^{C_D \frac{\rho A}{M_1} s} = \frac{V_0^2}{V_r^2}\,.$$

EQUATIONS OF MOTION

With all these considerations the equations of motion in Chapter 7 when the torpedo is rolled through an angle $\phi(s)$ and decelerating become:

Vertical Plane.

$$m\Omega + m_2\alpha' + C_l\alpha = -C_{\lambda_e}\xi_0 \cos\phi - C_{\lambda_r}\delta_0 \sin\phi + \frac{2(W-B)e^{C_D\frac{\rho A}{m_1}s}}{\rho A V_0^2}, \quad (56)$$

$$n\Omega' + C_K\Omega + C_m\alpha = C_{\mu_e}\xi_0 \cos\phi + C_{\mu_r}\delta_0 \sin\phi + \frac{2Bae^{C_D\frac{\rho A}{m_1}s}}{\rho A V_0^2}, \quad (57)$$

where it has been assumed that $\cos\theta = 1$.

Horizontal Plane.

(essentially replacing $\Omega \rightarrow \omega$, $\beta \rightarrow \psi$)

$$m\omega + m_2\psi' + C_l\psi = C_{\lambda_e}\xi_0 \sin\phi - C_{\lambda_r}\delta_0 \cos\phi\,, \quad (58)$$
$$n\omega' + C_K\omega + C_m\psi = -C_{\mu_e}\xi_0 \sin\phi + C_{\mu_r}\delta_0 \cos\phi\,. \quad (59)$$

ROLL, $\phi(s)$.

In order to obtain a solution of these equations, it is necessary to know how ϕ varies with s. To obtain this dependence it appears that one must revert to experiment. In the case of the Mark 13 torpedo with a shroud ring, the torpedo roll appears to attenuate exponentially from a maximum value at the beginning of this stage of motion. Without the shroud ring the roll continues to increase for a distance of about 250 ft and then begins to damp out. A possible explanation for this behavior is that the shroud ring increases the effectiveness of the fins so that they are able to damp out the motion more rapidly. A typical curve of roll angle versus distance is given in Figure 66 for the Mark 13 torpedo with a shroud ring when entering right side up and upside down. This is the second effect of the shroud ring on the Mark 13 torpedo that has been encountered. The first effect discussed in Section 6.4 was to increase the tail lift and hence to increase the radius of curvature of the path in the cavity stage and to decrease the mean pitch and yaw angles. For torpedoes without controls, no knowledge of the roll is necessary in this approximation. In general, the roll angle as a function of distance must be obtained experimentally since it depends on the roll velocity at the beginning of this stage and on the damping in roll of the torpedo.

In order for equations (56 and 57) to be amenable to analytic integration ϕ must be expressed as a linear function of s. If this cannot be done, the equations may be integrated numerically. The fact that with

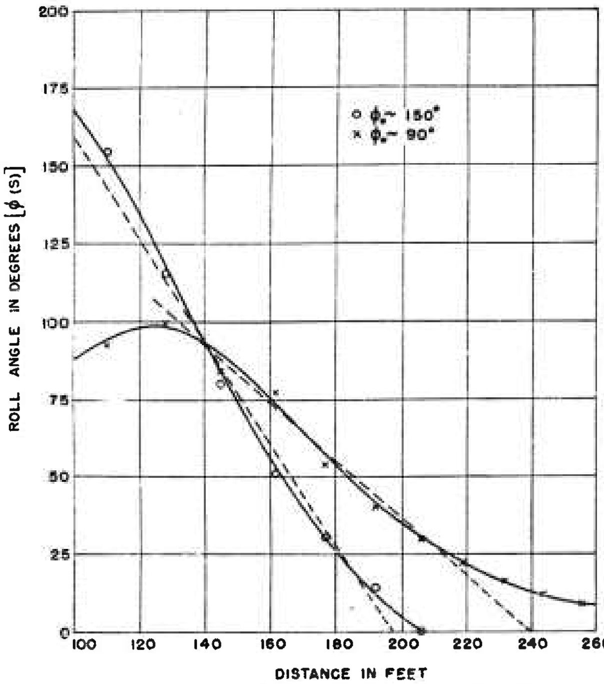

FIGURE 66. Roll of Mark 13 torpedo with shroud ring versus distance from entry.

the shroud ring the roll seems to attenuate exponentially indicates that the motion is over-damped. Hence it might be expected that $\phi = \phi_0 e^{-as}$. Then as this expression is expanded and two terms retained thus

$$\phi = \phi_0(1 - as),$$

where ϕ_0 is the roll angle at the beginning of this stage and a is obtained from the slope of the curve of $\phi(s)$ in Figure 66 (s is in torpedo lengths). It appears that for $\phi_0 = 90°$, $a\phi_0 = -12.5$ degrees/torpedo length and for $\phi_0 = 150°$, $a\phi_0 = -21.5$ degrees/torpedo length, approximately $a = 0.14$ per torpedo length.

This approximation must be treated somewhat differently without a shroud ring since there is a very small attenuation of roll. Clearly, it is also applicable to torpedoes without controls.

Then, writing

$$A_1 = C_{\lambda_e}\xi_0 \cos\phi_0\,, \qquad A_1' = C_{\lambda_r}\delta_0 \cos\phi_0\,,$$
$$A_2 = C_{\lambda_e}\xi_0 \sin\phi_0\,, \qquad A_2' = C_{\lambda_r}\delta_0 \sin\phi_0\,,$$
$$A_3 = C_{\mu_e}\xi_0 \cos\phi_0\,, \qquad A_3' = C_{\mu_r}\delta_0 \cos\phi_0\,,$$
$$A_4 = C_{\mu_e}\xi_0 \sin\phi_0\,, \qquad A_4' = C_{\mu_r}\delta_0 \sin\phi_0\,,$$

the equations of motion become:

Vertical Plane.

$$m\Omega + m_2\alpha' + C_l\alpha = -(A_1 + A_2')\cos(as\phi_0)$$
$$(A_2 - A_2')\sin(as\phi_0) + \frac{2(W-B)e^{C_D\frac{\rho A}{m_1}s}}{\rho A V_0^2}\,, \quad (60)$$

$$n\Omega' + C_K\Omega + C_m\alpha = (A_3 + A_4')\cos(as\phi_0)$$
$$+ (A_4 - A_3')\sin(as\phi_0) + \frac{2Bae^{C_D\frac{\rho A}{m_1}s}}{\rho A V_0^2}\,. \quad (61)$$

Horizontal Plane.

$$m\omega + m_2\psi' + C_l\psi = (A_2 - A_1')\cos(as\phi_0) - (A_1 + A_2')\sin(as\phi_0), \quad (62)$$

$$n\omega' + C_K\omega + C_\mu\psi = -(A_4 - A_3')\cos(as\phi_0) + (A_3 + A_4')\sin(as\phi_0). \quad (63)$$

These equations are integrated up to a value of s such that $\phi = 0$, at which distance the torpedo is right side up. Since the motion is over-damped, from that position onwards $\phi \sim 0$. Hence at the value of s such that $\phi(s) = 0$ the new equations of motion are dealt with, which are the same as the ones up to this point, except that it is assumed $\phi = 0$ on the right side of equations (56) to (59).

SOLUTION OF EQUATIONS OF MOTION

The general solution of the equation is:

Vertical Plane.

$$\Omega = \Omega_1 e^{p_1 s} + \Omega_2 e^{p_2 s} + \Omega_3\cos(\phi_0 as) + \Omega_4\sin(\phi_0 as) + \Omega_5 e^{\gamma s} + \Omega_6\,,$$

$$\alpha = \alpha_1 e^{p_1 s} + \alpha_2 e^{p_2 s} + \alpha_3\cos(\phi_0 as) + \alpha_4\sin(\phi_0 as) + \alpha_5 e^{s} + \alpha_6\,.$$

The value of p_1 and p_2 is determined by the requirement that a necessary and sufficient condition for the equations,

$$m\Omega_i + (m_2 p_i + C_l)\alpha_i = 0\,,$$
$$(np_i + C_K)\Omega_i + C_m\alpha_i = 0\,,$$

to have a nonzero solution is that the determinant of the coefficients of α_i and Ω_i must vanish. Hence

$$p_i = -\frac{(nC_l + m_2C_K) \pm \sqrt{(nC_l + m_2C_K)^2 - 4nm_2(C_lC_K - mC_m)}}{2nm_2}$$

$$(i = 1, 2)\,.$$

The constants α_1, α_2, Ω_1, and Ω_2 are determined from the initial conditions of the motion, α^* and $\Omega^* = l/R$ as given in Section 6.4, and also by the equations of motion (56 and 57) setting $s = 0$. Thus α^* and Ω^* with the equations of motion (60 and 61) at $s = 0$ determine α_1, α_2, Ω_1, and Ω_2. Thus there are really only two independent constants since the other constants α_3, α_4, α_5, α_6, Ω_3, Ω_4, Ω_5, and Ω_6, are completely determined. Equating coefficients of cos $(\phi_0 as)$ and sin $(\phi_0 as)$ one obtains four equations with the four unknowns α_3, α_4, Ω_3, and Ω_4 which may easily be solved, thus determining α_3, α_4, Ω_3, and Ω_4. In a similar manner, α_5 and Ω_5 may be determined from the equations of motion simply by equating coefficients of $e^{\gamma s}$. The constants α_6 and Ω_6 are determined by equating coefficients of the constant terms in the equations of motion. When $\phi(s) = 0$, the equations of motion become

$$m\Omega + m_2\alpha' + C_l\alpha = -(C_\lambda\xi_0 - \bar{w}_0) - \bar{w}_0 F e^{\gamma s}\,,$$
$$n\Omega' + C_K\Omega + C_m\alpha = (C_\mu\xi_0 + \bar{b}_0) - \bar{b}_0 F e^{\gamma s}\,,$$

where

$$\bar{w}_0 = \frac{2(W-B)}{\rho A V^2[(\phi = 0)]}\,,$$

$$\bar{b}_0 = \frac{2Ba}{\rho A V^2[(\phi = 0)]}\,,$$

and $(C_\lambda\xi_0 - \bar{w}_0)$ and $(C_\mu\xi_0 + \bar{b}_0)$ are constants. $V^2[(\phi = 0)]$ means V^2 evaluated at the value of s where $\phi = 0$.

Then the general solution is

$$\alpha = \alpha_1 e^{p_1 s} + \alpha_2 e^{p_2 s} + \alpha_3 e^{s} + \alpha_4\,,$$
$$\Omega = \Omega_1 e^{p_1 s} + \Omega_2 e^{p_2 s} + \Omega_3 e^{s} + \Omega_4\,.$$

The constants of integration may be obtained as outlined earlier.

Then, since $\theta = \alpha + \beta$, the change in depth is given by

$$D = D_0 - \int_0^s \sin(\alpha + \beta) ds \approx D_0 - \int_0^{s(\phi = 0)} (\alpha + \beta) ds - \int_{s(\phi = 0)}^s (\alpha + \beta) ds ,$$

$$x = x_0 + \int_0^s \cos(\theta + \beta) ds \approx x_0 + s ,$$

where $\beta(s) = \beta_0 + \int_0^s \Omega ds$ and D_0 is the depth at the beginning of this stage of the motion (or at the end of the transition stage as given under *Condition of the Torpedo When Effectively in Noncavitating Motion* in Section 6.4.4. β_0 may also be obtained from *Condition of the Torpedo When Effectively in Noncavitating Motion*, Section 6.4.4. Thus $\beta_0 = \theta^* - \alpha^*$.

It has been assumed that $(\alpha + \beta)$ is usually small enough so that $\sin(\alpha + \beta) = \alpha + \beta$. This is sufficiently accurate for upturning trajectories and some downturning trajectories. For most torpedoes going to the top of the cavity the trajectory angle becomes large so that $(\alpha + \beta) >> \sin(\alpha + \beta)$. The integration can be carried through graphically or numerically in such a case.

In the horizontal plane there is a completely analogous solution, except that $\beta_5 = \Omega_5 = \beta_6 = \Omega_6 = 0$. D becomes the course deviation in the horizontal plane.

It is to be noted that in the special case where the torpedo does not have controls $C_\lambda \xi_0 = C_\mu \xi_0 = C_\lambda \delta_0 = C_\mu \delta_0 = 0$ and the equations of motion are very much simplified.

CONTROLS

Torpedoes with controls possess a control system that transmits signals to the elevators and rudders. The signals transmitted depend on the orientation and the position of the torpedo. Two types of control systems may be considered, an ideal one and one similar to that of the Mark 13 torpedo.

We shall take as an ideal system, one in which

$$\xi = \xi_r - \lambda\beta - \sigma h ,$$

where ξ_r is the steady running elevator angle, λ and σ are constants depending on the control.

An actual control system usually includes a pendulum, and in a system similar to that in the Mark 13 torpedo

$$\xi = \xi_r - r(\beta + X) - \sigma h ,$$

where X is the angle the pendulum makes in space, so that $-(\beta + X)$ is the angle the pendulum makes with the torpedo axis. This relationship between the attitude of the torpedo and the elevator position is correct only in the case of steady motion. A deceleration will change the reference direction and produce a spurious response. Although both of these expressions refer to controls of the proportional type, similar considerations are also applicable to on-off (two-position) controls since they behave like proportional controls in many respects (see Section 8.4).

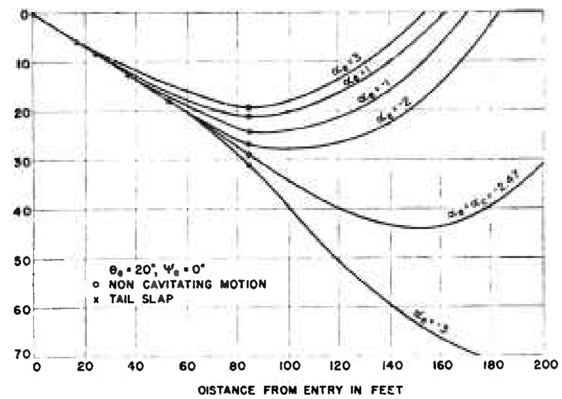

FIGURE 67. Theoretical trajectories for CIT Steel Dummy for various pitch angles at entry.

In the ideal case, the controls govern the elevators when the value of ξ called for by β and h is not greater than ξ_0. Similarly, the controls of the Mark 13 torpedo take over when β and X have the values such that $|\xi| \leq \xi_0$. This may be obtained from the equation of motion of the pendulum, equation (1) in Chapter 12.

At this point along the trajectory the equations of motion given in Chapter 7 are used, and the value of ξ as given by the control equations is inserted in them. Then the set of differential equations is readily integrated.

In the horizontal plane, the controls of the Mark 13 torpedo are of the on-off type. Hence the vertical rudder is usually over against the stop until the angle between the torpedo axis and the gyroscope becomes zero.

As an example of the calculation of the trajectory for a torpedo without controls the equations of motion in the vertical and horizontal plane for the CIT Steel Dummy can be solved.

In the vertical plane, the theoretical trajectories for $\theta_e = 20°$ are drawn for various pitch angles at entry in Figure 67. One case is included where the pitch angle at entry is more nose-down than the

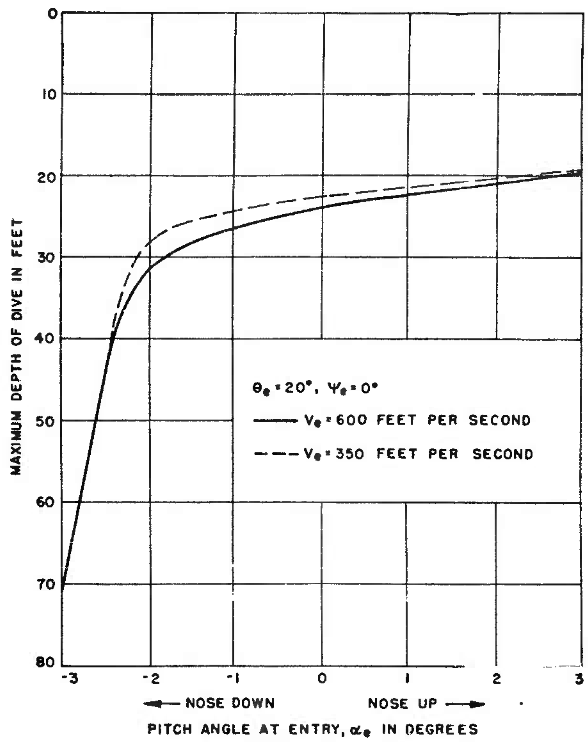

FIGURE 68. Theoretical maximum depth of dive versus pitch angle at entry.

critical pitch angle. These trajectories are in close agreement with observed trajectories at the CIT-TLR. In Figure 68 the theoretical maximum depth of dive for $\theta_e = 20°$, $\psi_e = 0°$, is plotted against the entry pitch angle. From this figure the dependence of the maximum depth of dive on entry velocity is seen to be very slight.

In the horizontal plane, by theory it is readily found that for $\psi_e = 3.5°$, $\alpha_e = -2°$, the lateral course deflection of the Steel Dummy at 550 ft from entry is about 40 ft, which is very close to the observed results. In Figure 69 a graph is plotted of the theoretical and observed results for the angle in the horizontal plane between the torpedo axis and the direction of launching. A fair agreement with experiment is noted.

By methods outlined, similar calculations can be carried out for torpedoes with controls whose hydrodynamic constants are known. If the dependence of the entry whip on the trajectory angle is known, it is a simple matter to calculate the depth of dive as a function also on the trajectory angle at entry. In the absence of precise knowledge of this dependence, it could probably be assumed that the variation is as the cot θ_e for which there is some evidence.

6.5.3 Description of Motion in Recovery Stage

GENERAL BEHAVIOR

Generally, the torpedo begins the stage with a large pitch angle (nose-up or nose-down) and a yaw angle. Until these are reduced to small values so that the

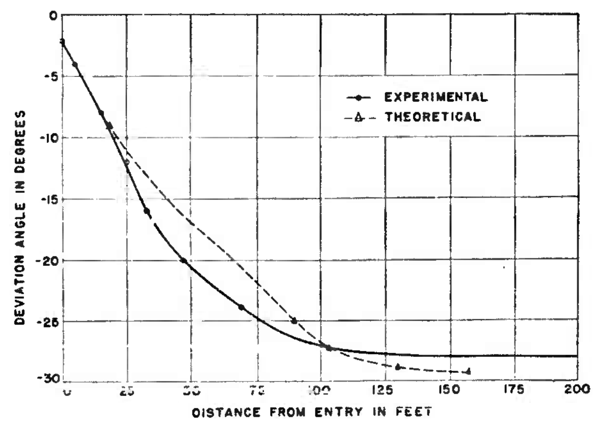

FIGURE 69. Angle in horizontal plane between axis of Steel Dummy and direction of launching.

torpedo is "on its trajectory," large lift and cross forces are experienced. Thus, if the torpedo is on the bottom of the cavity, the large initial nose-up pitch angle produces a lift force that counteracts the effect of the controls even if the torpedo is upside down. If the torpedo is at the top of the cavity, even if it is right side up, the forces due to the nose-down pitch continue the torpedo on its downturning trajectory, causing a great depth of dive. Thus there is a transition region during which the torpedo settles down to a steady motion, the transients damp out, and the torpedo tends to line up with its trajectory.

In the horizontal plane, since the torpedo possesses an initial yaw angle and angular velocity and also since the torpedo is generally rolled over initially there are forces tending to produce a course deflection, and the path curves away from the straight line in which the torpedo was aimed. Clearly, this deflecting force and moment diminish for two reasons as the torpedo proceeds along its trajectory. First, the yaw angle and hence the cross force diminishes; and, secondly, the torpedo is righting itself, and the effect of the elevators in producing a course deflection diminishes as the torpedo rights itself, while the effect of the rudders in straightening the path continues to increase. As a result of these effects the path curves toward the desired direction until it finally straightens out. The net result is a lateral displacement of of the path of the torpedo.

The effect of the controls in producing a hook is probably considerably greater than the effect of the initial yaw angle ψ_e that causes the torpedo to ride on one side of the cavity. The effect of the elevators in producing this hook is indicated by observations at the CIT-TLR. On most of the launchings the torpedo is rolled at the beginning of this stage of the motion between 0 and $-180°$ (a counterclockwise roll). As a result a left hook is expected. However, this hook has been considerably diminished, and even a right hook has been produced by means of the counter pendulum and anti-pendulum. By these devices the elevators are held in a neutral or down position for a short time after entry.

Effect of Shroud Ring

During the open cavity stage it was seen that the shroud ring produced an additional lift at the tail and thus increased the radius of curvature of the trajectory. This effect tends to create a greater depth of dive for the torpedoes on the bottom of the cavity and a shallower depth of dive for torpedoes on the top of the cavity than is the case of a torpedo that has no shroud ring. It also tends to produce a smaller hook for torpedoes striking the side cavity wall.

The principal effect of the shroud ring probably takes place after cavity collapse and may be traced to the decrease in the effectiveness of the elevators and rudders, the increase of the static stability of the Mark 13 torpedo, and the increased damping of roll which it produces. The first effects combine to increase the turning radius of the torpedo both in the horizontal and vertical planes by roughly a factor of 4 to 5. As a result, the large hook effected by a torpedo without the shroud ring is considerably diminished since the torpedo turns in a much larger circle. Some tests were run with the shroud ring in a position somewhat farther forward on the fins than the standard position. On the Mark 13 torpedo the forward position of the shroud ring gives the controls an intermediate effect and hence an intermediate turning radius, and probably does not damp out the roll as rapidly as the aft position. Hence an intermediate value in the number and extent of the hooks for the forward position may be effected. All these conclusions have been observed in full-scale launchings at various naval torpedo stations.

The effect of the shroud ring on the depth of dive may also be explained by the differences produced in the hydrodynamic constants of the torpedo. The turning circle in the vertical plane is of considerably larger radius with the shroud ring aft than without the shroud ring and is roughly intermediate between these two values for the shroud ring forward. Hence, for a given set of conditions at the beginning of this stage of the motion, the torpedo without the shroud ring will tend to turn up in a very tight circle (or turn down if it is rolled over), while with the ring it will turn up in a comparatively large circle. As a result, it is expected that the depth of dive without the ring will be less than with the ring aft and the depth of dive with the ring forward will be in between. These conclusions have also been verified in full-scale tests at various naval torpedo stations.

Broaching

Many torpedoes emerge from the water after traveling some distance beneath the surface. This is called a broach. The cause of broaching lies in the trajectory during the open cavity stage as well as in the torpedo controls. Clearly, if the cavity does not close until the torpedo has progressed some distance under water and if the torpedo strikes the bottom side of the cavity, it will pursue an upturning trajectory which has been shown to be roughly circular in form. Consequently, the torpedo may emerge from the water while in this open cavity stage, as appears to be the case in very high speed rockets. In addition, even if the cavity closes while the torpedo is still submerged but the torpedo has turned up sufficiently so that it is headed toward the surface of the water, it may also broach. Thus it may be said that broaching will depend on the trajectory angle at entry θ_e since at cavity closure $\theta = \theta_e - \Delta\theta$ and $\Delta\theta$ is approximately constant. In addition, it is necessary for the torpedo to be on the bottom side of the cavity if it is to pursue an upturning trajectory, hence broaching will depend on whether $\alpha_e > \alpha_c$ or $\alpha_e < \alpha_c$. Furthermore, the more nose-up α_e the shorter will be the distance to tail slap, S, and the less will be θ at cavity closure. Broaching will also depend somewhat on V_e since the greater V_e the longer the time to cavity closure and hence the smaller θ, with a resulting greater tendency to broach. These conclusions have been verified in model and full-scale tests of bombs. Also, most rockets broach, and this may be attributed to small θ_e and large V_e.

In the case of torpedoes with controls there is an additional effect. It has been seen that at the beginning of the stage where the motion is in noncavitating water the torpedo is below set depth and decelerating, with the elevators, as a result, hard up. Even when the torpedo has reached its set depth it may still be decelerating sufficiently that the elevators remain hard up with the torpedo coming out of the water. It is expected that this phenomenon is more prevalent the higher V_e and has been so observed in British torpedo launchings.

When the torpedo broaches, its heading may change as it leaves the water. The torpedo may hook in either direction and it also may not rotate about a transverse axis in air with the result that it lands tail first. In this instance, there is another effect of the shroud ring. Due to the ring there is a restoring moment at the tail of the torpedo; when the nose emerges this moment tends to give the torpedo a nose-down angular velocity so that it re-enters head first. In addition, this moment tends to keep the torpedo on course so that the hook is small at broaching.

Chapter 7

UNDERWATER RUN

7.1 ESTIMATES OF COEFFICIENTS

Values of the drag coefficient C_D, the moment coefficient C_M, and the lateral force coefficient C_L, defined in equations (3), (1), and (2) of Chapter 4, can be determined from model tests or from towing, wind tunnel, or running tests with the full-scale torpedo. Because of the inaccuracy inherent in scaling up the drag from model to prototype, C_D would probably best be determined from a full-scale run in which the propeller thrust was measured by apparatus contained in the torpedo. In practice, however, model measurements are much easier to perform, and an extrapolation of C_D determined in the high-speed water tunnel as a function of Reynolds number is actually used.

The moment and force coefficients have been measured using 1/11-scale models in the high-speed water tunnel at the California Institute of Technology and 1/5-scale models in the wind tunnel at Gould Island. Values obtained in these two tunnels are not in complete agreement, and it appears that the discrepancies increase as the l/d ratio. They are probably due primarily to the smallness of the particular forces and moments being measured and to the difficulty of correcting for interference between model and support shield.

The moment increases from zero as the attack angle increases from zero, linearly at first, and less rapidly than this for larger angles. It has the sign of an upsetting moment, tending to increase the attack angle for small values of this quantity. It is because of this that torpedoes are generally regarded as being statically unstable; however, as will be shown in Section 7.2, this is largely irrelevant to the actual dynamic behavior of the torpedo in the water. The lateral force also increases linearly with attack angle for small angles and somewhat faster than linearly for larger angles. It has the same sign as the lift of an airfoil section: the torpedo tends to translate in the direction of the deflection of its nose. Typical curves of C_D, and of C_M and C_L as functions of attack angle for 0° and 2° elevator (horizontal rudder) angle are shown in Figure 1. These are rough provisional values for the Mark 13-2 torpedo, with and without the 8° cone angle shroud ring in the aft position; the vertical rudders are about one-tenth as effective as the elevators. The overall length of this torpedo is $l = 13.42$ ft, the maximum cross-sectional area is $A = 2.75$ sq ft, and the density of sea water is $\rho = 2$ slugs per cu ft.

In addition, it is often useful to remember that, since the center of pressure of the elevator lift is close to the elevator stock, the ratio of the elevator moment coefficient (C_μ) divided by the elevator lift coefficient (C_λ) is given by λ/l, where λ is the distance from center of gravity to the elevator stock and l is the torpedo length. Since for many torpedoes (for example, the Mark 13-2) $\lambda = l/2$; $C_\mu/C_\lambda = 0.5$. Similar considerations hold for the rudder coefficients.

The damping moment and force coefficients C_K and C_F are much more difficult to estimate since the torpedo or model must be rotating as well as translating through the water. They could, in principle, be determined experimentally from oscillating models in the water tunnel, from straight models in a curved tunnel or curved models in a straight tunnel, from rotating arm or curved rail towing tests with model or prototype, or from free turning tests with powered models or full-scale torpedoes. The last is the only method that has been used; photographs of circular runs have been made at the California Institute of Technology, and depth and roll records have been collected from figure running torpedoes at Newport. It is indicated in Section 7.2 how a relation between C_K and C_F may be obtained from the measured turning radius with known rudder angle; it is, of course, impossible to determine both of these unknowns from a single piece of data.

In this connection further information may be obtained from a theoretical calculation based on the moments and lateral forces measured on models of the bare hull and the complete torpedo. It is assumed that the damping moment and force arise principally from the tail empennage and are due to the fact that the attack angle at the tail differs from that at the center of gravity by $\omega\lambda/V$ radians, where λ is the distance from the center of gravity to the center of pressure of the empennage (see Section 4.4). The dependence of empennage force on attack angle and the magnitude of λ can be inferred from the difference

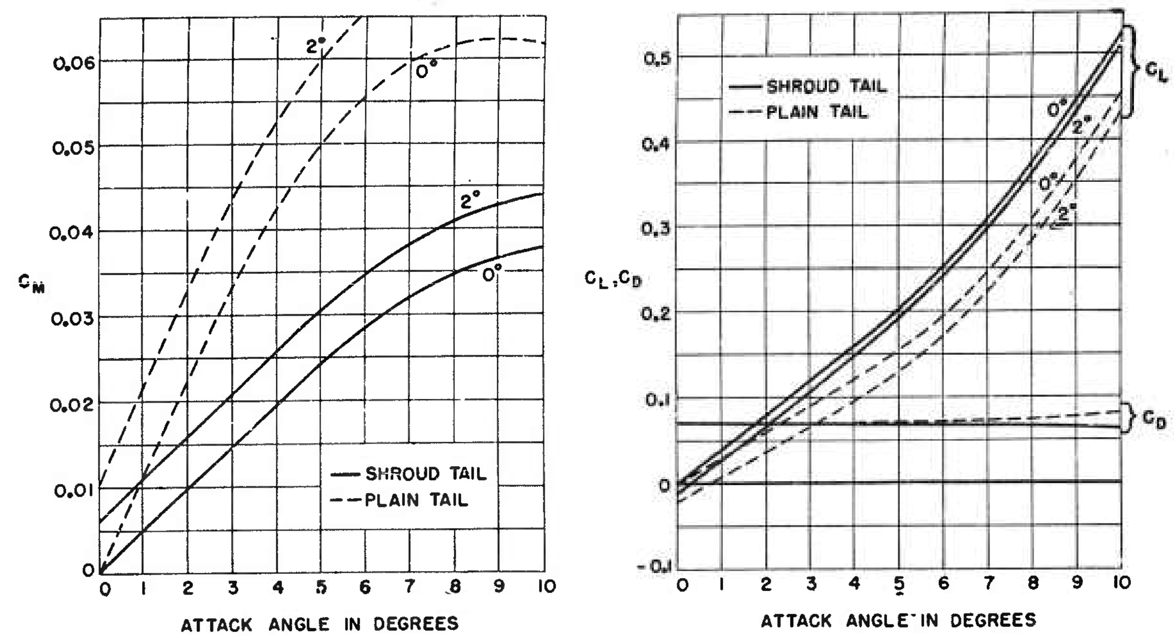

FIGURE 1. C_D, C_M, and C_L as functions of attack angle for 0° and 2° elevator (horizontal rudder) angle.

between the forces and moments experienced by the complete torpedo and the bare hull; from these, values of C_K and C_F are readily estimated. The British Torpedo Manual (p. 122 of the 1929 edition) recommends that C_K be increased slightly beyond the value obtained in this way to take account of the hull damping moment. The following provisional numerical values for the Mark 13-2 torpedo were arrived at by considering both the experimental and theoretical approaches: for the plain tail, $C_K = 0.44$, $C_F = 1.01$; for the shroud ring tail, $C_K = 0.48$, $C_F = 1.16$. Incidentally, it appears on the basis of this discussion that for conventional torpedo shapes C_K and C_F may be related to C_{Mf} and C_{Lf}, where the subscript f refers to the corresponding coefficient for the fins.

Up to the present, practically all static testing, like the tests run in the water tunnel and wind tunnel were made on torpedoes without propellers. It is a well-known fact from other fields (i.e., airplanes, ships, etc.) that the propellers exert a side force. As a result they create some stabilizing effect ($\partial C_M/\partial\alpha$ is diminished), the propellers produce a lift force, and they contribute very significantly to C_K and C_F. Hence the omission of propellers probably leads to large errors in the various constants, C_M, C_L, C_K, and C_F. Although C_K and C_F have been determined primarily from full-scale turning results, the relation between C_K and C_F depends on C_M and C_L which are certainly in error. Recently, in the Gould Island wind tunnel the Mark 13-2 torpedo was tested with free-wheeling (windmilling) propellers. It is as yet not known whether results obtained with freewheeling propellers may be taken as the results obtained with powered propellers, even though both are rotating at close to the same speed. However, the observed results, which are presented below, are indicative of the effect of propellers on the static constants.

	$-\frac{\partial C_M}{\partial \alpha}$	$\frac{\partial C_L}{\partial \alpha}$
Bare hull	0.952	1.16
Bare hull plus free props	0.796	1.46
Bare hull plus plain tail	0.640	1.80
Bare hull plus plain tail plus props	0.466	2.14
Bare hull plus shroud ring tail	0.419	2.26
Bare hull plus shroud ring tail plus props	0.363	2.36

From these results it appears that in addition to the large effect of propellers there is an interference effect with the shroud ring and propellers. These results are only preliminary, and it is to be remembered that the propellers are freewheeling.

It thus appears that the status of the hydrodynamic constants of torpedoes is at present very unsatisfactory and the knowledge inadequate. The static constants C_M and C_L are in error since the torpedo models have been tested without propellers. The dynamic constants C_K and C_F are in error since the wrong static constants were used in their calculation, the turning circle data must be corrected for roll (as will be seen in Section 7.2). In addition, the turning circles very often are not reproducible. It appears that future work in determining these constants by means of models with propellers (preferably powered at least to see the limits of freewheeling propellers) as well as curved motion tests is definitely required. In fact, it appears that results of this type may soon be obtained in towing and rotating arm tests.

7.2 EQUATIONS OF MOTION AND STABILITY

In studying the dynamic behavior of a torpedo, it is convenient to separate the motion into components in a horizontal plane, in a vertical plane, and about the longitudinal axis of the torpedo. This is a natural separation from the point of view of the control system, for the steering, depth and heel are handled independently. In general, the interaction between them is small (see Section 8.5), and the approximation is both valid and useful. The equations are developed here for motion in a vertical plane (depth-keeping); however, they are readily adapted to the steering motion in the horizontal plane. Rolling and heeling will be considered in Chapter 9.

The three degrees of freedom in the vertical plane are best taken as the components of the motion of the center of gravity along and perpendicular to the longitudinal axis of the torpedo and the angle of rotation about a horizontal transverse axis through the center of gravity. The choice of axes fixed in the torpedo rather than in space or with respect to the trajectory of the center of gravity has the advantage that accelerations along and perpendicular to the axis of the torpedo are treated separately so that the accession to the inertia of the torpedo due to entrained water, which is different for the two directions, can be readily taken into account. The equations of motion are

$$\begin{aligned} &M_1\dot{u} - M_2 v\dot{\beta} \\ &\quad = P - D\cos\alpha + L\sin\alpha + (W - B)\sin\beta\,, \end{aligned} \tag{1}$$

$$\begin{aligned} &M_2\dot{v} + M_1 u\dot{\beta} \\ &\quad = -L\cos\alpha - D\sin\alpha + (W - B)\cos\beta + F\dot{\beta}\,, \end{aligned} \tag{2}$$

$$Q\ddot{\beta} = M - K\dot{\beta} + Ba\cos\beta\,, \tag{3}$$

where the left sides are the inertia terms given by Lamb[a] and the right sides are the hydrodynamic forces and moments; Lamb's term $(M_2 - M_1)uv$ is included in the measured moment M, and terms arising from fore-and-aft asymmetry are neglected. Here, M_1 and M_2 are the mass in slugs of the torpedo corrected for entrained water in longitudinal and transverse accelerations, respectively; Q is the similarly corrected moment of inertia in slug-ft²; u and v are the longitudinal and transverse components of the velocity V in ft per sec; β is the orientation angle, α the attack angle, and $\theta = \beta + \alpha$ the course or trajectory angle, all in radians; W is the weight, B the buoyancy and P the propeller thrust, all in lb, and the remaining forces and moments are measured in lb and ft units; ξ is the elevator angle in radians and a the distance of the center of buoyancy (CB) aft of the CG in ft; dots represent time derivatives.

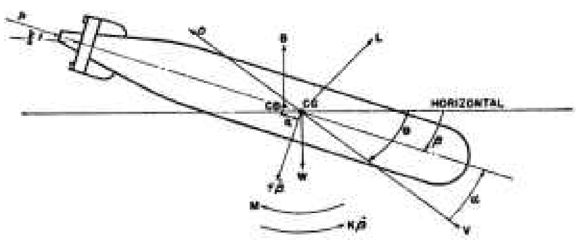

FIGURE 2. Diagram showing positive direction for various parameters.

Figure 2 illustrates the sense in which the various parameters are taken positive. M and L are, of course, functions of α and ξ; however, D appears to be practically independent of these quantities (see Figure 1).

For motion in the horizontal plane, equations of the above form are valid, except that the terms involving W and B no longer appear. Then equations (2) and (3) may be applied to steady turning, if $\dot{u}$, $\dot{v}$, and $\ddot{\beta}$ are set equal to zero. It is then apparent that the turning radius is $V/\dot{\beta}$ so that $\dot{\beta}$ as well as ξ is measurable. Then α can be eliminated from the two equations and a relation obtained between K and F; this is the relation referred to in Section 7.1. In interpreting this relation a correction should be applied for the heeling of the torpedo in the turn; however,

[a] *Hydrodynamics*, H. Lamb, Fourth Edition, 1916, Chapter VI, pages 124, 127.

this correction is both small and of uncertain magnitude and has generally been neglected.

In order to treat types of motion in which α, β, and $\dot\beta$ are small, it is convenient to linearize equations (1), (2), and (3); indeed, it is only in this way that analytic solutions may be obtained. One can then put $\cos\beta = \cos\alpha = 1$, $\sin\beta = \beta$, $\sin\alpha = \alpha$, $u = V$, $v = V\alpha$, $M = -c\alpha + d\xi$, $L = e\alpha + f\xi$, and assume that P, D, F, and K are independent of β and ξ. Then to first order in the small quantities β, $\dot\beta$, α, $\dot V$, and $W - B$, these equations become

$$M_1\dot V = P - D\,, \tag{4}$$

$$M_2 V\dot\alpha + M_1 V\dot\beta = -e\alpha - f\xi - D\alpha + (W - B) + F\dot\beta\,, \tag{5}$$

$$Q\ddot\beta = -c\alpha + d\xi - K\dot\beta + B\alpha\,. \tag{6}$$

In analogy with equations (1), (2), and (3) it is convenient to define moment and force coefficient derivatives as follows:

$$\begin{aligned} D + e &= \tfrac{1}{2}\rho V^2 A C_l\,, & f &= \tfrac{1}{2}\rho V^2 A C_\lambda\,, \\ c &= \tfrac{1}{2}\rho V^2 A l C_m\,, & d &= \tfrac{1}{2}\rho V^2 A l C_\mu\,, \end{aligned} \tag{7}$$

so that

$$C_L + C_D\alpha = C_l\alpha + C_\lambda\xi\,, \quad C_M = -C_m\alpha + C_\mu\xi\,. \tag{8}$$

One can also define a dimensionless independent variable s such that $dt = (l/V)ds$ is the time required for the torpedo to travel ds lengths at the instantaneous speed V; then

$$\dot\alpha = \frac{d\alpha}{dt} = \frac{ds}{dt}\frac{d\alpha}{ds} = \frac{V}{l}\alpha'\,, \quad \text{etc}\,,$$

where primes represent derivatives with respect to s. With equation (4) and the additional substitutions:

$$\begin{aligned} m_1 &= \frac{2M_1}{\rho A l}\,, & m_2 &= \frac{2M_2}{\rho A l}\,, \\ n &= \frac{2Q}{\rho A l^3}\,, & m &= m_1 - C_F\,, \\ w &= \frac{2(W - B)}{\rho A V^2}\,, & b &= \frac{2BA}{\rho A l V^2}\,, \\ \Omega &= \beta'\,, \end{aligned} \tag{9}$$

equations (5) and (6) become to first order

$$\begin{aligned} m_2\alpha' + C_l\alpha + m\Omega &= -C_\lambda\xi + w\,, \\ C_m\alpha + n\Omega' + C_K\Omega &= C_\mu\xi + b\,. \end{aligned} \tag{10}$$

Equation (4) is not of interest for the case in which the speed V is constant; it was used in Section 6.5, in connection with deceleration during the initial dive.

For motion in the horizontal plane the same development of the equations of motion follows as in the vertical plane except that the terms involving w and b no longer appear.

An important feature of equations (10) is that neither the t nor the speed V appear explicitly except for the speed-dependent terms w and b. Thus in the horizontal plane (in which w and b do not appear) the space trajectory described with fixed rudder is independent of the speed, even if the speed is not constant. In particular it is of interest to consider the motion in the horizontal plane with neutral rudder ($\xi = 0$). This provides a criterion for dynamic stability of the torpedo itself before the control system is added.

The equations to be solved are

$$\begin{aligned} m_2\alpha' + C_l\alpha + m\Omega &= 0\,, \\ C_m\alpha + n\Omega' + C_K\Omega &= 0\,; \end{aligned} \tag{11}$$

since these are homogeneous linear differential equations with constant coefficients, the only non-vanishing solutions for α and Ω are of exponential form:

$$\begin{aligned} \alpha &= \alpha_1 e^{p_1 s} + \alpha_2 e^{p_2 s}\,, \\ \Omega &= \Omega_1 e^{p_1 s} + \Omega_2 e^{p_2 s}\,. \end{aligned} \tag{12}$$

Substitution of (12) and (11) gives the following equations for the coefficients of each of the exponential factors:

$$\begin{aligned} (m_2 p_i + C_l)\alpha_i + m\Omega_i &= 0\,, \\ C_m\alpha_i + (np_i + C_K)\Omega_i &= 0\,, \end{aligned} \tag{13}$$

where $i = 1, 2$. Equations (13) have non-vanishing solutions for α_i and Ω_i only if the determinant of their coefficients vanishes. This results in a quadratic equation for the characteristic exponents p_i:

$$nm_2p_i^2 + (m_2C_K + nC_l)p_i + (C_lC_K - mC_m) = 0 \tag{14}$$

which has the two solutions:

$$p_{1,2} = \left[-h \pm \frac{\sqrt{h^2 - 4nm_2(C_l C_K - mC_m)}}{2nm_2} \right]. \tag{15}$$

where $h = m_2 C_K + nC_l$.

Now in order for the torpedo to be dynamically stable without controls, any initial disturbance (nonvanishing initial values of α or Ω) must be damped out as the motion progresses; this means that the exponents p_1 and p_2 must have negative real parts. It is apparent that this is equivalent to the requirement that the three coefficients of equation (14) have the same sign; since the first two are necessarily positive, this means that the criterion for dynamic stability is

$$C_l C_K - mC_m > 0. \tag{16}$$

It is worth noting that the torpedo need not be statically stable in order to be dynamically stable, and the latter requirement is of much greater significance so far as the behavior of the torpedo in the water is concerned. Indeed, all known torpedoes are statically unstable and are dynamically stable. As remarked in Section 7.1, static stability implies that C_m be negative so that a small attack angle produces a restoring moment. While according to (16) this is practically always a sufficient condition for dynamic stability, it is evidently not a necessary condition. The Mark 13-2 torpedo with either the plain or shroud ring tail is dynamically stable, even though C_m is positive; this has been shown both by computation and by free running trials with rudders removed.

Approximate values for the characteristic exponents p_1 and p_2 are readily calculated from equation (15) with the help of the provisional values of the coefficients which are collected in Section 9.1. The results are

	Plain	*Shroud*
p_1	−0.23	−0.56
p_2	−2.91	−2.72

Since in each case p_2 is much larger in magnitude than p_1, the rate of recovery of the uncontrolled torpedo from an initial disturbance is determined principally by p_1. This recovery is roughly exponential, the disturbance being reduced to $1/e$ of its initial value in approximately 4.3 lengths for the plain tail torpedo and 1.8 lengths for the shroud tail torpedo. Thus the addition of the shroud ring significantly increases the stability and also makes the control problem much less critical as will be seen in Part III. This improvement is due primarily to the decrease in C_m caused by the shroud ring. It should be remarked that recovery from an initial disturbance implies only that α, Ω and hence $\dot{\beta}$ approach zero as the motion progresses. It does not, of course, mean that the new straight course is parallel to the initial course, and, in general, this is not the case; on the other hand, dynamic stability means that a small initial disturbance does not cause the torpedo to wind up into a spiral or circular trajectory.

As a result of this discussion it appears that a torpedo is dynamically stable if a perturbation of the yaw angle or angular velocity diminishes in time with a resulting relatively small course deviation. For example, if an uncontrolled torpedo (with rudders neutral) which is traveling in a straight course suddenly receives a small yaw angle and/or angular velocity, if the torpedo is dynamically stable the yaw angle and angular velocity will both decrease to zero, and the torpedo will resume a new straight course which is generally close to the original course. If the torpedo were dynamically unstable the yaw angle and angular velocity would both increase, the path tending to become a spiral, until finally due to nonlinearities in the hydrodynamic constants the torpedo becomes dynamically stable when the yaw angle and angular velocity become large enough and the trajectory winds up into a circle. For an uncontrolled dynamically stable torpedo on a straight course, one readily finds from equations (11), (12), and (15) that the final course angle when the torpedo has an initial yaw angle α_0 and angular velocity Ω_0 is given by

$$\theta(\infty) = \theta_0 + \frac{nC_l\Omega_0 - m_2 C_m \alpha_0}{C_l C_K - mC_m}. \qquad \text{[Equation (20), Chapter 11]}$$

It is interesting to note the mechanism of dynamic stability. This is best done by considering a statically unstable torpedo which possesses, for example, an initial yaw angle to starboard and angular velocity to starboard. Due to the yaw angle a lift force is produced in the starboard direction, thus giving the torpedo a velocity in the starboard direction, which is seen to be effectively some yaw angle in the port direction. Due to the initial angular velocity and the increase in this velocity due to the static instability, a damping moment is produced tending to diminish this angular velocity, and a damping force is produced which essentially helps the lift force in reducing the initial yaw angle. Hence it is clear that the essential mechanism of dynamic stability is that the torpedo can move transversely and as a result an initial disturbance is reduced or compensated for by a generally small course deviation. From this discussion the main reason for the inadequacy and impracticability of static stability as any criterion for the motion is fairly obvious. The reason is that static stability is strictly defined for a torpedo which cannot move transversely, and it is precisely this motion which is the essence of the mechanism of dynamic stability.

7.3 STEADY RUNNING

To obtain the steady-state (or mean) running conditions of the torpedo, we simply set all derivatives (remembering that $\Omega' = \beta'$) equal to zero in the equations of motion above. One then readily finds that, for $\alpha' = \Omega' = \Omega = 0$,

$$\alpha_r = \frac{bC_\lambda + wC_\mu}{C_lC_\mu + C_mC_\lambda} = \frac{\dfrac{Ba}{l}C_\lambda + (W - B)C_\mu}{C_lC_\mu + C_mC_\lambda}\,\frac{2}{\rho A V^2}, \quad (17)$$

$$\xi_r = -\frac{bC_l - wC_m}{C_lC_\mu + C_mC_\lambda} = -\frac{\dfrac{Ba}{l}C_l - (W - B)C_m}{C_lC_\mu + C_mC_\lambda}\,\frac{2}{\rho A V^2}. \quad (18)$$

From these equations it is seen that for a given torpedo the steady-state pitch angle and elevator angle become smaller as V, the running speed, increases. One also sees from these equations that for a given torpedo there is a minimum speed at which it can be run, if there is a lower stop in the elevator so that ξ is limited.

From the second equation it is clear that one can choose the center of buoyancy and center of gravity in such a relative position that $\xi_r = 0$. This may be of significance since when the torpedo is heeled over in a turn ξ_r affects the turning circle. However, if $\xi_r = 0$, there will be no effect of the elevators on the circle. If $\xi_r < 0$, the elevators will aid the rudders in a turn and so contribute to a tighter circle.

7.4 STEADY CIRCLING

The condition of a dynamically stable torpedo going around in a steady turn may be obtained simply by setting $\alpha' = \Omega' = 0$, which corresponds to a circling condition. Then from equations of motion in the horizontal plane it follows that:

$$\Omega = \frac{l}{R} = \frac{C_lC_\mu + C_mC_\lambda}{C_lC_k - mC_m}\,\xi, \quad (19)$$

where R is the radius of the turning circle.

Also

$$\alpha = \frac{C_kC_\lambda + mC_\mu}{C_lC_k - mC_m}\,\xi,$$

or

$$\Omega = \frac{C_lC_\mu + C_mC_\lambda}{mC_\mu + C_kC_\lambda}\,\alpha. \quad (20)$$

These equations indicate a linear relation between Ω and ξ and between Ω and α.

However, the above treatment is really an unwarranted oversimplification of the problem of the circling of a dynamically stable torpedo because the heel in the turn is completely neglected. Most torpedoes in the steady-running condition normally have a down elevator [b is negative in equation (18)]. This is not necessarily true since it will depend on the relative position of the center of gravity and center of buoyancy as discussed above. In addition, practically all torpedoes have the center of gravity below the center of buoyancy so that, if the torpedo rolls a little about its longitudinal axis, a restoring moment is produced. Then, if no torque is set up by an inequality in rudder or fin area, reducing the problem of a circling torpedo to a static problem we may see that a heel will be produced in the turn and obtain the approximate magnitude of the heel. Consider the torpedo going around in a circle of radius R and heeled through an angle ϕ. Then, taking moments about the center of buoyancy of the torpedo, we find that, if the metacentric height is G,

$$\frac{MV^2}{R}G\cos\phi = MgG\sin\phi,$$

where the left side represents the torque of the centrifugal force and the right side the restoring moment of the metacentric height. It then follows that the heel in the turn is given by

$$\phi = \tan^{-1}\left(\frac{V^2}{gR}\right). \quad (21)$$

This angle is not particularly small. If we consider the Mark 13 torpedo without a shroud ring, $R \sim 250$ ft, $V = 56$ ft per sec, so that $\phi = 21.3°$.

Remembering that for most torpedoes the running elevator position is down, when the torpedo is heeled over in a turn it is clear that the elevators will tend to have an opposite effeet from the rudders and so tend to make a larger turning circle. Sinee the elevators are generally mueh larger than the rudders, this effect is of considerable importance.

In order to ealculate the effect of a steady heel we shall assume that the heel only affects the motion through the components of the elevator and rudder in the horizontal and vertical plane and that to this first approximation the hydrodynamic constants in the equations of motion are unaltered. This assumption is discussed in more detail in Section 6.5.2. From that section we see that the right sides of the equations of motion are altered. From equations (56) and (57) in that seetion we see that the relation for ξ_r as given by equation (18) above, becomes

$$\xi_r = -\frac{C_l b - C_m w}{C_{\mu e} C_l + C_{\lambda m}} \sec\phi - \frac{C_l C_{\mu e} + C_m C_{\lambda e}}{C_l C_{\mu e} + C_m C_\mu} \delta_0 \tan\phi\,, \quad (22)$$

where δ_0 is the rudder angle in the turn and $C_{\mu e}$, $C_{\lambda e}$, are the elevator coefficients.

Thus, when the torpedo is heeled over in a turn, the running elevator angle is less down by the amount noted in the second term. From the equations of motion in Section 6.5.2 we find that in a steady turn:

$$\Omega = \frac{l}{R}$$

$$= \frac{(C_l C_\mu + C_\lambda C_m)\delta_0 \cos\phi - (C_l C_{\mu e} + C_{\lambda e} C_m)\xi_r \sin\phi}{C_l C_K - m C_m}, \quad (23)$$

where ξ_r is the mean elevator angle in the turn and may be reeorded by some instrument or given by equation (22) above. It is seen, as was reasoned earlier, that since generally $\xi_r > 0$, a roll angle in the turn increases the radius of the turning circle. Since ϕ varies with V^2/R, Ω will be a function of the veloeity. This equation is the one referred to earlier relating C_K to C_F.

One method of obtaining the damping moment coefficient C_K and damping force coefficient $C_F (m = m_1 - C_F)$ in the past has been from an analysis of turning circle data. With a knowledge of R and assuming a relation between C_K and C_F generally the ratio is approximately $C_K/C_F = 0.5$; corresponding to the assumption that most of the damping force arises at the torpedo tail these constants were estimated. However, the effect of heel in the turn must be considered since if it is neglected an artificially large C_K is deduced (since a heel and increasing C_K both increase the turning circle radius). This method will probably also be used in the future and it is therefore necessary to note the large effect of heel.

PART III

CONTROL SYSTEM

Chapter 8

GENERAL DISCUSSION OF CONTROLS

8.1 PURPOSE OF CONTROLS

It was shown in Section 7.2 that the Mark 13-2 torpedo is dynamically stable with respect to motion in the horizontal or steering plane. While this is a desirable state of affairs, it is not sufficient to guarantee good course-keeping; for any asymmetry in the torpedo or its propulsive plant, or any external disturbance will cause the torpedo to depart from its original course. It is necessary, therefore, to provide a correction which tends to restore the torpedo to its original course; this is supplied by a gyroscope and steering engine which operate the vertical rudders.

The situation with regard to motion in the vertical plane (depth-keeping) is more critical since it is usually desired that the torpedo run within narrow limits of depth and quite close to the surface. Because of the inhomogeneous terms in equations (10) of Chapter 7, that is, because of the necessity for balancing both the unbuoyed weight $W - B$ and the moment Ba of the torpedo, a horizontal rectilinear path ($\Omega = \dot{\Omega} = \dot{\beta} = 0$) will not be obtained unless the attack angle α and the horizontal rudder or elevator angle ξ have precisely the right values, as given by equations (17) and (18) of Chapter 7. This adjustment requires a depth-control system which is sensitive to depth and which must therefore contain at least a hydrostat and a depth engine for operating the elevators. It will be shown in Section 12.1, however, that a control of this type makes the torpedo dynamically unstable. It is therefore necessary to add an element which indicates incipient deviations from running depth before they develop to such an extent that the hydrostat cannot handle them. Such an element can be provided by a pendulum arranged to indicate deviations from running orientation angle; other arrangements involving gyroscopes and depth differentiators are possible as well.

Apart from the maintenance of course and depth during the steady run, the control system must on occasion provide predetermined course changes in both the horizontal and vertical planes. Thus angle shots, in which the torpedo is brought to a new course after launching, and recovery from the initial dive must be taken into consideration in designing the control. The first is relatively simple, since it is only necessary that the gyro pick-off be preset so that the torpedo runs at a fixed angle to the gyro axis. The second, however, requires that the depth control be constructed so that the large decelerations inherent in the initial dive and recovery do not prevent it from bringing the torpedo to running depth quickly and without excessive broaching.

8.2 TYPES OF CONTROLS

There are two extreme control types which can be applied to either the course-keeping or depth-keeping problem. These are the linear or proportional system, and the limited or two-position system. A proportional control is one in which the rudder displacement is some linear combination of the magnitudes of the factors to be controlled (orientation, depth, etc.) and possibly their time derivatives. A two-position control is one in which the rudder is always in one of two positions or in relatively rapid transit between them, the position selected again depending on the factors to be controlled.

The torpedo together with a proportional control can be represented, at least for small deviations from running conditions, by a set of simultaneous linear differential equations with constant coefficients. The control is stable if a small disturbance produces a motion which damps out in time, that is if the real parts of all the characteristic exponents of the differential equations are negative. If the control is not stable the motion will build up until the rudder motion is limited by stops. When the instability is of an oscillatory character so that the exponents with positive real parts are complex, the rudder stops act as a limiter, and the control has many of the properties of the two-position type. Such transitional cases are best considered along with the ideal two-position control.

The two-position control operates stably when the rudder oscillates periodically between its two positions and the torpedo motion is correspondingly periodic; then the motion following a small disturbance tends to resume this periodic character. It is possible for a two-position control to be unstable in the sense that the oscillatory motion of the torpedo increases in period and amplitude; this can, of course, also occur for an unstable proportional control which is operating in the transitional range.

8.3 METHODS OF ANALYSIS: PROPORTIONAL CONTROL

The most straightforward method of analyzing a proportional control consists in writing down the simultaneous linear differential equations that describe the torpedo motion and the control system and solving them by the method of characteristic exponents already applied in Section 7.2. The torpedo equations have already been given in (10) of Chapter 7 and a relation between the rudder angle ξ and the torpedo parameters must be added. The steady-state values of the parameters can be found first and will in general be different from zero if inhomogeneous terms like w and b are present in the equations. The transient part of the motion can then be found as a sum of exponential terms like e^{ps} or e^{pt}, depending on whether the distance in lengths s or the time t is used as the independent variable. These are to be substituted into the homogeneous equations that result when the steady-state terms are subtracted out. The requirement that a solution exist for the coefficients of the exponentials gives rise to an algebraic equation in the exponents p. This "secular" equation can be solved by trial and error using synthetic division, or in other ways, and the coefficients of the exponentials evaluated in terms of the initial conditions. In this way the explicit motion of the torpedo following a transient disturbance or during the recovery from the initial dive can be found.

For many purposes it is sufficient to know simply that the control is stable, without knowing even the values of the characteristic exponents. In this case the Hurwitz criterion[a] can be applied directly to the coefficients of the secular equation. This criterion states that the necessary and sufficient condition that the real parts of all the roots of the algebraic equation

$$a_0p^n + a_1p^{n-1} + a_2p^{n-2} + \cdots + a_{n-1}p + a_n = 0 \quad (1)$$

be negative is that all the quantities

$$a_0, a_1, \begin{vmatrix} a_1 & a_0 \\ a_3 & a_2 \end{vmatrix},$$

$$\begin{vmatrix} a_1 & a_0 & 0 \\ a_3 & a_2 & a_1 \\ a_5 & a_4 & a_3 \end{vmatrix} \cdots \begin{vmatrix} a_1 & a_0 & 0 & 0 & \cdots & 0 \\ a_3 & a_2 & a_1 & a_0 & \cdots & 0 \\ \cdots & \cdots & \cdots & \cdots & \cdots & \cdots \\ 0 & 0 & 0 & \cdots & \cdots & a_n \end{vmatrix} \quad (2)$$

be greater than zero.

[a] *Differentialgleichungen der Physik*, Frank and von Mises, Vol. I, p. 163.

Another less direct but often more convenient method for dealing with the problem of the response and stability of the control system is based on an analogy with a linear feed-back amplifier. A feed-back amplifier is one in which a part of the output of a conventional electronic amplifier is fed back to the input. Great improvement in frequency response and freedom from distortion can be obtained in this way by proper design, but care must be taken that the circuit does not oscillate by itself or possess too slowly damped transients. Information as to the behavior of the circuit in this respect can be obtained from a study of the overall response function of the amplifier and feed-back network. Suppose that the feed-back network is disconnected from the amplifier input and a sinusoidal signal voltage of unit amplitude is applied to the input. The magnitude and phase lead of the voltage that appears at the terminals of the feed-back network, when it is terminated by the input impedance of the amplifier, may be plotted as a function of signal frequency in polar coordinates. If the resulting curve and its image in the polar axis enclose the point which is unit distance from the origin along the polar axis, the complete feed-back amplifier will be unstable and oscillate with an amplitude which is limited by the non-linearities of the amplifier circuit. The circuit is stable when the unit point is not enclosed, but if the curve passes too close to it the circuit will possess slowly damped transients. These results were first obtained by Nyquist.[b]

The torpedo and control system can be regarded as a feed-back amplifier. For example, motion of the rudder produces a motion of the torpedo as a whole (amplifier) which produces a motion of the control system (feed-back network) and in turn actuates the

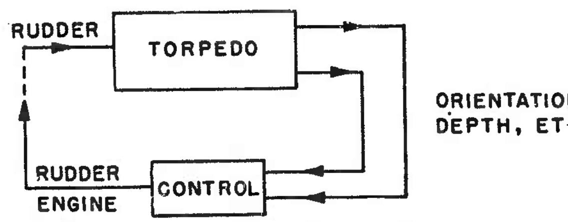

FIGURE 1. Nyquist criterion applied to torpedo and control system.

rudder. If the control is disconnected from the rudder, an overall response function can be defined in terms of the steering or depth engine motion produced by a sinusoidal rudder motion of given fre-

[b] H. Nyquist in *Bell System Technical Journal*, Vol. 11, 1932, p. 126.

quency. The use of the Nyquist criterion in this connection has the great advantage that the overall response function can be broken up into two parts: one for the torpedo and one for the control system. Thus the torpedo response function need be calculated only once and can be used in connection with various control response functions. Moreover, it can be seen from an examination of the response function what changes must be made in the control to improve the stability.

The overall response function, once it is known, can also be used to find the torpedo motion resulting from some periodic external disturbance, such as a wavy sea. A straightforward, but less simple, calculation enables one to calculate the transient response to an aperiodic disturbance by expressing it as a Fourier integral.

8.4 METHODS OF ANALYSIS: TWO-POSITION CONTROL

The ideal two-position control contains a limiter which switches the rudder instantaneously from one extreme position to the other when the controlling signal reaches a specified value from one direction and reverses the process when it reaches the same value from the other direction. A straightforward but difficult method for analyzing such a system consists in integrating the supposedly linear equations of motion of the torpedo in intervals during each of which the rudder position has one of its extreme positions and matching boundary conditions at the instants when the rudder makes its traversals.

A far simpler method is based on the fact that the torpedo response to rudder motion has the general properties of a low-pass amplifier so that high-frequency components of the rudder motion are strongly attenuated. One can then assume that the rudder has a periodic square-wave motion, and this can be analyzed in a Fourier series. Because of the decrease in amplitude of the harmonics with frequency and the high-frequency attenuation, only the fundamental component of this series will be significant in the torpedo motion, which will therefore be very nearly sinusoidal. The response of the control and hence the phase of the limiter action can be predicted from this motion, and this must of course agree with the originally assumed phase of the rudder motion. Since the phase lags of the torpedo-response function and the control are generally increasing functions of the frequency, there will, in general, be one frequency for which the phases of the assumed rudder motion and the resulting limiter action agree; this is the frequency at which the system oscillates.

When the overall phase lag is an increasing function of the frequency, the oscillation obtained in this way is stable. This can be seen from the following argument. Suppose then an external disturbance momentarily retards the rudder motion. This introduces lower frequency components into the rudder and hence into the torpedo motion. This in turn decreases the overall phase lag, making the limiter action take place more quickly and restoring the motion to its original periodic character. Similarly, a momentary speed-up of rudder action introduces higher frequency components, increases the phase lag and hence slows the motion down towards the original frequency. By the same argument, an oscillation fre-

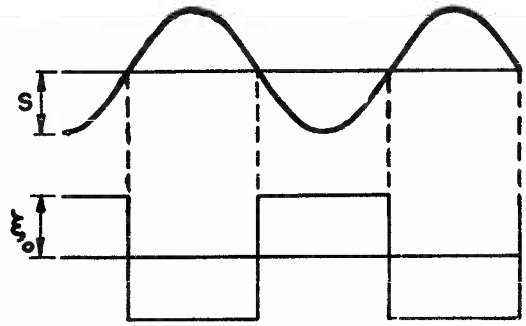

FIGURE 2. Effect of a low-frequency external disturbance on a stably oscillating two-position control.

quency which occurs when the overall phase lag is a decreasing function of frequency is not stable. When this occurs, the phase lag will generally increase eventually with frequency and produce a higher frequency oscillation which is stable. On the other hand, if an external disturbance causes the frequency to start decreasing from the unstable point, it is possible that an unstable oscillatory motion will result in which the period and amplitude increase with time.

It is possible to find in a simple way the response of a stably oscillating two-position control to an external disturbance which is of low frequency compared to the control-oscillation frequency and whose amplitude at the limiter is small compared to the control-signal amplitude. Suppose the control-signal amplitude at the limiter is S and the disturbance is a steady signal of magnitude s at the limiter. If the limiter action takes place when the total signal crosses the zero value, as is usually the case, the effect of the disturbance is to cause the rudder to spend slightly more time in one position than the other; this adds a small component of rudder in that direction without affecting the phase of the limiter or rudder action, and hence without affecting the frequency of the steady oscillation. The rudder then spends a fraction $(\frac{1}{2} + s/\pi S)$ of a cycle in one direction and a fraction $(\frac{1}{2} - s/\pi S)$ of a cycle in the other direction, so that the net steady rudder component is $2s\xi_0/\pi S$, where $\pm\xi_0$ is the rudder throw. But the amplitude of the fundamental component of the rudder motion is $4\xi_0/\pi$ so that the ratio of steady to fundamental component of the rudder is $s/2S$.

While the proof given here applies only to extremely slow disturbance frequencies, it has been shown that this applies for all lower frequencies and for amplitude ratios at the limiter of the order of ½ or less. Thus the ideal two-position control acts like a linear amplifier for external disturbances, and the oscillations can be ignored from this point of view. This approach is useful in considering response to waves and the effect of initial conditions. Also it is this approach which permits the treatment of on-off systems subject to disturbances as though they are proportional systems. This enables one to calculate practically all the behavior characteristics of a torpedo with an on-off system that one could calculate for a torpedo with a proportional system.

As a simple but instructive application of this very useful theorem we shall calculate the trajectory in the horizontal plane of a dynamically stable torpedo with proportional depth controls and two position (on-off) steering when the torpedo is heeled over clockwise by an angle ϕ. Essentially, we shall look for the final course angle of the torpedo.

Clearly, for such a torpedo we have the case of an on-off system subject to a disturbance (caused by the steady component of the elevators in the horizontal plane) which is of lower frequency than that of the on-off system, in fact in this case the disturbance is of zero frequency.

One can then readily write down the equations of motion in the *horizontal plane* (where the hydrodynamic constants are taken to be independent of heel in this approximation).

$$m\Omega + m_2\alpha' + C_l\alpha = -C_\lambda\delta\cos\phi + C_{\lambda e}\xi_r\sin\phi\,,$$
$$n\Omega' + C_k\Omega + C_m\alpha = C_\mu\delta\cos\phi - C_{\mu e}\xi_r\sin\phi\,,$$

$$\Omega = \beta'\,,$$
$$\delta = -\gamma\beta\,.$$

δ is the steady rudder component, ξ_r is the steady running elevator angle. From the previous theorem it is evident that

$$\gamma = \frac{2\delta_0}{\pi\beta_0}$$

where δ_0 is the rudder throw and β_0 is the amplitude of the yawing oscillations. The general solution of these differential equations is

$$\alpha = \alpha_1 e^{p_1 s} + \alpha_2 e^{p_2 s} + \alpha_3 e^{p_3 s} + \alpha_4\,,$$
$$\beta = \beta_1 e^{p_1 s} + \beta_2 e^{p_2 s} + \beta_3 e^{p_3 s} + \beta_4\,.$$

One may take as the initial conditions of the motion

$$\beta_i = \beta_i' = \alpha_i = 0\,.$$

If the body is dynamically stable the real parts of p_1, p_2, and p_3 must be negative.

For example, for the Mark 13 torpedo with shroud ring the real parts of the characteristic exponents have the magnitudes -2.2, -0.51, -0.51, the last two being the same since two of the roots are complex conjugates.

Since these exponents are to be multiplied by s, it is clear that the corresponding terms will damp out. Since we are interested in what will happen for large values of s (the course deviation at the end of many torpedo lengths), it is evident that (for s large)

$$\alpha \cong \alpha_4\,,$$
$$\beta \cong \alpha_4\,,$$

since α_4 and β_4 are constants independent of s.

Substituting into the equations of motion, one finds

$$\alpha_4 = \frac{(C_\lambda C_{\mu e} - C_{\mu e}C_\lambda)\xi_r\sin\phi}{(C_lC_\mu + C_\lambda C_m)}\,,$$

$$\beta_4 = \frac{(C_{\mu e}C_l + C_{\lambda e}C_m)\xi_r\tan\phi}{\gamma(C_lC_\mu + C_\lambda C_m)}\,.$$

Since the center of pressure of the rudder and elevator lift forces is almost exactly the same distance from the center of gravity

$$\frac{C_\mu}{C_\lambda} = \frac{C_{\mu e}}{C_{\lambda e}} = \lambda\,,$$

where λ is the fraction of a torpedo length by which the center of pressure of the lift forces of the elevators and rudders (approximately the elevator or rudder stock) lies aft of the center of gravity.

With this consideration one finds

$$\alpha_4 = 0\,,$$

$$\beta_4 = \frac{(C_m + \lambda C_l)C_{\lambda_e}\xi_r \tan\phi}{\gamma(C_m + \lambda C_l)C_\lambda} = \frac{C_{\lambda_e}}{\gamma C_\lambda}\,\xi_r \tan\phi\,.$$

Remembering that $\gamma = \dfrac{2}{\pi}\dfrac{\delta_0}{\beta_0}$,

$$\beta_4 = \frac{\pi}{2}\frac{C_{\lambda_e}}{C_\lambda}\frac{\xi_r}{\delta_0}\beta_0 \tan\phi\,.$$

Naturally for heel angles of interest (which are generally small) one can replace $\tan\phi$ by ϕ in radians. Thus the torpedo travels with zero yaw angle and with the average angle between the torpedo axis and the direction of the gyroscope setting being β_4. The trajectory angle is given by $\theta = \alpha + \beta = \beta_4$. Thus the angle the course pursued makes with the set direction, when the torpedo is heeled over, is given by β_4.

The course deflection or the distance between the actual torpedo position and its desired position is given by

$$y = \int_0^s \beta_4 ds = \frac{\pi}{2}\frac{C_{\lambda_e}}{C_\lambda}\frac{\xi_r}{\delta_0}\beta_0 s \tan\phi\,.$$

For the Mark 13 torpedo with shroud ring, using β_0 as given in Chapter 10, $\beta_0 = 0.77°$, $C_{\lambda_e}/C_\lambda = 10$, $\xi_r = 2.2°$, $\delta_0 = 9°$, we find

$$\theta = \beta_4 = 3° \tan\phi$$

or the deflection is given by $y = (3 \tan\phi/57.3)s$ torpedo lengths. One may also say that the deflection is given by

$$\text{Deflection} = 52.7 \tan\phi \text{ mils}$$
$$= 52.7\,\phi \text{ mils} \quad \text{(for small } \phi \text{ where } \phi \text{ is in radians).}$$

Thus, if the Mark 13-6 torpedo is heeled over about 5.5° in its steady run, it will suffer a course deflection of about 5 mils.

This result is in good agreement with verbal reports of statistical studies made of runs at the Newport Torpedo Station.

Since most torpedoes have some heel (probably due primarily to lack of complete torque balance of the propellers), it is seen that this is a very large effect compared to the restrictions commonly imposed on torpedo gyroscopes.

We see from this result that a clockwise heel will produce a nose-right course deflection for down elevator running angles.

It is also seen that decreasing ξ_r (the elevator running angle) and decreasing the time lag in steering (which from Chapter 10 is seen to diminish β_0) will diminish the deflection due to heel.

The reason for the torpedo to run at an angle β_4 between its axis and the direction of the gyroscope is that this angle is necessary to produce the steady component of the vertical rudder, since it behaves like a proportional system and the steady component is proportional to β, which will overcome the steady effect of the elevators in the horizontal plane.

The discussion thus far has been restricted to ideal two-position controls. An actual control may differ from this in three principal ways. First, the rudder does not switch instantaneously, but requires a finite time to travel from one position to the other. Second, there may be a time delay in the transmission of the switching signal from the limiter to the rudder. Third, the control values at which the switching action takes place need not be the same for the two directions. All three of these effects introduce additional phase lags.

The Fourier analysis method outlined above may also be applied to the study of unstable proportional controls in which the amplitude of the rudder oscillation is limited by stops. In such a transitional system, the amplitude and phase relations between rudder and torpedo motion must usually be considered simultaneously.

8.5 INTERACTION BETWEEN DEPTH-KEEPING, STEERING, AND ROLL

It is assumed throughout most of this report that the motions of the torpedo in the vertical and horizontal planes can be treated separately. It is evident, however, that if the torpedo rolls or heels, the vertical rudders act to a certain extent as elevators (horizontal rudders), and vice versa. The resulting interaction between depth-keeping, steering, and roll may be of importance in two situations. First, in the recovery from the initial dive, large rolls are encountered which may affect the operation of the depth controls.

Second, in steering with a two-position control, a certain amount of roll having the same frequency as the steering oscillation is produced by the vertieal rudder action and the displacement of the center of buoyancy above the center of gravity of the torpedo. Attempts are made to minimize this roll by making the upper vertical rudder larger than the lower one and the lower vertical fin larger than the upper one. However, the elevator effect of this vertical rudder motion is roughly proportional to the product of the roll angle and the rudder displacement and hence has twice the frequency of the steering oscillation. Thus in the absence of heel the steering action can influence the depth-keeping, but this influence will not react back significantly on the steering since it has twice the frequency. When the torpedo is heeled over, however, there is also an elevator effect component of the vertical rudder motion that has the same frequency, and in this case one should solve the combined equations of motion. Although little quantitative work has been done on this effect, it seems likely that it provides the explanation for the synchronous depth and roll oscillations sometimes observed when the torpedo is heeled over.

Chapter 9

PROPORTIONAL CONTROL

THIS CHAPTER applies the methods discussed in Section 8.3, to the detailed consideration of the horizontal steering of the Mark 13-2 torpedo. It is assumed that the torpedo is provided with a linear steering control in which the steady-state deflection of the vertical rudder is proportional to the deviation of the gyroscope axis from the desired heading. This will not be true in general for varying gyro signals since some delay in transmission is inevitable with rapid variations. Thus, in addition to the torpedo equations (10) of Chapter 7, with $w = b = 0$, there is a connection between the orientation angle θ and the rudder angle ξ (both in radians) which may be written as follows:

$$\tau\dot{\xi} + \xi = -\gamma\beta . \tag{1}$$

This equation would result, for example, if a pneumatic transmission possessing viscous friction and stiffness described by a time constant τ were used to transmit the gyro signal to the rudder. The equations of motion of the system may then be written

$$\begin{aligned} m_2\alpha' + C_l\alpha + m\Omega &= -C_\lambda\xi , \\ C_m\alpha + n\Omega' + C_K\Omega &= C_\mu\xi , \\ \xi + \sigma\xi' &= -\gamma\beta , \\ \beta' &= \Omega , \end{aligned} \tag{2}$$

where $\sigma = V\tau/l$.

9.1 HURWITZ CRITERION

In this method a substitution of the form e^{ps} is made for each of the variables, resulting in the following secular determinantal equation:

$$\begin{vmatrix} m_2p + C_l & m & C_\lambda & 0 \\ C_m & np + C_K & -C_\mu & 0 \\ 0 & 0 & \sigma p + 1 & \gamma \\ 0 & 1 & 0 & -p \end{vmatrix} = 0 . \tag{3}$$

This may be rewritten as a fourth degree algebraic equation in the characteristic exponent p:

$$a_0p^4 + a_1p^3 + a_2p^2 + a_3p + a_4 = 0 ,$$

$$\begin{aligned} a_0 &= m_2n\sigma, \\ a_1 &= m_2n + \sigma(nC_l + m_2C_K) , \\ a_2 &= (nC_l + m_2C_K) + \sigma(C_lC_K - mC_m) , \\ a_3 &= C_lC_K - mC_m + m_2C_\mu\gamma , \\ a_4 &= \gamma(C_lC_\mu + C_mC_\lambda) . \end{aligned} \tag{4}$$

Application of the Hurwitz criterion (2) of Chapter 8 to this equation is equivalent to the requirement that all of the coefficients be positive and that

$$a_1a_2a_3 - a_0a_3^2 - a_1^2a_4 > 0 . \tag{5}$$

For a dynamically stable torpedo such as the Mark 13-2, equation (16) of Chapter 7 states that $C_lC_K - mC_m > 0$; thus in this case all of the coefficients are positive, and equation (5) is by itself a necessary and sufficient condition for stability of the controlled torpedo.

Some of the numerical parameters representative of the Mark 13-2 torpedo have been given in Section 7.1, and Figure 1 of Chapter 7. The inertia parameters m_1, m_2, and n may be calculated from the mass and moment of inertia of the torpedo, with the corrections for entrained water being made approximately on the basis of Lamb's calculation for prolate spheroidal shapes. Provisional numerical values are collected below for this torpedo with plain and shroud ring tails. These are intended for use as illustrative parameters and are not definitive magnitudes.

	Plain	Shroud
m_1	1.80	1.84
m_2	3.11	3.20
n	0.176	0.188
C_m	0.650	0.279
C_μ	0.295	0.173 (horizontal elevator)
C_μ	0.030	0.017 (vertical rudder)
C_l	2.01	2.30
C_λ	0.606	0.344 (horizontal elevator)
C_λ	0.061	0.034 (vertical rudder)
C_K	0.44	0.48
C_F	1.01	1.16
m	0.79	0.68

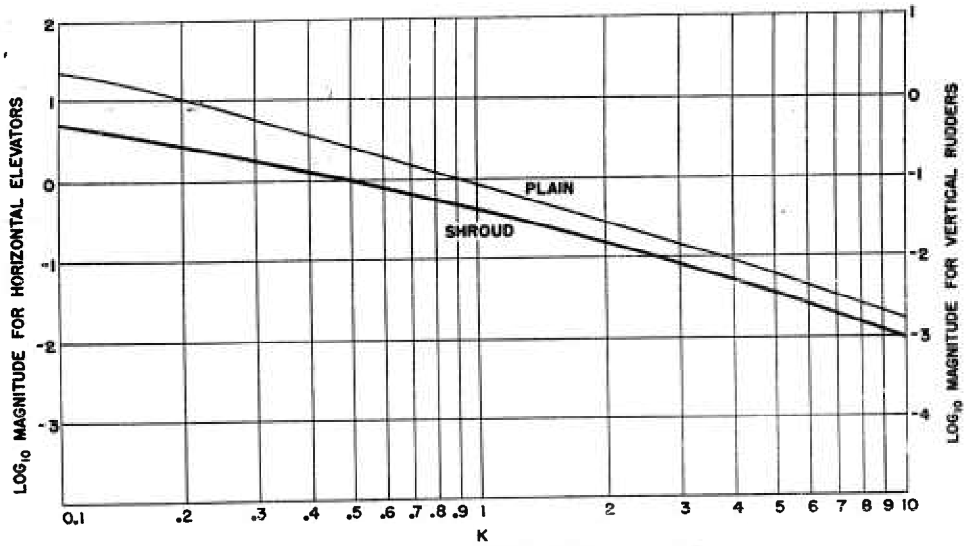

FIGURE 1. Log_{10} magnitude of β_0/ξ_0 versus k.

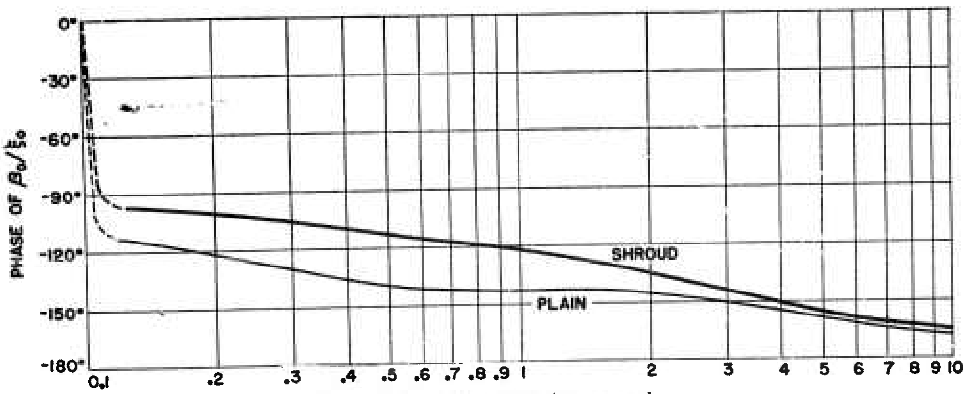

FIGURE 2. Phase of β_0/ξ_0 versus k.

Substitution of these numbers into equations (4) and (5) shows that the motion is stable for any value of γ if there is no time delay ($\sigma = 0$). For $\sigma = 0.5$, which corresponds to $\tau = 0.10$ sec for 40 knots and $\tau = 0.12$ sec for 33½ knots, the plain tail torpedo is stable if $\gamma < 28$, and the shroud tail torpedo is stable if $\gamma < 99$. Thus the improvement in dynamic stability of the uncontrolled torpedo produced by the addition of the shroud ring (see end of Chapter 7) is reflected here as an increase in the range of control parameters over which stable operation occurs.

9.2 NYQUIST CRITERION

In this method the θ response to a sinusoidal rudder motion ξ is calculated first, and then the rudder motion ξ^* produced by this θ motion through the control. The two together give the overall response of the controlled torpedo, and from a plot of this as a function of frequency the stability may be inferred. In performing the calculation it is convenient to use complex exponentials rather than sines and cosines. Thus if $\xi = \xi_0 e^{i\omega t} = \xi_0 e^{iks}$ is substituted on the right sides of the first two of equations (2) and the steady state solutions $\Omega = \Omega_0 e^{iks}$ and $\beta = \beta_0 e^{iks}$ found, the complex ratio Ω_0/ξ_0, for example, may be written as $|\Omega_0/\xi_0| e^{i\psi}$, where the magnitude is the amplitude ratio and ψ is the phase lead in radians of Ω over ξ. The β response is readily obtained from the fourth of equations (2), and ξ_0^*/β_0 may be found from the third of these equations. The complex overall response function is then given by the product of the three factors:

$$\frac{\xi_0^*}{\xi_0} = \left(\frac{\Omega_0}{\xi_0}\right)\left(\frac{\beta_0}{\Omega_0}\right)\left(\frac{\xi_0^*}{\beta_0}\right). \tag{6}$$

From Section 7.2, the relation between the frequency ν in cycles per sec, the angular frequency ω in

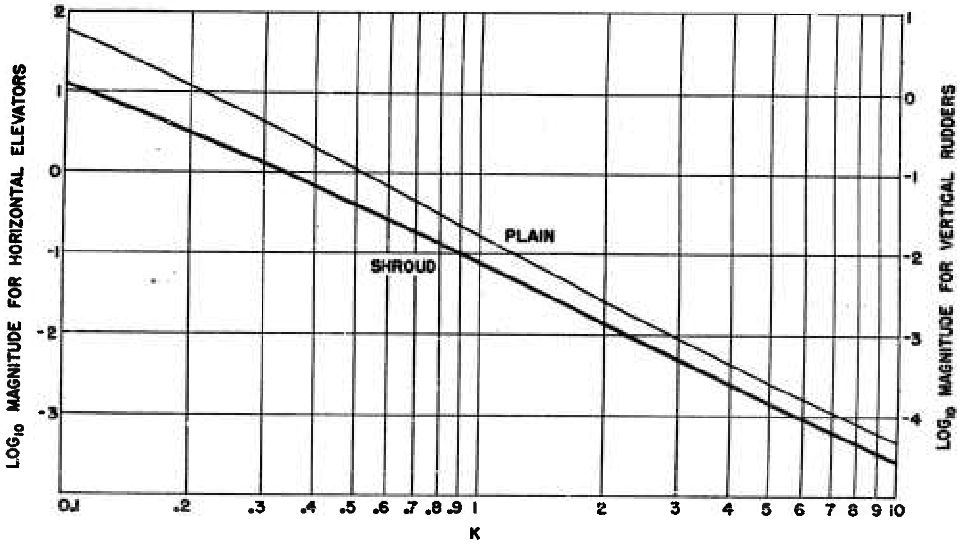

FIGURE 3. Log_{10} magnitude h_0/ξ_0 versus k.

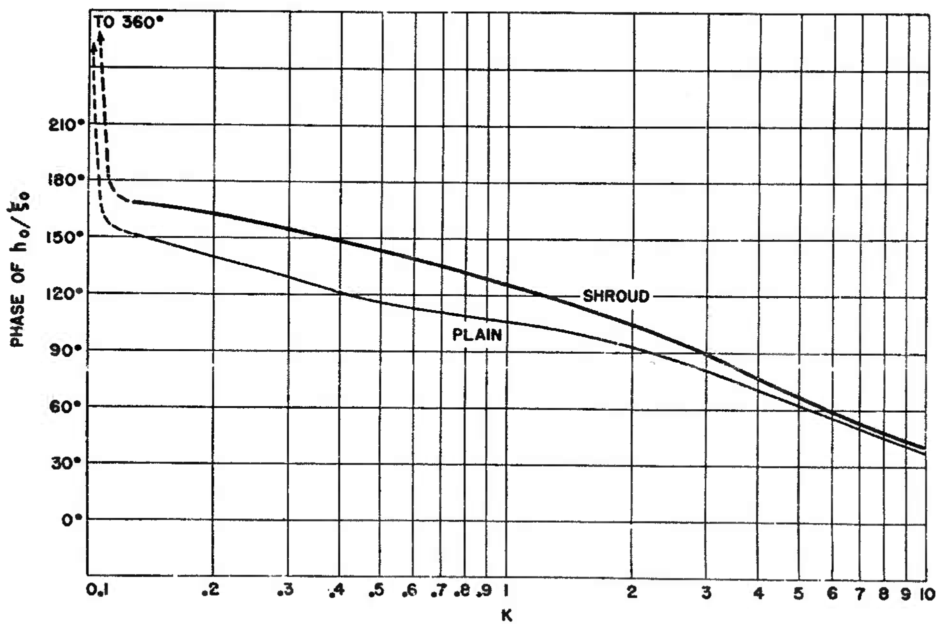

FIGURE 4. Phase of h_0/ξ_0 versus k.

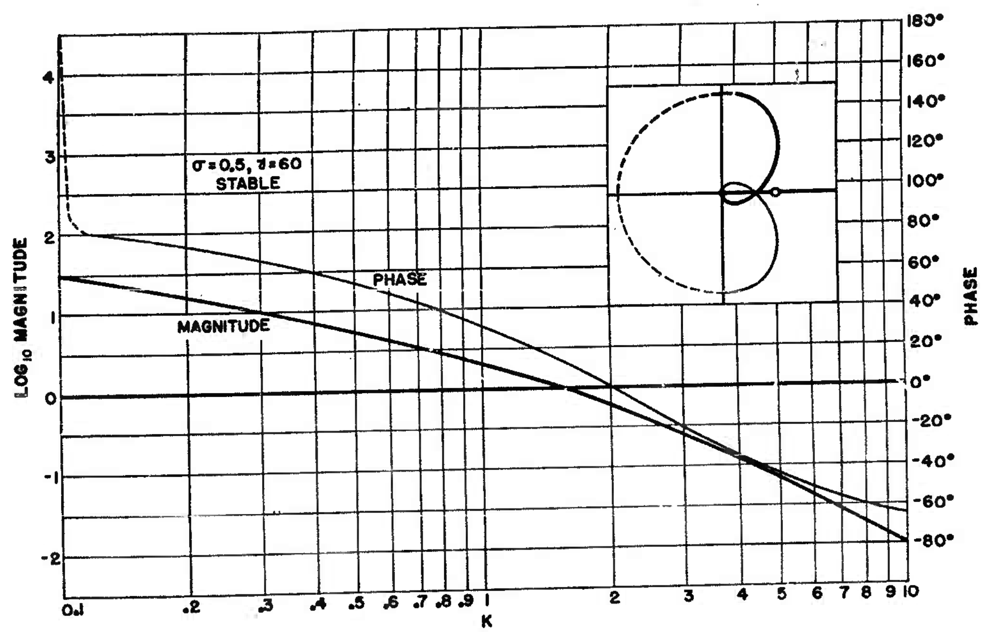

FIGURE 5. Phase of and $\log_{10}$ magnitude of ξ_0^*/ξ_0 for shroud-tail steering versus k.

radians per sec, and the dimensionless quantity k is

$$2\pi\nu = \omega = \frac{V}{l} k .$$

Thus, for the Mark 13-2 torpedo at 40 knots, $\nu = 0.79k$, and at $33\frac{1}{2}$ knots, $\nu = 0.66k$.

The solutions of the first two of equations (2) are

$$\frac{\alpha_0}{\xi_0} = \frac{(mC_\mu + C_K C_\lambda + iknC_\lambda)}{\Delta} ,$$

$$\frac{\Omega_0}{\xi_0} = -\frac{(C_m C_\lambda + C_l C_\mu + ikm_2 C_\mu)}{\Delta} , \tag{7}$$

$$\Delta = nm_2k^2 - (C_l C_K - mC_m) - ik(nC_l + m_2 C_K) .$$

The last two of equations (2) give

$$\frac{\beta_0}{\Omega_0} = \frac{1}{ik} , \tag{8}$$

$$\frac{\xi_0^*}{\beta_0} = -\frac{\gamma}{1 + ik\sigma} , \tag{9}$$

The quantity $\beta_0/\xi_0 = (\Omega_0/\xi_0)(\beta_0/\Omega_0)$ can be computed from (7) and (8) with the numerical values of Section 9.1; its phase and the logarithm of its magnitude are plotted as a function of k for the plain and shroud ring tails in Figures 1 and 2. Similar curves of h_0/ξ_0, where h is the lateral deviation from straight course, are plotted in Figures 3 and 4 (see Chapter 12). The left ordinate scales for Figures 1 and 3 refer to the horizontal elevators and the right ordinate scales to the vertical rudders.

Before completing the study of this control by Nyquist's method, it is necessary to discuss a peculiarity of the torpedo problem which does not arise in most other control problems. This is the singularity in β_0/ξ_0 at $k = 0$, which makes it impossible to apply Nyquist's criterion directly. Physically, this singularity means that if the rudder is oscillated slowly enough, the angular excursions of the torpedo can be made arbitrarily large with fixed rudder amplitude; this is to be expected so long as the nonlinearity of the equations for such large angles is neglected. It can be shown that the way in which to deal with this singularity is to bring the phase of the β_0/ξ_0 response function from the smallest k of practical interest to $k = 0$ along the dotted curves indicated in Figure 2 and keep the magnitude constant. This corresponds to avoiding the singularity by replacing e^{iks} by e^{ps} for small k, where the contour in the complex p-plane is taken along the imaginary axis

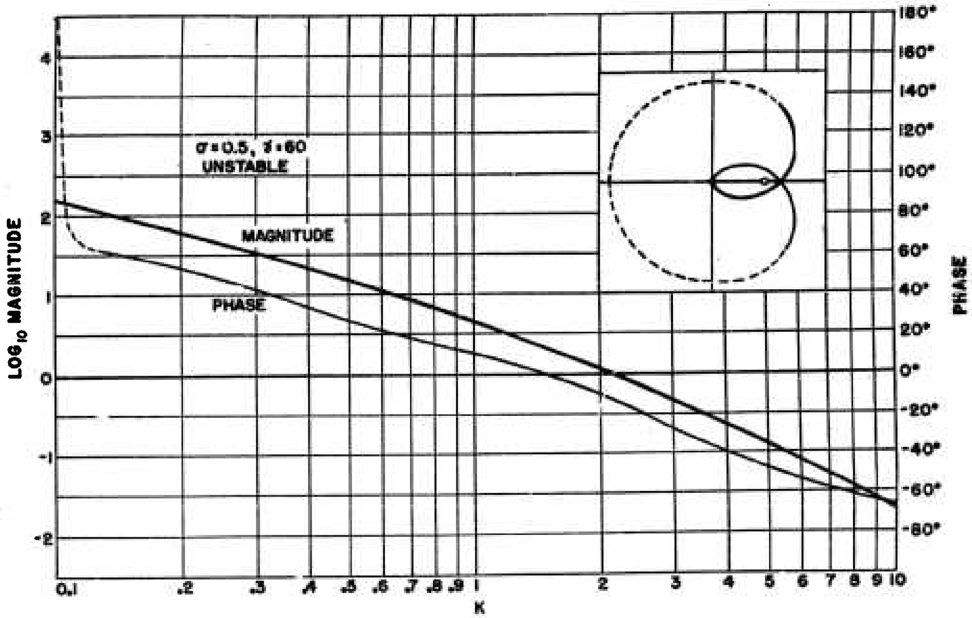

FIGURE 6. Phase of and $\log_{10}$ magnitude of ξ_0^*/ξ_0 for plain tail steering versus k.

($p = ik$) in to a small value of k, and then around the origin to the right. When this procedure is followed, Nyquist's criterion may be used.[a]

The phase and the logarithm of the magnitude of the overall response function (6) are plotted as a function of k in Figures 5 and 6, the circuit of the origin being indicated by dotted curves. The control parameters chosen are $\sigma = 0.5$, $\gamma = 60$, for which, according to Section 9.1, the shroud tail torpedo should be stable and the plain tail not. The inserts of Figures 5 and 6 show schematically (not to scale) the shape of the Nyquist diagrams in polar coordinates, the positive real polar axis being to the right and the unit point being marked with a circle; it is evident that these diagrams agree with the results of Section 9.1. A comparison of the curves and the inserts shows that it is necessary to examine the response function only in the region of k near which the magnitude is unity and the phase zero. If the phase crosses zero (from positive to negative as k increases) at a smaller value of k than that at which the magnitude crosses unity (decreasing as k increases) so that the magnitude is greater than unity when the phase is zero, the system is unstable; otherwise, it is stable. This last statement of the Nyquist criterion is of course special to this problem, but it does apply to a large group of torpedoes and controls; in case of doubt the whole of the Nyquist diagram should be drawn.

It might appear from the foregoing discussion that the Hurwitz criterion is easier to apply than the Nyquist criterion. This is generally true if only a single control and a single type of motion need be considered. But if, for example, one wishes to consider both proportional and two-position systems or if one wishes to compare a number of different types of proportional control on a single torpedo, then the decomposition of the overall response function into a product of torpedo and control response functions saves a great deal of numerical work. It should also be noted that the relatively simple fourth degree equation (4) for p becomes a sixth or higher degree equation for a pendulum type depth control.

Another advantage of the Nyquist method is that it is possible to do some problems that cannot be treated at all by the Hurwitz method. These are problems in which frequency-independent time delays occur or in which part of the overall response function, say that of the steering or depth engine, is measured empirically. Although the Nyquist method has been rigorously justified only for systems that can be described by a set of linear differential equations of finite order, it seems very plausible that the

[a] It is worth noting, as is easily proved, that Nyquist's criterion gives incorrect results when applied to torpedoes that are dynamically unstable; this does not, however, affect its application to the Mark 13-2 torpedo.

method is applicable to systems with time delays or mild nonlinearities. As an example, the friction-stiffness time constant assumed in the problem worked out above could be replaced by a fixed time delay τ simply by introducing an additional phase lag $2\pi\nu\tau = k\sigma$ radians into the overall response function. This could not, on the other hand, be treated by the Hurwitz method since a fixed delay can only be represented by a differential equation of infinite order. Thus, in order to represent

$$\xi(s + \sigma) = -\gamma\theta(s)$$

in place of the third of equations (2), one would require the differential equation:

$$\xi + \sigma\xi' + \frac{\sigma 2\xi''}{2!} + \cdots = -\gamma\theta\,.$$

The convergence of this equation would have to be investigated in particular cases of interest. It should be noted, however, that in order to calculate the motion and trajectory of the torpedo the characteristic exponents must be determined.

Chapter 10

TWO-POSITION CONTROL

This chapter applies the second (approximate) method discussed in Section 8.4 to the detailed consideration of the horizontal steering of the Mark 13-2 torpedo. It is assumed that the torpedo is provided with a two-position steering control which possesses characteristics similar to those of the standard pallet mechanism. Thus, if the desired heading is $\beta = 0°$ and the gyroscope axis is in this direction, the mechanism is set into motion when the heading becomes $\pm\beta_c$ and the rudder moves very quickly from stop to stop a time τ after this.

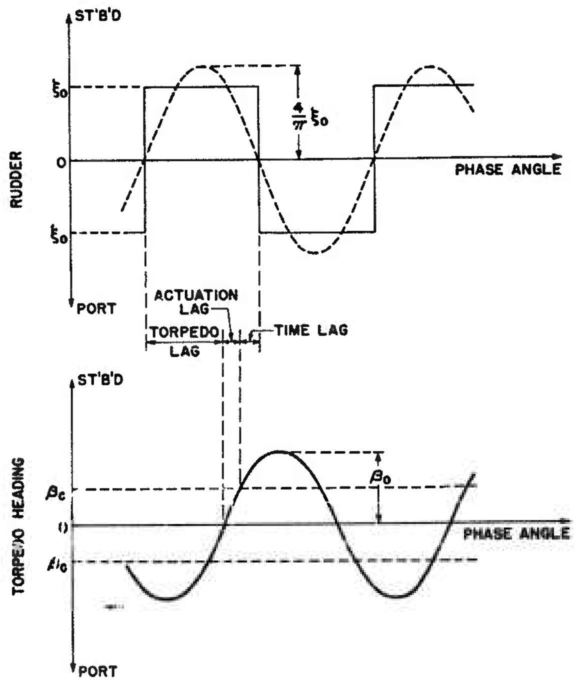

Figure 1. Phase lags caused by torpedo motion, the finite actuation angle β_c, and the time delay.

A square-wave rudder motion of amplitude ξ_0 and of definite frequency or k value (see Section 9.2) is assumed, and the torpedo motion corresponding to its fundamental component is calculated. The phase at which the β motion causes the control to operate the rudders is found, and this corrected for the time delay τ must agree with the originally assumed phase of the rudder motion. If the time of transit of the rudder from stop to stop is appreciable, it may be taken into account by increasing the time delay by half the transit time and correcting the amplitude of the fundamental component of the rudder motion in accordance with the departure from square-wave form; the second of these effects is usually negligible whereas the first is not.

The relationships between the phase lags due to the torpedo motion, to the finite actuation angle β_c, and to the time delay τ are shown schematically in Figure 1. It is clear from this that the sum of the three phase lags must be 180° in order for a steady oscillation of this type to persist. The torpedo phase lag is the negative of the phase of β_0/ξ_0 plotted in Figure 2 of Chapter 9, and the phase lag due to the time delay is simply $2\pi\nu\tau = k\sigma$ radians, where again $\sigma = V\tau/l$. The actuation phase lag is seen from Figure 1 to be $\sin^{-1}(\beta_c/\beta_0)$, where β_0 is the amplitude of the oscillation of the torpedo heading. β_0 may be computed from Figure 1 of Chapter 9 (using the right ordinate scale) for any k value by multiplying the magnitude of β_0/ξ_0 by $4\xi_0/\pi$, which is the amplitude of the fundamental component of the rudder motion.

The rudder throw in the Mark 13-2 torpedo is $\xi_0 = 12.1°$. Figure 2 shows the three component phase lags and their sum as functions of k for the shroud tail torpedo, under the assumption that $\beta_c = 0.5°$ and $\sigma = 0.5$, which corresponds to $\tau = 0.10$ sec at 40 knots and $\tau = 0.12$ sec at 33½ knots. Figure 3 shows similar curves for the plain tail torpedo. Since the total phase lags increase with ν or k in each case, the 180° crossings represent stable oscillations (see Section 8.4). These crossings happen to occur at $k = 0.76$ for both tails. A similar calculation for $\sigma = 0.4$ corresponding to $\tau = 0.10$ sec at 33½ knots, gives crossings which were used to construct the following table.

Mark 13-2 Torpedo

Period (T) in seconds and amplitude (β_0) for steering. $\xi_0 = 12.1°$, $\beta_c = 0.5°$, $\tau = 0.1$ sec.

	Shroud tail		Plain tail	
	T	β_0	T	β_0
40 knots:	1.66	0.82°	1.66	1.98°
33½ knots:	1.89	0.77°	1.84	1.73°

Both the assumed parameters and the calculated periods are in good agreement with observation; no experimental data are available on β_0.

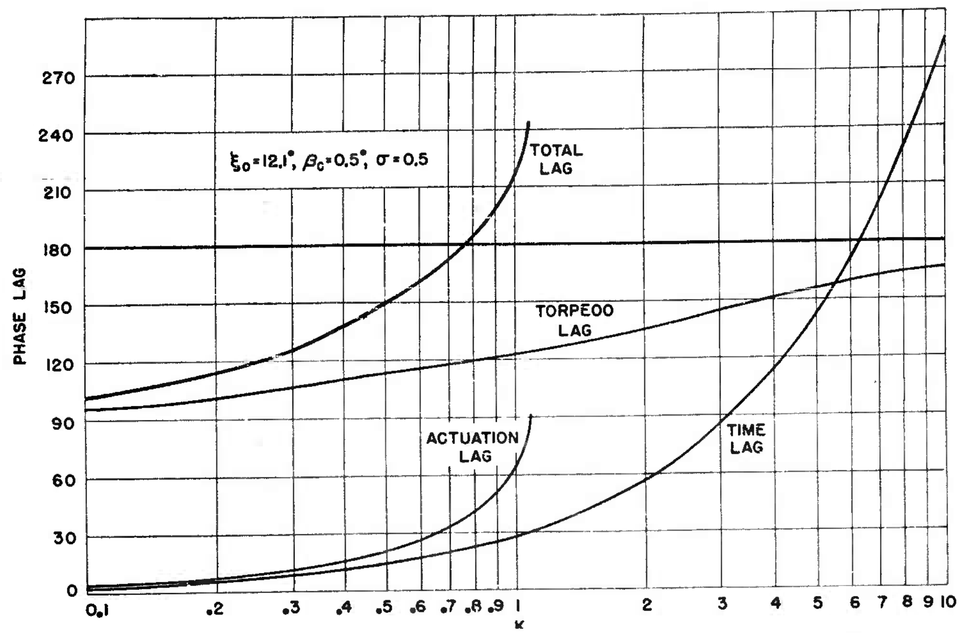

FIGURE 2. Three component phase lags and their sum as functions of k for the shroud tail torpedo.

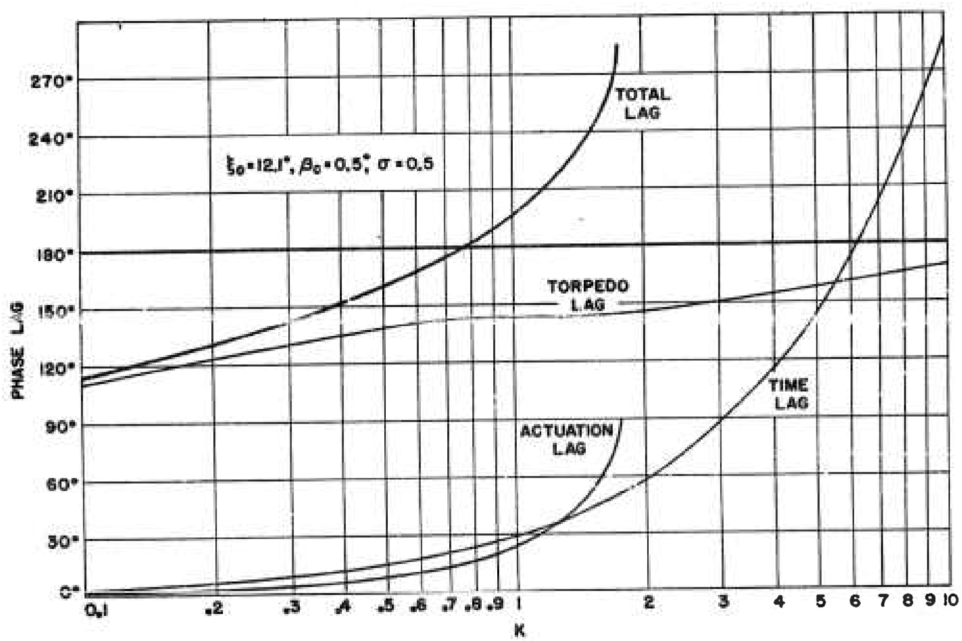

FIGURE 3. Three component phase lags and their sum as functions of k for the plain tail torpedo.

It will be noticed that increase in θ_c and decrease in θ_0 increases the actuation lag, increase in τ or σ increases the time lag, and removal of the shroud ring increases the torpedo lag. All of these changes increase the overall phase lag and hence increase the period of oscillation. Thus the close agreement between the values for the periods with and without the shroud tail is due to a compensation between the increase in torpedo phase lag caused by removal of the shroud ring and the decrease in actuation phase lag caused by the increase in β_0 that accompanies this removal. In similar fashion, increase in speed causes k to decrease for given ν and hence causes the torpedo lag and the actuation lag to decrease; the time lag is unchanged. Thus the overall lag and hence the period of oscillation decrease.

Chapter 11

STEERING CONTROL

The steering of the Mark 13-2 torpedo has been used to provide a numerical example of a proportional control in Chapter 9 and of a two-position control in Chapter 10. The methods available for constructing these controls will be discussed in Section 11.1; Sections 11.2 and 11.3 deal with problems that arise in maneuvering in the horizontal plane. Before proceeding further, it is worth emphasizing that the use of a gyroscope as a standard of course direction is fundamental to all devices intended to steer the torpedo or to maneuver it in a predetermined manner. The long time errors that make an uncorrected gyro unsuitable for use as a compass are of little importance in the case of a torpedo, where the short duration of the run makes it possible to use a gyro of quite moderate dimensions and speed.

11.1 AVAILABLE METHODS

The problem to be discussed here is that of making available a force large enough to move the vertical rudders in accordance with the information supplied by the gyroscope, without producing a reaction on the gyro large enough to cause it to precess appreciably.

The standard pallet mechanism puts the valve of a pneumatically operated steering engine in one of two positions in accordance with the orientation of the outer gimbal of the gyro with respect to the torpedo body. The energy for moving the valve comes from the propeller shaft, which oscillates the pallet in such a way that it is tripped in one direction or the other by a blade on the gimbal without reacting back appreciably on the gimbal. Since the pallet carries the information to the valve only once per cycle, there is an inherent time delay in this system which is of the order of the period of oscillation. In addition, the torpedo must deviate from course by a finite angle before the pallet is tripped, and machining tolerances prevent this angle from being as small as might be desired. As was shown in Chapter 10, both of these effects lengthen the steering period, and hence increase the amplitude of horizontal oscillation and of roll.

Another device that operates in the same general manner has recently been developed for use in some electric torpedoes by the Westinghouse Electric and Manufacturing Company. A light roller attached to the gyro gimbal is arranged so that it makes a contact whenever the torpedo is off course in one direction, and breaks it when it is off course in the other direction. The contact is connected in series with a relay which passes current through one or the other of two solenoids which move the rudders in opposite directions. In this case the actuation phase lag (see Chapter 10) is negligible, but the time delay can still be appreciable if the relay and solenoids are not properly designed.

A pneumatic control that has a more rapid response than the pallet mechanism and can also be used as a proportional control has been developed by Columbia University and the American Can Company for use on the Mark 25 torpedo. This consists of a semicircular blade mounted on the gyro outer gimbal and coaxial with it, which interrupts two jets of high-pressure air moving radially outward at opposite ends of the diameter of the semicircle. Air is supplied from a single source to both jets and, after traversing the small gap in which the blade moves, goes into two receptive orifices which lead it to opposite sides of the steering engine piston. When the gyro is centered with respect to the torpedo axis, the blade interrupts both air streams equally, and the pressures developed on the two sides of the piston are equal. A small motion of the blade causes more air to go to one side of the piston than the other and moves the piston and hence the vertical rudders accordingly. The quite small reaction of the air stream back on one edge of the blade is nearly cancelled by that on the other edge.

The hydrodynamic pressure on the vertical rudders produces a restoring force which is approximately proportional to the rudder deflection. Since the piston force is also nearly proportional to the blade deflection, the entire system acts as a proportional control with properties somewhat like those assumed in Chapter 9; the time constant assumed there is significant if the connecting air lines from the blade to the engine are more than a few inches in length. In a well-designed practical system, with line pressure of the order of 500 psi and piston area of the order of one square inch, the hydrodynamic restoring force is so small that for the time constant encountered the quantity γ in equation (1) of Chapter 9 can be made to exceed the maximum value at which the system operates as a stable proportional control (see Chapter 9). It then operates as a transitional system and for large γ may be treated as a two-position control.

A proportional system may be developed along these lines by loading the steering engine output with springs large enough to reduce γ to the stable range. This is referred to as a force-proportional control. It is the force exerted by the steering engine rather than its position which is proportional to the blade deflection, and the engine or rudder position is proportional to this only if the restoring force has a fixed proportionality constant and static or Coulomb friction can be neglected. The hydrodynamic restoring force depends on the speed but is generally much smaller than the spring restoring force, which can be made quite constant and reproducible.

While in principle positioning type engines and phase advance schemes may be applied to the steering problem, this has not been attempted thus far, and it seems unlikely that it will be in the near future. These techniques will be discussed in Section 12.1 in connection with depth controls.

11.2 MANEUVERING: APPROACH TO TURN

It is sometimes useful to be able to predict the trajectory of a torpedo in the horizontal plane when the rudder is manipulated in accordance with some predetermined plan. The two examples to be worked out in this section and the next illustrate the principal features of calculations of this type. In the first example, it is assumed that the torpedo is running on a straight course when the rudder is suddenly thrown hard over and maintained that way. The torpedo then makes the transition from the straight run to the steady turning circle. In the second example (Section 11.3), it is assumed that the torpedo is in its steady turn when the rudder is suddenly brought amidships, and the transition to a straight course is to be found. These examples provide the elements of the calculation of an angle shot, and extensions of the calculations to other problems of practical interest can be made.

For illustrative purposes it is permissible to leave the actual steering mechanism out of consideration and to assume that the only rudder motion is a rapid transit from center position to hard over, or vice versa. This gives sensible results if the torpedo is dynamically stable (see Section 7.2) since then the undisturbed torpedo will run on a straight course with rudder amidships. Since the Mark 13-2 torpedo, with or without the shroud ring, is dynamically stable (and all other torpedoes that have been studied appear to be as well), the methods of this section are of practical interest. If it were ever necessary to study a dynamically unstable torpedo, however, the present treatment would be inadequate, and it would be necessary to include the steering control as a fundamental factor in the motion.

The equations to be solved are (10) of Chapter 7 with $w = b = 0$:

$$m_2\alpha' + C_l\alpha + m\Omega = -C_\lambda\xi_0\,, \qquad C_m\alpha + n\Omega' + C_K\Omega = C_\mu\xi_0\,. \tag{1}$$

The solutions of these inhomogeneous equations are the same as for the homogeneous equations considered in Section 7.2, except for the addition of constant terms:

$$\alpha = \alpha_1 e^{p_1 s} + \alpha_2 e^{p_2 s} + \alpha_3\,, \qquad \Omega = \Omega_1 e^{p_1 s} + \Omega_2 e^{p_2 s} + \Omega_3\,. \tag{2}$$

The characteristic exponents p_1 and p_2 are as given in equation (15) of Chapter 7.

For the first example, in which the torpedo is going from straight course into a turn, ξ_0 is the full rudder angle, and the initial conditions (at $s = 0$) are $\beta = \alpha = \Omega = 0$. In this treatment the roll angle of the torpedo in a turn is neglected. The initial values of α' and Ω' are also required in order to evaluate the coefficients in (2), and these may be obtained from the equations of motion (1) at $s = 0$; the results are

$$\alpha_0' = -\frac{C_\lambda\xi_0}{m_2}\,, \qquad \Omega_0' = \frac{C_\mu\xi_0}{n}\,. \tag{3}$$

The values of α_3 and Ω_3 may be obtained by substituting (2) into (1) and equating terms independent of s. The solution of the resulting equations is

$$\beta_3 = -\frac{(C_K C_\lambda + mC_\mu)\xi_0}{(C_l C_K - mC_m)}\,, \qquad \Omega_3 = \frac{(C_l C_\mu + C_m C_\lambda)\xi_0}{(C_l C_K - mC_m)}\,. \tag{4}$$

The initial values of α, Ω and their derivatives then give the following equations for the other coefficients of (2):

$$\alpha_1 + \alpha_2 = -\alpha_3\,, \qquad p_1\alpha_1 + p_2\alpha_2 = \frac{-C_\lambda\xi_0}{m_2}\,,$$
$$\Omega_1 + \Omega_2 = -\Omega_3\,, \qquad p_1\Omega_1 + p_2\Omega_2 = \frac{C_\mu\xi_0}{n}\,. \tag{5}$$

The solutions of equations (5) are

$$\alpha_1 = \frac{(-C_\lambda\xi_0/m_2 + p_2\beta_3)}{(p_1 - p_2)}\,,$$
$$\beta_2 = \frac{(C_\lambda\xi_0/m_2 - p_1\beta_3)}{(p_1 - p_2)}\,, \tag{6}$$
$$\Omega = \frac{(C_\mu\xi_0/n + p_2\Omega_3)}{(p_1 - p_2)}\,,$$
$$\Omega_2 = -\frac{(C_\mu\xi_0/n + p_1\Omega_3)}{(p_1 - p_2)}\,.$$

Equations (2), (4), and (6) give the complete solutions for α and Ω as functions of the distance s along the trajectory measured in torpedo lengths.

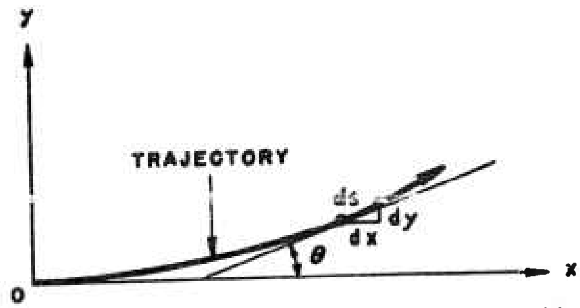

FIGURE 1. Illustrative diagram of trajectory with coordinates along and perpendicular to the original course.

The orientation angle β may be obtained by integrating the equation $\beta' = \Omega$, and the course or trajectory angle is then $\theta = \beta + \alpha$ (see Figure 2 of Chapter 7). Now if x and y are rectangular coordinates along and perpendicular to the initial course of the torpedo, measured in lengths, the following relations are valid:

$$\frac{dx}{ds} = \cos\theta\,, \qquad \frac{dy}{ds} = \sin\theta\,. \tag{7}$$

Equations (7) may be integrated to give

$$x(s) = \int_0^s \cos\theta(z)dz\,,$$
$$y(s) = \int_0^s \sin\theta(z)dz\,. \tag{8}$$

Since θ will be given in terms of exponentials of its argument, the integrals in (8) cannot be evaluated analytically except as infinite series. For many purposes, the leading terms of these series are sufficient; these are obtained by putting $\cos\theta = 1$, $\sin\theta = \theta$, when

$$x(s) = s\,, \qquad y(s) = \int_0^s \theta(z)dz\,. \tag{9}$$

The trajectory given by (9) is accurate so long as the course angle θ does not become large. Thus, for the errors to be less than 10 per cent, θ must be less than 0.45 radian = 26°. It is evident, however, that since the torpedo is going into a circle, θ will become arbitrarily large after a sufficiently long time. This does not affect the usefulness of (9) so long as the motion becomes circular before θ is large since then the steady turning circle can be fitted on to the transient phase of the motion which is described by equations (9). An explicit expression for the course angle is obtained by integrating Ω as given by (2) and adding α:

$$\theta(s) = \alpha_1 e^{p_1 s} + \alpha_2 e^{p_2 s} + \alpha_3 + \Omega_1\frac{(e^{p_1 s} - 1)}{p_1} + \frac{\Omega_2(e^{p_2 s} - 1)}{p_2} + \Omega_3 s\,. \tag{10}$$

The asymptotic form of this as s becomes large is

$$\theta(s) \longrightarrow \left(\alpha_3 - \frac{\Omega_1}{p_1} - \frac{\Omega_2}{p_2}\right) + \Omega_3 s\,, \tag{11}$$

which makes the trajectory a circle of radius (measured in lengths) $\rho = 1/\Omega_3$.

The question as to the accuracy of (9) may now be put as follows: does the $\theta(s)$ given by (10) approach the asymptotic form (11) sufficiently closely before θ becomes large enough to invalidate the approximations made in deriving (9)? Retaining the 10 per cent criterion of accuracy, the requirement is that

$$e^{p_1 s_0} \leqq 0.1 \text{ for } \theta(s_0) = 0.45\,. \tag{12}$$

The smaller exponent p_1, given by the upper sign in equation (15) of Chapter 7, is used since it furnishes the more stringent criterion. In calculating s_0 from the second part of (12), the asymptotic form (11) may be used.

If now it is assumed that the criterion (12) is satisfied, the complete trajectory is readily calculated. An important parameter of this motion is the distance parallel to the initial course from the point at which the rudder is thrown over to the center of the steady

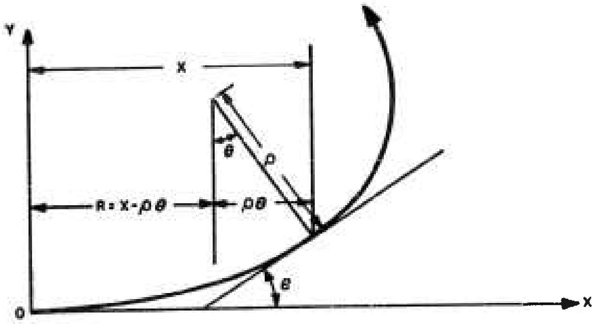

FIGURE 2. Diagram illustrating torpedo reach and method of calculation.

turning circle. This "reach" R of the torpedo is seen from the diagram in Figure 2 to be given approximately by

$$R = x - \rho\theta = s - \frac{\theta}{\Omega_3}. \qquad (13)$$

Substitution of (11) into (13) gives

$$R = \frac{(\Omega_1/p_1 + \Omega_2/p_2 - \alpha_3)}{\Omega_3}, \qquad (14)$$

which is independent of s, as, of course, it must be for the method of calculation to be valid. Equation (14) may be simplified with the help of (4) and (6) to

$$R = \frac{C_K - \lambda(m_2 - m)}{C_m + \lambda C_l} + \frac{nC_l + m_2 C_K}{C_l C_K - mC_m}. \qquad (15)$$

Here $\lambda \equiv C_\mu/C_\lambda$ is the fraction of the torpedo length aft of the CG at which the effective rudder force is applied. It is interesting to note that R is independent of ξ_0 and hence of the turning circle radius ρ for a given torpedo. From (12) and (11), s_0 is seen to be

$$s_0 = \frac{(0.45 - \alpha_3 + \Omega_1/p_1 + \Omega_2/p_2)}{\Omega_3} = \frac{R + 0.45}{\Omega_3}. \qquad (16)$$

Thus the accuracy criterion becomes

$$-p_1 s_0 = |p_1| \cdot (R + 0.45\rho) \geqq 2.3\,; \qquad (17)$$

this does depend on ρ and hence on ξ_0.

Substitution of the provisional torpedo parameters given in Section 9.1, into the above equations gives the following approximate numerical values for the Mark 13-2 torpedo with and without the shroud ring:

	Shroud	Plain
ρ (lengths)	88.5	17.7
ρ (feet)	1,190	238
R (lengths)	1.61	4.22
R (feet)	21.6	56.7
$-p_1 s_0$	23.2	2.80

The accuracy criterion, which is barely satisfied by the plain tail torpedo, is very well met by the shroud tail torpedo. In general, a small value of R is associated with a large degree of dynamic stability; the more stable the torpedo, the more rapidly it approaches a new state of steady motion.

11.3 MANEUVERING: PULL-OUT FROM TURN

As the second example, a solution of the equations of motion will be obtained for the case in which the rudder is suddenly set amidships while the torpedo is in a steady turn. The equations are now (1) with $\xi_0 = 0$, from which it is seen that the solution is (2) with $\alpha_3 = \Omega_3 = 0$. The coefficient α_1, α_2, Ω_1, and Ω_2 can be found as in Section 11.2 in terms of the initial conditions. It will be assumed that at $s = 0$, when the rudder is thrown amidships, the orientation of the torpedo is $\beta = 0$ and the torpedo is circling to the left. Since in the steady turn the torpedo noses in toward the center of the turn, the initial value of α is negative and equal in magnitude to the α_3 calculated from the first of equations (4). In similar fashion, the initial value of Ω is positive and equal to the Ω_3 calculated from the second of equations (4). The initial values of α' and Ω' may be found from the equations of motion, as before.

The solution for the course angle θ is given by (10) with $\beta_3 = \Omega_3 = 0$ so that asymptotically θ approaches a constant value θ_∞ and the motion approaches a straight line. The trajectory may be found by integrating the approximate equations (9):

$$y(x) = -\left(\frac{\Omega_1}{p_1} + \frac{\Omega_2}{p_2}\right)x + \frac{(\alpha_1 + \Omega_1/p_1)\,(e^{p_1 x} - 1)}{p_1} + \frac{(\alpha_2 + \Omega_2/p_2)\,(e^{p_2 x} - 1)}{p_2} \quad (18)$$

where x has been substituted for s. The asymptotic form of this is the straight line:

$$y(x) \longrightarrow \theta_\infty x - \delta\,. \quad (19)$$

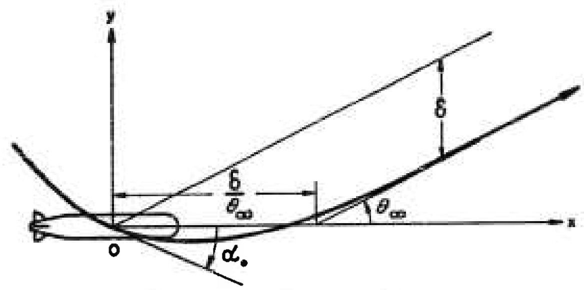

FIGURE 3. Illustrative diagram.

Substitution of the torpedo parameters into the expressions for α_1, etc., gives

$$\theta_\infty = \frac{-m_2 C_m \alpha_0 + n C_l \Omega_0}{C_l C_K - m C_m}, \quad (20)$$

$$\delta = \frac{-[C_K(C_l C_K - m C_m) + C_m(n C_l + m_2 C_K)]\,m_2 \alpha_0}{(C_l C_K - m C_m)^2} + \frac{[C_l(n C_l + m_2 C_K) - (m_2 - m)(C_l C_K - m C_m)]\,n \Omega_0}{(C_l C_K - m C_m)^2}\,.$$

For the situation illustrated in the Figure 3, α_0 is negative and Ω_0 is positive. Since α_0 and Ω_0 are proportional to the rudder throw ξ_0 in the initial turn (see equations 4), δ and θ_∞ are also, and the quantity δ/θ_∞ is independent of ξ_0 and hence of the initial turning radius.

Numerical values may be obtained with the help of the approximate constants given in Section 9.1. Equations (20) then become

$$\theta_\infty = -0.98\alpha_0 + 0.473\Omega_0\,, \qquad \delta = -3.79\alpha_0 + 0.505\Omega_0 \quad \text{(shroud)}\,;$$

$$\theta_\infty = -5.45\alpha_0 + 0.954\Omega_0\,, \qquad \delta = -28.9\alpha_0 + 3.33\Omega_0 \quad \text{(plain)}\,. \quad (21)$$

From the results of Section 11.2

$$\alpha_0 = -.0065 \text{ radian} = -0.37^\circ\,, \qquad \Omega_0 = .0113, \quad \text{(shroud)}\,;$$

$$\alpha_0 = -.0284 \text{ radian} = -1.63^\circ\,, \qquad \Omega_0 = .0565\,, \quad \text{(plain)}\,. \quad (22)$$

Substitution of (22) in (21) gives finally

	Shroud	Plain
θ_∞	0.7°	12.0°
δ	0.030	1.01
θ_∞	2.6	4.8

δ and δ/θ_∞ are, of course, measured in lengths. It is apparent that the increase in stability that accompanies the addition of the shroud ring greatly reduces the angle by which the torpedo overshoots the desired new heading.

Chapter 12

DEPTH CONTROL

12.1 AVAILABLE PRINCIPLES AND METHODS

It is natural to think of the depth of a torpedo as being controlled simply by a hydrostatic bellows or some similar pressure-indicating device. According to such a scheme, if the torpedo rises above set depth, the hydrostat calls for down elevator, and conversely. However, it is easy to see from the Nyquist criterion discussed in Section 9.1 that a proportional control based on this principle would be unstable. If h is the distance of the torpedo above set depth and ξ is the elevator angle, the relation between the two quantities should be $\xi = -\sigma h$, where σ is a positive proportionality constant. According to the curves of the phase of h_0/ξ_0 presented in Figure 4 of Chapter 9, this would give a Nyquist diagram of the form shown schematically in Figure 1. Since this encloses the unit point for any value of σ, the system is unstable. In similar fashion, since the lag of h behind ξ is always greater than 180°, the discussion of Chapter 10 shows that a two-position control based on hydrostat indication alone will not give satisfactory operation.

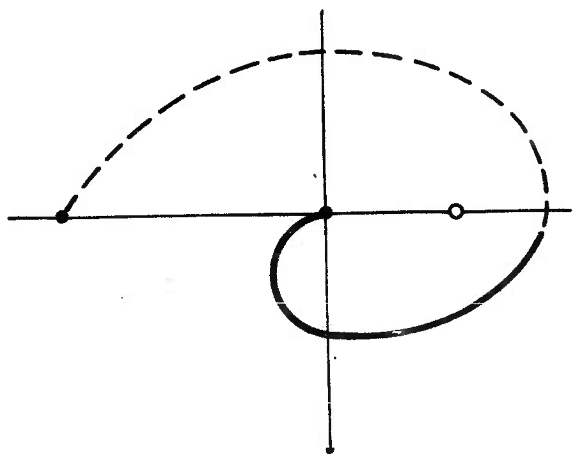

Figure 1. Nyquist diagram from curves in Chapter 9, Figure 1.

From a physical viewpoint, it may be said that the hydrostat fails to give stable control because it does not anticipate incipient deviations from set depth before they develop to such a point that they cannot be handled. This lack of anticipation is equivalent mathematically to excessive phase lag (greater than 180°). In order to get a stable control it is necessary to introduce an anticipatory device, which has the effect of decreasing the overall phase lag of the system. This can be done in a variety of ways, but in each case it is necessary to retain the hydrostat as part of the control mechanism in order that the torpedo may have an indication as to the depth at which it is supposed to run. Thus the problem of depth control during the steady run may be said to be the resolution of a conflict between too much anticipation and too little hydrostat on the one hand, which permits minor disturbances to give rise to excessive wandering from set depth, and too little anticipation and too much hydrostat on the other hand, which leads to instability. This situation manifests itself both when proportional and two-position controls are used.

The most widely used anticipatory device is the pendulum. The hydrostat is usually coupled to the pendulum through a linkage and the pendulum to the elevators through a depth engine. Thus the orientation of the pendulum with respect to the torpedo, and hence the position of the elevators, depends both on the orientation angle β of the torpedo in space and on the force exerted on it by the hydrostat. Since the torpedo usually noses up before decreasing its depth, the pendulum, insofar as it indicates inclination of the torpedo, serves the desired purpose. The diagrams in Figure 2 show schematic Nyquist curves (derived from Figures 2 and 4 of Chapter 9) for a pendulum control alone, for which $\xi = -\gamma\beta$, and for combined pendulum-hydrostat controls, for which $\xi = -\gamma[\beta + h/(W/V)]$, where for the present purpose β is measured in degrees and h in feet. The W/V ratio is the number of feet of depth change that is equivalent to 1° of change of inclination. It is clear from the diagrams that too small a W/V leads to instability; as pointed out above, too large a W/V suppresses the hydrostat effect so that the torpedo may be too insensitive to depth. W/V values now in use range for the most part from 2 to 4.

The foregoing discussion assumes that the system

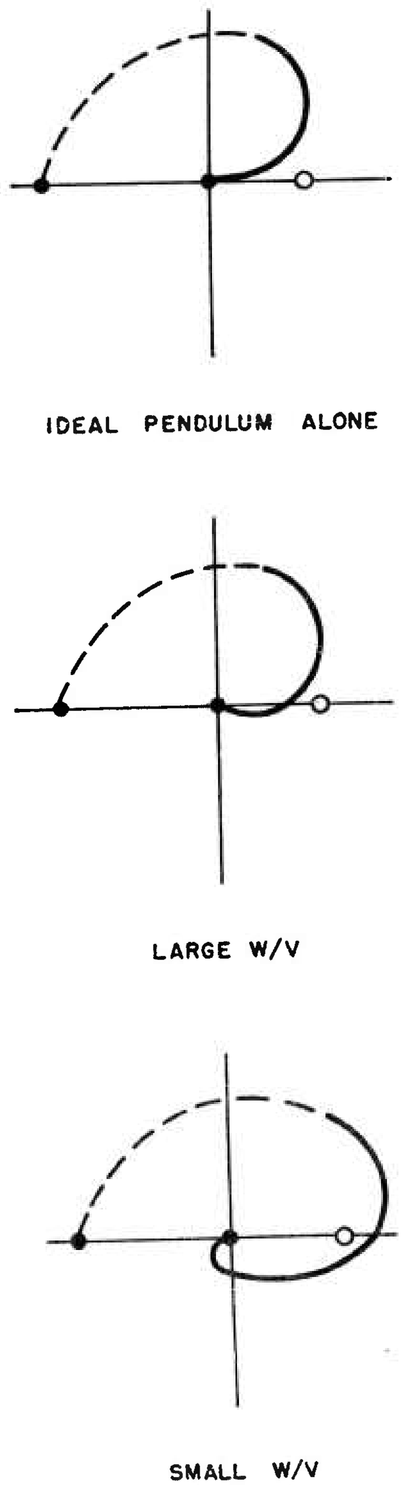

FIGURE 2. Nyquist diagrams for various pendulum controls.

is ideal in the sense that the hydrostat indicates depth, the pendulum indicates inclination, and the combined signal is transmitted without delay to the elevators. Actual depth controls fall short of this ideal in all three respects. The hydrostat indicates pressure rather than depth, and this varies from point to point over the torpedo and with its speed and pitch. Enough data are available on dynamic pressure distributions to take this into account in making the calculations. The effect is generally small and can be made negligible by suitably placing the hydrostat intake.

The pendulum is acted upon both by gravity and accelerations and, moreover, possesses inertia which affects its displacement. The accelerations acting on the pendulum depend not only on the translational motion of the torpedo, but on its rotational motion as well since the pendulum is usually mounted some distance from the CG of the torpedo. The effect of accelerations and inertia on the motion of a pendulum is best found by setting up the Lagrangian equation of motion in terms of the orientation angle χ of the pendulum in space, when the torpedo range traveled r, height h, and orientation angle $-\beta$ are specified functions of the time. Suppose that the pendulum pivot is mounted a distance x_0 aft of and y_0 above the torpedo CG, that L is the distance from its center of mass to the pivot, and that its mass and moment of inertia about the pivot are M and I. Then the equation of motion is

$$\text{External torques } \underbrace{MgL \times \sin\chi}_{\text{(gravity)}} + \underbrace{I\ddot{\chi}}_{\text{(inertia)}}$$

$$+ \underbrace{ML\ddot{r}\times\cos\chi}_{\substack{\text{(longitudinal}\\ \text{acceleration)}}} + \underbrace{ML\ddot{h}\times\sin\chi}_{\substack{\text{(vertical}\\ \text{acceleration)}}} + \underbrace{MLX\dot{\beta}^2}_{\substack{\text{(centrifugal}\\ \text{acceleration)}}} + \underbrace{MLY\ddot{\beta}}_{\substack{\text{(angular}\\ \text{acceleration)}}}, \tag{1}$$

where the origin of each term is indicated in parentheses beneath it. Here $X \equiv x_0 \cos(\chi + \beta) - y_0 \sin(\chi + \beta)$ is the distance from the torpedo CG to the pendulum along a line perpendicular to the pendulum, and $Y \equiv x_0 \sin(\chi + \beta) + y_0 \cos(\chi + \beta)$ is the distance from the pendulum pivot to the point of intersection of this line with the pendulum, measured positive when the pivot is above the intersection point.

Equation (1) can be linearized by assuming that all angles are small. It is of interest to express the motion in terms of the angle $\psi \equiv \chi + \beta$ that the pendulum makes with the perpendicular to the torpedo axis since it is the orientation of the pendulum relative to the torpedo that provides a useable signal. The result is

$$I\ddot{\psi} + MgL\psi = \text{External torques} - ML\ddot{r} - ML\chi_0\ddot{h} - [(I - MLY)\ddot{\beta} + MgL\beta]\ . \quad (2)$$

The first term on the left side is the inertia of the pendulum, and the second term is the gravitational restoring torque. Among the external torques may be a spring restoring torque proportional to ψ which would modify the gravitational term and a viscous damping torque proportional to $\dot{\psi}$. The next two

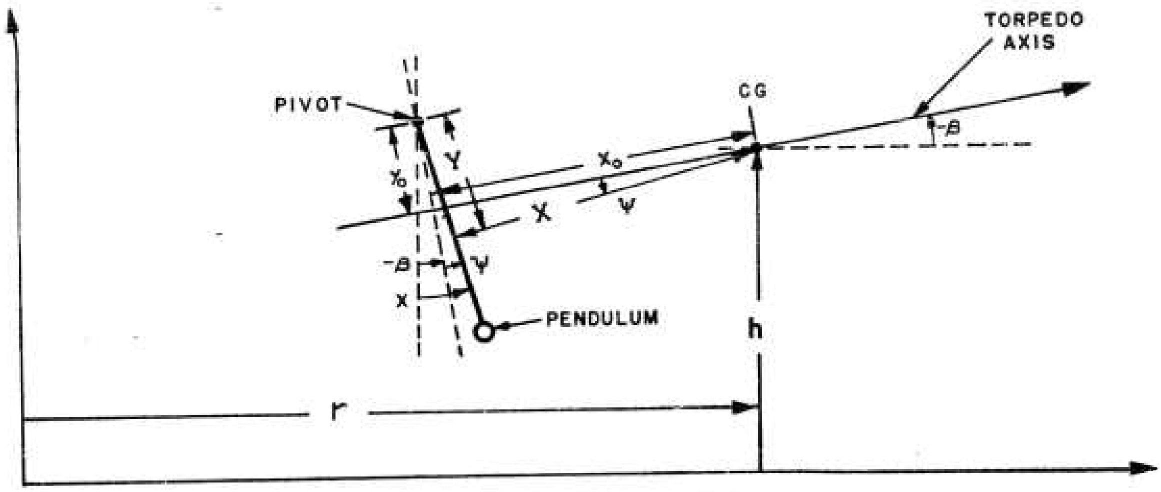

FIGURE 3. Diagram of pendulum in torpedo.

terms on the right side are the torques produced by longitudinal and vertical accelerations; the latter of these vanishes if the average orientation angle χ_0 of the pendulum is zero (vertical in space). The last terms on the right side include the additional gravitational torque due to inclination of the torpedo, and the effect of angular acceleration of the torpedo.

Suppose now that the hydrostat coupling (which appears as one of the external torques) is neglected for the moment, and a spring restoring torque $K\psi$ and damping torque $R\dot{\psi}$ are introduced. Then equation (2) becomes

$$I\ddot{\psi} + R\dot{\psi} + (MgL + K)\psi = -ML\ddot{r} - ML\chi_0\ddot{h} - [(I - MLY)\ddot{\beta} + MgL\beta]\ . \quad (3)$$

This may be thought of as a pendulum having an impedance characterized by the inertia, damping, and stiffness coefficients on the left side and driven by the forcing terms on the right side. Of these latter, the β terms are of particular interest since the pendulum was originally introduced to provide a measure of β. It is evident that the effect produced by change of orientation depends in general on the rate or frequency of the angular motion of the torpedo. In particular, there is a frequency of sinusoidal oscillation,

$$\omega_A = \left[\frac{g}{I/(ML - Y)}\right]^{1/2}, \quad (4)$$

for which there is no pendulum motion contributed by the β terms. This is referred to as an antiresonance frequency, in contrast with the resonance frequency

$$\omega_R = \left[\frac{MgL + K}{I}\right]^{1/2} \quad (5)$$

which is the natural frequency of the pendulum and springs (provided the damping term R is not too large). The antiresonance frequency is equal in magnitude to the natural frequency of a simple pendulum the length of which is equal to the distance of the center of percussion of the pendulum below the point of intersection of the pendulum with a line through the torpedo CG perpendicular to the pendulum. If the center of percussion of the pendulum is above the intersection point, the antiresonance phenomenon does not occur. Considered from the point of view of the Nyquist diagram, the resonance and antiresonance can each introduce phase lags of the order of 180°; since the former is associated with a large amplitude and the latter with zero amplitude, the order in which they occur as the frequency increases may be of importance in determining the stability of the control. This is discussed further in Section 12.2.

It is clear, therefore, that a pendulum is far from an ideal device and can introduce additional phase lags and amplitude changes which may be (and generally are) undesirable. This has led to the investigation of other methods for obtaining the anticipatory action necessary for satisfactory operation. The pendulum inertia and resonance may be eliminated by capturing the pendulum so that its motion is severely limited. A pneumatic proportional control has been developed along these lines by the Foxboro Corporation in which a feed back link supplies a torque which is just sufficient to keep the pendulum from moving. The same torque operates the elevators so that the system supplies a signal proportional to the right side of equation (3) and eliminates the impedance lag inherent in the left side. A very simple captured pendulum has been used by the Westinghouse Electric and Manufacturing Company on some of their electric torpedoes. This is a two-position control in which the pendulum is permitted just enough motion to make or break an electric contact which supplies current through a relay to solenoids that move the elevators. While controls of this type remove the impedance lag, they cannot, of course, make the pendulum insensitive to accelerations.

For some applications it is important to have a depth control which is unresponsive to accelerations. Controls of this type have been constructed by the United Shoe Machinery Corporation, using a gyroscope as a standard of orientation in the vertical plane. An uncorrected gyro is unsatisfactory for this purpose, even though it can be used for steering, since the limitations on depth are far more severe than those on deflection. The USMC controls have therefore evolved along two lines. First, the gyro is precessed by friction so that it tends to be oriented perpendicular to the torpedo axis. In this arrangement the gyro corrects for small deviations from running orientation angle, and the hydrostat adjusts the average depth. Second, the primary anticipation is provided by a rate of change of depth indicator, and additional stability is obtained from a spring captured gyro which indicates rate of change of orientation angle. Although this latter system has not as yet been tried, analysis indicates that it should be successful with reasonable values of the parameters. The hydrostat-rate of depth control without the gyro had been tried earlier by Foxboro and preliminary results were unsatisfactory. The computed margin of stability turns out to be very small with such a control, particularly with the plain tail Mark 13-2, which is somewhat less stable than the present shroud tail torpedo. Addition of the captured gyro should make this a practical device.

Thus far, very little has been said about the transmission of the depth-control signal to the elevators. This is the third point at which the overall system can deviate from the ideal. All American torpedoes with the exception of some of those under development by Westinghouse use proportional depth controls and therefore require a depth engine which will transmit the desired indication without delay or change in amplitude and with sufficient force output to operate the elevators. Such proportional engines may be grouped into two classes: force-proportional engines and positioning engines. Force-proportional steering controls were discussed in Section 11.1. A pneumatic device of the type described there has also been developed by Columbia University and the American Can Company for the depth control of the Mark 25 torpedo. A force-proportional electric control has been used experimentally by Westinghouse. This control has a multi-contact unit (Silverstat) which changes the current through the elevator solenoids in discrete steps as the pendulum orientation changes; as with the pneumatic control, the elevators are loaded with springs to insure proportional action.

The standard depth engine used until recently on all American torpedoes is of the positioning or displacement-proportional type. In this engine any difference in displacement of the piston and the valve stem, which is attached to the pendulum, produces an unbalanced air force on the piston which tends to bring it into line with the valve. It suffers from the drawback that, due to close machining tolerances, it is difficult to manufacture and adjust and, unless maintained in optimum condition, will not respond to rapid motions of the pendulum. An improvement on this has recently been developed in conjunction with the blade type force-proportional control for possible use on the Mark 25 torpedo. In this device the pendulum carries a jet which feeds high pressure air into one or the other of two receptive orifices, causing the pendulum support to move until whatever force is being exerted on the pendulum is balanced by a spring and the pendulum remains in its neutral orientation. The pendulum support is rigidly connected to the elevators and hence displaces them in proportion to the pendulum torque.

All of these engines suffer to a greater or lesser extent from phase lags, and these impair the operation of both proportional and two-position systems. Such lags tend to make the former unstable (see Section 9.2) and increase the period of the latter until the amplitude of the depth wave is excessive (see Chapter 10). The best way in which to reduce such lags is by careful design, construction, and maintenance. In pneumatic controls, connecting air lines should be as short as possible, high pressure air should be used, and provision should be made for exhausting as well as filling engine cylinders. In electric controls, relay operation should be made as rapid as possible and time delays due to current build-up in solenoids should be reduced by proper design. In two-position controls in particular, phase advance schemes have been employed with considerable success to partially compensate for time delays and other phase lags that cannot be eliminated. These may involve spring-dashpot systems mounted on the pendulum which add derivatives of the pendulum displacement to the signal supplied to the depth engine. Perhaps the most successful attempt along these lines is that employed by Westinghouse in one of their two-position electric controls. The pendulum is allowed to swing nearly freely and a contact-relay system is set up so that the elevators are thrown up when the pendulum leaves one of two contacts spaced a finite angle apart, and thrown down when it leaves the other. Although the relay system is more complicated here than in the single contact captured pendulum, the gain from the advanced phase at which elevator action takes place more than compensates for the slight increase in relay time delay.

Two effects which have not as yet been given the attention which they deserve from an analytical point of view are Coulomb or static friction and free play. Static friction can affect the motion of the pendulum, or the engine motion directly in a force-proportional system. Free play can occur in the pendulum-hydrostat linkage or in the engine output. Both of these are non-linear effects and hence difficult to take into account without great theoretical complications. It seems, however, that both of these effects will introduce additional phase lags into any control, and this is their principal effect in two-position controls. In proportional controls they may also produce oscillations, not necessarily periodic in character, of sufficient amplitude to take up the frictional force or the displacement free play. In well-designed systems these oscillations are probably too small to observe in the overall motion of the torpedo, but might be detected with suitable instrumentation.

12.2 EXAMPLE: PENDULUM-HYDROSTAT PROPORTIONAL CONTROL

As an illustrative example of a depth control, a simple pendulum-hydrostat proportional system will be considered in this section with the help of the Nyquist criterion. It will be assumed that the pendulum is mounted vertically in space when the torpedo is at its running orientation angle so that $\chi_0 = 0$. Since the drag and propeller thrust depend only very slightly on attack angle, equation (4) of Chapter 7 indicates that the longitudinal acceleration is zero. Then the pendulum equation (3) becomes

$$\begin{aligned} I\ddot{\psi} + R\dot{\psi} + (MgL + K)\psi \\ = -[(I - MLY)\ddot{\beta} + MgL\beta] + \frac{MgL}{W/V}h\,, \end{aligned} \tag{6}$$

where a hydrostat torque has been added corresponding to a particular W/V ratio; angles are measured in degrees and depth in feet. It will be assumed that the depth engine is an ideal one of the positioning type so that

$$\xi = \sigma\psi\,. \tag{7}$$

In using the Nyquist method, it is necessary to find the steady response of the pendulum to oscillating β and h of angular frequency ω ($\beta = \beta_0 e^{i\omega t}$, etc.). In the notation of Section 9.2, equation (6) gives

$$\psi_0 = \frac{+[MgL-(I-MLY)\omega^2]\beta_0 + [MgL/(W/V)]h_0}{(MgL + K) - I\omega^2 + iR\omega}\,. \tag{8}$$

With the substitutions

$$\begin{aligned} \gamma &\equiv \frac{\sigma MgL}{MgL + K}\,, \\ \rho &\equiv \frac{2\pi R}{MgL + K}\,, \\ \nu_A &\equiv \frac{\omega_A}{2\pi}\,, \\ \nu_R &\equiv \frac{\omega_R}{2\pi}\,, \end{aligned} \tag{9}$$

where ω_A and ω_R are defined by (4) and (5), equation (7) becomes

$$\xi_0^* = -\frac{\gamma[-\beta_0(1 - \nu^2/\nu_A^2) + h_0/(W/V)]}{[1 - \nu^2/\nu_R^2 + i\rho\nu]}. \quad (10)$$

This may be expressed in terms of the torpedo-response functions plotted in Figures 1, 2, 3, and 4 of Chapter 9 to give an overall response function for the torpedo plus control:

$$\frac{\xi_0^*}{\xi_0} = -\frac{\gamma[(\beta_0/\xi_0)(1-\nu^2/\nu_A^2)+(h_0/\xi_0)/(W/V)]}{1 - \nu^2/\nu_R^2 + i\rho\nu}. \quad (11)$$

Current practice with the Mark 13-2 torpedo favors values close to $\gamma = 3$, $W/V = 3$; ν_R is generally about 1 c, and ν_A may vary over a wide range. It is clear then from a comparison of Figures 1 and 3 of Chapter 9 that for a considerable frequency range around 1 c, which corresponds to $k = 1.3$ at 40 knots, the magnitude of β_0/ξ_0 is much greater than the magnitude of $(h_0/\xi_0)/(W/V)$. Thus the β term is the dominant one, except near ν_A, where it vanishes because of the antiresonance. For moderate values of the damping coefficient ρ, the resonance will cause the overall response to become large near ν_R. Now both the resonance and the antiresonance have phase lag increases of the order of 180° associated with them. Thus the structure of the Nyquist curve is altered in a fundamental way as ν_A is changed from a value less than ν_R to a value greater than ν_R. This is illustrated schematically in Figure 4. In each case, the curve passes close to the origin near the antiresonance frequency and describes a large semicircle near the resonance frequency. It follows that the system is stable when $\nu_A < \nu_R$ and unstable when $\nu_A > \nu_R$.

The standard Mark 13-2 depth control appears to fall in the latter class, with ν_A slightly greater than ν_R. However, the pendulum damping is large, and this has the effect of reducing the magnitude of the resonance peak. A careful computation, which is based on the best available parameters for both torpedo and control and which considers other effects omitted in the discussion of this section (dependence of hydrostat pressure on attack angle and the finiteness of χ_0), shows that the plain tail torpedo is just on the edge of instability at 40 knots. Reduction of the speed to 33½ knots, or addition of the shroud ring, or both, serve to put the torpedo well into the region of stable operation. Reduction of speed reduces the phase lag and increases the gain, but the former effect is more important than the latter; addition of the shroud ring decreases both phase lag and gain. Thus both of these changes improve the stability.

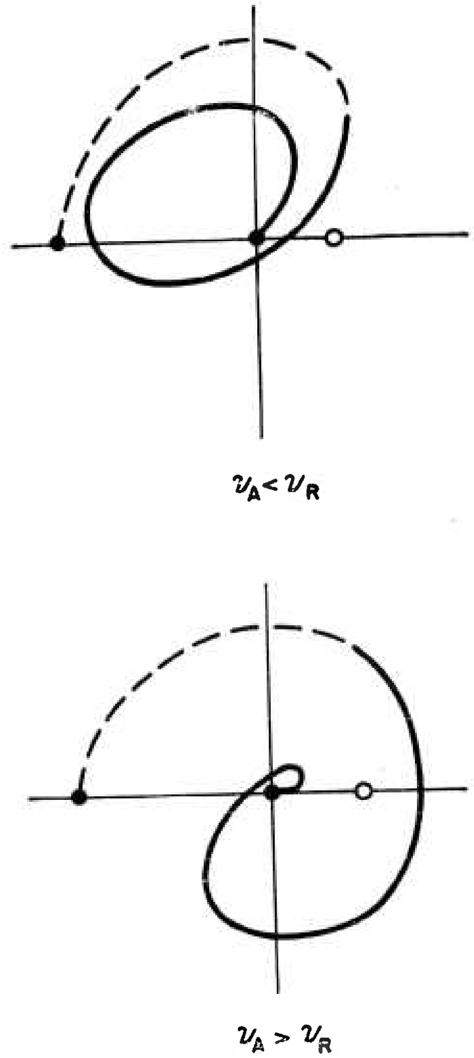

FIGURE 4. Variation of Nyquist curves with the change in the ν_A (pendulum antiresonant frequency), ν_R (pendulum resonant frequency) relationship.

Chapter 13

POWER PLANT

When this report was first projected, it was planned to include a discussion of torpedo power plants. However, while this report was being prepared the United States Navy Coordinator of Research and Development requested the National Defense Research Committee to undertake a torpedo survey under Project N-121. A panel of experts was assembled, and among the subjects upon which a report was presented was torpedo power plants.

As this report is presumably available to interested parties through the Office of Naval Research and is quite comprehensive, it is not thought necessary to present here in a degree the same material.

For additional detailed information on torpedo power plants the reader is referred to the Bibliography.

BIBLIOGRAPHY

Numbers such as Div. 6-800-M1 indicate that the document listed has been microfilmed and that its title appears in the microfilm index printed in a separate volume. For access to the index volume and to the microfilm, consult the Army or Navy agency listed on the reverse of the half-title page.

GENERAL

1. *Selected Index of British Reports on Torpedoes*, Richard H. Bolt, CUDWR,[a] March 1944. Div. 6-800-M1
2. *Program Analysis of the Torpedo Division*, OEMsr-287, HUSL,[b] May 30, 1944. Div. 6-800-M2
3. *Conference on Program Analysis of the Torpedo Division of Harvard Underwater Sound Laboratory Held in the New York Division Six Office, June 5, 1944*, Richard H. Bolt, June 1944. Div. 6-800-M3
4. *Report on Studies Made in Connection with Projects AC-70 and NO-177*, William V. Houston, OSRD 53, NDRC 6.1-sr1131-1182, CUDWR, Oct. 25, 1944. Div. 6-800-M5
5. *A Theoretical Study of the Effectiveness of a 20-Knot Acoustic Torpedo and of Possible Modifications Having Lower Speeds With or Without an Automatic Speed-Changing Mechanism*, Conyers Herring and E. Ward Emery, NDRC 6.1-sr1131-1882, CUDWR, Nov. 22, 1944. Div. 6-912.4-M1
6. *Summary Report of the CIT Morris Dam Group of Division 3 NDRC*, L. B. Slichter and others, CIT,[c] 1945.

HYDRODYNAMICS AND AERODYNAMICS

7. *Hydrodynamics*, H. Lamb, 4th Edition, 1916, Chap. VI, pp. 124, 127.
8. *Report of Investigation of Torpedoes with Screws Running*, Conducted in the Aerodynamics Department, National Physical Laboratory, British, January 1928.
9. *Analysis of Aircraft Torpedo Drops, The Effect of Entry Conditions and Underwater Roll on the Initial Dive*, L. W. Parkin and K. D. Tocher, OSRD WA-1241-4, Report TDU/18/1943, Torpedo Development Unit, RAF Station, Gosport, August 1943. Div. 6-810.21-M3
10. *The Underwater Behavior of the 11.75-in. Aircraft Rocket*, I. S. Bowen, OEMsr-418, Division 3 Report IPC 65, CIT, Oct. 25, 1944. AMP-406-M4
11. *Tests of Darts at the New London Escape Tower*, L. J. Hooper, Report D1/1318, NLL,[d] Sept. 26, 1941. Div. 6-810.22-M1
12. *Free Fall of Streamlined Bodies in Water*, R. G. Folsom and Morrough P. O'Brien, UCDWR,[e] Oct. 22, 1941. Div. 6-810.2-M1
13. *A Preliminary Study of the Ballistics of a Submerged Projectile*, Report 603, CIT, Oct. 23, 1941. Div. 6-810.2-M2
14. *Free Fall Tests of 1" x 6" Brass Darts at the Alden Hydraulic Laboratory, Worcester Polytechnic Institute, Worcester, Massachusetts*, L. J. Hooper, Laboratory Report D1/1983, NLL, Feb. 10, 1942. Div. 6-810.22-M2
15. *High Speed Photography of 1" x 6" Darts at the Alden Hydraulic Laboratory, Worcester Polytechnic Institute, Worcester, Massachusetts*, L. J. Hooper, Laboratory Report D1/1985, NLL, Feb. 16, 1942. Div. 6-810.22-M3
16. *Summary, Coefficients of Drag and Terminal Velocities, Models of Underwater Projectiles*, Report D16/2206, NLL, Mar. 10, 1942. Div. 6-810.2-M3
17. *The Trajectory of Stable Underwater Projectiles for the Case in which the Trajectory is Nearly Vertical and the Projectile is Traveling at Terminal Velocity*, G. A. Gongwer, Laboratory Report D10/2258, NLL, May 1, 1942. Div. 6-810.21-M1
18. *Investigation of the Control in Air of a Torpedo with Fixed Tailplane and Gyro-Controlled Ailerons*, L. W. Parkin, OSRD WA-1378-26, Torpedo Development Unit, July 1942. Div. 6-810.1-M1
19. *British Studies of Hydrodynamics of Projectiles Discussion with Dr. V. O. Knudsen*, D. P. Fullerton, Report G2/3873, NLL, Sept. 1, 1942.
20. *Memorandum on Water Tunnel Tests of 2" Diameter Projectiles with Hemispherical Noses and Square Ends*, Robert T. Knapp, HML Report ND-10, CIT, Nov. 10, 1942. Div. 6-722.7-M1
21. *Initial Underwater Torpedo Trajectories After Dropping*, C. H. Tindal, NDRC 6.1-sr287-778, HUSL, May 25, 1943. Div. 6-810.21-M1
22. *Aircraft Torpedo Trajectory*, U. S. Navy Torpedo Station, Newport, Rhode Island, October 1943.
23. *Selected Index of British Reports on Water Entry ond Water Travel*, William V. Houston, Project No. 176, CUDWR, November 1943. Div. 6-810.2-M4
24. *Selected Index of California Institute of Technology and Miscellaneous Reports on Water Entry and Water Travel*, William V. Houston, CUDWR, November 1943. Div. 6-810.2-M5
25. *Relationship between Cavitation Bubble and Entrance Air Bubble of Torpedoes and Other Projectiles* (Memorandum), Robert T. Knapp, OEMsr-207, CIT, Nov. 6, 1943. Div. 6-810.23-M1

---

[a] Columbia University Division of War Research.
[b] Harvard Underwater Sound Laboratory.
[c] California Institute of Teehnology.
[d] New London Laboratory.
[e] University of California Division of War Research.

26. *Observations on the Water Entry of a Torpedo* (Local Intermediate Report), R. W. Ager, Report IOC-14, CIT, Nov. 23, 1943. Div. 6-810.21-M4

27. *Wind Tunnel Tests Prior to Dropping Full Sized Torpedoes*, Harvey A. Brooks and Carl M. Herget, HUSL, Dec. 21, 1943. Div. 6-810.1-M2

28. *Preliminary Remarks on the Cavity Made by a Projectile Entering Water*, B. D. Blackwell, OSRD WA-1927-3d, Report SRE/UT/4, Department of Scientific Research and Experiment, Great Britain, February 1944. AMP-401.2-M4

29. *Ricochet off Water*, Garrett Birkhoff, George D. Birkhoff, and others, OEMsr-1007, AMP[f] Memorandum 42.4M, AMG-C 157, May 1944. AMP-401.1-M5

30. *The 24-ft. Wind Tunnel Tests on Four Torpedo Air Tails*, P. J. Pearsall and T. B. Owen, OSRD WA-2764-3, Technical Note Aero. 1442, Royal Aircraft Establishment, Farnborough, May 1944. Div 6-810.1-M3

31. *A Method of Prediction of the Upturning Underwater Trajectories of Rockets in Two Dimensions*, B. D. Blackwell, Report SRE/UT/8, UBRC-31, Department of Scientific Research and Experiment, Admiralty, Great Britain, June 1944. AMP-406-M7

32. *Impact Forces*, Garrett Birkoff, OEMsr-1384 AMP Memorandum 42.6M, AMG-Harvard, September 1944. AMP-404-M1

33. *Prediction of Underwater Behavior from Wind Tunnel Measurements*, R. A. Shaw, OSRD WA-3024-14C, H/Arm/Res. 23, Marine Aircraft Experiment Establishment, Helensburgh, Great Britain, Sept. 26, 1944. AMP-401-M6

34. *Visit to California Institute of Technology, August 27–September 3, 1944*, G. F. Wislicenus, Project NO-176, CUDWR, Sept. 9, 1944. Div. 6-800-M4

35. *Theoretical Depth Trajectories 149-B* (Memorandum), Harvey A. Brooks and Nelson M. Blachman, HUSL, Oct. 31, 1944. Div. 6-810.21-M5

36. *Drag Coefficients of Spherical and Conical Motion Underwater*, R. W. Duncan and F. E. Bradley, OSRD WA-3519-2, Technical Note Arm. 301, Royal Aircraft Establishment, Great Britain, November 1944. AMP-401.3-M4

37. *Information on Mk 13 Dynamics*, Harvey A. Brooks, HUSL, Nov. 13, 1944. Div. 6-820.1-M2

38. *The Effect of Trajectory Angle and Pitch Angle on the Initial Underwater Trajectory of the Torpedo*, Marvin Gimprich, NDRC 6.1-sr1131-1881, CUDWR, Nov. 18, 1944. Div. 6-810.21-M6

39. *Tunnel Characteristics and Test Procedure for Bodies of Revolution. Cavitation Tests in the Iowa Variable-Pressure Water Tunnel*, Hunter Rouse, John S. McNown, and En-Yun-Hsu, OEMsr-1353, Informal Report to Section 12.1, State University of Iowa, Nov. 30, 1944. Div. 6-810.23-M2

40. *Moment of Inertia Characteristics of Mark-13 Type Torpedoes*, Memorandum to Chief, Bureau of Aeronautics Section, Naval Torpedo Station, Newport, R. I., Dec. 1, 1944.

41. *Cylindrical Body with Hemispherical Head, Cavitation Tests in the Iowa Variable-Pressure Water Tunnel*, Hunter Rouse, John S. McNown, and En-Yun-Hsu, OEMsr-1353, Informal Report to Section 12.1, State University of Iowa, Dec. 4, 1944. Div. 6-810.23-M3

42. *Cylindrical Body with Blunt Head, Cavitation Tests in the Iowa Variable-Pressure Water Tunnel*, Hunter Rouse, John S. McNown, and En-Yun-Hsu, OEMsr-1353, Informal Report to Section 12.1, State University of Iowa, Dec. 8, 1944. Div. 6-810.23-M4

43. *Head Studies*, J. H. Wayland, Report TLP 28, TL-D 351, CIT, January 1945.

44. *Initial Dive and Recovery of Aircraft Torpedoes*, Leonard I. Schiff, Project NO-176, CUDWR, Feb. 14, 1945. Div. 6-810.21-M7

45. *Underwater Performance of One Inch Diameter Models of a Family of Cone Head Rockets*, R. A. Shaw and P. E. Naylor, OSRD WA-3996-9, Report H/Arm/Res.25, Marine Aircraft Experimental Establishment, Great Britain, Feb. 7, 1945. AMP-406-M6

46. *Heat Treatment of Standard Mk 13 Torpedo Propellers to Withstand Entry Impact Forces*, W. Harry Johns, Jr., NDRC 6.1-sr1131-1886, CUDWR, Feb. 8, 1945. Div. 6-810.2-M7

47. *Cavitation Tests on a Systematic Series of Torpedo Heads. Water Tunnel Characteristics and Test Procedure*, Hunter Rouse, John S. McNown, and En-Yun-Hsu, NDRC 6.1-sr1353-2190, State University of Iowa, Institute of Hydraulic Research, Feb. 22, 1945. Div. 6-810.23-M5

48. *The Mechanism of Pitch Sensitivity of Aircraft Torpedoes*, Harold Wayland, Report NOC-47.1, CIT, Feb. 27, 1945. Div. 6-810.1-M4

49. *Cavitation Tests on a Systematic Series of Torpedo Heads, Hemispherical Head*, Hunter Rouse, John S. McNown, and En-Yun-Hsu, OSRD 5059, NDRC 6.1-sr1353-2191, State University of Iowa, Institute of Hydraulic Research, Feb. 28, 1945. Div. 6-712-M5

50. *Cavitation Tests on a Systematic Series of Torpedo Heads, Blunt Head*, Hunter Rouse, John S. McNown, and En-Yun-Hsu, OSRD 5056, NDRC 6.1-sr1353-2192, State University of Iowa, Institute of Hydraulic Research, Mar. 5, 1945. Div. 6-712-M6

51. *Cavitation Tests on a Systematic Series of Torpedo Heads, 1/4 Caliber Rounded Head*, Hunter Rouse, John S. McNown, and En-Yun-Hsu, NDRC 6.1-sr1353-2193, State University of Iowa, Institute of Hydraulic Research, Mar. 10, 1945. Div. 6-810.23-M6

[f] Applied Mathematics Panel

52. *Cavitation Tests on a Systematic Series of Torpedo Heads, 1/8 Caliber Rounded Head*, Hunter Rouse, John S. McNown, and En-Yun-Hsu, NDRC 6.1-sr1353–2194, State University of Iowa, Institute of Hydraulic Research, Mar. 15, 1945. Div. 6-810.23-M7

53. *Cavitation Tests on a Systematic Series of Torpedo Heads, 1-Caliber Ogival Head*, Hunter Rouse, John S. McNown, and En-Yun-Hsu, OSRD 5055, NDRC 6.1-sr1353–2195, State University of Iowa, Institute of Hydraulic Research, Mar. 20, 1945. Div. 6-712-M8

54. *Cavitation Tests on a Systematic Series of Torpedo Heads, 2-Caliber Ogival Head*, Hunter Rouse, John S. McNown, and En-Yun-Hsu, OSRD 5054, NDRC 6.1-sr1353–2196, State University of Iowa, Institute of Hydraulic Research, Mar. 26, 1945. Div. 6-712-M9

55. *Analysis of Aircraft Drops of Mark 13-2A and Mark 13-3 Torpedoes fitted with Eight Degree Cone Angle Shroud Ring Tail*, K. H. Keller, Dec. 14, 1944. In: *Analysis of Aircraft Launchings of Torpedoes Equipped with Shroud Rings*, Karl H. Keller, Marvin Gimprich and W. H. Wilson, NDRC 6.1-sr1131–1887, Project NO–176, CUDWR, Mar. 26, 1945. Div. 6-810.1-M5

56. *Summary of Cavitation Tests on a Systematic Series of Torpedo Heads* (Final Report), Hunter Rouse, John S. McNown, and En-Yun-Hsu, NDRC 6.1-sr1353–2330, State University of Iowa, Institute of Hydraulic Research, May 31, 1945. Div. 6-810.23-M8

57. *Water Entry Bibliography*, OEMsr-1384, AMP Memorandum 42.8M, AMG-II 11, June 1945. AMP-401-M10

58. *Values of Lift and Moment Coefficient Derivatives for the American Mark 13 Aircraft Torpedo*, B. G. Neal, OSRD WA–4557–3, Report SRD/UT/9, Department of Scientific Research and Experiment, Great Britain, June 1945. Div. 6-810.1-M6

59. *A Study of the Depth of Initial Dive of a Mark-13 Torpedo with Shroud Ring*, Marvin Gimprich, OSRD 5244, NDRC 6.1-sr1131–1889, June 9, 1945. AMP-405.3-M8

60. *Hydrodynamic Forces Resulting from Cavitation on Under-Water Bodies*, James W. Daily, OSRD 5756, NDRC 6.1-sr207–2242, Division 6 Laboratory Report ND–31.2, MIT,[g] July 21, 1945. AMP-401.5-M4

61. *Attitude of Torpedoes Released from Airplanes* (Interim Report), Marvin Gimprich, NDRC 6.1-sr1131–1893, Dec. 21, 1945. Div. 6-810.1-M7

CONTROL OF UNDERWATER RUN

62. *Bell System Technical Journal*, Harry Nyquist, Vol. II, 1932, p. 126.

63. *Differentialgleichungen der Physik*, Frank and von Mieses, Vol. I, p. 163.

64. *Determination of Running Depth of Test Torpedoes by a Sonic Method*, Donald A. Proudfoot, Memorandum for file G/10/R165, NLL, Feb. 18, 1943. Div. 6-820.22-M1

65. *Analysis of Search and Pursuit Patterns Employing Mechanical Depth Control*, H. Poritsky and L. J. Savage, NDRC 6.1-sr1131–1155, Project NO-181, CUDWR, Dec. 22, 1943. Div. 6-820.22-M2

66. *Memorandum on Torpedo Steering.* William V. Houston [CUDWR], Feb. 14, 1944. Div. 6-820.21-M1

67. *Steering Control of the Mark 13-2 Torpedo*, Leonard I. Schiff, Project NO–176, CUDWR, May 29, 1944. Div. 6-820.21-M2

68. *Proportional and On-Off Control Systems*, J. C. Lozier, Report 44-3510-JCL-GH, Bell Telephone Laboratories, Aug. 15, 1944. Div. 6-820.1-M1

69. *Depth Turning Radius of Mark 13 with Shroud Rings in Forward Position*, Gilford G. Quarles, HUSL, Oct. 30, 1944. Div. 6-820.22-M3

70. *Supplement to "Depth-Turning Radius of Mark 13 with Shroud Ring in Forward Position"* (Memorandum), Gilford G. Quarles, HUSL, Oct. 31, 1944. Div. 6-820.22-M4

71. *Hydrodynamic Properties of the Mark 13-2 and 13-2A Torpedoes with Plain and Shroud Ring Tails*, Leonard I. Schiff, Project NO–176, CUDWR, Nov. 7, 1944. Div. 6-810.2-M6

72. *Development of Depth and Steering Controls for the Mark 25 Torpedo*, William V. Houston, NDRC 6.1-sr1131–2348, Project NO–176, CUDWR, July 12, 1945. Div. 6-820-M1

POWER PLANT

73. *Preliminary Experiments with Mixtures of Tetranitromethane and Iso-Octane*, OEMsr-124, Report 607, CIT, Nov. 20, 1941. Div. 6-830.2-M1

74. *Studies of the Restricted Burning of Certain Heterogeneous and Colloidal Propellants*, OEMsr-124, Report 609, Department of Chemical Engineering, CIT, Apr. 15, 1942.

75. *Study of Utilization of Tetranitromethane and Gasoline as Fuel in Jet Propulsive Equipment*, OEMsr-124, Report 610, Department of Chemical Engineering, CIT, Apr. 22, 1942. Div. 6-830.2-M3

76. *Dynamometer Test of Aircraft Torpedoes*, George Farnell and Ascher H. Shapiro, Project NO–176, Research Project DIC–6228, Report D-1, MIT, May 23, 1944. Div. 6-830-M1

77. *Dynamometer Tests of Aircraft Torpedoes*, George Farnell and Ascher H. Shapiro, Project NO–176, Research Project DIC–6228, Report D–2, MIT, June 30, 1944. Div. 6-830-M1

78. *Torpedo Igniter Type B Developed by Remington Arms Company, Inc.*, A. E. Buchanan, Jr., NDRC 6.1-sr1131–1851, prepared by Remington Arms Co., Inc., for Special Studies Group, Sept. 5, 1944. Div. 6-830.1-M1

79. *Thermodynamic Analysis of the Combustion of Ethyl Alcohol*, John A. Goff, Project NO–176, NDRC 6.1-sr1131–1847, CUDWR, Sept. 18, 1944. Div. 6-830.2-M4

[g] Massachusetts Institute of Technology.

80. *Gas Generating Systems for Torpedoes. An Experimental Study of Systems Using Ethyl Alcohol and Air for Combustion and Either Water or Ethyl Alcohol as a Coolant*, George Farnell, Chas. S. Hofmann, Don G. Jordan, William A. Reed, Dumont Rush, and Ascher H. Shapiro, NDRC 6.1-sr1198–2111, Project NO–176, Research Project DIC–6228, Report R-1, MIT, Nov. 4, 1944. Div. 6-830.2-M5

81. *Gas Generating Systems for Torpedoes. An Experimental Study of the Mark EX–25–0 Combustion Pot Using Ethyl Alcohol and Air for Combustion and Ethyl Alcohol as a Coolant*, George Farnell, Chas. S. Hofmann, Don G. Jordan, William A. Reed, Dumont Rush, and Ascher H. Shapiro, NDRC 6.1-sr1198–2112, Project NO–176, Research Project DIC–6228, Report R-2, MIT, Jan. 11, 1945. Div. 6-830.2-M6

82. *Progress Report on Decomposition Studies* (Memorandum to: Glenn C. Williams, Ernest P. Neumann, and Howard S. Gardner), Charles N. Satterfield and Wilburn H. Hoffman, OEMsr-1289, Project NO–236, MIT, Jan. 30, 1945. Div. 6-830.21-M1

83. *An Explorative Study of the Combustion of Nitropropane with Air and of Nitroethane with Air*, William A. Reed and Ascher H. Shapiro, Project NO–176, Research Project DIC–6228, Report C-1, MIT, Feb. 13, 1945. Div. 6-830.2-M7

84. *Thermodynamic Analysis of the Energy Producing Capabilities of Hydrogen Peroxide*, Harold S. Mickley, NDRC 6.1-sr1289–2118, Project NO–236, Research Project DIC–6249, Report T-1, MIT, Mar. 28, 1945. Div. 6-830.2-M8

85. *Torpedo Fuels*, G. C. Williams and E. P. Neumann, NDRC 6.1-sr1829–2119, Project NO–236, Research Project DIC-6249, Progress Report A–1, MIT, Apr. 11, 1945. Div. 6-830.2-M9

86. *Torpedo Fuels*, G. C. Williams and E. P. Neumann, NDRC 6.1-sr1289–2119, Project NO–236, Research Project DIC-6249, Progress Report A-2, MIT, May 14, 1945. Div. 6-830.2-M9

87. *Thermodynamic Analysis of the Energy Producing Capabilities of Hydrogen Peroxide*, NDRC 6.1-sr1289–2118, Project NO–236 and Research Project DIC-6249, Progress Report T–2, MIT, June 14, 1945. Div. 6-830.2-M8

88. *Decomposition of 50 Weight Per Cent Hydrogen Peroxide Solution Using Calcium and Sodium Permanganate*, Charles N. Satterfield and Wilburn H. Hoffman, NDRC 6.1-sr1289–2336, Project NO–236, Research Project DIC–6249, Progress Report C–1, MIT, June 28, 1945. Div. 6-830.21-M2

89. *Torpedo Igniter Design and Pyrotechnics Investigation*, J. P. Catlin, W. L. Finlay and T. B. Johnson, NDRC 6.1-sr1131–2333, Aug. 31, 1945. Div. 6-830.1-M2

90. *An Experimental Investigation of Torpedo Power Plants* (Final Report), C. Richard Soderberg and Ascher H. Shapiro, OSRD 6348, NDRC 6.1-sr1198–2385, Research Project DIC–6228, MIT, Aug. 31, 1945. Div. 6-830-M2

91. *Investigation of Torpedo Fuels — An Experimental Study of the Peroxide-Ethanol Cycle* (Final Report), NDRC 6.1-sr1289–2391, MIT, Nov. 14, 1945. Div. 6-830.2-M10

92. *Design of the Mark 25 Torpedo* (Section 2 of the Final Technical Report), OEMsr-1131, OSRD 6673, NDRC 6.1-sr1131–2393, Project NO–176, Dec. 31, 1945. Div. 6-800-M6

93. *Sea-Water Batteries* (Final Report), OSRD 6420, NDRC 6.1-sr1069–2128, Bell Telephone Laboratories, Nov. 30, 1945. Div. 6-647-M1

CONTRACT NUMBERS, CONTRACTORS, AND SUBJECTS OF CONTRACTS

Contract Number	Name and Address of Contractor	Subject
OEMsr-20	The Trustees of Columbia University in the City of New York New York, New York	Studies and experimental investigations in connection with and for the development of equipment and methods pertaining to submarine warfare.
OEMsr-1131	The Trustees of Columbia University in the City of New York New York, New York	Conduct studies and investigations in connection with the evaluation of the applicability of data, methods, devices, and systems pertaining to submarine and subsurface warfare.
OEMsr-207	California Institute of Technology Pasadena, California	Construction and operation of a high-speed water tunnel, and use of such water tunnel in research and experimental investigations involving underwater projectiles and detection equipment.
OEMsr-1105	American Can Company New York, New York	Conduct studies and experimental investigations in connection with (i) the modification and improvement of torpedo design, with the general purpose of (a) enabling torpedoes to be dropped from aircraft without damage at higher speeds than is now possible and (b) improving the operating characteristics of torpedoes designed for high underwater speed; and (ii) the construction of experimental models of torpedoes or parts thereof for test purposes.
OEMsr-1198	Massachusetts Institute of Technology Cambridge, Mass.	Conduct studies and experimental investigations in connection with (i) torpedo power plants and (ii) the general problem of power-plant design.
OEMsr-1289	Massachusetts Institute of Technology Cambridge, Mass.	Conduct studies and experimental investigations in connection with new and improved fuels for torpedoes, including survey of power supplies for jet-propelled missiles.
OEMsr-1342	Newark College of Engineering Newark, New Jersey	Conduct studies and experimental investigations in connection with a development and test program for Navy Project NO-176.

SERVICE PROJECT NUMBERS

The projects listed below were transmitted to the Executive Secretary, NDRC, from the War or Navy Department through either the War Department Liaison Officer for NDRC or the Office of Research and Inventions (formerly the Coordinator of Research and Development), Navy Department.

Service Project Number	*Subject*
NO-176	Torpedoes for high-speed aircraft
NO-236	Investigation of torpedo fuels
N-121	Torpedo survey

INDEX

The subject indexes of all STR volumes are combined in a master index printed in a separate volume. For access to the index volume consult the Army or Navy Agency listed on the reverse of the half-title page.